



Discovery of Novel Targets in the Hedgehog Signaling Pathway

Dissertation

zur Erlangung des akademischen Grades eines

Doktors der Naturwissenschaften

(Dr. rer. nat.)

an der Fakultät für Chemie und Chemische Biologie

der Technischen Universität Dortmund

vorgelegt von

M. Sc. Summersing Patil

Geboren am 15.06.1990

in Bodwad, India

Dekan: Prof. Dr. Roland Winter

1. Gutachter: Prof. Dr. Dr. h.c. Herbert Waldmann

2. Gutachter: PD. Dr. Leif Dehmelt

Erklärung / Declaration

Die vorliegende Arbeit wurde in der Zeit von September 2013 bis September 2017 am Max-Planck-Institut für Molekulare Physiologie Dortmund unter der Anleitung von Prof. Dr. Dr. h.c. Herbert Waldmann durchgeführt.

Hiermit versichere ich an Eides statt, dass ich die vorliegende Arbeit selbstständig und nur mit den angegebenen Hilfsmitteln angefertigt

The work described in this Dissertation was performed from September 2013 to September 2017 at the Max Planck Institute of Molecular Physiology Dortmund under the guidance of Prof. Dr. Dr. h.c. Herbert Waldmann.

I hereby declare that I performed the work independently and did not use any other but the indicated aids.

Teile dieser Arbeit wurden bereits in folgenden Publikationen

The present work was partly published in the following papers:

A ligand-directed divergent catalytic approach to establish structural and functional scaffold diversity

Lee, Y.-C., **Patil, S.**, Golz, C., Strohmann, C., Ziegler, S., Kumar, K., & Waldmann, H. (2017). *Nature Communications*, 8, 14043.

दिलों में तुम अपनी बेताबियाँ लेके चल रहे हो, तोह जिंदा हो तुम
नज़र में ख़्वाबों की बिजलियाँ लेके चल रहे हो, तोह जिंदा हो तुम

If you have eagerness in your heart, it means you are alive

If your eyes are filled with dreams, it means you are alive

Javed Akhtar

Zindagi na milegi dobara

Dedicated to my parents and my wife Kalyani

Table of contents

1	Summary.....	1
2	Zusammenfassung.....	3
3	Introduction.....	5
3.1	Chemical Genetics.....	5
3.1.1	Phenotypic Screening.....	7
3.1.2	Approaches to target identification.....	8
3.2	The Hedgehog signaling pathway.....	18
3.2.1	Maturation of Hh proteins.....	19
3.2.2	The Hh signaling cascade in vertebrates.....	20
3.2.3	The Hh pathway in disease and cancer.....	23
3.3	Modulators of the Hh signaling pathway.....	24
3.3.1	SMO inhibitors in clinical trials.....	24
3.3.2	Inhibitors upstream of SMO.....	25
3.3.3	Inhibitors downstream of SMO.....	26
3.3.4	Activators of Hh signaling pathway.....	26
4	Motivation and aim of the thesis.....	28
5	Results and discussion.....	31
5.1	Phenotypic screening to identify Hh pathway modulators.....	31
5.2	Biological evaluation of <i>df</i> -oxindoles.....	33
5.2.1	Confirmation of biological activity by secondary assays.....	33
5.2.2	SMO binding of YCL-220.....	36
5.2.3	Effect on the ciliary transport of SMO.....	40
5.2.4	Summary and outlook for <i>df</i> -oxindole YCL-220.....	42
5.3	Biological evaluation of bridged bispyrrolidines.....	43
5.3.1	Confirmation of biological activity by secondary assays.....	43
5.3.2	Computational target prediction.....	46
5.3.3	Target identification by chemical proteomics.....	50
5.3.4	Target identification by chemical proteomics.....	56
5.3.5	Regulation of RHO GTPases by RHOGDI.....	60
5.3.6	RKN-1043 binds to the GerGer binding pocket of RHOGDI1.....	64
5.3.7	Genetic validation of RHOGDI1 as target of RKN-1043.....	70
5.3.8	Effect of RKN-1043 on stress fibers.....	77

5.3.9	Summary and outlook for RKN-1043.....	79
5.4	Biological evaluation of bis-nitrophenyl-bipyridines	80
5.4.1	Confirmation of biological activity by secondary assays	81
5.4.2	Target identification.....	85
5.4.3	Target validation	89
5.4.4	Polyamine biosynthesis.....	94
5.4.5	Influence of MJD-1314 on MTAP enzymatic activity	97
5.4.6	Genetic validations.....	99
5.4.7	Effect of MJD-1314 on the localization of MTAP	103
5.4.8	Immunoprecipitation of interacting partners of MTAP	104
5.4.9	Summary and outlook for the bis-nitrophenyl-bipyridine MJD-1314.....	108
6	Materials	109
6.1	Chemicals	109
6.2	Laboratory consumables	110
6.3	Laboratory equipment	111
6.4	Commercial Kits	112
6.5	Buffers and solutions.....	113
6.6	Cell lines.....	116
6.7	Mammalian cell culture medium.....	116
6.8	Bacterial strains	117
6.9	PCR primers	117
6.10	siRNAs.....	117
6.11	Plasmids.....	118
6.12	Primary antibodies	119
6.13	Secondary antibodies	119
7	Methods.....	120
7.1	Cell culture	121
7.1.1	Determination of cell number	121
7.1.2	Osteoblast differentiation assay	121
7.1.3	CellTiter-Glo [®] viability assay.....	122
7.1.4	Gli-dependent reporter gene assay.....	122
7.1.5	SMO binding assay using fluorescence microscopy	123
7.1.6	SMO binding assay using flow cytometry.....	123
7.1.7	SAG1 competition assay.....	124
7.1.8	Ciliary localization of SMO.....	124

7.2	Molecular biology methods.....	124
7.2.1	RNA isolation	124
7.2.2	cDNA preparation.....	125
7.2.3	Quantitative PCR	125
7.2.4	Transformation of competent <i>E. coli</i> with plasmid DNA.....	126
7.2.5	Glycerol stock preparation.....	126
7.2.6	Plasmid DNA isolation	126
7.3	Biochemical methods	127
7.3.1	Purification of recombinant MTAP protein.....	127
7.3.2	Protein concentration determination	127
7.3.3	SDS polyacrylamide gel electrophoresis (SDS-PAGE)	128
7.3.4	Immunoblotting.....	128
7.3.5	Colloidal coomassie staining of proteins	128
7.3.6	PTP1B enzymatic assay	129
7.3.7	MTAP enzymatic assay	129
7.4	Chemical proteomics.....	129
7.4.1	Cell lysate preparation for affinity <i>pull-down</i> experiments	129
7.4.2	Cell lysate preparation for co-immunoprecipitation.....	130
7.4.3	Affinity chromatography enrichment of compound-bound proteins (Pull-down) 131	
7.4.4	On bead tryptic digestion and STAGE (STop And Go Extraction) tips desalting	131
7.4.5	Cell lysate preparation for stable isotope labeling with amino acids in cell culture (SILAC)	132
7.4.6	Determination of heavy amino acid incorporation efficiency	132
7.4.7	Co-immunoprecipitation.....	133
7.4.8	Mass spectrometric and data evaluation	133
7.4.9	Target engagement by affinity enrichment.....	135
7.5	Biophysical methods	135
7.5.1	Cell lysate preparation for cellular thermal shift assay.....	135
7.5.2	Cellular thermal shift assay.....	136
7.5.3	Differential scanning fluorimetry	136
7.5.4	Fluorescence polarization	136
7.5.5	Liposome sedimentation assay	137
7.5.6	Liposome flotation assay	137
7.5.7	Surface plasmon resonance (SPR).....	138

7.6	Genetic validation	139
7.6.1	siRNA-mediated knockdown.....	139
7.6.2	Overexpression	139
7.7	Kinase profiling at Eurofins	140
7.8	GPCR screening at Eurofins	140
7.8.1	Synthesis of the <i>pull-down</i> probes	141
8	Appendix.....	151
10	List of abbreviations	160
12	References.....	163
13	Acknowledgements.....	173
14	Curriculum vitae	176

1 Summary

A forward chemical genetics approach in order to identify novel modulators of Hh signaling pathway led to identification of three novel inhibitor classes with novel targets in Hh signaling. The identification of proteins involved in Hh signaling regulation sheds light on the complexity of Hh signaling pathway.

An osteoblast differentiation assay that monitors Hh pathway activity identified YCL-220 as an inhibitor of Hh signaling. Orthogonal assays revealed YCL-220 as a potent inhibitor of GLI transcription factor-mediated Hh signaling pathway. Mechanistic insights showed that YCL-220 acts as a SMO antagonist that inhibits SMO localization to cilia, similar to vismodegib. The SMO binding of YCL-220 was reversed upon a washout step, thus indicating the non-covalent and reversible mode of SMO binding. The mutations in SMO demands for new strategies to modulate SMO functions, therefore reversible inhibition of SMO by YCL-220 can be further investigated as future SMO targeted strategies.

In addition, a pyrrolidine, RKN-1043, was identified as a Hh signaling pathway inhibitor acting downstream of SMO. Affinity chromatography coupled to proteomics for target identification revealed RHOGDI1 as a potential target of RKN-1043. Biophysical experiments showed that RKN-1043 inhibits RHOGDI1-mediated extraction of prenylated RAC1-GDP from liposomes. Furthermore, RKN-1043 competed with GerGer-RAB1 peptide for binding to the GerGer binding pocket of RHOGDI1 which makes it the first molecule to bind to the GerGer binding pocket of RHOGDI1, thus inhibiting its function. Genetic alterations revealed involvement of RHOGDI1 as a negative regulator of Hh signaling.

Overall, RKN-1043 is a novel inhibitor of Hh signaling as well as of RHOGDI1. In-depth analysis of the effect of RKN-1043 on the activation state of RHO GTPases will further support the mechanism of action for RKN-1043-mediated Hh signaling inhibition.

The third compound, MJD-1314 was prepared as a result of diversity-oriented synthesis by using metathesis cascades to prepare substrates for inter- and intramolecular Diels-Alder reactions. The substance was characterized as a potent inhibitor of osteogenesis and GLI-mediated Hh signaling pathway acting downstream of SMO. Chemical proteomics experiments revealed MTAP as a potential target for MJD-1314. Thermal

stability experiments validated the target engagement by inducing thermal stabilization of MTAP. Although MJD-1314 binds to MTAP, it had no effect on enzymatic activity of MTAP. Additionally, MTDIA, an inhibitor of MTAP failed to inhibit GLI-mediated Hh signaling. These results indicated a possible non-canonical function of MTAP in Hh signaling regulation. Genetic alterations of MTAP indicated a contradicting mode of involvement, i.e. as a positive regulator or negative regulator of Hh signaling. Furthermore, MJD-1314 binding to MTAP did not alter its localization. Efforts to identify novel interaction partners of MTAP that may link MTAP to Hh signaling were unsuccessful.

To explore the influence of MJD-1314 on the MTAP function in cells, the cell metabolic state upon compound treatment will be analyzed. Furthermore, in order to elucidate the mode of action of MJD-1314 in Hh pathway inhibition, gene expression profiling can facilitate a global picture of effect of MJD-1314 on the physiological state of the cells.

The work presented in this thesis led to the identification of novel Hh signaling inhibitors and uncovered novel players in Hh signaling pathway. The approach followed in this study stresses on the importance of using a combination of methods for identification and validation of small-molecule targets in order to establish the mechanism of action of small molecule modulators.

2 Zusammenfassung

Ein vorwärtsgerichteter chemisch-genetischer Ansatz zur Identifizierung neuer Modulatoren des Hedgehog (Hh)-Signalweges führte zur Entdeckung von drei Inhibitoren mit neuen Zielproteinen innerhalb der Signalkaskade. Die Ermittlung von Proteinen mit Beteiligung am Hh-Signalweg gibt Aufschluss über die Komplexität des Signalweges.

Ein Osteoblasten-Differenzierungstestsystem, mit dessen Hilfe die Hh-Signalaktivität analysiert wurde, führte zur Identifizierung von YCL-220 als Inhibitor der Hh-Signalkaskade. Orthogonale Experimente wiesen die Verbindung als potenten Inhibitor der GLI-vermittelten Signalaktivität aus. Mechanistische Untersuchungen zeigten, dass YCL-220 als SMO-Antagonist wirkt und analog zu Vismodegib den Transport von SMO in die Zilien verhindert. Die Bindung an SMO konnte durch Auswaschen aufgehoben werden, was auf einen reversiblen, nicht-kovalenten Bindungsmechanismus hindeutet. Mutationen in SMO erfordern neue Strategien zur Regulierung der Proteinfunktion, weshalb die reversible Inhibition durch YCL-220 zukünftig detaillierter untersucht werden sollte.

Des Weiteren wurde das Pyrrolidin RKN-1043 als Inhibitor des Hh-Signalweges identifiziert, der unterhalb von SMO wirkt. Durch Affinitätschromatographie und Proteomik zur Zielproteinidentifizierung wurde RHOGDI1 als potentielles Zielprotein ermittelt. Biophysikalische Experimente zeigten eine Inhibition der RHOGDI1-vermittelten Extraktion von prenyliertem RAC1-GDP aus Liposomen. RKN-1043 konkurriert als erstes entdecktes Molekül mit dem GerGer-RAB1-Peptid um die Bindung an die GerGer-Bindetasche in RHOGDI1 und inhibiert dadurch dessen Funktion. Genetische Veränderungen wiesen RHOGDI1 als negativen Regulator des Hh-Signalweges nach.

Abschließend konnte RKN-1043 als neuer Inhibitor des Hh-Signalweges und von RHOGDI1 identifiziert werden. Weiterführende Analysen des Effektes von RKN-1043 auf den Aktivierungszustand von RHO-GTPasen können genauere Informationen zum Wirkungsmechanismus der Substanz liefern.

Die dritte Verbindung MJD-1314 wurde mittels diversitätsorientierter Synthese durch eine Metathesenkaskade erhalten, die zur Herstellung von Substraten für inter- und

intramolekulare Diels-Alder-Reaktionen durchgeführt wurde. Die Substanz wurde als potenter Inhibitor der Osteogenese und GLI-vermittelten Hh-Signalkaskade erhalten, der unterhalb von SMO wirkt. Mittels chemischer Proteomik wurde MTAP als potenzielles Zielprotein identifiziert und eine thermische Stabilisierung des Proteins infolge der Substanzbindung bestätigt. Trotz der Bindung an MTAP konnte jedoch kein Effekt der Substanz auf die enzymatische Aktivität des Proteins aufgezeigt werden. Ebenso war keine Inhibierung des Hh-Signalweges durch den MTAP-Inhibitor MTDIA nachweisbar. Diese Ergebnisse wiesen auf eine mögliche nicht-kanonische Funktion von MTAP hin. Genetische Veränderungen von MTAP ergaben widersprüchliche Wirkungen des Proteins auf den Hh-Signalweg. Des Weiteren wurde keine Änderung der intrazellulären Lokalisierung infolge der Bindung des Inhibitors ermittelt. Ansätze zur Identifizierung neuer Interaktionspartner von MTAP, die eine Verbindung zum Hh-Signalweg aufzeigen könnten, waren nicht erfolgreich.

Zur Untersuchung des Einflusses von MJD-1314 auf die intrazelluläre Funktion von MTAP wird die metabolische Aktivität der Zellen nach Substanzbehandlung untersucht werden. Weiterhin kann eine Genexpressionsprofilierung eine globale Darstellung des Effektes auf den physiologischen Zustand der Zellen ermöglichen, was detaillierte Informationen zum Wirkungsmechanismus von MJD-1314 liefern kann.

Die hier präsentierte Arbeit führte zur Identifizierung neuer Inhibitoren des Hh-Signalweges und bislang unentdeckter Bestandteile der Signalkaskade. Diese Studie verdeutlicht die Wichtigkeit einer Kombination verschiedener Methoden zur Identifizierung und Validierung von Zielproteinen niedermolekularer Substanzen, um deren Wirkungsmechanismen aufzeigen zu können.

3 Introduction

The advent of whole genome sequencing in the beginning of 21st century has led to overwhelming high throughput information on genes expressed in an organism. The study of genes and genetic variation i.e. genetics, has been used widely to study biology by manipulating the biological system at the level of the genes. This manipulation is achieved by knocking out the gene of interest, which prevents the expression of the corresponding proteins. Additionally, an increased number of gene copies or use of hyper active promoter results in an increased protein expression. Moreover, protein function can be altered by introducing missense mutation in the corresponding gene.¹ Using these genetic perturbations, basic biological processes such as cell cycle in the yeast *Saccharomyces cerevisiae*,² programmed cell death in the nematode *Caenorhabditis elegans*,³ as well as early embryonic development in the *Drosophila melanogaster* have been elucidated.⁴

A classical genetics approach also termed as forward genetics, involves unbiased gene perturbation giving rise to a phenotype of interest followed by identification of the gene responsible for the phenotype. Recent advances in genome editing techniques have given rise to a reverse genetics approach to deconvolve gene function. Reverse genetics involves perturbation of a specific gene of interest followed by close examination of resulting phenotypes.

3.1 Chemical Genetics

The use of chemical compounds in the form of plant extracts for treatment of many diverse ailments has been a part of human history. Advances in scientific understanding of the importance of chemical compounds have led to the introduction of antibiotics in the form of pure small-molecule treatment in the twentieth century. Recently, the use of small molecules as therapeutics has increased significantly with an impact on the understanding of all areas of life sciences. This chemical intervention to understand biological systems is termed “chemical genetics”.⁵

Contrary to the routinely used genetic approaches, chemical genetics employs small molecules to modulate biomolecule (nucleic acid, lipid and protein) function in order to

understand biology.⁶ Chemical genetics is divided into forward chemical genetics and reverse chemical genetics (see Figure 1). A forward chemical genetics approach involves screening of small molecule libraries in unbiased phenotypic assays.⁶ “Hit” compounds which affect a given cellular phenotype are then selected for further characterization and the biomolecules that are modulated are identified using various approaches discussed in the following sections. In reverse chemical genetics, small molecules are tested for their ability to directly modulate a biomolecule of interest. The small molecules that bind to the biomolecule of interest are selected and tested in phenotypic assays relevant to the biomolecule of interest. Hit compounds selected from forward and reverse chemical genetics approaches are then subjected to in-depth biological evaluation. The reverse chemical genetics approach is further extended to a genome-wide scale under the newly emerging field termed chemical genomics. Chemical genomics describes the search for small-molecule modulators for functions of all the gene products.⁷

Forward and reverse chemical genetics approaches are widely used to identify small-molecule modulators. However, these approaches have their own advantages and disadvantages. The forward chemical genetics approach relies on phenotypic assays and thus does not require prior information about a potential target. Therefore, there is a possibility to identify multiple or new targets regulating the phenotype studied. Limitation of this approach is the requirement of large libraries of diverse small molecules. Also, optimization of an initial hit compound which is cell permeable and metabolically stable can be challenging and time-consuming. Contrary to forward chemical genetics, reverse chemical genetics requires prior knowledge of the function of the target. In-depth knowledge of the natural ligand (if present) and binding pocket in the case of proteins facilitates the optimization of a newly identified small molecule modulator. However, the dynamic nature of the protein can complicate the design of small molecule modulator. The reverse chemical genetics approach to identify small molecule modulators is only limited to biomolecules under experimental study, as such new targets cannot be discovered by this approach.

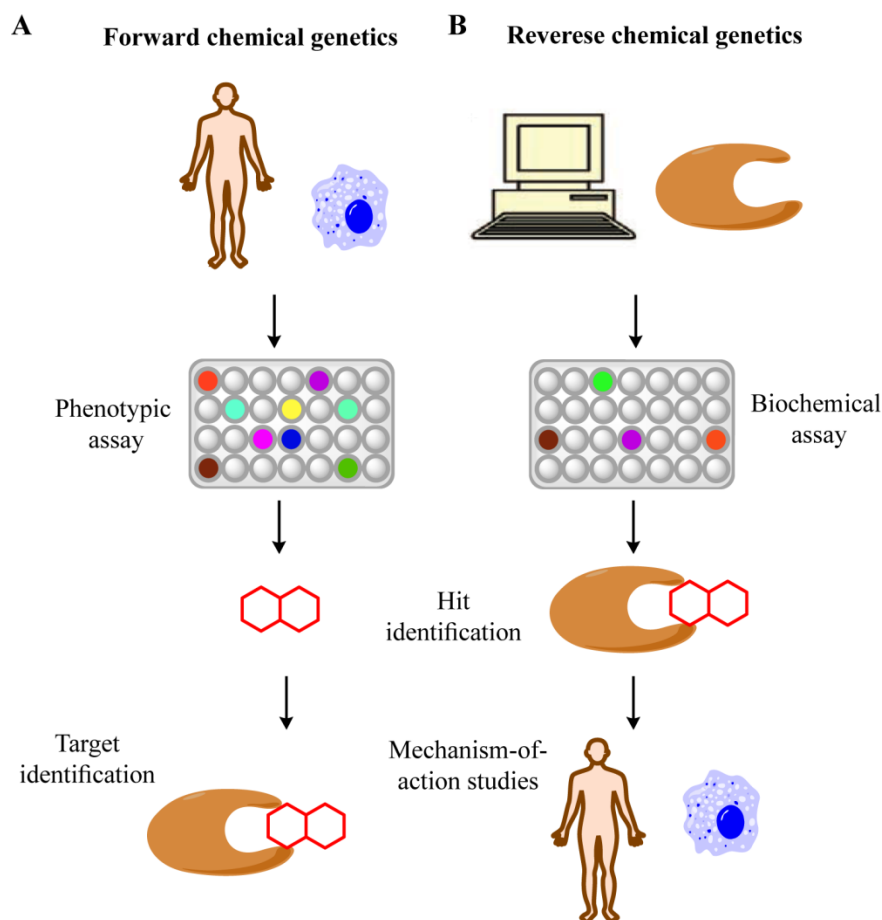


Figure 1. Mechanism-of-action and target identification in chemical genetics.

(A) In forward chemical genetics, phenotypic assays are employed to identify small molecule modulators. Mechanism of action and target identification is undertaken to establish the biomolecule responsible for the phenotype. (B) In reverse chemical genetics small molecules are screened in a biochemical assay to identify modulators of a biomolecule under study. Exploration of the mechanism of action and possible side effects of the small-molecule modulator are undertaken. (Modified from Monica Schenone et al., 2013)⁶

3.1.1 Phenotypic Screening

Phenotypic screens are the starting point of forward chemical genetics. They offer the possibility of identifying small-molecule modulators of targets that have not yet been linked to the studied phenotype. Moreover, as they are active in cellular assays, these identified small molecule modulators are cell permeable and metabolically stable.⁶

The choice of physiologically-relevant phenotypic assay is critical in forward chemical genetics. Commonly used readout modalities are based on the physiological properties of the cell.⁸ In order to measure the transcriptional activity of the cell, reporter gene assays are the preferred readout. A reporter gene is a gene that is attached to the regulatory

sequence of gene of interest. Expression of this reporter gene along with gene of interest, renders measurable characteristic such as fluorescence and luminescence.⁹ The activity of phenotype-relevant promoter can also be measured by placing the reporter gene under the control of promoter. The reporter gene products are mostly fluorescent proteins (e.g. Green fluorescent protein, GFP) or enzymes (e.g. Firefly luciferase) that hydrolyze substrate thereby generating light (i.e. luminescence) to obtain quantifiable signal. Reporter gene assays are developed to identify modulators of signaling pathways such as Hedgehog (Hh), Wnt and Notch by introducing the reporter gene under the control of pathway-specific transcription factors.¹⁰

Cell viability assays are considered to identify cytotoxic compounds. Cell viability is measured by monitoring metabolic activity, membrane leakage or by visible cell growth.¹¹ Metabolic activity of the cell is measured by using formazan-based dyes (e.g. MTT, XTT and WST) or by measuring the metabolite levels of ATP by using CellTiter-Glo[®] assay. Cell viability is also measured by monitoring cell growth under the microscope. Advanced imaging instruments such as IncuCyte[™] developed by Essen Biosciences measure cell confluency as a measure of cell growth.

Sophisticated robotic systems are used to screen large compound libraries in disease-relevant phenotypic assays. Hit compounds identified from these phenotypic screens are taken up for target identification process.

3.1.2 Approaches to target identification

In the forward chemical genetics approach, which includes phenotypic screening, the identification of the target(s) of small molecule modulators is the most important and challenging step. Target identification serves the purpose of establishing the mechanism of action of a small-molecule modulator. In order to identify the target(s) of small molecules, several strategies have been developed. Within the scope of this thesis, target identification strategies to identify protein targets are discussed. These strategies can broadly be divided into affinity-based methods, genetic methods and computational methods. The affinity-based method takes advantage of the direct interactions of a target protein and small molecule. For target identification, genetic methods rely on the alteration of the quantity of a target under investigation in order to change the activity of a small molecule in the phenotypic assay. Contrary to these experimental approaches,

computational methods are used to generate target hypothesis by comparing the structural similarity of the hit molecule with established ligand-target pairs.

3.1.2.1 Affinity chromatography-based methods

The most widely used method to identify target proteins is based on the direct affinity between a target protein and the small molecule (see Figure 2 A). The chemically modified active and inactive analogs of a hit compound are functionalized with a linker to synthesize affinity probes. The affinity probes are immobilized on a stationary phase and cell lysates are passed over the stationary phase in order to capture the proteins having an affinity towards the small molecule derived probe. The capture of the proteins is followed by stringent washing to remove nonspecifically bound proteins. Appropriate elution steps are used to release the bound proteins followed by mass spectrometry analysis to identify potential binders. Statistical analysis is performed to identify the proteins that are selectively enriched in active affinity probe.¹²

Stable isotope labeling by amino acids in cell culture (SILAC) is used in affinity chromatography in order to facilitate quantification of the identified proteins (see Figure 2 B).¹³ In this method, cell lysates are prepared from cells that are grown in “heavy” or “light” medium, that are supplemented with $^{13}\text{C}_6, ^{15}\text{N}_2$ L-lysine and $^{13}\text{C}_6, ^{15}\text{N}_4$ - L-arginine, and with $^{12}\text{C}_6, ^{15}\text{N}_2$ L-lysine and $^{12}\text{C}_6, ^{14}\text{N}_4$ - L-arginine, respectively.¹⁴ Complete incorporation of the labeled amino acids into the proteome is achieved by growing the cells in heavy or light medium for at least five cell divisions. The heavy and light cell lysate is passed over both of the immobilized active and inactive probes. After stringent washing and elution, the heavy proteins bound to the active probe are mixed with light proteins bound to the inactive probe. Similarly, heavy proteins bound to the inactive probe are mixed with light proteins bound to active probe followed by mass spectrometry analysis. The mixing allows less stringent washing steps and comparative quantification of the enriched proteins, therefore increases confidence in identification of the weakly bound proteins. SILAC has been used successfully to identify tubulin and exportin-2 as target proteins for tetrahydropyran-containing compound Tubulexin. It was experimentally shown that the compounds bind to the vinca alkaloid binding site of tubulin.¹⁵ BCR-ABL was confirmed as a target for Imatinib-a drug marketed by Novartis pharmaceutical for the treatment of acute myeloid leukemia.¹⁶ The SILAC approach can

also be extended to the whole organism such as mouse,¹⁷ *C. elegans* and *D. melanogaster*.¹⁸ Stable incorporation of labeled amino acids is critical and long term cultivation of cells in heavy medium is necessary. Therefore, cells such as blood platelets cannot be used for SILAC techniques as they can only be cultivated for a short time.¹²

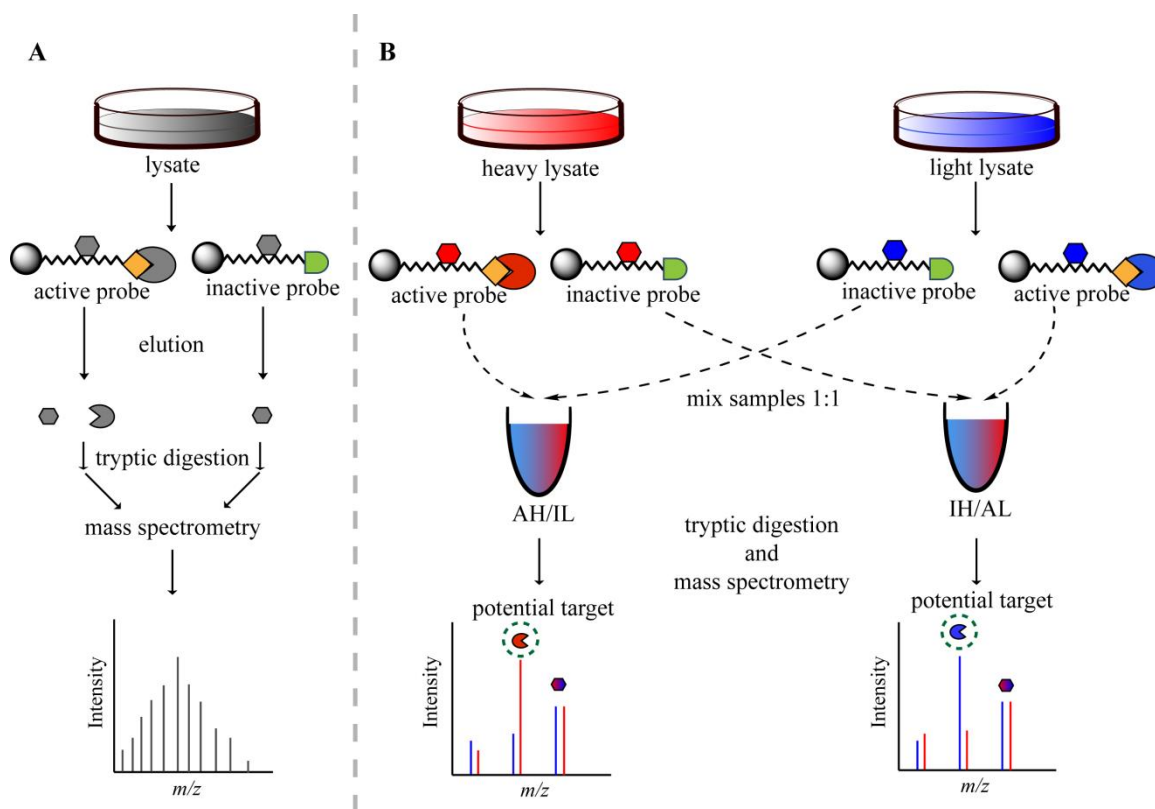


Figure 2. Affinity chromatography based methods for target protein identification.

(A) Label-free affinity chromatography. For protein binding, cell lysate is passed over active and inactive analogs of small molecule-affinity-probe immobilized on solid support. The probes are then washed and bound proteins are finally eluted. The eluted proteins are tryptically digested and analyzed by mass spectrometry. (B) Quantitative affinity chromatography with SILAC. Cells are grown in “light” and “heavy” isotope-labeled amino acids supplemented growth medium in order to incorporate isotope-labeled amino acids in the proteome of the cells. The resultant “heavy” and “light” lysates are passed over active and inactive analogs of the small molecule-affinity-probe immobilized on solid support. The probes are washed and the heavy proteins bound to active probe (AH) are mixed with light proteins bound to inactive probe (IL). Similarly, heavy proteins bound to inactive probe (IH) are mixed with light proteins bound to active probe (AL) followed by mass spectrometry analysis. By quantifying the ratios of “light” and “heavy” peptides between AH and IL as well as IH and AL signals, a potential target protein is identified.

The success of affinity chromatography is dependent on several factors including the lysis buffer, the affinity of the small molecule towards the target protein and the expression level of the protein in the employed cell line.¹⁹ The affinity of the small molecule towards its target protein, which is critical for this method, can be greatly affected by the chemical modification required for preparation of affinity linker attachment (Figure 3 A). Therefore, in depth understanding of the structure-activity-relationship (SAR) is

necessary in order to retain the affinity while attaching the small molecule to an affinity linker. In some cases, addition of the affinity linkers on to the small molecule causes a significant drop in the bioactivity of the small molecule and thus its affinity towards target protein.²⁰ To overcome this problem, small alkyne or azide groups are used to functionalize the small molecule (see Figure 3 B). In order to retain the sensitivity of the small molecule towards target, the small molecule is first added to the cell lysate and using “click-chemistry”, linker tag is added on to this functionalized small molecule.²¹ Additionally, small photoreactive groups such as benzophenone, diazirine, or arylazide are used to stabilize weak protein-small molecule interactions by inducing covalent cross linking (see Figure 4 C).²² The functionalization of hit molecules by photoaffinity tags further enhances the sensitivity of the target identification process by allowing to identify weakly bound targets. One such example is of Imatinib, BCR-ABL oncogenic receptor kinase is an established target of Imatinib. However, using photoreactive aryl azide modification, g-secretase activating protein (gSAP) was found to be the additional target of Imatinib.²³

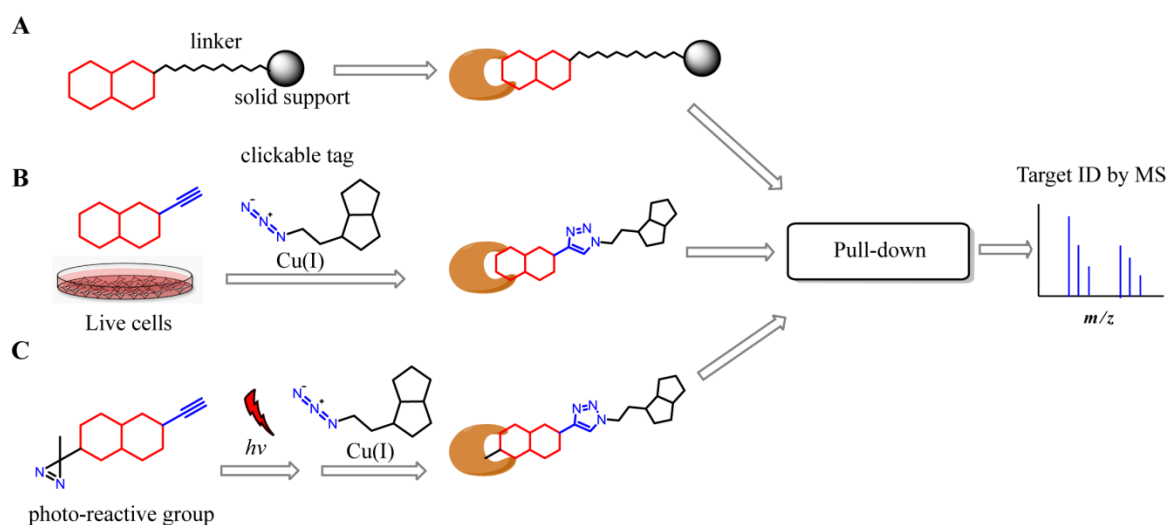


Figure 3. Chemical modification of active hit for affinity-chromatography.

(A) The active-affinity-probe is directly immobilized on solid support. Proteins bound to the probe are analyzed by mass spectrometry. (B) The small molecule is modified with a ‘clickable’ group and incubated with live cells. A tag is added on to this functionalized small molecule *via* a linker upon incubating with cell lysate for protein binding followed by mass spectrometry. (C) A small molecule is equipped with a photo-reactive group (e.g. diazirine) to induce covalent cross-link between the small molecule and the target protein(s). (Modified from Jiyoun Lee et al., 2013)²⁰

Despite these advances in the affinity chromatography-based target identification techniques, for some compound classes even small changes in their structure can cause a significant reduction in bioactivity. Moreover, for some compounds target protein or

additional off-targets cannot be identified as a result of reduced bioactivity. Therefore, label-free approaches are of increasing importance as chemical modification of the hit compound is not necessary.

3.1.2.2 Label-free techniques

Label-free target ID approaches do not require chemical modification of the small molecule. Therefore the time duration and complexity of the target identification process is significantly reduced.²⁰ These methods take advantage of the change in the thermodynamic properties of target protein upon binding to a small molecule. The cellular thermal shift assay (CETSA) relies on the change in the thermal stability of the target protein upon binding to small molecule ligand (see Figure 4 A).²⁴ The small molecule may change the thermodynamic properties of the target protein(s) leading to thermal stabilization or destabilization. The small molecule is incubated with cellular extracts or live cells to allow binding to the target proteins. These extracts are then aliquoted and heated to different temperatures to induce protein melting at higher temperatures. Upon ultra-centrifugation, only the soluble fractions collected from these aliquots are analyzed by western blotting to detect the change in the melting behavior of the target protein. Thus, allowing the target validation for small molecule. Alternatively, for widening the applicability of CETSA, the soluble fraction are labeled with tandem mass tags (TMT) to analyze the proteome-wide melting behavior by mass spectrometry. As a proof of concept, PD0332991 was used, which showed specificity towards CDK4/6 by stabilizing the kinase at higher temperatures.²⁵ Another label-free approach is drug affinity responsive target stability (DARTS), which relies on changes in the sensitivity of proteins toward proteolytic enzymes upon binding with small molecule ligand (see Figure 4 B). Cell lysates are treated with a ligand or vehicle followed by limited digestion by using proteases.²⁶ The samples are then analyzed by gel electrophoresis or mass spectrometry to detect the disappearance of a protein from small molecule treated fraction as compared to vehicle treated sample. DARTS has been successfully used to identify molecular targets of rapamycin, FK506, didemnin B, and resveratrol.²⁷ Similar to DARTS, stability of proteins from rates of oxidation (SPROX) depends on sensitivity of the protein-small molecule complex towards oxidative conditions (See Figure 4 C).²⁸ An oxidizing agent (H₂O₂) and a chemical denaturant are used to induce oxidation of the methionine residues in target proteins. The reaction is quenched and the oxidized and

non-oxidized proteins are identified following quantification by mass spectrometry. The small molecule-bound proteins are more resistant to the denaturant and therefore show larger shift in the rate of oxidation at higher denaturant concentration. As a proof of concept, cyclophilin A and UDP-glucose-4-epimerase were identified as targets for the immunosuppressive drug cyclosporine A.²⁹

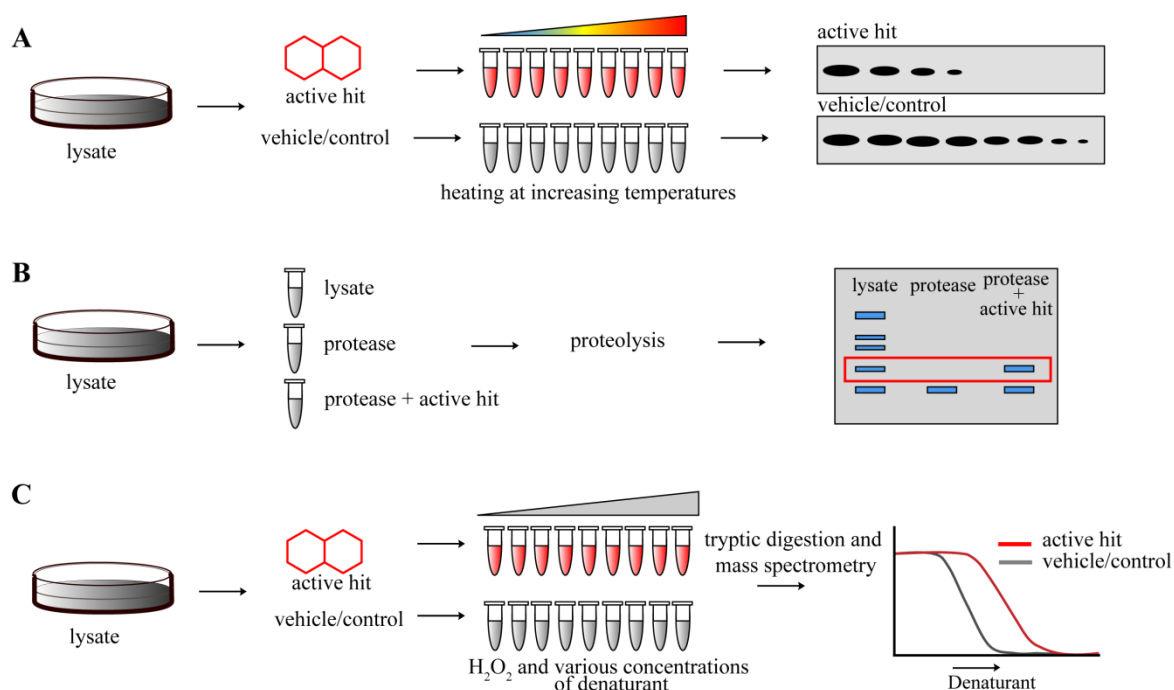


Figure 4. Label-free techniques for target identification.

(A) Cellular thermal shift assay (CETSA). Cell lysates are incubated with a small hit molecule or control (e.g. DMSO) and aliquoted. The aliquots are heated at a range of temperatures in order to denature the proteins. The soluble protein fractions are analyzed by immunoblotting using an antibody against the protein of interest. (B) Drug affinity responsive target stability (DARTS) relies on the increased stability of the target protein-small molecule complex against proteolytic cleavage. Lysate is incubated with small hit molecule followed by exposure to a protease. Proteins that are more resistant to proteolysis are analyzed by SDS-PAGE. (C) Stability of proteins from rates of oxidation technique is based on the sensitivity of protein-small molecule interaction under oxidative conditions in various concentrations of chemical denaturant. Lysates are incubated with active hit small molecule and control and are exposed to H₂O₂ and various concentrations of chemical denaturant. Small molecule bound proteins are more resistant towards chemical denaturant. Therefore proteins that show denaturant-concentration dependent denaturation are identified by mass spectrometry. (Modified from Kapoor et al 2016 and Jiyoun Lee et al., 2013)^{20,30}

As described in the previous section, advances in affinity-based approaches have led to deconvolution of target proteins for many small molecules. The label free approaches significantly improve the versatility of the affinity based target identification process, as they do not require exploration of SAR and preparation of affinity probes. However, the identification weak binding or membrane protein target for small molecule remains challenging.

3.1.2.3 Genetic methods

The completion of the human genome sequencing has revolutionized biomedical research. The knowledge of genes and their effects on the biological system has given a new perspective to the target identification process. The function of genes and proteins has been determined by employing genomics tools such as analysis of gene expression profile, resistance-conferring mutations and RNAi libraries. Gene expression profiling generates a global picture of the effect of small molecule treatment on all the genes expressed in a cell/tissue or animal (see Figure 5 A). Generally, gene expression profiling is a choice for generating hypothesis for future research. Sometimes the data generated is too complex and therefore can give rise to several interpretations. Therefore gene expression profiling is always used in combination with other chemical biology tools to establish a mode of action for a small molecule modulator. Gene expression analysis of wide range of cancer lines upon treatment with 6-(4-(diethylamino)-3-nitrophenyl)-5-methyl-4,5-dihydropyridazin-3(2H)-one (DNMDP) led to the identification of phosphodiesterase 3A (PDE3A) as a target. CRISPR/Cas9-mediated knockout of the PDE3A rescued the DNMDP mediated cytotoxicity, therefore validating PDE3A as a molecular target of DNMDP.³¹

Genetic approach to identify and establish the functionality of a target is based on comparing the phenotypic outcome as a result of the small molecule and interfering RNA (RNAi) treatment to deplete the target (See Figure 5 B).^{32,33} Similarity in both phenotypes is then used to generate a target hypothesis. It is expected that the knockdown should result in a phenocopy of the small molecule inhibitor. The use of RNAi in combination with small molecule inhibition should result in a more potent induction of the phenotype depending on the nature of the target gene. Genome-wide RNAi experiments are performed to search for genes that have a similar effect when knocked down as the small-molecule inhibitors.³⁴ RNAi is also used in more focused experiments when the probable target for the small molecule modulator is known.

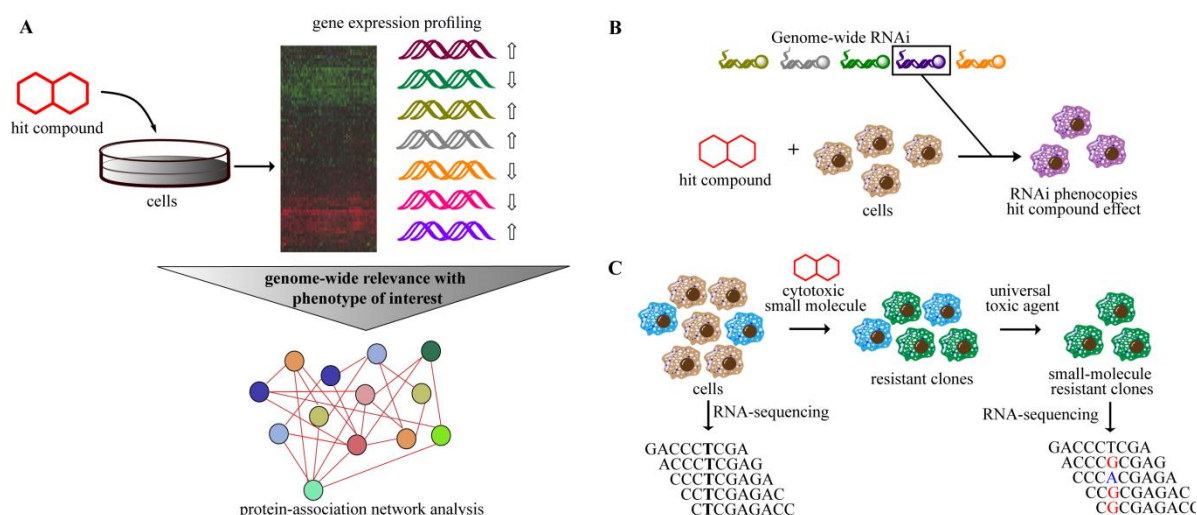


Figure 5. Genetic methods for target identification.

(A) To identify the target and establish a mechanism of action of a hit compound, gene expression profiling is performed to characterize changes in the gene expression level as a result of compound treatment. Bioinformatics tools are utilized to establish the relevance of gene expression profile with the phenotype under study. (B) Phenotypes as a result of small molecule treatment are compared with phenotypes from genome-wide RNAi studies. Similarities in the phenotype provide a hint that the depleted gene product is a possible target of the small molecule. (C) Exposure of cells to a cytotoxic small molecule leads to the development of compound-resistant clones. Clones that are resistant to multiple compounds are excluded by treating the cells with a universal toxic agent. The remaining resistant clones are analyzed by transcriptome sequencing to compare parental and resistant clones to identify mutated genes. (Modified from Kapoor et al., 2016 and Schenone et al., 2013)^{6,30}

Another approach to identify the target protein is to identify resistance-conferring mutations upon exposure to toxic small molecules (See Figure 5 C).³⁵ Cells grown in sublethal concentrations of the toxic small molecule can develop resistance to the toxic small molecule. These surviving cells are then analyzed by transcriptome sequencing to detect the genes that are mutated in the resistant cells. PLK1 was identified as the target of the small molecule BI2536 by analyzing BI2536-resistant clones of HCT116 cells that carried a mutation in the BI2536 binding site in PLK1.^{36,37} However the approach is currently only limited to molecules that are cytotoxic to the cells.³⁰

3.1.2.4 Computational approaches

Advances in computational techniques have opened up a new dimension in target identification research. *In silico* predictions of the molecular targets of small molecules are based on ligand and network-based computational approaches.

The Similarity Ensemble Approach (SEA) clusters proteins by employing 2D structural similarity of their bound ligands to predict small molecule targets. All ligands are ranked according to the ratio of the number of features common to both molecules to the total number of features (Tanimoto coefficient). SEA can be used for predicting the off-target activities of small molecules. One such example is Fabahistin, for which the serotonin receptor 5-HT_{5A} was predicted as a target. Fabahistin proved to have a K_i of 130 nM for 5-HT_{5A}, which was better than the K_i for its canonical target, the histamine H1 receptor. Moreover, the predicted target 5-HT_{5A} was experimentally validated to be potently modulated by fabahistin.³⁸

Self-organizing map-based prediction of drug equivalence relationship (SPiDER) is a self-organizing-maps (SOM)-based technique developed by Schneider et al., to predict the molecular targets of a small molecule modulator. SPiDER uses pharmacophoric similarity of well-established drugs with small molecules under study to predict the molecular targets. The similarity is based on the topological features, scaffold connectivity, and target interaction potential of small molecule under study, but is independent of molecular weight.³⁹ Using this tool, target prediction was performed for molecules synthesized by using amprenavir, a HIV1 protease inhibitor, as a template. Surprisingly, in addition to the HIV1 protease, bradykinin receptor B1 was predicted as a target with a significant score. Moreover, the small molecules showed higher experimental affinities towards bradykinin receptor B1 than for HIV1 protease.

Although there is no generic method for identification and validation of small-molecule targets, combination of these complementary methods as described in Figure 6 are used to establish the mechanism of action of small molecule modulators.

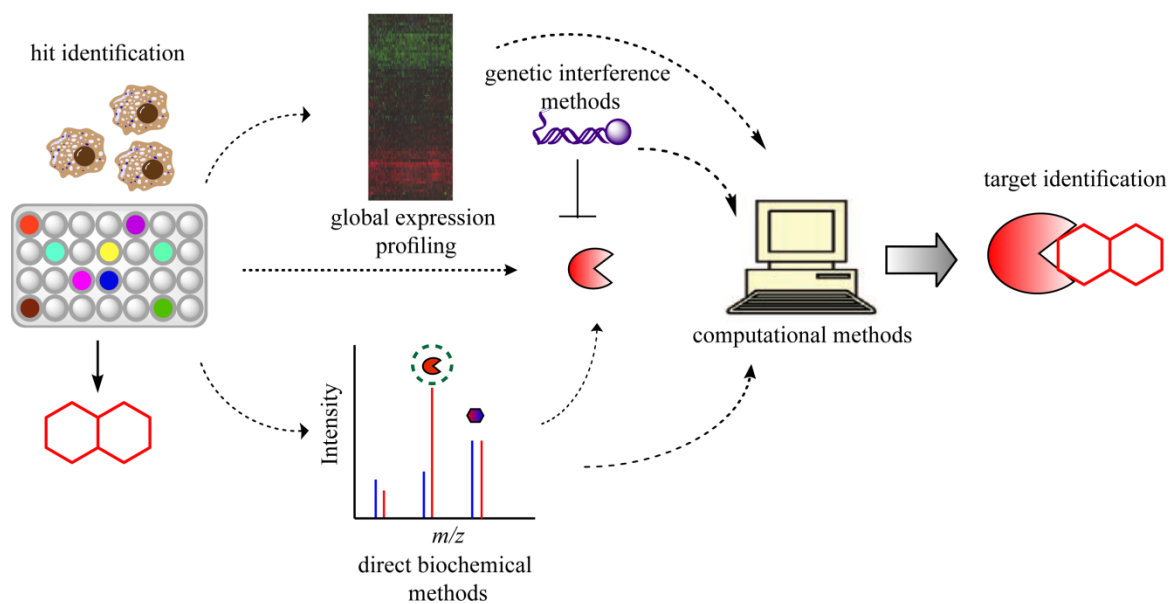


Figure 6. General approaches to target identification.

In order to identify the target of a small molecule, combination of direct biochemical methods, genetic techniques and/or computational approaches are employed. The relationship between data from multiple platforms might lead to successful deconvolution of the target protein. (Modified from Schenone et al., 2013)⁶

3.2 The Hedgehog signaling pathway

The Hedgehog gene (Hh) was identified by C. Nüsslein-Volhard and E. F. Wieschaus while studying genetic mutations in *Drosophila melanogaster*.⁴ They identified 50 genes that had an effect on the embryonic development of the larvae. One such gene when mutated gave rise to spine-like features on the dorsal side of the larvae with similarity in appearance to a hedgehog. Therefore, the gene responsible for this phenotype was termed Hedgehog. In 1993 three paralogues were identified and named as Sonic Hh (Shh), Indian Hh (Ihh) and Desert Hh (Dhh).⁴⁰⁻⁴³ The Hh genes are highly conserved across vertebrates and they govern various processes such as proliferation, differentiation tissue patterning, and tissue repair.⁴⁴ However, anomalies in Hh signaling are linked to various types of cancers, basal cell carcinoma (BCC) and medulloblastoma being the most prominent. Cancers of the pancreas, prostate, lung, and breast are also linked to aberrations in Hh signaling.⁴⁵ Therefore, modulators of the Hh signaling pathway may have therapeutic potential. Stimulators of the Hh pathway may have applications in the induction of angiogenesis and promotion of wound healing. Inhibitors of Hh signaling have applications in the treatment of cancers and other type of Hh pathway-related developmental anomalies.⁴⁶

3.2.1 Maturation of Hh proteins

Posttranslational modification of the Hh protein is a prerequisite to release the active form of Hh from cells to activate Hh signaling.⁴⁷ A ~45 kDa precursor signal sequence is removed from the N-terminus of Hh followed by autocatalytic cleavage between GlyCys residues, that is part of the highly conserved GlyCysPhe tripeptide (Figure 7). This N-terminal signaling domain is further modified by addition of cholesterol at the C-terminal glycine to generate the ~19 kDa signaling domain. Cholesterol itself is not necessary for the activity of the signaling domain but is important for anchorage as well as transport of Hh ligand within the cells. It has been shown that other sterol modifications can substitute for the cholesterol modification.⁴⁵ In the final step, fully functional Hh protein is formed after palmitoylation of the N-terminal cysteine by the enzyme Hedgehog acyl transferase (Hhat). A highly conserved CysGlyProGlyArg-sequence is necessary for palmitoylation to occur. The general hydrophobic effect rendered by palmitoylation contributes to the potency of Hh protein to activate Hh signaling.⁴⁷

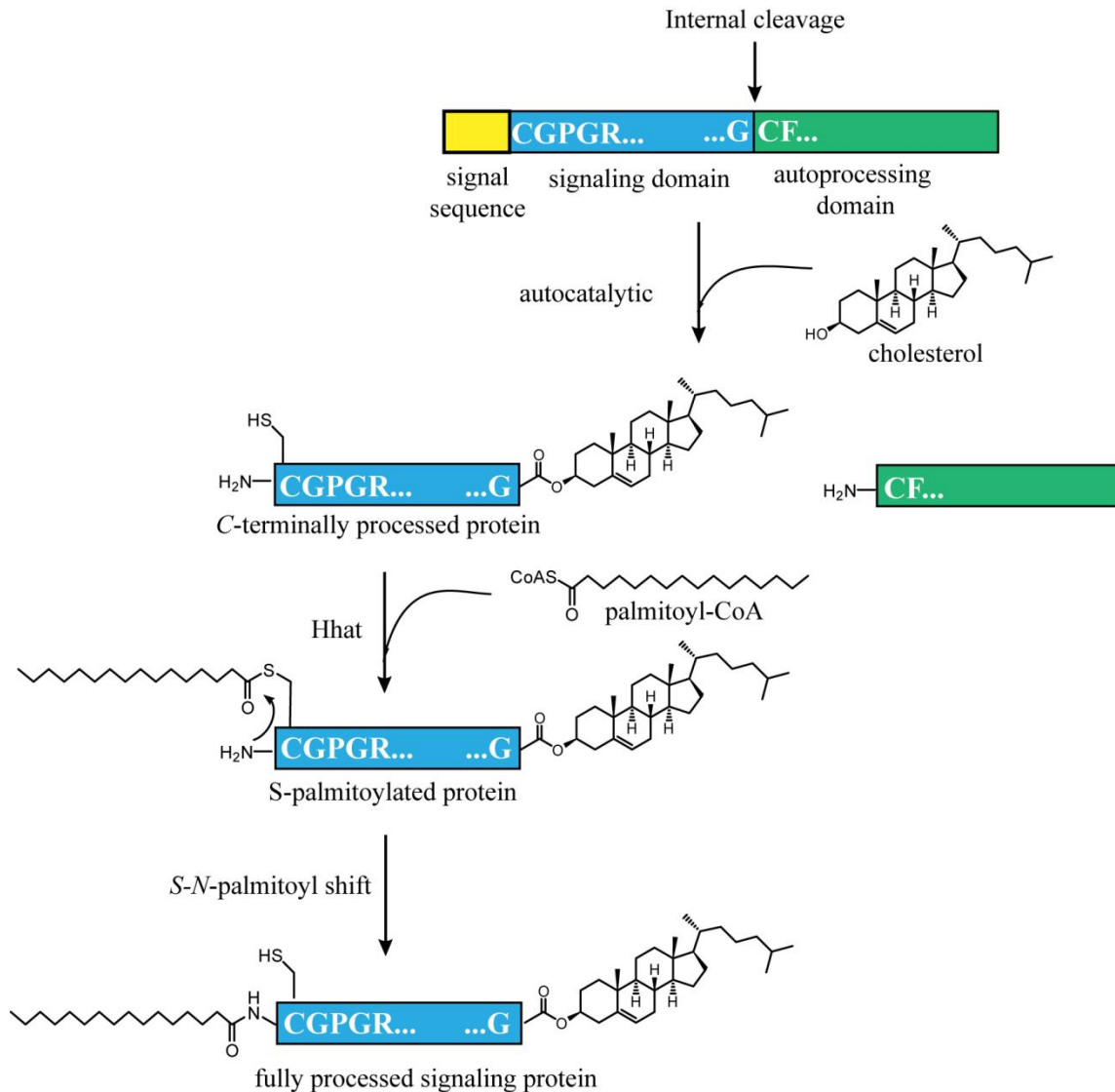


Figure 7. Posttranslational modification of Hh protein.

A ~45 kDa polypeptide encoded by Hh genes undergoes internal proteolysis and N-terminal signaling sequence cleavage followed by acylation. As a result a ~19 kDa segment is produced by endoproteolytic cleavage at the GlyCysPhe sequence. The signaling domain is decorated by cholesterol at the C-terminal Gly. Hhat adds a palmitoyl moiety at the N-Terminal Cys followed by a spontaneous rearrangement (*S-N*-acyl shift) to generate mature Hh ligand capable of activating the Hh signaling cascade upon binding to PTC1. (Modified from Heretsch et al., 2010)⁴⁸

3.2.2 The Hh signaling cascade in vertebrates

Hh signaling starts by binding of the Hh ligand to its receptor Patched1 (PTC1). PTC1 inactivation relieves repression of the seven transmembrane receptor Smoothed (SMO), initiating the signaling cascade (see Figure 8). This results in the activation of glioma-associated oncogene (GLI) transcription factors and the expression of Hh target genes. The transcription factor GLI has three homologs: GLI1, GLI2 and GLI3.⁴⁹ GLI1 is a

transcriptional activator, GLI2 is a major pathway activator and GLI3 functions as a repressor (GLIR). The Suppressor of Fused (SUFU) is a Hh pathway inhibitor that inhibits Hh signaling by maintaining GLI in an inactive state. In vertebrates, Hh signaling occurs at the primary cilium.⁵⁰ The intraflagellar transport (IFT) protein, kinesin II (KIF3 family) and dynein-2 (DYNC2) motors regulate the constant shuttling of Hh pathway components between the cilia and the cytoplasm.⁵¹ Transport and accumulation of Hh pathway-related proteins into the cilium is necessary but not sufficient for Hh pathway activity. Therefore, mutations in the ciliary transport genes lead to aberrations in Hh signaling.⁵²

In vertebrates, Hh signaling exists in an on or off state depending on the presence or absence of fully matured Hh ligand. In the absence of Hh ligand, PTC1 and the recently discovered G protein-coupled receptor (GPCR) GPR161 are present in the cilia. SMO is maintained in the inactive state by PTC1, while GPR161 activates protein kinase A (PKA).⁵³ Upon activation, PKA together with Casein kinase 1 (CK1) and glycogen synthase kinase 3 β (GSK3 β) phosphorylates the GLI transcription factors which undergo proteolytic processing into C-terminally GLI repressor (GLIR) form. Transport of GLIR to the nucleus results in repression of Hh target genes, thus maintaining Hh signaling in the inactive state.^{54,55} Upon binding of mature Hh ligand to PTCH1, PTCH1 and GPR161 are internalized and PTC1 undergoes lysosomal degradation. In the absence of PTCH1 and GPR161 in the primary cilium, SMO repression is relieved. In the absence of active PKA, SMO is phosphorylated by CK1 and G protein-coupled receptor kinase (GRK2).⁵⁶ The phosphorylated SMO is transported into the cilium by the kinesin KIF3A and anchored near the base of the cilium by Ellis-van Creveld syndrome proteins EVC1/EVC2.⁵⁷ The active state of SMO inhibits GLI phosphorylation and thus full-length GLI2/3 (GLI FL) in complex with SUFU accumulates at the tip of cilia where they dissociate and exit the cilium.⁵⁸ The GLI FL are transported to the nucleus, where they activate Hh target genes such as *GLI1*, *PTCH1*, and *HIP*. The transport of GLI FL to the nucleus is important for maintaining the GLI FL and GLIR ratio to regulate Hh signaling.⁵⁹ Hedgehog interacting protein (HHIP) is another negative regulator of Hh signaling that binds to PTC1 with similar affinity as the Hh ligand.⁶⁰ The expression level of Hh activator or repressor genes regulates Hh signaling by feedback mechanisms.⁶¹ Hh ligands can also trigger non-canonical pathways *via* SMO that are independent of GLI transcription factors.⁶²

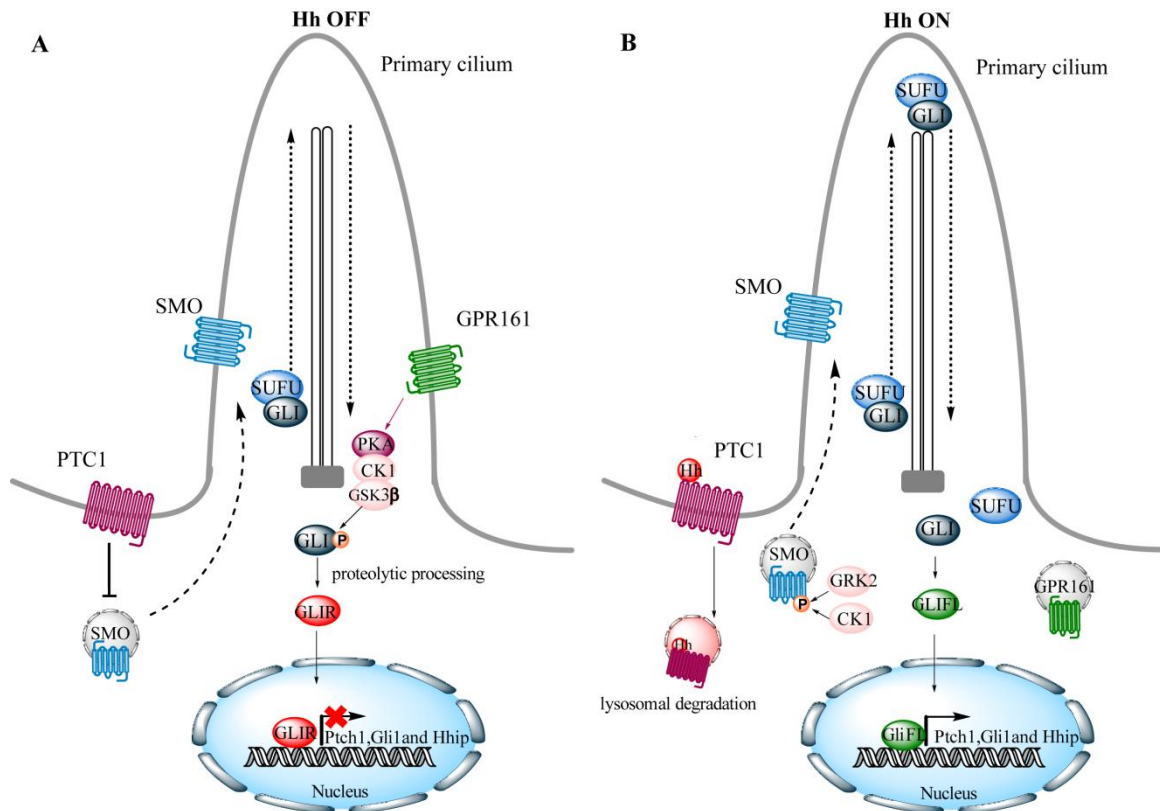


Figure 8. The Hh signaling pathway in vertebrates.

(A) In the absence of Hh ligand, PTC1 inhibits ciliary transport of SMO. GLI2 and GLI3 are maintained in the inactive form by SUFU. GPR161 present in the cilium activates protein kinase A (PKA), which, together with Casein kinase 1 (CK1) and glycogen synthase kinase 3 β (GSK3 β) phosphorylates GLI2 and GLI3 at the base of the cilium. The phosphorylated GLI2 and GLI3 are processed to GLI repressor (GLIR) form by the proteasome. (B) When Hh ligand binds to PTC1, PTC1 and GPR161 are internalized and PTC1 undergoes lysosomal degradation. In the absence of PTC1, SMO is phosphorylated by CK1 and GSK3 β . The phosphorylated SMO is transported and anchored to the base of the cilium. The SUFU - GLI complex accumulates and dissociates at the tip of the cilium. The full-length GLI (GLI FL) is then transported to the nucleus where it activates Hh target genes. (Modified from Tatiana Gorjankina et al., 2016)⁵²

The activation of SMO and the downstream signaling cascade are still not fully understood. How SMO is inhibited by PTC1, and how the signal transduction from SMO to GLI occurs are questions that are intriguing for the Hh research community. It is proposed that SMO activation is a two-step process comprising ciliary localization and C-terminal phosphorylation. This could explain the inhibition of SMO by cyclopamine but not the fact that it is still transported to cilia.⁵² It is shown that there is no direct physical interaction between SMO and PTC1.⁶³ However, PTC1 regulates SMO by controlling the influx of sterols, specifically cholesterol, into the cytoplasm. Cholesterol allosterically binds to the cysteine rich domain (CRD) of SMO and triggers conformational changes sufficient for SMO activation. It is proposed that PTC1 maintains low levels of cholesterol in the ciliary membrane, thereby ensuring that SMO will not be activated.⁶⁴ However, upon PTC1 inhibition by SHH, cholesterol concentration in the cilia increases,

leading to SMO activation. The open form of SMO is accessible to kinesin protein KIF3 which drives SMO localization to the base of cilia. The GPCR like activation of SMO is proposed *via* a G α i protein that couples with the open conformation of SMO in the cilium.⁶⁵ Once active inside the cilium, SMO activity is regulated by the concentration gradient of cholesterol. This gradient is dependent on Hh ligand concentration which regulates cholesterol influx through PTC1.⁶⁶

3.2.3 The Hh pathway in disease and cancer

Aberrations in Hh signaling regulation are responsible for various types of cancers. There are three types of Hh pathway activity models proposed in cancer (See Figure 9).⁶⁷

In type 1 cancers, the Hh pathway is abnormally activated because of ligand-independent mutations (see Figure 9 A). Activating mutations in SMO or inactivating mutations in PTC1 result in constitutively active Hh signaling independent of Hh ligand. The type 1 model was first observed in patients with Gorlin syndrome that harbored inactivating mutations in PTC1. Therefore, patients with Gorlin syndrome are prone to BCC, medulloblastoma and rhabdosarcoma.⁶⁸ Inactivating mutations are also reported for SUFU which renders resistance to drugs acting upstream of SUFU. Therefore, drugs acting downstream of SUFU are needed for treatment of cancers originating due to type I cancers.

Type 2 cancers are a result of ligand-dependent Hh signaling in an autocrine or juxtacrine manner. The Hh ligand produced by the tumor cell acts on the same or nearby cells in an autocrine or juxtacrine manner respectively, thereby stimulating the growth and proliferation of cancerous tissue. This type of model is observed in colon cancer. Inhibitors acting upstream or downstream of SMO may show effectiveness in type 2 Hh-driven cancers. In type 3 cancers (see Figure 9 B and C) the Hh ligand overproduced by tumor cells, stimulates stromal cells in a paracrine manner. The stimulation of stromal cells leads to secretion of growth factors (VEGF, IGF etc) which in turn support growth and survival of tumor cells (see Figure 9 B). Alternatively, Hh ligand is secreted by stromal cells which stimulate growth and proliferation of tumor cells. This type of model is known as reverse paracrine signaling mode (see Figure 9 C).

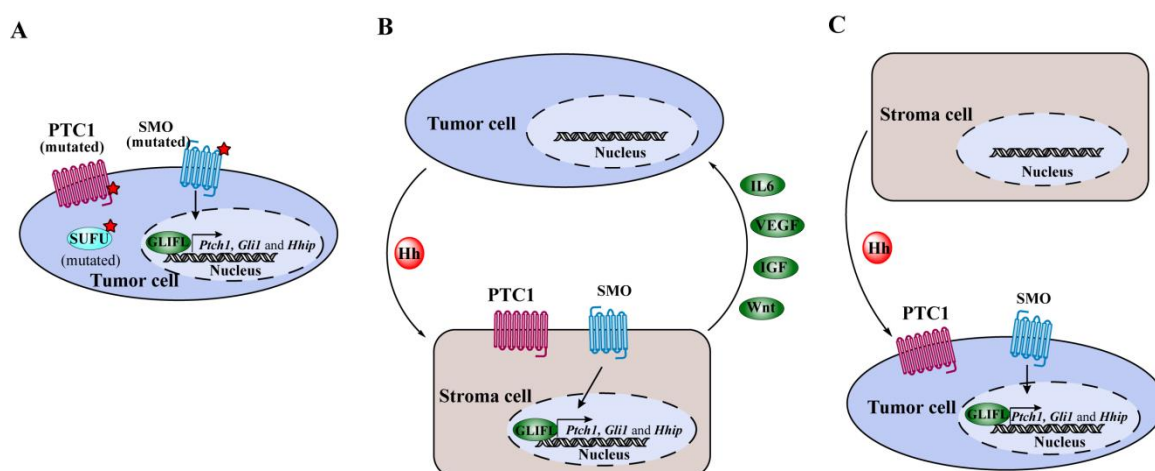


Figure 9. Models of Hh pathway activation in cancer.

(A) Inactivating mutations in the negative repressors PTC1 and SUFU or activating mutations in the positive regulator SMO lead to ligand-independent activation of the Hh pathway. (B and C) Ligand-dependent activation occurs through paracrine (B) or “reverse paracrine” mechanisms (C). (B) Tumor cells secrete Hh ligand that stimulates surrounding cells (e.g., stromal cells) in a paracrine manner. In response to stimulation by Hh, the stromal cells release tumor-supporting factors such as IL6, VEGF, IGF and Wnts. (C) In reverse paracrine activation, Hh ligand is produced by surrounding non-tumor cells that stimulate the growth of tumor cells. (Modified from Fujia Wu et al., 2017)⁶⁷

3.3 Modulators of the Hh signaling pathway

3.3.1 SMO inhibitors in clinical trials

The natural product cyclopamine was the first known inhibitor of SMO. Cyclopamine was discovered for causing cyclopia, when sheep that ingested *Veratrum californicum* during their gestation period gave birth to progeny with birth defects including cyclopia. The steroid alkaloid causing this was isolated from the plant extract of *Veratrum californicu* and named cyclopamine.⁴⁸ However, cyclopamine was not tested clinically for its use in cancer therapy because of moderate inhibition of Hh target gene expression, poor aqueous solubility and lack of stability in acidic pH.⁶⁹ SMO is the most druggable target in Hh signaling and all small molecules that have reached clinical trials are antagonists of SMO (see Figure 10 A). Vismodegib was the first molecule to enter clinical trials and gain FDA approval in 2012 for the treatment of BCC. Vismodegib was co-developed by Curis and Genentech and marketed under the tradename ErivedgeTM. Novartis Institute of Biomedical Research developed NVP-LDE225 (Sonidegib) as a potent SMO antagonist. Sonidegib is in phase I/II clinical trials for the treatment of BCC, acute leukemia and medulloblastoma.⁷⁰ PF-04449913 (Glasdegib) was developed by

Pfizer as a potent SMO antagonist which is currently in phase I/II clinical trials for the treatment of acute myeloid leukemia and myelodysplastic syndrome.⁷¹ BMS-833923 was developed by Bristol-Myers Squibb in collaboration with Exelixis and is being evaluated in phase I and II as a single agent as well as in combination for the treatment of various cancers.⁷² LY2940680 (Taladegib) developed by Eli Lilly is in phase I and II trials for the treatment of pediatric medulloblastoma and small cell lung cancer.⁷³ Table 1 summarizes the bioactivity of above mentioned SMO antagonists.

Table 1. Established SMO inhibitors in clinical trials.

SMO inhibitors in clinical trials and their sensitivity towards cell with the D473H point mutation.

Compound	IC ₅₀ wild-type SMO	IC ₅₀ D473H SMO	Development status
Vismodegib	3-22 nM	Loss of activity	Clinically approved
NVP-LDE2225	2.5 nM	Loss of activity	Phase III
PF-04449913	5 nM	Not reported	Phase II
BMS-833923	21 nM	Not reported	Phase II
LY2940680	2.4 nM	Active	Phase II

3.3.2 Inhibitors upstream of SMO

Interfering with binding of the Hh ligand to Ptch1 is another attractive strategy to inhibit Hh signal transduction. The monoclonal antibody 5E1 was developed at Howard Hughes Medical Institute (Maryland, USA) to block the binding of Hh ligand to PTC1 with low nanomolar potency.⁷⁴ However, the antibody failed to advance to clinical development because of moderate activity in cells. RU-SKI-43 was identified as an inhibitor of Hhat-mediated palmitoylation of SHH - a post-translational modification necessary for activity of SHH. However, RU-SKI-43 did not display any anti-cancer activities *in vitro* or *in vivo*.⁷⁵ Researchers at the Broad Institute (Cambridge, USA) developed robotnikinin, which binds to the active N-terminal fragment of SHH, thereby inhibiting Hh signal transduction.⁷⁶ Statins are another class of molecules that inhibit Hh upstream of SMO. Progeny of pregnant women administered statins like cerivastatin, simvastatin, lovastatin

or atorvastatin, displayed birth defects like holoprosencephaly. Statins reduce cholesterol biosynthesis by inhibiting 3-hydroxy-3-methylglutaryl CoA (HMG-CoA) reductase. The reduction of cholesterol biosynthesis leads to inhibition of cholesterol-dependent Hh pathway.⁷⁷ Therefore, compactin- a statin derived molecule was developed to deplete cholesterol levels in the cell and thereby maturation of the Hh protein (See Figure 10 B).⁷⁸

3.3.3 Inhibitors downstream of SMO

Mutations upstream in the Hh signaling pathway components result in Hh-dependent type 1 cancers. Therefore, therapies that act downstream of SMO and SUFU are desired to overcome mutation-related resistance. GLI transcription factors are attractive targets for inhibiting Hh signaling at the transcriptional level. GANT58 and GANT61 are two structurally different inhibitors that were identified to inhibit GLI transcription in a screen performed in HEK293 cells.⁷⁹ Two independent studies have shown that arsenic trioxide (ATO) inhibits GLI transcription factors *via* different mechanisms. ATO improved the survival of SMO M2 mutation-expression model of medulloblastoma.⁸⁰ Hh pathway inhibitor (HPI 1-4) were identified as potent inhibitors of Hh signal transduction. It was demonstrated by Chen *et al.* that these inhibitors act at or below the level of SUFU. Among these four inhibitors, HPI 1 is the most potent inhibitor of Hh pathway activity. It is proposed that these compounds inhibit Hh pathway by interfering with GLI processing or primary cilia formation (see Figure 10 C).¹⁰ In another high-throughput screen, the natural product physalin F was identified as a potent inhibitor of GLI1. Physalin F inhibited GLI transcriptional activity with an IC₅₀ of 0.66 μM.⁸¹

3.3.4 Activators of Hh signaling pathway

Purmorphamine, a purine derivative, was identified as Hh pathway agonist in an osteoblast differentiation assay performed in mouse mesenchymal C3H/10T1/2 cells.⁸² C3H/10T1/2 cells undergo osteoblast differentiation, i.e. osteogenesis, upon Hh pathway activation. Levels of alkaline phosphatase (ALP), a gene expressed as a result of osteogenesis, are quantified as a measure of Hh pathway activity. The molecular target of purmorphamine was identified to be SMO, as the activity of purmorphamine was unchanged in *PTCH1*^{-/-} cells and significantly affected in *SMO*^{-/-} cells. Also, purmorphamine displaced BODIPY-cyclopamine in HEK293T cells overexpressing SMO which indicative of binding to SMO.⁸³

SAG (SMO Agonist) is another Hh pathway activator found in high-throughput screening in Shh-Light2 cells. Experimentally it was shown that SAG binds to SMO and activated GLI-mediated transcriptional activity. SMO is locked in open form upon binding of SAG to heptahelical bundle of SMO (See Figure 10 D)⁴⁸

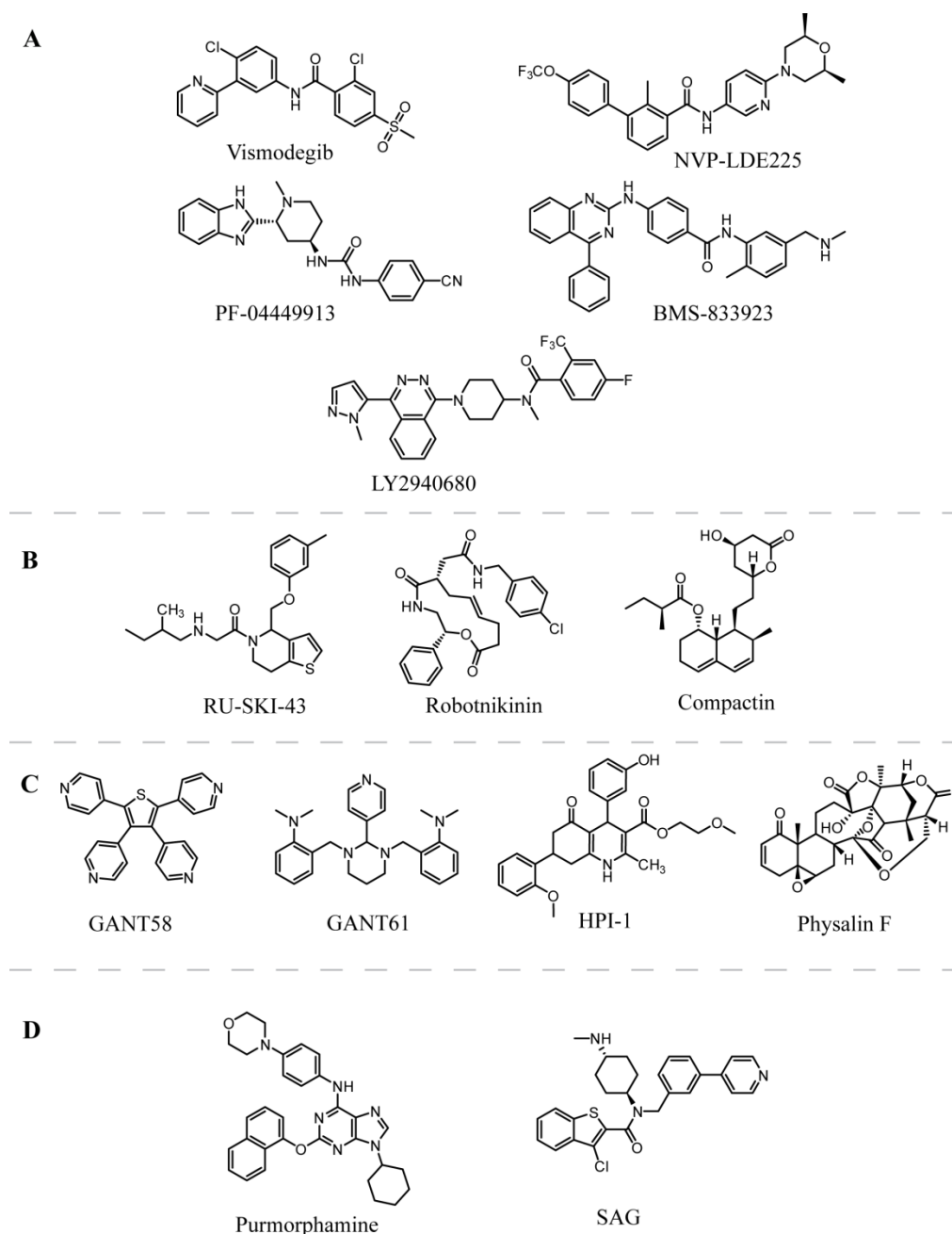


Figure 10. Synthetic small molecule modulators of Hh signaling pathway.

(A) Established SMO inhibitors in clinical trials. (B) Hh pathway inhibitors acting upstream of SMO. (C) Hh pathway inhibitors acting downstream of SMO. (D) Hh pathway activators acting at the level of SMO.

4 Motivation and aim of the thesis

The Hh signaling pathway is vital for organ development and body patterning during embryogenesis. However, its inappropriate activation is linked to several types of cancers.⁴⁴ Therefore, development of small molecule modulators of Hh pathway is of utmost importance in the cancer research.

SMO is the most druggable target in Hh signaling and all small molecules that have reached clinical trials are antagonists of SMO. However, there is a need to impinge the pathway downstream of SMO due to recently discovered mutations in the SMO.⁸⁴

In this regards, the aim of the thesis is to identify novel modulators of the Hh signaling pathway and establish their mode of action. In order to identify the novel modulators of Hh signaling pathway a cell-based screening will be performed. The “hits” from this primary screening will be chosen for validation in orthogonal assays. Where needed, exploration of structure activity relationship (SAR) for the hit compounds should enable attachment of a linker for the purpose of affinity-based proteomics in order to identify the targets of hit compounds. Validation and mode of action studies will be based on the nature of the targets identified.

Figure 11 summarizes the workflow for identification of novel modulators of Hh signaling pathway. The primary cell-based screening will be done in compound management and screening center (COMAS) to identify the Hh pathway modulators. Hit compounds from this screen will be tested for their ability to modulate GLI transcription factor-mediated Hh pathway activity. Since SMO is the most druggable target, the ability of the Hh modulators to bind to SMO will be determined by BODIPY-Cyclopamine displacement assay. For non-SMO binders SAR exploration followed by affinity-based chemical proteomics will be performed in order to identify the targets of hit compounds. Target identification process will be followed by target validation experiments, e.g. modulation of the identified targets the by hit compounds will be determined by biophysical, genetic and target-functional assays.

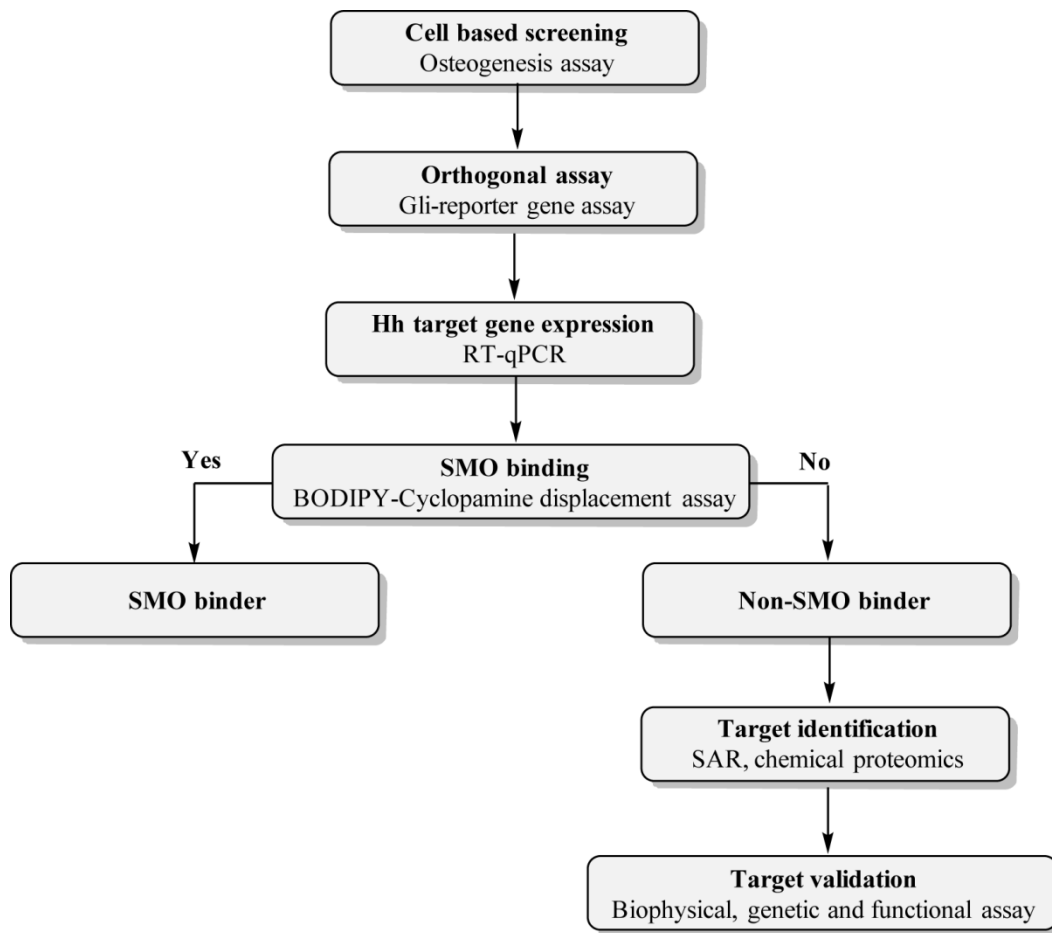


Figure 11. Workflow for identification and characterization of novel modulators of Hh signaling pathway

The success of this strategy would enlighten the mechanism of action that modulates Hh signaling pathway. Moreover, identification novel targets may allow novel entry points for therapeutic intervention downstream of SMO.

5 Results and discussion

5.1 Phenotypic screening to identify Hh pathway modulators

To investigate the biological activity of small molecules, the phenotype-based approach, i.e. forward chemical genetics approach, was followed. As opposed to reverse chemical genetics, forward chemical genetics does not need information about biological targets and moreover library of diverse molecules can be screened for bioactivity.⁶ COMAS library comprising 200,000 compounds was screened in several cell-based phenotypic assays, including monitoring the modulation of autophagy, Wnt signaling, glucose uptake, Hh signaling.

To examine Hh signaling pathway modulation, Hh responsive pluripotent mouse mesenchymal C3H/10T1/2 cells were used. These multipotent progenitor cells undergo osteogenesis to differentiate into osteoblasts. Osteogenesis is the process of bone formation by osteoblasts. As a result of osteogenesis, cells produce Alkaline Phosphatase (ALP), an enzyme necessary for mineralization during the process of bone formation.⁸⁵ The level of ALP can be used as a marker of Hh pathway activity and is quantified by using the CDP-*Star* reagent. CDP-*Star* is dephosphorylated by ALP and converted to a meta-stable dioxetane-phenolate anion. The resulting unstable product undergoes decay, emitting light which can be quantified by measuring the luminescence.⁸⁶

The high throughput screening (HTS) of the 160,000 compounds yielded 1500 low micromolar inhibitors of the Hh pathway, which dose dependently decreased the luminescence with low micromolar IC₅₀s. The compounds that inhibited Hh signaling without affecting cell growth and other tested signaling pathways (e.g. Wnt, autophagy, glucose uptake etc.) were regarded as hits, and selected for follow-up biological evaluation. Within the scope of this thesis, three such hit compounds were selected from *df*-oxindole, bispyrrolidines and bis-ntrophenyle-bipyridine compound classes for biological evaluation are depicted in Figure 12.

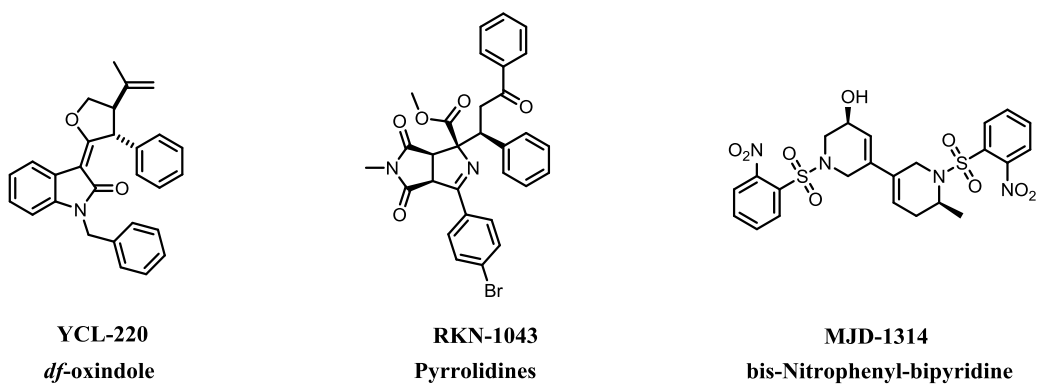


Figure 12. Hh pathway inhibitor analogues chosen for biological evaluation and target identification.

A workflow for evaluation of Hh pathway modulators as noted in Figure 11 was followed in an attempt to decipher the mode of action of these hit compounds.

5.2 Biological evaluation of *df*-oxindoles

5.2.1 Confirmation of biological activity by secondary assays

The *df*-oxindole compound library was synthesized by Yen-Chun Lee, a PhD student in the department of chemical biology at the Max Planck Institute of Molecular Physiology, Dortmund, Germany, in an effort to design a ligand-directed gold catalysis approach to access diverse scaffolds. The library comprised of 21 compounds was assayed in the osteoblast differentiation assay at COMAS. Out of 21 tested compounds, seven compounds inhibited Hh signaling with low micromolar IC₅₀ (see Table 9). The most active compounds MPI-YENLEE-YCL-220 and MPI-YENLEE-YCL-225, here after referred to as YCL-220 and YCL-225, had an IC₅₀ of 3.13 μM and 2.75 μM respectively. Further, YCL-220 and YCL-225 were assayed in GLI-reporter gene assay - an orthogonal assay that is closer to physiological condition of Hh signaling pathway.⁸⁷ The assay is performed using in Shh-LIGHT2 cells, a NIH/3T3 derived cell line stably transfected with GLI-dependent firefly luciferase and constitutive *Renilla* luciferase reporters (Figure 13 A).

The ability of the compounds to inhibit purmorphamine induced activation of Hh pathway in Shh-LIGHT2 cells was monitored by measuring the firefly luciferase signal and normalizing it to the signal for renilla luciferase. In this assay, YCL-220 and YCL-225 also inhibited the Hh pathway dose-dependently with IC₅₀ of 0.8 ± 0.15 μM and 1.75 ± 0.42 μM respectively, which are in the same range as the IC₅₀ generated in the osteogenesis assay (Figure 13 B). Both the compounds did not affect the *Renilla* luciferase activity, which is under the control of thymidine kinase promoter, therefore suggesting GLI-specific inhibition of transcription upon treatment with YCL-220 and YCL-225. YCL-220 was chosen for follow-up biological characterization as it was the most potent GLI-transcription inhibitor in this series.

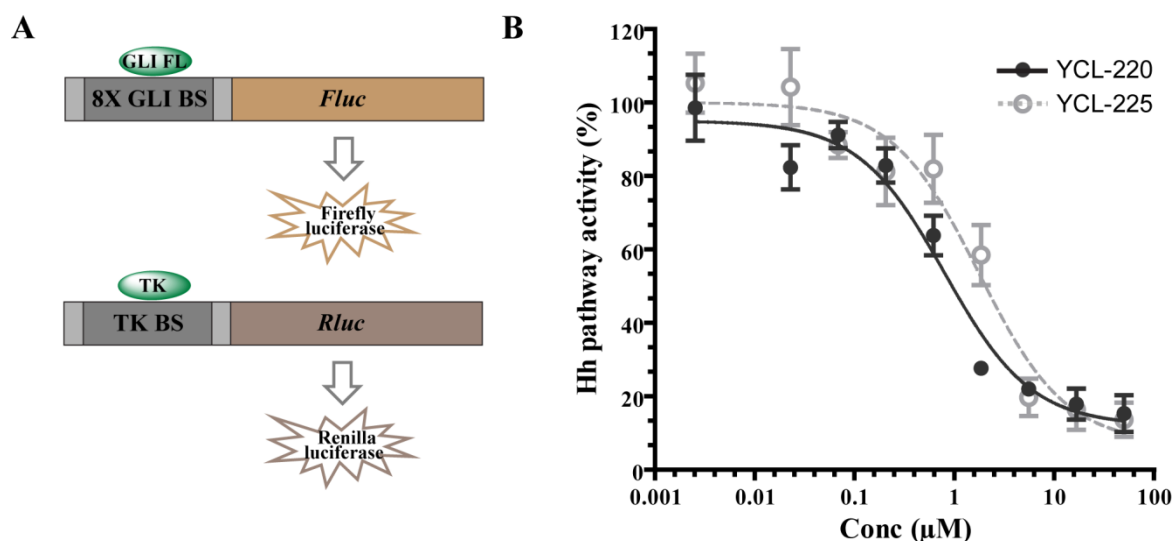


Figure 13. Influence of YCL-220 and YCL-225 on the GLI-mediated reporter gene expression in Shh-LIGHT2 cells.

(A) Reporters in Shh-LIGHT2 cells, a NIH/3T3 derived cell line stably transfected with GLI-dependent firefly luciferase (Fluc) and constitutive renilla luciferase (Rluc) reporters. (B) YCL-220 and YCL-225 inhibit GLI-dependent reporter gene expression in Shh-LIGHT2 cells. Cells were treated with 1.5 µM purmorphamine and different concentrations of compounds for 48 h. Firefly and renilla luciferase activities were determined and ratios of firefly luciferase/Renilla luciferase signals were calculated, which are a measure of Hh pathway activity. Nonlinear regression analysis was performed using a four parameter fit. All data are mean values of three independent experiments ($n = 3$) \pm s.d.

To further inspect the inhibition of GLI-specific transcription, expression of Hh target genes upon YCL-220 treatment was monitored by RT-qPCR. The activation of the Hh pathway by stimulation with an agonist, in this case purmorphamine, results in a cascade of events which culminates in the activation GLI-dependent transcription of Hh pathway-specific target genes such as *Ptch1* and *Gli1*.⁸⁸ PTC1 is a negative regulator and GLI1 is positive regulator of the Hh pathway. Upon Hh pathway activation, expression of these genes is necessary for the Hh pathway regulation, as these proteins control the Hh pathway activity by feedback regulation of the pathway. The level of expression of *Ptch1* and *Gli1* was monitored in C3H/10T1/2 cells. Upon treatment with various compound concentrations along with purmorphamine, total RNA was isolated and cDNA was synthesized by a reverse transcription reaction. The cDNA was used in the qPCR experiment in order to quantify the expression of *Gapdh*, *Ptch1* and *Gli1*. The expression of *Gapdh*, used as reference gene, was used to normalize the expression of *Ptch1* and *Gli1*. Both the target genes had basal levels of expression upon treatment with DMSO. Highest levels of *Ptch1* and *Gli1* expression was detected upon treatment with 1.5 µM purmorphamine and these values were set to 100% in all further experiments. The RT-

qPCR experiments further confirmed the Hh-specific transcriptional inhibition by YCL-220, which dose dependently inhibited the expression of *Ptch1* and *Gli1* (Figure 14). Upon treatment with 5 μ M YCL-220 target gene expression was reduced to 40%, which further dropped to 10% at 20 μ M. These results confirm the GLI-transcription factor dependent inhibition of Hh pathway by YCL-220.

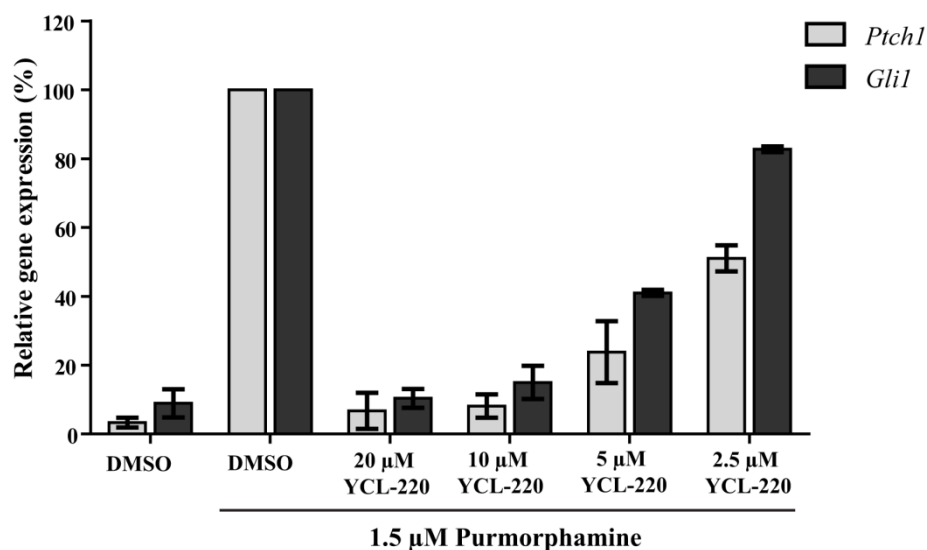


Figure 14. Effect of YCL-220 on Hh target gene expression.

C3H/10T1/2 cells were treated with purmorphamine (1.5 μ M) and different concentrations of YCL-220 or DMSO as a control for 48 h before isolation of total RNA. Following cDNA preparation, the relative expression levels of *Ptch1*, *Gli1* and *Gapdh* were determined by means of quantitative PCR employing specific oligonucleotides for *Ptch1* and *Gli1* or *Gapdh* as a reference gene. Expression levels of *Ptch1* and *Gli1* were normalized to the levels of *Gapdh* and are depicted as percentage of gene expression in cells activated with purmorphamine (100%). All data are mean values of three independent experiments ($n = 3$) \pm s.d.

5.2.2 SMO binding of YCL-220

In order to explore the biological target of the YCL-220, the ability of YCL-220 to directly bind to SMO was explored. SMO appears to be the most druggable Hh pathway component. Vismodegib and Cyclopamine are the most studied examples of small molecule inhibitors of the Hh signaling which directly bind to the seven transmembrane pocket of SMO. A BODIPY-cyclopamine displacement assay was performed in HEK-293T cells transiently transfected with SMO-expressing construct to determine whether compounds competitively bound SMO at this site. BODIPY-cyclopamine binds to cells expressing SMO, which is detected as green fluorescent cell staining (Figure 15 A). Upon treatment with Vismodegib, BODIPY-cyclopamine is displaced from the cells as indicated by loss of the green fluorescence. YCL-220 treatment resulted in decreased BODIPY fluorescence in cells indicating that YCL-220 binds to SMO. In order to quantify the displacement of BODIPY-cyclopamine, flow cytometry was used to count the cells displaying green fluorescence. Cells that were treated with BODIPY-cyclopamine and DMSO displayed the maximum BODIPY intensity, and were normalized to 100% (Figure 15 B). Upon treatment with various concentrations of YCL-220, a concentration-dependent displacement of BODIPY-cyclopamine from the cell was observed similar to vismodegib at 5 μM .

As an additional confirmation of the SMO binding nature of the YCL-220, the inhibition of Hh pathway by YCL-220 upon activation of Hh signaling by 0.1 μM and 1 μM of SAG was investigated using the GLI-reporter gene assay. SAG is a SMO agonist which activates the Hh pathway by binding to SMO. At higher concentrations, i.e. 1 μM , it saturates the binding sites on SMO, resulting into drop in the inhibitory activity of SMO antagonists.¹⁰ As a proof of concept, the activity of vismodegib and GANT61, which inhibit the Hh pathway at different levels, was assayed. Upon activation of Hh signaling by 1 μM SAG, a drop in the activity of vismodegib was observed (Figure 16 A). Conversely, the activity of GANT61, a non-SMO binder, was unaffected when the pathway was activated by 1 μM SAG (Figure 16 B). In a similar manner, when Hh signaling was activated by 1 μM SAG, YCL-220 was less potent in inhibiting the GLI-mediated Hh pathway activity (Figure 16 C). This data supports the observation that YCL-220 inhibits Hh signaling by binding to SMO.

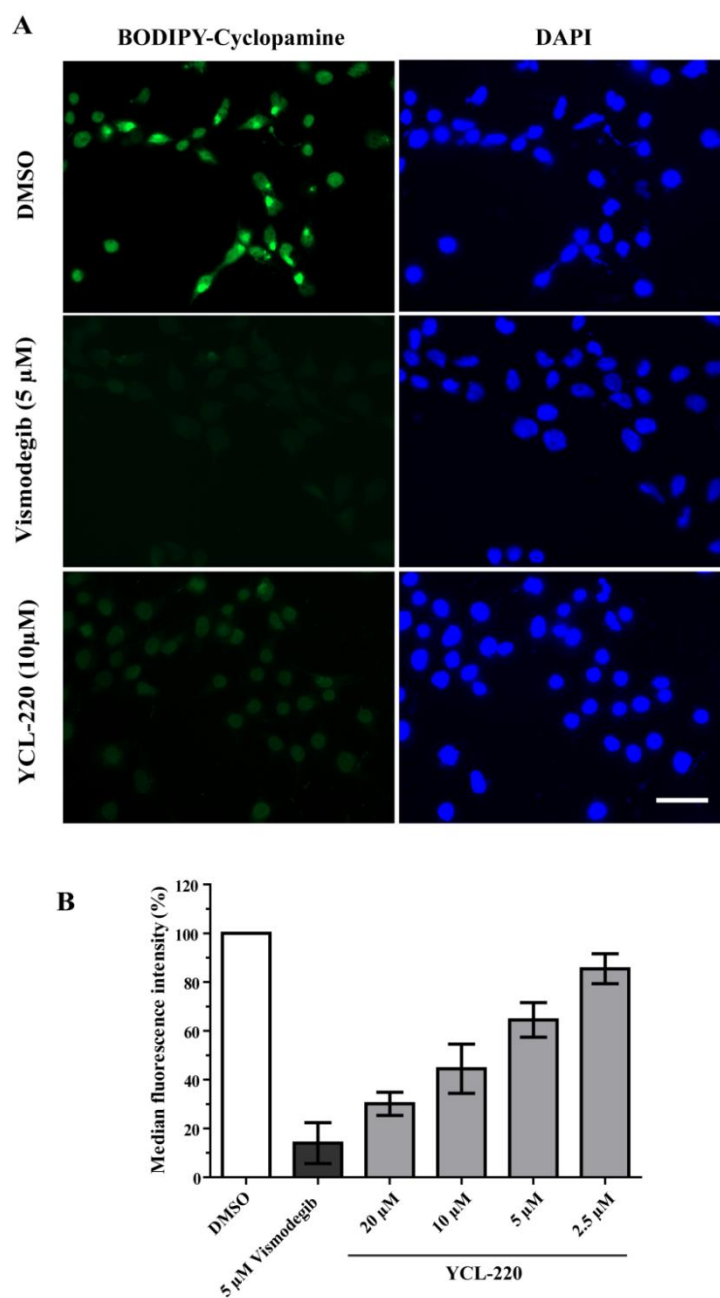


Figure 15. Effect of YCL-220 on SMO-bound BODIPY-cyclopamine.

(A) HEK293T cells were transiently transfected with SMO expressing plasmid or empty vector. 48 h later cells were treated with BODIPY-cyclopamine (5 nM, green) followed by addition of 10 μM of YCL-220 or 5 μM vismodegib and DMSO as controls and incubation for 1 h. Cells were then fixed and stained with DAPI to visualize the nuclei (blue). Scale bar: 20 μm (B) HEK 293T cells ectopically expressing SMO were treated with different concentration of YCL-220 or vismodegib and DMSO as controls in the presence of BODIPY-cyclopamine (5 nM) for 5 h. The graph shows the percentage of cell-bound BODIPY-cyclopamine as detected by fluorescence-activated cell sorting. Data are mean values of three independent experiments ($n=3$) \pm s.d.

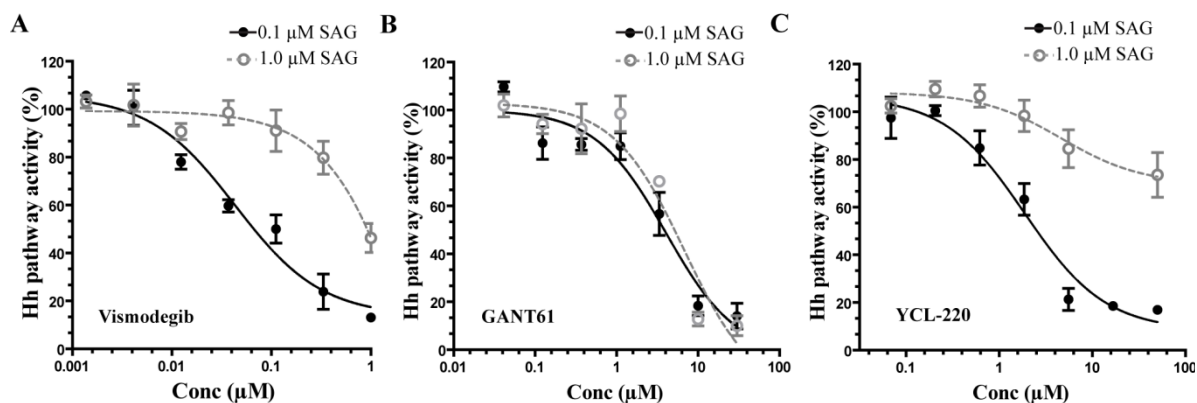


Figure 16. Effect of YCL-220 on GLI-mediated reporter gene expression upon Hh pathway activation by SAG.

(A) Influence of vismodegib, (B) GANT61 and (C) YCL-220 on GLI-mediated reporter gene expression upon Hh pathway activation in Shh-LIGHT2 cells by SAG (0.1 μM and 1 μM). Cells were treated with 0.1 μM or 1.0 μM SAG and different concentrations of compounds for 48 h. Nonlinear regression analysis was performed using a four parameter fit. Data are mean values of three independent experiments ($n=3$) \pm s.d. and were normalized to cells treated with the respective concentration of SAG (set to 100%).

The *df*-oxindoles possess potentially reactive Michael acceptor functionalities often responsible for covalent binding to cellular targets by addition of nucleophiles such as thiols in biomolecules. Therefore, to explore the mode of binding of YCL-220 to SMO, i.e. reversible or irreversible, a washout step was introduced in the BODIPY-cyclopamine displacement assay (Figure 17 A). HEK-293T cells were transfected with pGEM-SMO plasmid for 48 h followed by treatment with YCL-220 and DMSO as a control for 1 h. Cells were then washed three times with cell culture media in order to wash away the bound YCL-220. After the washing steps, cells were supplemented with 5 nM BODIPY-cyclopamine for 1 h prior to fixation and staining with DAPI to visualize the nuclei. For the cells wherein no washout step was introduced, YCL-220 was able to displace BODIPY-cyclopamine as indicated by loss of green fluorescence. Whereas, upon washout, YCL-220 failed to displace BODIPY-cyclopamine, indicating reversible binding of YCL-220 to SMO.

Furthermore, this reversible binding of the YCL-220 to SMO was assayed using the GLI-reporter gene assay with an extra washout step. Shh-LIGHT2 cells were treated with 1.5 μM purmorphamine and different concentrations of compound for 30 min. Cells were washed three times with cell culture medium followed by addition of fresh medium containing 1.5 μM purmorphamine or DMSO as a control and incubated for 48 h. Firefly and Renilla luciferase activities were determined. As seen in Figure 17 B, the washout

steps decreased the potency of YCL-220 when compared to no washout step as detected by shift in the curve confirming the reversible binding of YCL-220 to SMO.

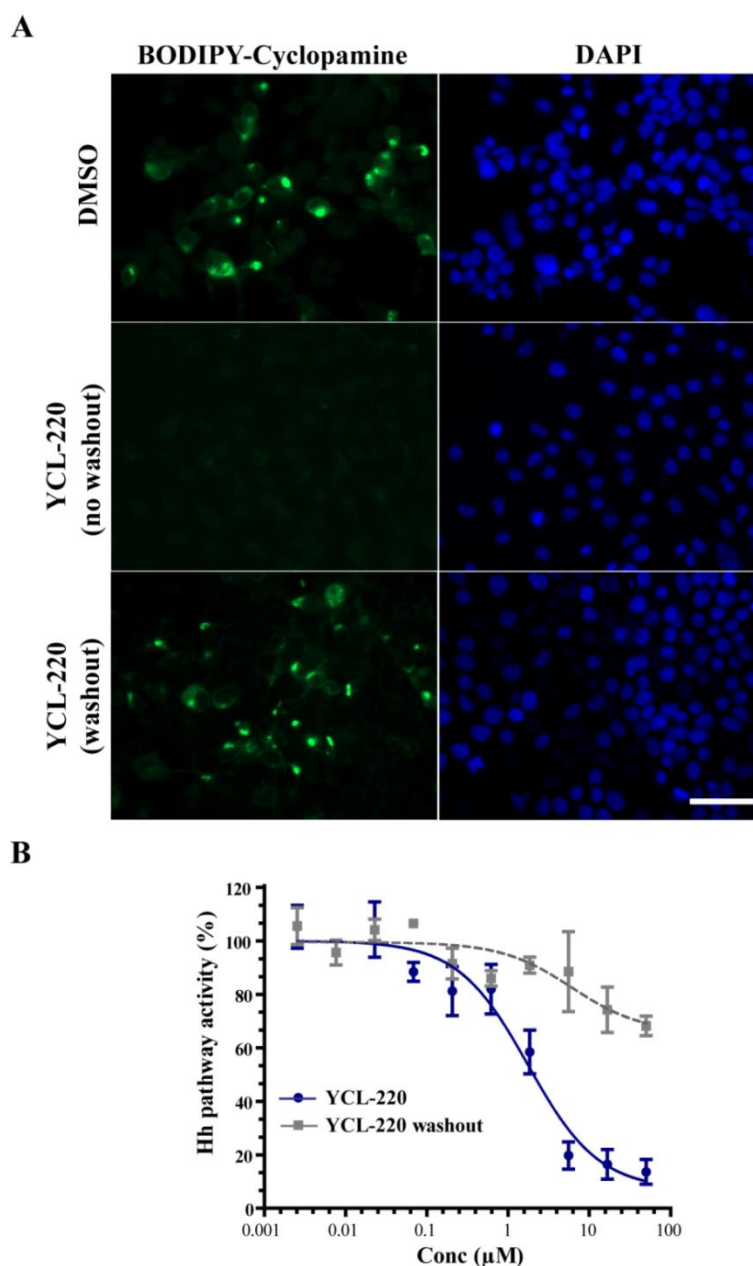


Figure 17. Washout experiment to access the mode of SMO inhibition by YCL-220.

(A) HEK293T cells were transiently transfected with SMO-expressing plasmid or empty vector. 48 h later cells were treated with 10 μM YCL-220 and DMSO as a control for one hour. Cells were then washed three times with medium, treated with 5 nM BODIPY-cyclopamine (green) for 1 h prior to fixation and staining with DAPI to visualize the nuclei (blue). Scale bar: 20 μm . (B) Hh signaling activity was determined using GLI-dependent reporter gene expression in Shh-LIGHT2 cells. Cells were treated with 1.5 μM purmorphamine and different concentrations of compounds for 30 min prior to washout followed by addition of fresh media containing 1.5 μM purmorphamine or DMSO as a control and incubation for 48 h. Firefly and renilla luciferase activities were determined. Ratios of firefly luciferase/renilla luciferase signals were calculated as a measure of Hh pathway activity. Nonlinear regression analysis was performed using a four parameter fit. Data are mean values of three independent experiments ($n = 3$) \pm s.d.

5.2.3 Effect on the ciliary transport of SMO

In vertebrate Hh signaling, Ptc1-induced inhibition of SMO is relieved upon Hh ligand binding. SMO in its active form initiates the cascade of Hh signaling events, which culminate in the transcription of Hh target genes. Most of the signaling cascade events occur in the primary cilium and involve mobilization of multiple pathway components to the cilium. Upon Hh pathway activation, SMO is laterally trafficked to the primary cilium *via* intraflagellar transport (IFT) through binding of the kinesin-like protein KIF3a. However, genetic studies showed that SMO is constantly cycling through the cilium without activating the Hh pathway. Thus the localization of SMO into the cilium is necessary but not sufficient for Hh pathway activity.⁸⁹

The Hh pathway inhibition due to SMO antagonism can have different effects on the localization of the SMO to the cilia. For example, vismodegib inhibits Hh pathway by antagonizing SMO and blocking its entry into the cilium. Contrary to this mode of inhibition, cyclopamine inhibits Hh pathway by antagonizing SMO but without blocking SMO entry into cilium. In order to investigate the effect of YCL-220 on SMO trafficking to the cilium, NIH/3T3 cells were treated with 1.5 μM purmorphamine and 2 μM vismodegib or 5 μM YCL-220 for 24 h. To visualize the localization of SMO to the primary cilium, cells were stained with an antibody against acetylated tubulin to stain cilium and against SMO protein followed by fluorescence microscopy. Upon purmorphamine treatment, SMO was localized to the cilium, as detected by co-localization of SMO with cilium, indicating the activation of Hh pathway (Figure 18). As reported in literature, treatment with vismodegib abolished the localization of SMO to the cilium. Similarly, upon treatment with YCL-220 purmorphamine-induced SMO localization into the cilium was inhibited.

The Michael acceptor functionalities in *df*-oxindoles may lead to instable compound upon reaction with cellular nucleophiles such as thiols in biomolecules. To address this concern, the stability of YCL-220 in the presence of glutathione (GSH) was determined after different incubation times (1, 24 and 48 h) in 5 mM GSH in PBS. Under the tested conditions, no reactivity of YCL-220 towards 5 mM GSH representing cellular concentrations of GSH was observed as indicated by the abundance of YCL-220 in the presence of 5 mM GSH (Figure 19). Therefore, YCL-220

appears to have a non-covalent and reversible mode of SMO binding and Hh pathway inhibition.

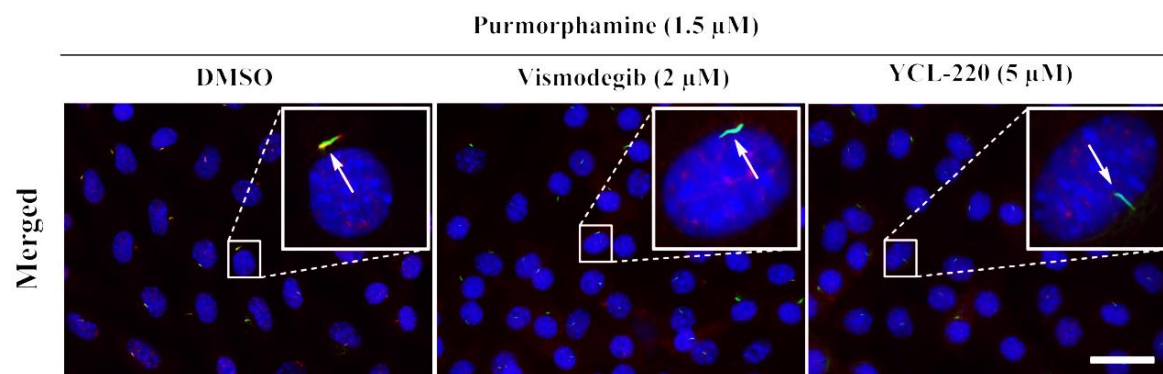


Figure 18. Effect of YCL-220 on ciliary localization of SMO.

NIH/3T3 cells were treated with purmorphamine (1.5 μ M) for 2 h followed by addition of 2 μ M vismodegib or 5 μ M YCL-220, and further incubation for 12 h. Cells were then fixed and stained with DAPI to visualize the nuclei (blue), SMO (red) and cilia (acetylated tubulin; green). Insets: representative single cilium. Scale bar: 10 μ m.

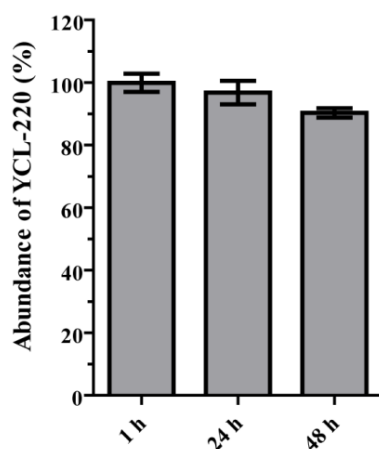


Figure 19. Reactivity of YCL-220 towards GSH.

YCL-220 (30 μ M) was incubated with 5 mM GSH or PBS. Reactivity of the compounds towards GSH was measured by HPLC. Numbers are percent abundance of the compound in GSH as compared to their abundance in PBS at the given time points. Data are mean values of three independent experiments ($n = 3$) \pm s.d.

5.2.4 Summary and outlook for *df*-oxindole YCL-220

In an effort to develop ligand-directed gold catalysis approach to diverse scaffold synthesis, Yen-Chun Lee synthesized 21 *df*-oxindole-based compounds. An osteoblast differentiation assay that monitors Hh pathway activity identified 7 out of 21 compounds as inhibitors of Hh signaling. Orthogonal assays revealed YCL-220 as a potent inhibitor of GLI - mediated inhibition of Hh signaling with an IC₅₀ value of 0.8 μM. Target identification efforts revealed reversible antagonism of SMO by YCL-220. Similar to Vismodegib, YCL-220 inhibited SMO by blocking SMO entry into the cilium, a necessary step in Hh pathway activation.

Although there are several compounds established as SMO inhibitors, *df*-oxindoles expand the *tool-kit* for studying the reversible binding to SMO.

5.3 Biological evaluation of pyrrolidines

5.3.1 Confirmation of biological activity by secondary assays

Dr. Rishikesh Narayan a post-doctoral researcher in the Department of Chemical Biology at the Max Planck Institute of Molecular Physiology, Dortmund, Germany reported a [3+2] cycloaddition-based enantioselective methodology to access functionalized tropanes. The screening for biological activity at COMAS of the resulting compound collection revealed potent inhibitors of Hh signaling pathway. Inspired by these results, Dr. Narayan and Dr. Erchang Shang further explored the chemical space, defined by these compounds. Towards this end, a small molecule library of pyrrolidines was synthesized and screened by COMAS for potential Hh pathway inhibition by employing the osteoblast differentiation assay.

The most active compounds RKN-1043 and SHANG-244 (Figure 20) had an IC_{50} value for inhibition of purmorphamine-induced osteogenesis of $1.5 \pm 0.2 \mu\text{M}$ and $1.8 \pm 0.0 \mu\text{M}$, respectively (Table 8). The Hh inhibitory activity of these compounds was confirmed in the orthogonal GLI-reporter gene assay with IC_{50} values $1.6 \pm 0.15 \mu\text{M}$ and $2.0 \pm 0.35 \mu\text{M}$ for RKN-1043 and SHANG-244 (Figure 21). Because of the fact that these two compounds are epimers and RKN-1043 is more potent in the osteoblast differentiation and GLI-reporter gene assay, RKN-1043 was chosen for further biological evaluation.

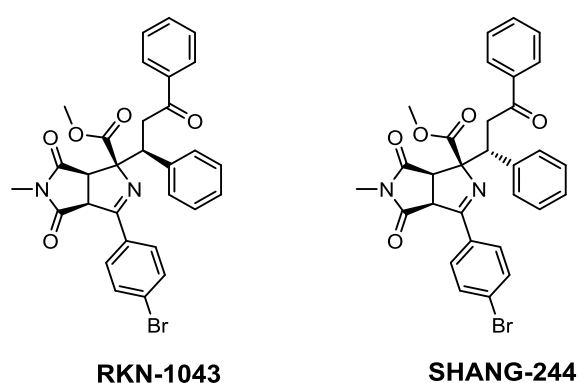


Figure 20. Chemical structures of RKN-1043 and SHANG-244.

RT-qPCR experiments further confirmed the inhibition of Hh target gene expression by RKN-1043, which dose dependently inhibited the expression of *Ptch1* and *Gli1* (Figure 21 B). Upon treatment with $10 \mu\text{M}$ RKN-1043 target gene expression was reduced to 20

to 30%, which further dropped to 10% at 20 μM . The qPCR experiments along with the GLI-reporter gene assay confirmed GLI-dependent inhibition of the Hh pathway by RKN-1043.

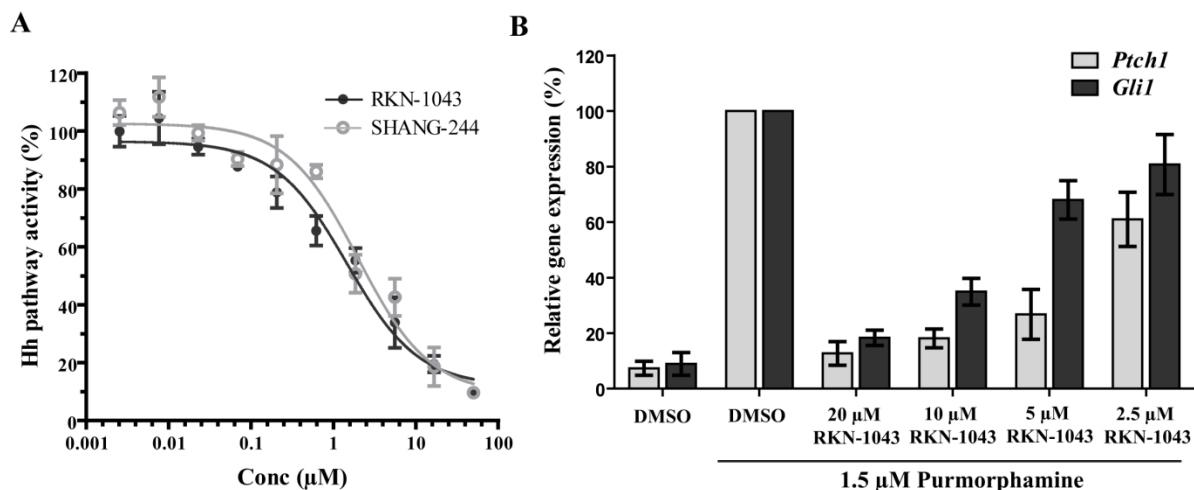


Figure 21. Influence on the GLI-mediated transcription by RKN-1043 and SHANG-244.

(A) RKN-1043 and SHANG-244 inhibit GLI-dependent reporter gene expression in Shh-LIGHT2 cells. Cells were treated with 1.5 μM purmorphamine and different concentrations of compounds for 48 h. Firefly and Renilla luciferase activities were determined and ratios of firefly luciferase/Renilla luciferase signals were calculated, which are a measure of Hh pathway activity. Nonlinear regression analysis was performed using a four parameter fit. All data are mean values of three independent experiments ($n = 3$) \pm s.d. (B) C3H/10T1/2 cells were treated with purmorphamine (1.5 μM) and different concentrations of RKN-1043 or DMSO as a control for 48 h before isolation of total RNA. Following cDNA preparation, the relative expression levels of *Ptch1*, *Gli1* and *Gapdh* were determined by means of RT-qPCR employing specific oligonucleotides for *Ptch1* and *Gli1* or *Gapdh* as a reference gene. Expression levels of *Ptch1* and *Gli1* were normalized to the levels of *Gapdh* and are depicted as percentage of gene expression in cells activated with purmorphamine (100%). All data are mean values of three independent experiments ($n = 3$) \pm s.d.

Furthermore, RKN-1043 treatment failed to displace BODIPY-cyclopamine from the cell indicating that RKN-1043 does not bind to the cyclopamine binding site of SMO (Figure 22). In order to quantify the displacement of BODIPY-cyclopamine, flow cytometry was used to count the cells displaying green fluorescence because of bound BODIPY-cyclopamine. Cells that were treated with BODIPY-cyclopamine and DMSO displayed the maximum BODIPY intensity, and were set to 100% (Figure 22 B). Treatment with various concentrations of RKN-1043 failed to displace BODIPY-cyclopamine from the cell surface therefore confirming the microscopy results.

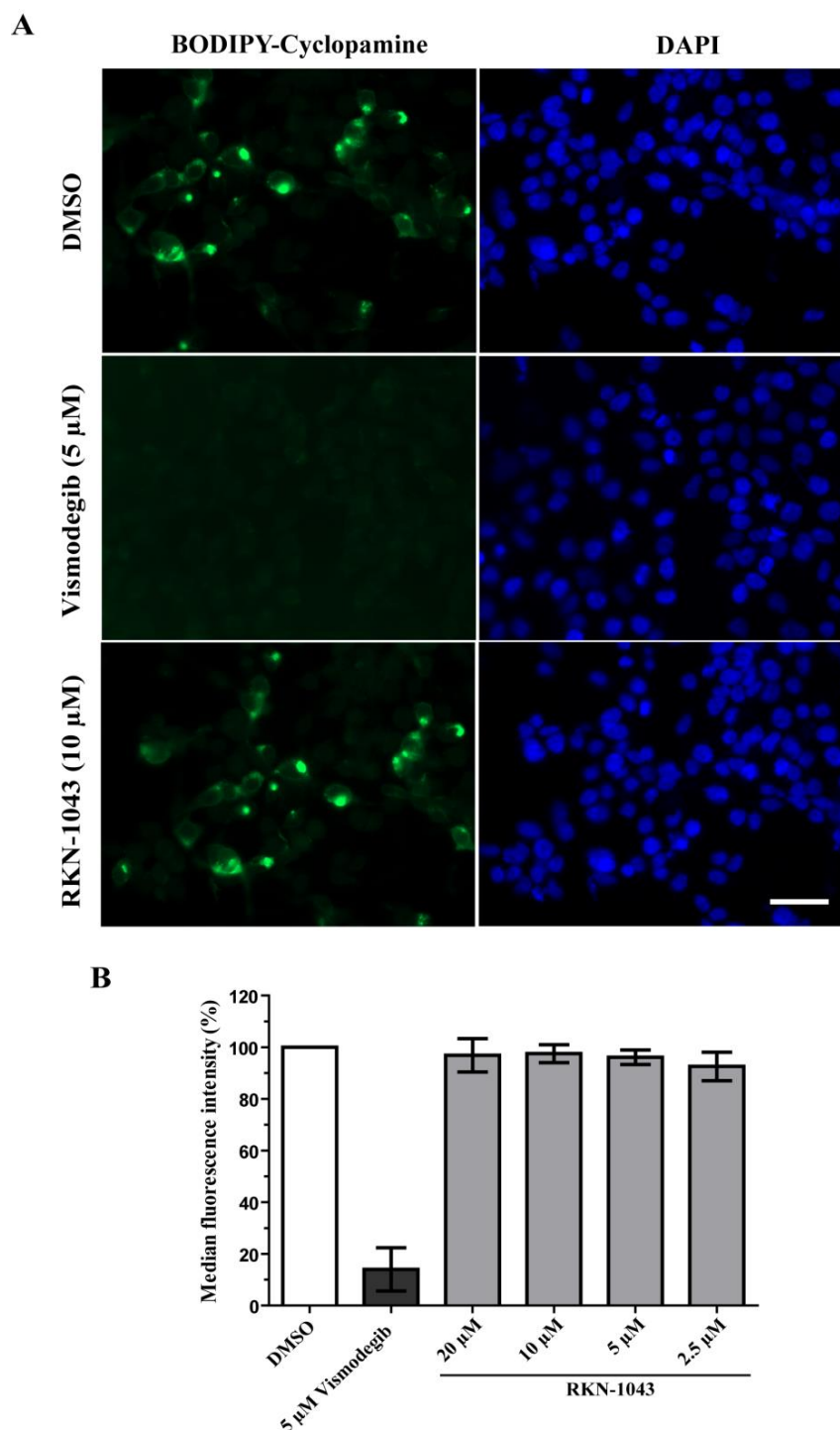


Figure 22. Effect of RKN-1043 on SMO-bound BODIPY-cyclopamine.

(A) HEK293T cells were transiently transfected with SMO expressing plasmid or empty vector. 48 h later cells were treated with BODIPY-cyclopamine (5 nM, green) followed by addition of 10 μ M of RKN-1043 or 5 μ M vismodegib and DMSO as controls and incubation for 1 h. Cells were then fixed and stained with DAPI to visualize the nuclei (blue). Scale bar: 20 μ m (B) HEK 293T cells ectopically expressing SMO were treated with different concentration of RKN-1043, vismodegib or DMSO as control in the presence of BODIPY-cyclopamine (5 nM) for 5 h. The graph shows the percentage of cell-bound BODIPY-cyclopamine as detected by fluorescence-activated cell sorting analysis. Data are mean values of three independent experiments (n=3) \pm s.d.

To rule out the interference of RKN-1043 with SMO localization to cilia, cells were treated with RKN-1043 along with purmorphamine. To visualize the localization of SMO to the primary cilium, cells were stained with an antibody against acetylated tubulin and SMO protein followed by respective secondary antibodies. SMO was localized to cilia upon Hh pathway activation by purmorphamine (Figure 23). However, RKN-1043 did not affect the localization of SMO into cilia as indicated by the co-localization of acetylated tubulin and SMO. Thus, indicating that RKN-1043 might be acting downstream of SMO for inhibition of the Hh pathway.

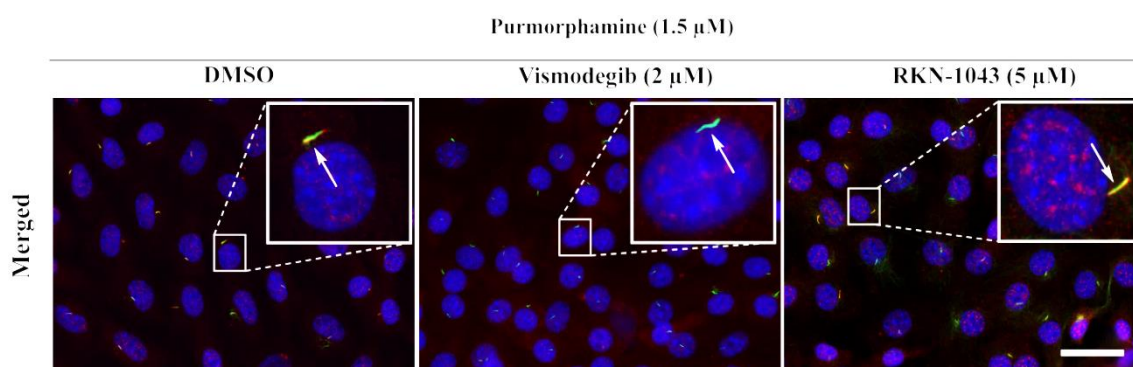


Figure 23. Effect of RKN-1043 on the ciliary localization of SMO.

NIH/3T3 cells were treated with 1.5 μ M purmorphamine for 2 h followed by addition of 2 μ M vismodegib or 5 μ M RKN-1043, and further incubation for 12 h. Cells were then fixed and stained with DAPI to visualize the nuclei (blue), SMO (red) and cilia (acetylated tubulin; green). Insets: representative single cilia. Scale bar: 10 μ m.

5.3.2 Computational target prediction

To identify the molecular targets of RKN-1043, computational target prediction using SPiDER was attempted in collaboration with the group of Prof. Gisbert Schneider, ETH, Zurich. SPiDER predictions were based on the topological features, scaffold connectivity, and target interaction potential similarity of well-established drugs with RKN-1043. SPiDER predicted the Cholecystinin receptor A and B (CCKA and CCKB), Glucagon receptor and protein tyrosine phosphatases 1 B (PTP1B) as putative targets of RKN-1043. It is paramount to experimentally validate the computationally predicted targets of RKN-1043 because the predicted binding does not guarantee the physiological modulation of the target by small molecule. Therefore, it is necessary to demonstrate that a small molecule binds directly to the target protein and leads to modulation of target protein function.

5.3.2.1 Influence of RKN-1043 on PTP1b enzymatic activity

Protein phosphorylation is one of the most important post-translational modification processes. Protein kinases and protein phosphatases reversibly regulate protein phosphorylation. PTP1B catalyzes the dephosphorylation of insulin receptor kinases and plays a critical role in insulin signaling.⁹⁰ For measuring the PTP1B activity, p-nitrophenyl phosphate (pNPP) was used as a substrate. Dephosphorylation of pNPP results in the production of p-nitrophenol (pNP), which causes an increase in the absorbance at 405 nm.

In order to determine the concentration of PTP1B to be used in enzymatic assay, various concentrations of PTP1B were incubated with 2 mM pNPP at 37 °C for 30 min and the generation of pNP was detected by monitoring the absorbance at 405 nm (Figure 24 A). Linear rate of pNPP conversion was observed with 0.15 µg of PTP1B and 2 mM of pNPP, therefore these conditions were used for determining the effect of RKN-1043 on the enzymatic function of PTP1B. For this, PTP1B was pre-incubated with various concentration of sodium orthovanadate or RKN-1043 followed by addition of pNPP to initiate the enzymatic reaction. Sodium orthovanadate, a general competitive inhibitor for PTP, inhibited the conversion of pNPP to pNP as indicated by decreasing absorbance at 405 nm (Figure 24 B). However, RKN-1043 did not affect PTP1B enzymatic function as indicated by complete conversion of pNPP to pNP (Figure 24 C). These results indicate

that RKN-1043 has no effect on the enzymatic activity of PTP1B, thus deprioritizing PTP1B as a potential target of RKN-1043. However, the probable binding of RKN-1043 to PTP1B and targeting its non-enzymatic functions cannot be completely ruled out and needs further investigations.

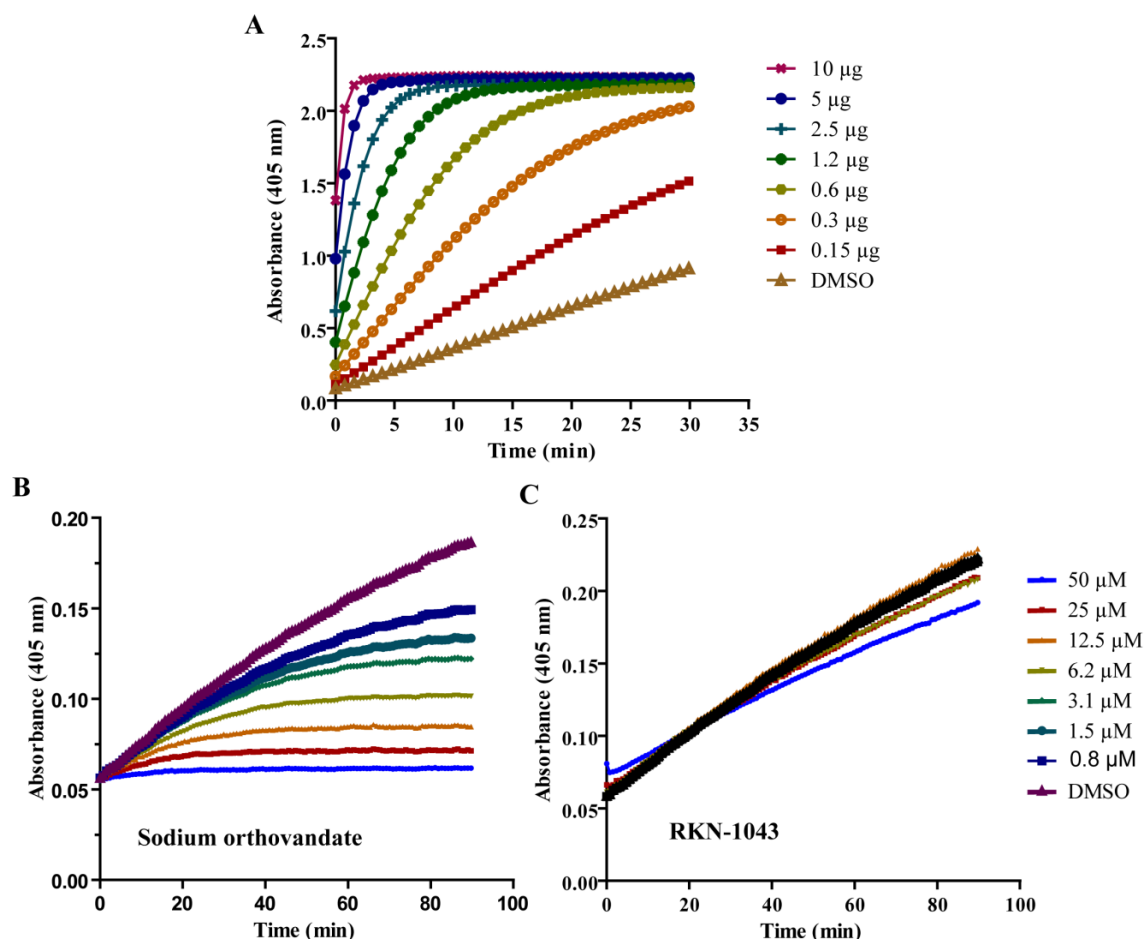


Figure 24. Influence of RKN-1043 on the enzymatic activity of PTP1B.

(A) PTP1B enzyme concentration optimization. Various concentrations of PTP1B were incubated with 2 mM pNPP at 37 °C. Conversion of pNPP to pNP was monitored by measuring the absorbance at 405 nm. (B) Effect of sodium orthovanadate and (C) RKN-1043 on the enzymatic activity of PTP1B. 0.15 µg of PTP1B was preincubated with various concentrations of the compounds and DMSO as a control. The enzymatic reaction was initiated by addition of 2 mM pNPP and the generation of pNP was monitored by measuring the absorbance at 405 nm. Data are representative of three independent experiments (n=3).

5.3.2.2 Effect of RKN-1043 on CCKA, CCKB and glucagon receptor

CCKA and CCKB are receptors for cholecystokinin, a peptide that acts as a peripheral hormone and as a central neurotransmitter.⁹¹ Glucagon receptor is class B GPCR that is activated by glucagon. Glucagon-mediated stimulation results in activation of adenylate

cyclase and increased levels of intracellular cAMP.⁹² This promotes the activation of adenylate cyclase and thus regulates hepatic glucose homeostasis.⁹³

In order to determine whether RKN-1043 binds to CCKA, CCKB and glucagon receptor, *in vitro* binding assays were performed by Eurofins BioPharma Product Testing. The GPCR binding assays were performed in whole membranes expressing high levels of GPCRs, the binding of RKN-1043 to GPCRs was calculated as a percent inhibition of the binding of a radioactively labeled ligand, which is specific for each target. Table 2 shows percent inhibition of radiolabeled CCKA [¹²⁵I]CCK-8s, CCKB [¹²⁵I]CCK-8s and [¹²⁵I]glucagon ligand binding to their respective GPCRs upon treatment with 10 μM RKN-1043. Minimal effect (less than 25 %) on the GPCR binding was observed with RKN-1043 treatment. However, such inhibition (or stimulation) lower than 25% is not considered significant and mostly attributable to variability of the signal around the control level. Based on these results it was concluded that RKN-1043 does not bind to any of the tested receptors. Therefore, the predicted target binding was de-validated and these targets were not pursued further.

Table 2. Influence of RKN-1043 on radioligand labelled GPCR binding.

The *in vitro* binding assays were performed by Eurofins BioPharma Product Testing. RKN-1043 binding was calculated as a percent inhibition of the binding of radiolabeled CCKA [¹²⁵I]CCK-8s, CCKB [¹²⁵I]CCK-8s and [¹²⁵I]glucagon ligand specific for each target. The values represent the percent inhibition of the ligand binding obtained from two (n) independent experiments and their mean.

GPCR	Inhibition of control specific binding (%)		
	n1	n2	Mean ± s.d.
CCK1 (CCKA) (<i>h</i>) (agonist radioligand)	-6.2	-2.1	-4.2 ± 2.9
CCK2 (CCKB) (<i>h</i>) (agonist radioligand)	-22.8	-14.5	-18.7 ± 5.9
Glucagon (<i>h</i>) (agonist radioligand)	-22.1	-19.5	-20.8 ± 1.8

The SPiDER based target predictions based on the pharmacophoric similarity to established drugs did not lead to successful identification of the targets for RKN-1043. One of the drawbacks for predictions based on pharmacophoric similarity is the reliability of the biological data available for the established drugs. In addition, the pharmacokinetic

and pharmacodynamic properties of the small molecules greatly influence the bioactivity. Therefore, the predictions arising from curating such data might lead to target predictions that cannot be validated experimentally.

5.3.3 Influence of RKN-1043 on kinases involved in Hh signaling

Protein kinases play predominant role in the regulation of cellular processes. Phosphorylation of proteins by kinases leads to functional changes in the target protein. Therefore the effect of RKN-1043 on the kinases that are known to regulate Hh signaling was determined by Eurofins. The biochemical inhibition of the tested kinase by 10 μ M RKN-1043 was determined by activity based assays (Table 10). However, RKN-1043 did not influence the tested kinases and therefore needs further efforts on identification of the novel regulators of Hh signaling pathway.

5.3.4 Target identification by chemical proteomics

The initial biological characterization data suggest that RKN-1043 is a potent inhibitor of Hh signaling acting downstream of SMO. The computationally predicted targets PTP1B, CCKA, CCKB and glucagon receptor were de-validated by in house or external assays. Therefore, in order to identify the molecular target(s) of RKN-1043, chemical proteomics, i.e. affinity-based chromatography (*pull-down*) was employed. For this technique, an active and control (inactive) affinity probe are required to enrich the molecular targets in *pull-down* experiments that can be analyzed by mass spectrometry. In order to synthesize the active and control linkers, primary screening data of the compounds synthesized by Dr. Rishikesh Narayan and Dr. Erchang Shang were taken into consideration to delineate a structure-activity relationship (SAR) (Figure 25).

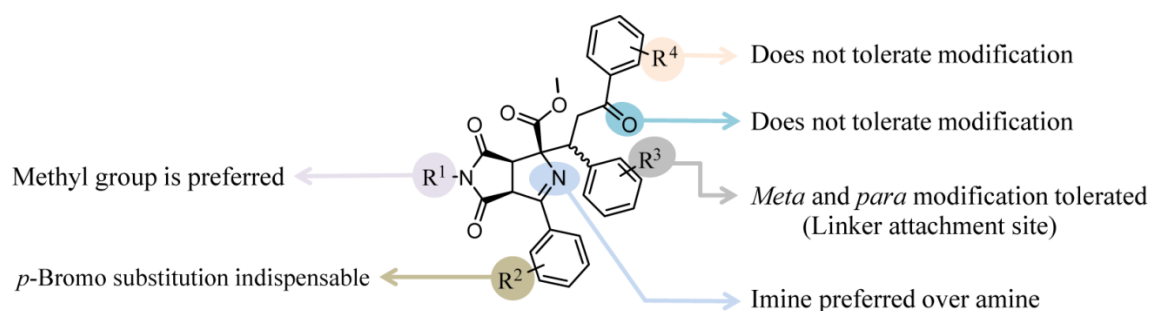


Figure 25. SAR for bridged bispyrrolidines based on the Hh pathway inhibition in osteogenesis assay and reporter gene assay.

Replacement of the methyl substituent on the bispyrrole at R^1 by a bulkier group led to decrease in bioactivity. *Para*-bromo substitution on the aryl ring (R^2) was indispensable for the bioactivity as other substitutions had a negative impact on the potency. The substitution pattern on the aryl rings (R^3 and R^4) of the chalcone was crucial for bioactivity. The aryl ring (R^3) tolerated modifications at *meta* and *para* positions with slight decrease in bioactivity. Modifications on the aryl ring (R^4) resulted in loss of bioactivity. Therefore, based on the SAR, R^3 was identified as suitable site for linker attachment as a range of substituents at *meta* and *para* position retained biological activity. Interestingly, RKN-1082, an analog with a bromine at the *para* position at R^4 was inactive in the GLI-reporter gene assay. Therefore, synthesis of an active and control *pull-down* probe was planned with linker attachment at the *para* position of R^3 on the chalcone part of the compound with or without bromine modification at the *para* position on R^4 . In addition, a simplified control probe was designed containing only the chalcone part.

The linker for the probe synthesis was prepared by mono-Boc protecting the amine on the 2,2'-(ethylenedioxy)-bis(ethylamine) (Figure 26). To avoid the di-Boc protection, one equivalent of di-*tert*-butyl dicarbonate was used with five equivalents of 2,2'-(ethylenedioxy)-bis(ethylamine). The resultant linker **1** was used without purification. 4-carboxy chalcone **2** was prepared by an aldol condensation of 4-carboxybenzaldehyde and acetophenone. Alternatively, compound **3** was prepared upon aldol condensation of 4-bromo-4-carboxybenzaldehyde and acetophenone. Finally, chalcone linker fragments **4** and **5** were prepared by amide coupling of **1** and **2** or **1** and **3**.

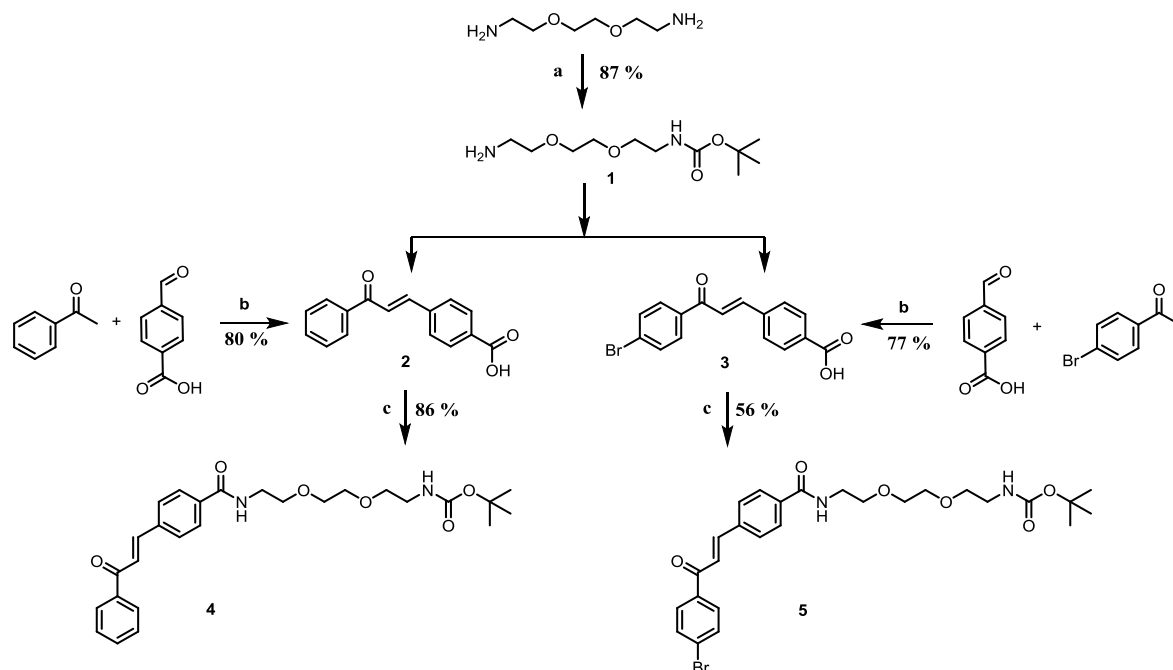


Figure 26. Synthetic scheme for chalcone-linker fragment synthesis.

(a) BOC₂O, DCM, 0 °C to rt, 18 h. (b) 20% KOH (aqueous) EtOH, rt, 16 h. (c) HBTU, Et₃N, DMF, rt, 16 h.

Compound **6** was prepared in two steps. In the first step, N-methyl maleimide and 4-bromo-iminoester underwent a [3+2] asymmetric cycloaddition catalyzed by tetrakis-(acetonitrile) copper(I) tetrafluoroborate to yield bispyrrole building block, which in a second step was oxidized by tert-butyl hydroperoxide to yield **6** (Figure 27).

In order to synthesize the active probe, **4** and **6** were stirred with tetrakis-(acetonitrile) copper (I) tetrafluoroborate and DBU to yield active probe **7** upon Michael addition. Similarly, **5** and **6** were stirred to prepare inactive probe **8**. The choice of control probe is crucial in the target identification process. Close similarity of the positive and negative linker is desired in order to reduce the number of proteins that bind non-specifically to the core scaffold. In this case, probes **7** and **8** are identical to each other except for the *para* substitution of bromine on the aryl ring (R⁴).

Compound **4** is a Michael acceptor, which may form covalent bonds to nucleophilic sites of proteins and DNA.⁹⁴ Therefore, to prepare the simplified control probe **9**, **4** was reduced by refluxing with dichloro(pentamethylcyclopentadienyl)iridium(III) dimer.

Having synthesized the desired probes, it was necessary to test their potency in the phenotypic assays. Therefore, the probes **7**, **8** and **9** were tested in GLI-reporter gene assay prior to Boc de-protection as the free amine group may interfere with the cell permeability and give rise to false negative outcomes (Figure 27). The desired active probe **7** ($IC_{50}=12.0 \mu\text{M}$) was less active than the hit molecule RKN-1043 ($IC_{50}=1.5 \mu\text{M}$). Attachment of the linker might have affected the cell permeability or the interaction with target molecule therefore leading to drop in activity. However, **7** was deemed sufficiently active to be used as a positive *pull-down* probe in affinity chromatography experiments. The planned control probe **8** and simplified control probe **9** were inactive with IC_{50} values of more than $50 \mu\text{M}$.

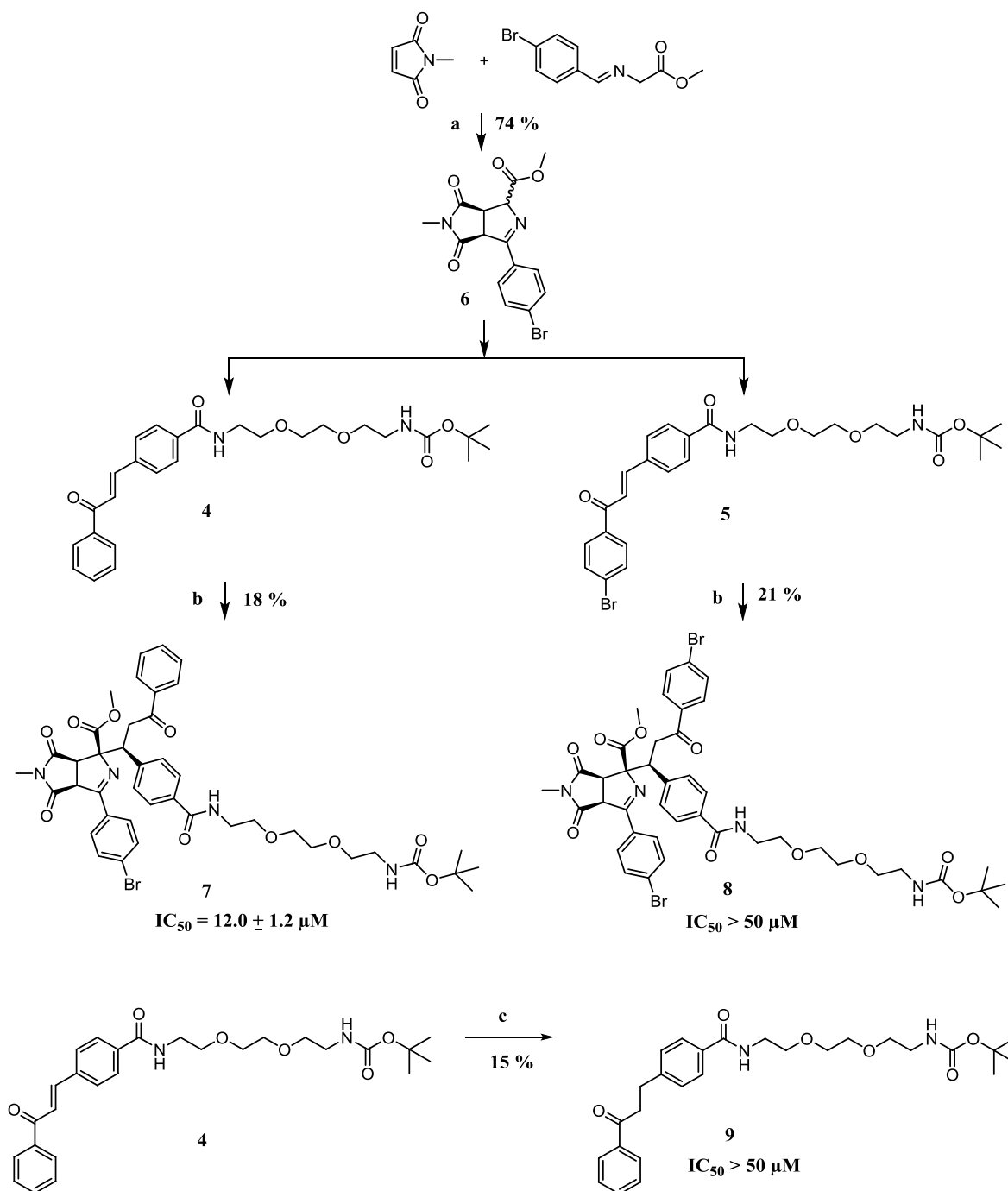


Figure 27. Synthetic scheme for the synthesis of pull-down probes.

(a) $\text{Cu}(\text{CH}_3\text{CN})_4\text{BF}_4$, (R)-Fesulphos, Et_3N , DCM, -10°C , 4 h. Then TBHP, rt, 4 d. (b) $\text{Cu}(\text{CH}_3\text{CN})_4\text{BF}_4$, DBU, DCM, rt, 16 h. (c) $[\text{IrCp}^*\text{Cl}_2]_2$, K_2CO_3 , iPrOH, 85°C 5 h. 7, 8 and 9 were tested in GLI-reporter gene assay in Shh-LIGHT2 cells. Cells were treated with $1.5 \mu\text{M}$ purmorphamine and different concentrations of 7, 8 and 9 for 48 h. Firefly and Renilla luciferase activities were determined and ratios of firefly luciferase/Renilla luciferase signals were calculated, which are a measure of Hh pathway activity. Nonlinear regression analysis was performed using a four parameter fit.

In order to use the probes in affinity chromatography experiments it was necessary to de-protect Boc group from the linkers in order to attach the probes on NHS-ester magnetic beads. The Boc protected linkers, **7**, **8**, and **9** were stirred with 20% trifluoroacetic acid in DCM at 25 °C. The solvent was evaporated under rotary evaporator to recover quantitative yields of **10**, **11**, and **12** in the form of TFA salts (Figure 28).

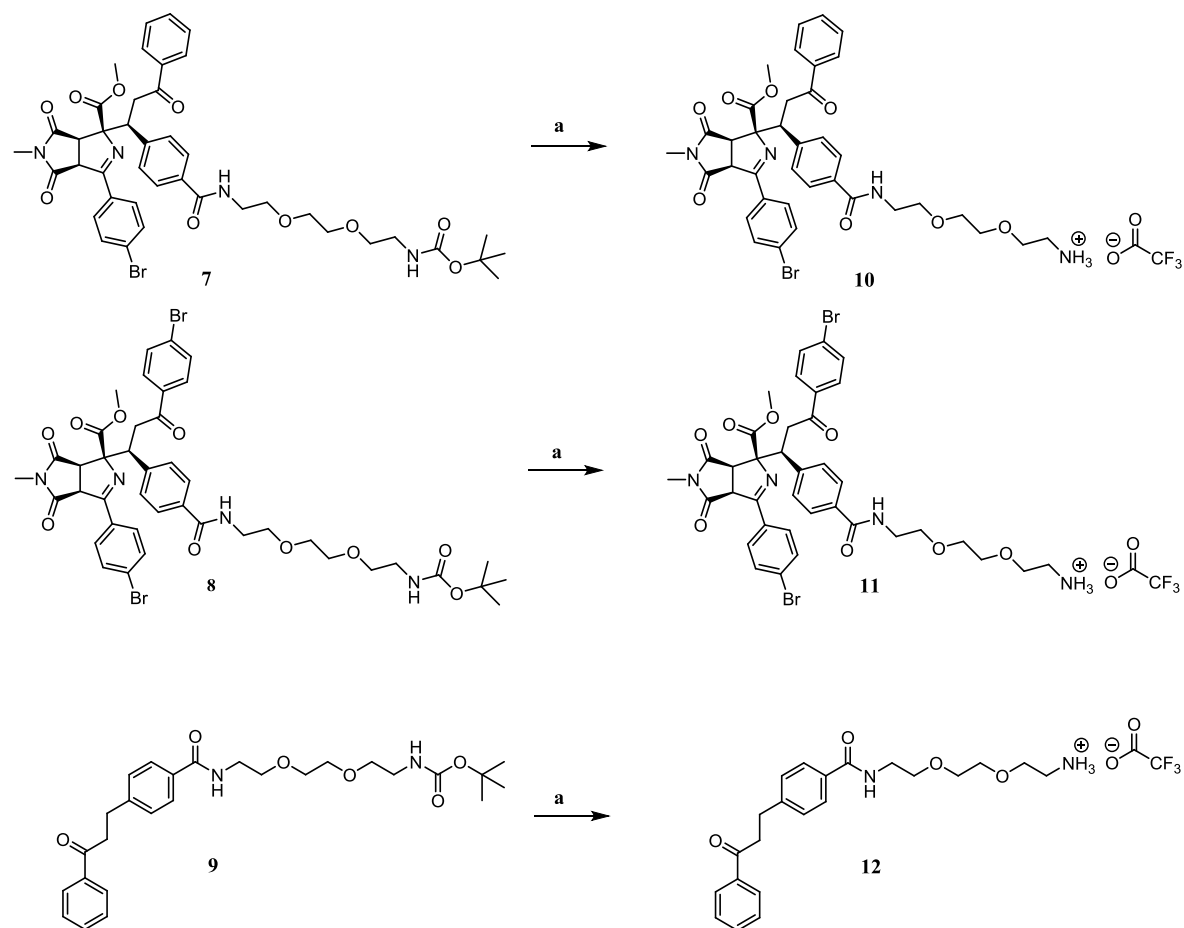


Figure 28. Synthetic scheme for synthesis of free amine *pull-down* probes.

(a) 20% TFA in DCM, rt, 5 h. The products **10**, **11** and **12** were recovered in quantitative yields.

5.3.5 Target identification by chemical proteomics

For affinity chromatography *N*-hydroxy-succinimide (NHS) ester magnetic beads were used as a solid support to immobilize *pull-down* probes **10**, **11** or **12**. The NHS functional group of the activated magnetic beads reacts with the primary amine group to form an amide linkage. In order to avoid non-specific binding of the proteins to residual active groups, the NHS ester groups were quenched with ethanolamine during the coupling stage. NIH/3T3 cell lysates were incubated with the immobilized probes to enable protein binding. Non-specifically bound proteins were removed by washing the immobilized probes with lysis buffer containing 25 mM magnesium chloride. For the enzymatic digestion of bound proteins, magnetic beads were incubated with trypsin and LysC endopeptidases that cleave within the polypeptide. Trypsin cleaves at the carboxyl side of the lysin or arginine except when they are followed by proline. The LysC peptidase acts on the carboxyl side of lysines. Trypsin and LysC were used in combination to achieve efficient peptide cleavage. The resulting peptides were purified as mentioned in section and analyzed by means of nano-HPLC / MS / MS. The mass spectrometry experiments were done at the HRMS facility at the MPI Dortmund and data analysis was performed by Dr. Petra Janning (MPI Dortmund). Statistical analysis was performed to quantify the proteins that were selectively enriched by the active probe as opposed to inactive probe.

The affinity chromatography experiments were performed in technical triplicates using the same lysate to increase reproducibility. Several proteins binding to the immobilized probes were identified indicating the successful immobilization of the probes on resin. Label-free quantification of proteins bound to active probe **10** and inactive probes **11** and **12** was performed to identify proteins that were enriched preferably with the active probe as compared to the inactive probes. Unfortunately, comparative analysis of active probe **10** with simplified probe **12** did not yield any statistically significant hits (data not shown). However, comparative analysis of active probe **10** with inactive probe **11** yielded 10 potential hits with statistical significance (Table 3).

The ratio column in Table 3 represents the fold enrichment of the proteins in active probe **10** against inactive probe **11**. Identified proteins such as ATPase inhibitor, guanine nucleotide-binding protein, ribosome-recycling factor, 60S ribosomal protein L10a, 60S ribosomal protein L32, Hsc70-interacting protein and tropomyosin alpha-4 chain were regarded as non-specific binders because they had comparatively low enrichment in the

active probe and had been frequently identified in previous *pull-down* experiments in the department. RHO GDP-dissociation inhibitor 1 (RHOGDI1), Filamin-B and Filamin-C were considered as potential targets of the RKN-1043 because of the relatively high fold enrichment. RHOGDI1 was identified with 33 fold enrichment by the active probe. Filamin-B and filamin-C are scaffold proteins and are frequently found in the other *pull-down* experiments performed in the department because of their higher abundance in cell lysates. However, in these particular experiments Filamin-B and Filamin-C were highly enriched in the presence of the active probe.

Table 3. List of proteins enriched by active probe 10 as identified by means of affinity chromatography.

Active probe **10** and inactive probe **11** were immobilized on NHS ester magnetic beads. NIH/3T3 lysate was passed on to the probes and target protein identification was performed following the aforementioned protocol. The ratios indicate the fold excess of protein enriched in active probe **10** than inactive *pull-down* probe **11**.

Protein names	Gene names	Ratio (A/I)
RHO GDP-dissociation inhibitor 1	Arhgdia	33
ATPase inhibitor, mitochondrial	Atpif1	4
Filamin-B	Flnb	36
Filamin-C	Flnc	27
Guanine nucleotide-binding protein subunit beta-2-like 1;Guanine nucleotide-binding protein subunit beta-2-like 1, N-terminally processed	Gnb2l1	6
Ribosome-recycling factor, mitochondrial	Mrrf	3
Ribosomal protein;60S ribosomal protein L10a	Rpl10a	-
60S ribosomal protein L32	Rpl32	9
Hsc70-interacting protein	St13	4
Tropomyosin alpha-4 chain	Tpm4	4

Interestingly, the addition of a single bromine on the active linker led to a difference in biological activity and binding to proteins in the lysate. The successful identification of the potential targets is a validation of the *pull-down* probe synthesis strategy.

With intention of validation and better quantification of the identified proteins, SILAC lysates were used in the affinity chromatography experiments. Several proteins were

identified bound to active and inactive probes. Unfortunately, statistical analysis of the ratios of heavy isotope-labelled proteins bound to the active probe (AH) and light isotope labelled protein bound to inactive probe (IL) (AH/IL) and vice versa the heavy isotope labelled protein bound to inactive probe and light isotope labelled protein bound to active probe (IH/AL) did not lead to identification of any protein targets with statistical significant identification score. Only one protein, high-mobility group protein HMG-I/HMG-Y was identified as hit with 0.5 SILAC identification score.

Moreover, the SILAC experiments failed to identify Filamin-B, Filamin-C and RHOGDI1 proteins. It was speculated that the 1:1 mixing step in the SILAC procedure might have led to dilution of the bound proteins, therefore, leading to protein concentrations that are below the detection limits of the HRMS instrument. To overcome this problem, the SILAC experiments were repeated with the use of double concentrations of lysate and less stringent washing steps. The salt concentration was varied to retain the weakly bound proteins during the washing steps. However, the change in the lysate concentration and less stringent washing steps did not yield a reproducible identification of potential targets.

Affinity chromatography-based target identification methods are efficient in identifying proteins that are bound to affinity probes. However, due to unspecific binders, the list of potential targets might harbor false positive potential targets. In order to identify the true target for further biological studies, prioritization and validation of the identified proteins is necessary. At this stage, RHOGDI1 was prioritized because of its possible involvement in Hh pathway regulation *via* RHO GTPases that are positive regulators of Hh signaling (discussed later in 5.3.6.1).

In order to validate RHOGDI1 as a potential target, immunoblotting after the *pull-down* was performed. Active and inactive probes were immobilized on the magnetic beads and exposed to NIH/3T3 cell lysates. The beads were washed to remove non-specifically bound proteins and heated in SDS sample buffer to elute proteins from the beads and denature the bound proteins. The resulting samples were then analyzed by SDS-PAGE followed by immunoblotting using a RHOGDI1-specific antibody (Figure 29). Higher enrichment of RHOGDI1 in positive probe can be seen as compared to control probe in the representative immunoblot. Quantification of the western blot image for the intensity

of RHOGDI1 revealed almost 2.5 fold higher enrichment by the positive *pull-down* probe as compared to control probe (Figure 29 B).

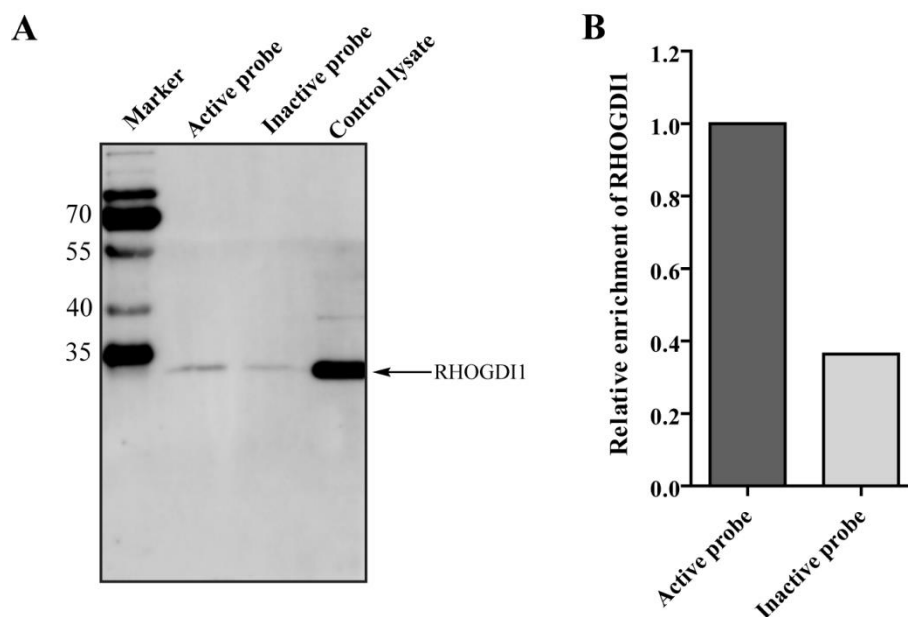


Figure 29. Validation of RHOGDI1 as a potential target of RKN-1043 by immunoblotting after the *pull-down*.

(A) Active probe **10** and inactive probe **11** were immobilized on NHS ester magnetic beads and exposed to NIH/3T3 lysates. Bound proteins were eluted and analyzed by immunoblotting using RHOGDI1 - specific antibody. (B) Quantification of RHOGDI1 enrichment in active probe (set to 1) against inactive probe. Data is representative of three independent biological replicates. (n=3)

This result confirms the target engagement of RHOGDI1 by the active *pull-down* probe. Therefore, further biophysical and genetic validation experiments were carried out to confirm RHOGDI1 as a target of RKN-1043.

5.3.6 Regulation of RHO GTPases by RHOGDI

The RAS homologous (RHO) family of GTPases regulates aspects of cell adhesion, migration and proliferation. RHO GTPases are a subfamily of the Ras superfamily of small GTPases. RHO GTPases are highly conserved in eukaryotes and CDC42, RAC1 and RHOA are the most studied members of the RHO GTPase family.⁹⁵ Formation of stress fibers and focal adhesion is controlled by RHOA,⁹⁶ whereas RAC1 regulates formation of membrane ruffles and lamellipodia⁹⁷ and CDC42 regulates the formation of actin microspikes and filopodia.^{98,99}

RHO GTPases like all G proteins act as molecular switches. The RHO GTPases are prenylated and cycle at the membrane between an active GTP-bound and inactive GDP-bound state (Figure 30). The GTPases bind and hydrolyze GTP for the generation of energy. The GTPases are regulated by GTPase activating proteins (GAPs), guanine nucleotide exchange factors (GEFs) and GDP-dissociation inhibitors (GDIs). RHOGEFs promote activation of RHO GTPases by stimulating the release of guanosine diphosphate (GDP) to allow binding of guanosine triphosphate (GTP)¹⁰⁰. Whereas, RHOGAPs bind to activated RHOGTPase and stimulate their GTPase activity that leads to inactive GDP-bound RHOGTPases.¹⁰¹ As an additional control, RHOGDIs act as negative regulators of RHO GTPases by sequestering the membrane bound inactive RHO GTPases (GDP-bound) to the cytoplasm to maintain them in a soluble inactive state.¹⁰² RHOGDIs constitutes a family of three mammalian members: RHOGDI1, RHOGDI2 and RHOGDI3.¹⁰³ Initially it was thought that RHOGDIs inhibit the loading and release of GDP and loading of GTP to GDP-bound RHO GTPase. However, later it was shown that RHOGDIs do not prevent loading of GDP or GTP to nucleotide-free GTPase but rather only inhibit the release of the GDP nucleotide.¹⁰⁴

At any given time point, the major fraction (90 - 95%) of prenylated RHO GTPases are maintained in stable soluble state in the cytosol by RHOGDI.¹⁰⁵ The isoprenoid moiety at the carboxy terminus of the RHO GTPases is essential for the proper folding, subcellular localization and signaling. However, in the absence of membranes, the highly hydrophobic isoprenoid moiety impairs the proper folding leading to the degradation of RHO GTPases. RHOGDI maintains the RHO GTPases in the cytosol and protects them from degradation by inserting the isoprenoid moiety in a hydrophobic geranylgeranyl (GerGer) binding pocket at the C-terminus of RHOGDI (Figure 31). In the absence of

RHOGDI the cytosolic fraction of GTPases is unstable and rapidly degraded by the proteasome.¹⁰⁵

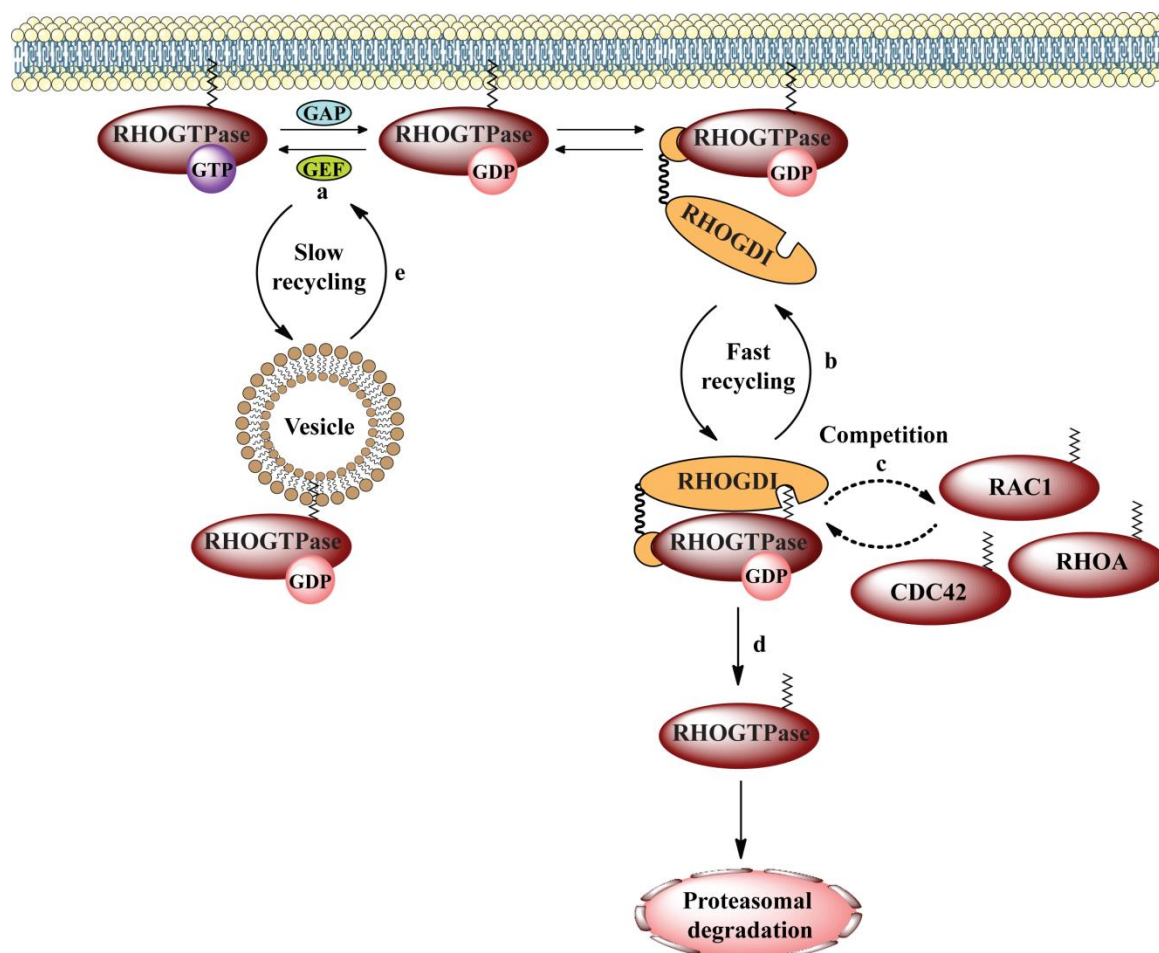


Figure 30. RHO GTPase regulation by RHOGDI.

(a) The prenylated RHO GTPase cycle at the membrane between an active GTP-bound and inactive GDP-bound state. Guanine nucleotide exchange factors (GEFs) promote activation of RHO GTPase by stimulating the release of guanosine diphosphate (GDP) to allow binding of guanosine triphosphate (GTP). Whereas, GTPase activating proteins (GAPs) bind to activated RHO GTPase (GTP bound) and stimulate their GTPase activity that leads to inactive GDP-bound RHO GTPases. (b) RHOGDIs act as negative regulators of RHO GTPases by sequestering the membrane bound inactive RHO GTPases (GDP-bound) in the cytoplasm in inactive soluble state. (c) Several RHO GTPases can associate with RHOGDIs and compete for binding. Overexpression of GTPase can displace the endogenous GTPase proteins from RHOGDI, targeting them for degradation. (d) Free prenylated cytosolic RHO GTPases are unstable and are rapidly degraded by the proteasome. (e) A slower pathway for recycling RHO GTPases through vesicle trafficking has also been postulated. (Adopted from Rafael Garcia-Mata *et al.*, 2011)¹⁰⁶

It is proposed that RHOGDIs act as molecular chaperones by stabilizing RHO GTPases in the cytosol and shuttling them between different membrane compartments. However, there is different evidence to support or oppose the chaperone-like function of RHOGDI. When mutants of constitutively active RAC1 and CDC42 were expressed in RHOGDI-null cells or wild type cells, no significant difference in the localization of RAC1 and CDC42 was found. This lead to the conclusion that RHOGDIs are not needed for the

translocation of RHO GTPases to the membrane compartments.^{107,108} Contrasting to these observations, a RAC1 double mutant with impaired binding to RHOGDIs failed to cycle between membranes. Also, a double mutant CDC42, which is unable to associate with RHOGDI, accumulated at the perinuclear region rather than translocating to the plasma membrane. Thus supports the chaperone-like function of RHOGDIs. Alternatively, studies in yeast have proposed RHO GTPase cycling *via* relatively slow vesicular trafficking.¹⁰⁹

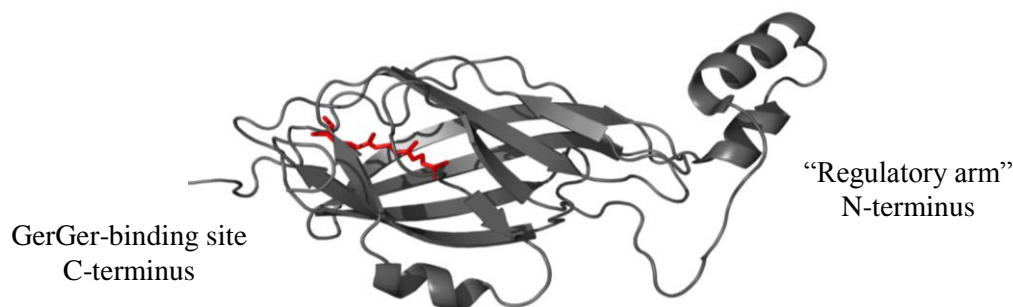


Figure 31. Crystal structure of RHOGDI1 in complex with a GerGer group (4F38).

The regulatory arm at the N-terminal domain of RHOGDI binds to the switch I and II domains of RHO GTPases. The GerGer group is represented in red bound to the binding pocket on the C-terminus of RHOGDI. The crystal structure is adapted from GerGer-RHOA in complex with RHOGDI1.¹¹⁰

The co-existence of two pathways for translocation of RHO GTPases to membranes thus explains the proper localization of constitutively active RHO GTPases that cannot interact with RHOGDI.^{107,108} Moreover, even in the absence of RHOGDI a small fraction of RHO GTPase is localized to the plasma membrane *via* slower vesicle trafficking that is sufficient for inducing the observable phenotype. Therefore, it is proposed that knockout of RHOGDI might lead to milder phenotypes due to alternative trafficking *via* vesicles.¹⁰⁶

5.3.6.1 RHO GTPases in Hh signaling

Literature evidence supports the cross-talks between RHO GTPases and Hh signaling (Figure 32). In a series of studies by Natalia Riobo *et al.*, it was demonstrated that Hh isoforms are capable of stimulating RHOA and RAC1 in a G_i -dependent manner. Stimulation of serum-starved HUVEC cells with SHH resulted in three fold increase in the levels of RHOA-GTP as indicated by *pull-down* assays. Interestingly, pre-incubation of serum-starved HUVEC cells with either 0.5 μ M KAAD-cyclopamine or 100 ng/mL pertussis toxin (inhibitor of G_i protein) prevented activation of RHOA by SHH indicating that RHOA activation by SHH involves SMO and G_i proteins.¹¹¹ Follow-up studies showed that stimulation of NIH/3T3 cells with SHH led to activation of RHOA and RAC1 dependent on SMO and independent of GLI transcription factors.

Interestingly, Kenji Kesai *et al.* have demonstrated that constitutive activation of RHOA induces GLI-mediated transcription, whereas dominant negative RHOA suppressed SHH-mediated activation of GLI transcription.¹¹² Extensive genetic studies by Steve Choi *et al.* in hematopoietic stem cells have shown that constitutively active mutant of *RAC1* induced higher expression of *GLI-2* and *SHH*. Conversely, blocking *RAC1* activity by dominant negative *RAC1* decreased the expression of *GLI-2* and *SHH*, therefore suggesting a GLI-dependent regulation of Hh signaling by RHO GTPases.¹¹³

The literature reports described above demonstrate a complex interplay between Hh signaling and RHO GTPases. These studies propose two types of non-canonical Hh signaling involving RHO GTPases that are dependent and independent of GLI transcription factors. Based on this it can be summarized that activation of RHO GTPase results in activation of Hh signaling, and inhibition of the RHO GTPases results in inhibition of Hh signaling.

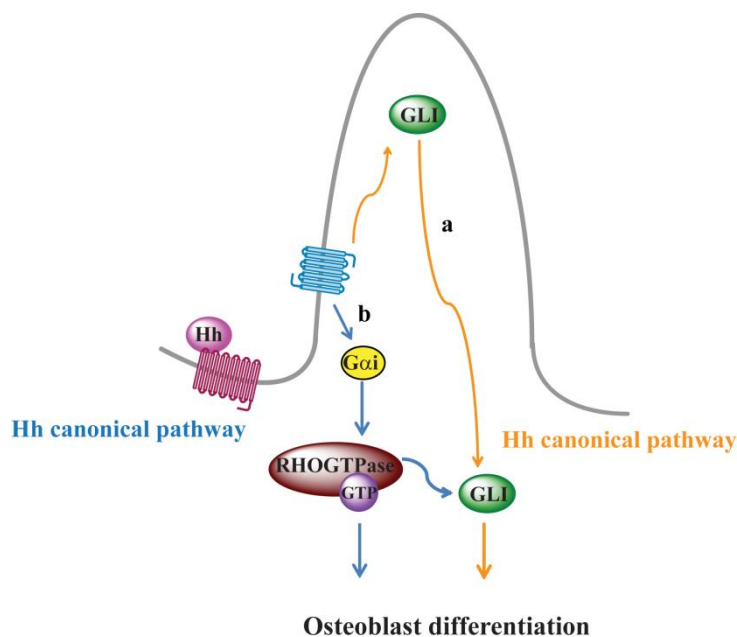


Figure 32. Cross-talks between RHO GTPases and Hh signaling.

Schematic representation of complex interplay between Hh signaling and RHO GTPase. (a) Canonical Hh signaling *via* SMO and GLI (orange arrows). (b) Two types of non-canonical Hh signaling involving RHO GTPases that are dependent and independent of GLI transcription factors (blue arrows).

5.3.7 RKN-1043 binds to the GerGer binding pocket of RHOGDI1

In order to further investigate the binding of RKN-1043 to RHOGDI1, the effect of RKN-1043 on RHOGDI1's interaction with RHO GTPases was investigated. RHOGDI1 sequesters GDP-bound inactive RHO GTPases as soluble fraction in the cytosol. It is proposed that binding of RHOGDI1 to RHO GTPases is a two-step process. In the first step the regulatory arm at the N-terminal domain of RHOGDI1 binds to the switch I and II domains of RHO GTPase. This binding leads to slower isomerization of RHOGDI1 and insertion of geranylgeranyl moiety into the hydrophobic pocket of RHOGDI1, resulting in RHO GTPase release from the membrane.

In order to determine the effect of RKN-1043 on RHOGDI1's binding to RHO GTPases, fluorescence polarization experiments were performed by Mohammad Akbarzadeh at Heinrich Heine University Düsseldorf. TAMRA-GDP-bound-RAC1 was titrated with increasing concentrations of RHOGDI1 in the presence or absence of 50 μ M RKN-1043 (Figure 33). The prenylated-RAC1 and RHOGDI1 have K_d value of >40 nm.¹¹⁴ However, the RAC1 used in these experiments was non-prenylated, as prenylated GTPases precipitate in the employed buffer, thus making it difficult to use in the experiments. In the absence of RKN-1043, RHOGDI1 could bind to non-prenylated RAC1 with

dissociation constant (K_d) of 14 μM which correlates with the earlier reported K_d of >10 μM for non-prenylated RAC1 and RHOGDI1.¹¹⁴ The higher K_d value is attributed to the use of non-prenylated RAC1 that has weaker binding affinity for RHOGDI1 because of the absence of the prenyl moiety. In the presence of RKN-1043, the K_d value for the RHOGDI1-RAC1 interaction was increased to 134 μM . The ~ 10 fold higher K_d value for RHOGDI1-RAC1 interaction indicates that RKN-1043 interferes with RHOGDI1's association with RAC1-GDP.

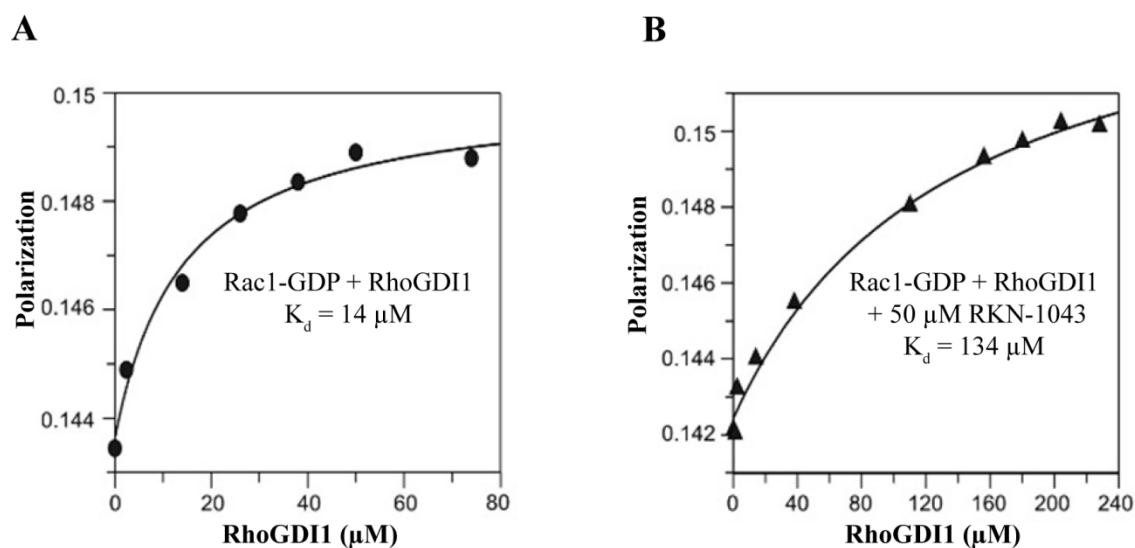


Figure 33. Influence of RKN-1043 on the binding of RAC1 to RHOGDI.

Fluorescence polarization measurements were performed by titrating 1 μM TAMRA-GDP-bound RAC1 with increasing concentrations of RHOGDI1 in the (A) presence of DMSO or (B) 50 μM RKN-1043. Data is representative of three independent experiments.

Further, the effect of RKN-1043 on the RHOGDI1 mediated extraction of prenylated RAC1-GDP from membranes was studied using a liposome sedimentation assay. Synthetic liposomes were prepared and prenylated GDP-bound RAC1 was immobilized on the liposomes. The presence of the prenyl moiety facilitates the insertion of RAC1 into the liposomes. RHOGDI1 was added to the liposomes followed by ultra-centrifugation to pellet the liposomes. The addition of RHOGDI1 to the liposome resulted in extraction of RAC1 as seen in Figure 34, wherein RAC1 is mostly detected in the supernatant fraction. Addition of RKN-1043 along with RHOGDI1 resulted in detection of RAC1 in the pellet containing liposomes, indicating the inhibition of RHOGDI1-mediated RAC1 extraction. As an additional control to confirm the specificity of RKN-1043, a structurally similar inactive analog of RKN-1025 was used in the sedimentation experiment. Addition of 50 μM RKN-1025 along with RHOGDI1 to the liposomes did not affect the function of

RHOGDI1 as RAC1 was detected in the supernatant. This suggests a RKN-1043 specific inhibition of RHOGDI1 function.

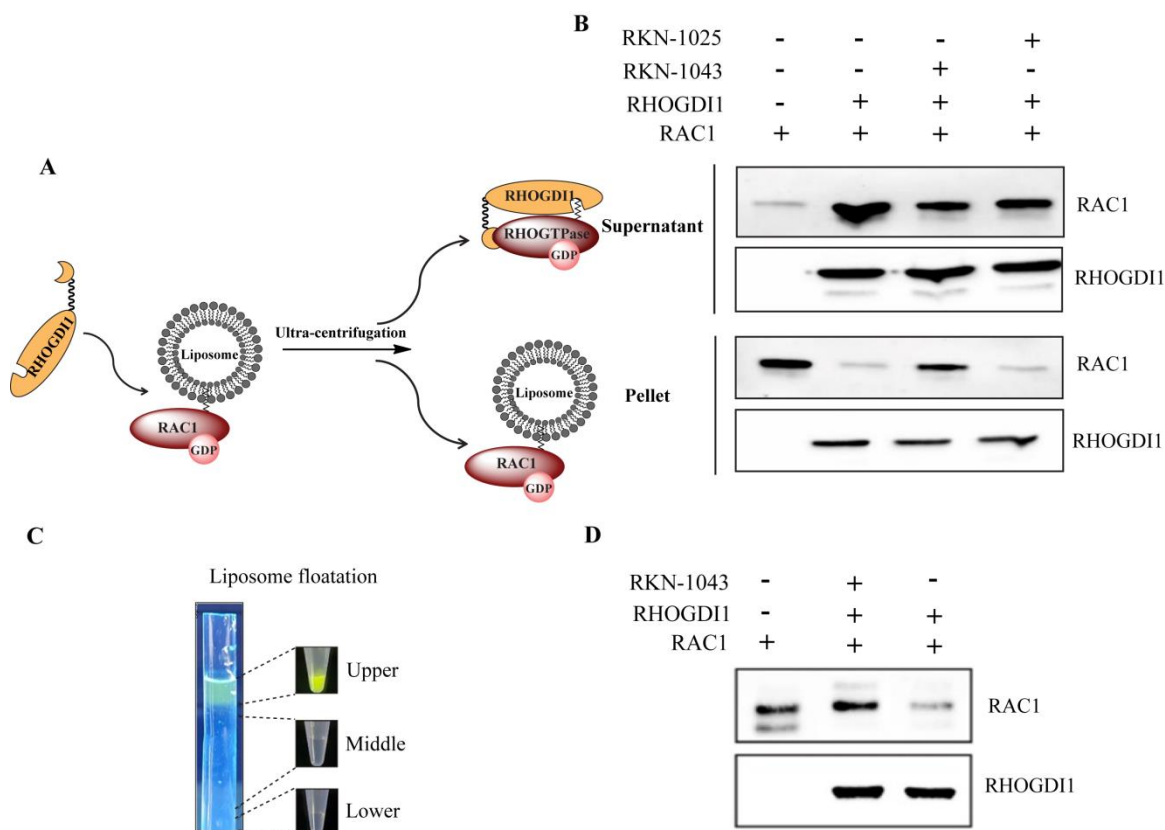


Figure 34. Influence of RKN-1043 on RHOGDI1-mediated extraction of prenylated RAC1-GDP from liposomes.

(A) Schematic representation of the liposome sedimentation assay. (B) Displacement of prenylated GDP-bound RAC1 from synthetic liposomes by GST-RHOGDI1 in the presence and in the absence of 50 μ M RKN-1043 or RKN-1025 was measured using liposome sedimentation assay. (C and D) Prenylated GDP-bound RAC1 displacement from liposomes by GST-RHOGDI1 in the presence or absence of 50 μ M RKN-1043 was analyzed under the same condition as in A by liposome floatation assay. (C) Fractions collected after gradient centrifugation. (D) The upper fraction containing liposomes was analyzed by WB. Data is representative of three independent experiments. (n = 3)

The long centrifugation step in the liposome sedimentation assay could lead to false positive results as protein precipitates can be confused with the liposome pellet. To overcome this shortcoming, liposome floatation assays were performed by Mohammad Akbarzadeh (Figure 34 C and D). The principle of the floatation assay is similar to the sedimentation assay except for the use of a sucrose gradient to separate the liposomes. The synthetic liposomes were prepared using 0.2% fluorescent NBD-PE as mentioned in section 7.5.6. Upon addition of RHOGDI1 to the liposome-associated RAC1, liposomes were separated by centrifugation under sucrose gradient. Upon centrifugation, the liposomes were detected in the upper fraction as indicated by fluorescent color of

liposomes. The liposome-containing fractions were analyzed by immunoblotting using RAC1-specific antibodies. Similar to the sedimentation assay, RHOGDI1 could extract RAC1 from liposomes as indicated by the low intensity band in the Figure 34 D. Addition of 50 μM RKN-1043 along with RHOGDI1, inhibited RHOGDI1s ability to extract RAC1 from liposomes as indicated by the presence of a RAC1 band in the liposome fractions. Overall, these experiments demonstrate that RKN-1043 specifically interferes with the RHOGDI1-RAC1 interaction and inhibits the RAC1 extraction by RHOGDI1. The inability of the inactive analog RKN-1025 to interfere with the RHOGDI1-RAC1 interaction in the sedimentation assay is an evidence of specificity of RKN-1043 towards RHOGDI1.

Surface plasmon resonance (SPR) experiments were performed as an additional proof of RKN-1043 interference with RAC1 extraction by RHOGDI1. SPR enables the detection of protein-protein interactions in real time, without the use of labels. The detection system is equipped with gold L1 sensor chip that changes refractive index upon binding of biomolecules on its surface. In Figure 35 A, an increase in the response units (RU) upon loading synthetic liposomes on the L1 sensor chip indicates the immobilization of liposomes on the chip. Further, the addition of 5 μM prenylated GDP-bound RAC1 to the immobilized liposomes resulted in a massive RU increase that indicates RAC1 binding to the liposomes on the chip (Figure 35 B). The signal remained relatively stable after washing with buffer but rapidly decreased upon injection of 25 μM RHOGDI1 mixed with 50 μM of the inactive derivative, RKN-1025. Addition of RHOGDI1 displaced liposome-bound RAC1 significantly slower as compared to RKN-1025 when 50 μM RKN-1043 was added. Calculated rate constants by mono-exponential fitting of RU decays were 0.002 and 0.0032 s^{-1} for RHOGDI1-mediated RAC1 displacement from the liposomes in the presence of RKN-1043 and RKN1025, respectively. This confirmed the ability of RKN-1043 towards inhibition of RAC1 extraction by RHOGDI1.

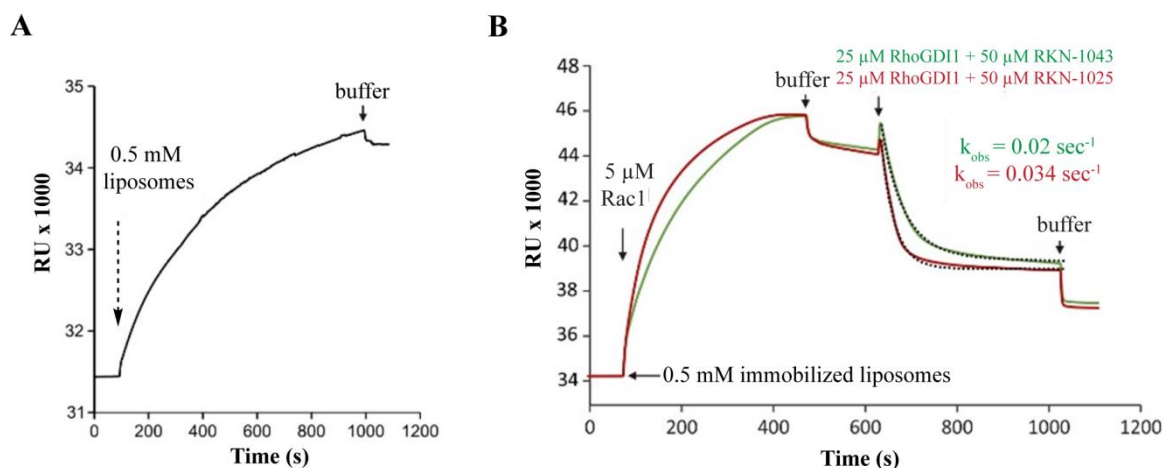


Figure 35. Influence of RKN-1043 on RHO GDI1 mediated extraction of GerGer-RAC1 from liposomes as determined by SPR.

(A) Synthetic liposomes were loaded on the L1 sensor chip for a period of 1000 sec. (B) Prenylated-GDP-bound RAC1 was next loaded on the immobilized liposomes. After washing with buffer 25 μ M RHO GDI1 premixed with 50 μ M RKN-1043 or RKN-1025 was added to the L1 chip and change in the RU was followed over time. Data are representative of three independent experiments.

The findings from the fluorescence polarization experiment, the liposome sedimentation assay, the liposome flotation assay and SPR measurements validate the interference of RKN-1043 with RHO GDI1's function. Reproducibility of this outcome in diverse assays indicates the definite interference of RKN-1043 with the membrane extraction function of RHO GDI1. However, the binding site of RKN-1043 cannot be deduced from the above mentioned experiments. Therefore, to elucidate the mode of inhibition and binding site of RKN-1043 on RHO GDI1, fluorescence polarization experiments with fluorescein (FITC)-labelled GerGer-Rab1 peptide were performed. Although RabGTPases bind to RHO GDI1 with weaker affinity than RHO GTPase, the interaction is sufficient to study whether RKN-1043 can bind to the GerGer binding pocket of RHO GDI1.¹¹⁵ A rapid increase in the polarization was observed upon addition of RHO GDI1 to FITC-GerGer-RAB1 peptide indicating RHO GDI1-Rab1 peptide binding as a result of insertion of the GerGer group into the hydrophobic pocket of RHO GDI1 (Figure 36). The addition of RKN-1043 to this setup in 10 μ M steps resulted in steady reduction in polarization. This stepwise drop in the polarization indicates competition of RKN-1043 with GerGer-RAB1 peptide for binding to the GerGer binding pocket. This finding demonstrates that RKN-1043 binds most likely to the GerGer binding hydrophobic pocket of RHO GDI1 thus explaining the inhibition of RHO GDI1-mediated extraction of RAC1-GDP.

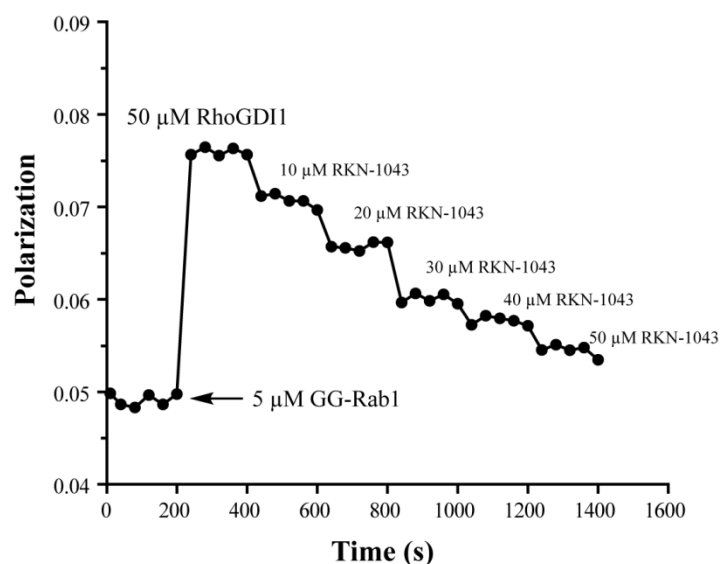


Figure 36. Competition of RKN-1043 with FITC-labelled GerGer-Rab1 peptide for binding to RHOGDI1.

Fluorescence polarization measurements were performed by titrating RKN-1043 into mixture of 5 μM FITC-labelled GerGer-Rab1 peptide and 50 μM RHOGDI1.

A small molecule library was synthesized by mimicking the biosynthesis of the natural product galanthamine on polystyrene beads. Screening of this library led to identification of secramine-an potent inhibitor of the endoplasmic reticulum-to-Golgi-to-plasma membrane transport of a viral glycoprotein fused to green fluorescent protein. Secramine is proposed to modulate CDC42 by stabilizing the RHOGDI1-CDC42 interaction thus leading to inhibition of endoplasmic reticulum-to-Golgi-to-plasma membrane transport of glycoproteins.¹¹⁶ The inhibitory effects of secramine were dependent on the presence of RHOGDI1. However, direct binding of secramine to RHOGDI1 was not proven experimentally. Therefore, RKN-1043 is the first molecule to bind directly to the GerGer binding pocket of RHOGDI1, thus inhibiting its function of membrane extraction.

5.3.8 Genetic validation of RHOGDI1 as target of RKN-1043

RHOGDI1 was identified as a potential target of RKN-1043 by affinity-based chemical proteomics. Biophysical experiments including a liposome sedimentation assay, fluorescence polarization assay and SPR binding assay confirmed the direct binding of RKN-1043 to the GerGer binding pocket of RHOGDI1. However, a direct involvement of RHOGDI1 in Hh pathway regulation is not known. Therefore, the effect of RKN1043-RHOGDI1 interaction on the regulation of Hh signaling needed to be explored. In order to understand the role of RHOGDI1 in the regulation of Hh signaling pathway, RHOGDI1 gene expression can be modified by dominant negative controls, antisense oligonucleotides, peptide nucleic acids, ribozymes, and siRNAs.¹¹⁷

5.3.8.1 siRNA-mediated RHOGDI1 knockdown

RNA interference (RNAi) offers a number of advantages over other techniques. The transient knockdown mediated by siRNA does not completely diminish the expression of a target gene. This is particularly advantageous when the target gene is necessary for cell survival as in the case of RHOGDI1 as it directly or indirectly governs cell proliferation and other vital cellular processes.¹¹⁸ siRNA can be synthetically designed to specifically target the gene isoform of interest, thus increasing specificity. Moreover, siRNA-mediated knockdown can be easily monitored by western blotting of the target protein or qPCR of the target mRNA.¹¹⁷ The siRNA has two strands of RNA, an antisense guide strand and a passenger strand. Upon liposome mediated delivery of siRNA into the cells, this double-stranded RNAs are processed by Dicer into a duplex of 19 to 25 bp in length with 3 dinucleotide overhangs. Subsequently, this duplex is incorporated into a silencing complex known as RNA-induced silencing complex (RISC). The siRNA-RISC complex recognizes and induces cleavage of the target mRNA.¹¹⁹

The siRNA-mediated target knockdown causes reduction in the concentration of the target protein within the cell, potentially leading to alterations in the observed phenotype.^{12,120} The target protein is regarded as a positive regulator of phenotype, if its knockdown phenocopies the effect of an inhibitor. In this case lower concentrations of inhibitor are required to observe the similar phenotype compared to the cells expressing normal target protein levels.¹⁹ However, if the knockdown of the target leads to increased

expression of a phenotype then the target is regarded as a negative regulator of phenotype.

5.3.8.1.1 siRNA-mediated RHOGDI1 knockdown

For the evaluation of the influence of RHOGDI1 knockdown on the Hh signaling pathway and the osteoblast differentiation assay, siRNA-mediated RHOGDI1 knockdown efficiency was optimized with regard to the siRNA sequence and the concentration of the siRNA.

Initially, three different RHOGDI1 siRNA sequences and a control siRNA were tested. The control siRNA has no specific complementary sequence to a mouse gene as it contains at least four mismatches to all mouse genes, and thus served as a reference for unspecific effects of siRNA transfection. In order to evaluate RHOGDI1's knockdown efficiency, C3H/10T1/2 cells were treated with 10 and 30 nM RHOGDI1 siRNAs along with 2% (v/v) DharmaFECT™ as a transfection reagent. Figure 37 A shows a successful knockdown of RHOGDI1 in C3H/10T1/2 cells. All three siRNAs reduced RHOGDI1 abundance as demonstrated by immunoblotting for all tested concentrations as compared to the control siRNA. Figure 37 B shows the quantification of the RHOGDI1 knockdown efficiency. Amongst the three siRNAs, RHOGDI1 siRNA-1 was most efficient in reducing the RHOGDI1 protein expression at 10 nM and 30 nM concentrations. Interestingly, RHOGDI1 siRNA-1 was most efficient when used at 10 nM showing only 18% RHOGDI1 expression. On the basis of these results, RHOGDI1 siRNA-1 and 2% (v/v) DharmaFECT™ were chosen for the following knockdown experiments.

In order to determine the effect of RHOGDI1 knockdown on Hh signaling pathway, an osteoblast differentiation assay was performed following RHOGDI1 knockdown. Two populations of C3H/10T1/2 cells were transfected with RHOGDI1 siRNA-1 and control siRNA following the optimized conditions. Cells were reseeded 48 h later in 96-well plates and treated with 1.5 µM purmorphamine and various concentrations of RKN-1043 or DMSO as a control. In the case of RHOGDI1 knockdown 2.5 fold stronger activation of Hh signaling was observed upon purmorphamine treatment as compared to purmorphamine treatment of cells transfected with control siRNA (Figure 37 C), thus indicating that RHOGDI1 is a negative regulator of Hh signaling. Figure 37 D shows the luminescence values upon treatment of the siRNA-transfected cells with various concentrations of RKN-1043. Both curves show a RKN-1043 concentration-dependent

reduction in the Hh pathway activity. Noticeably, the Hh pathway activity is significantly enhanced in cells with depleted RHOGDI1. In addition, RKN-1043 is less potent in inhibition of osteoblast differentiation in RHOGDI1-depleted cells as marked by the shift in inhibition curve to higher concentrations, thereby confirming the modulation of RHOGDI1 by RKN-1043 and involvement of RHOGDI1 in Hh regulation.

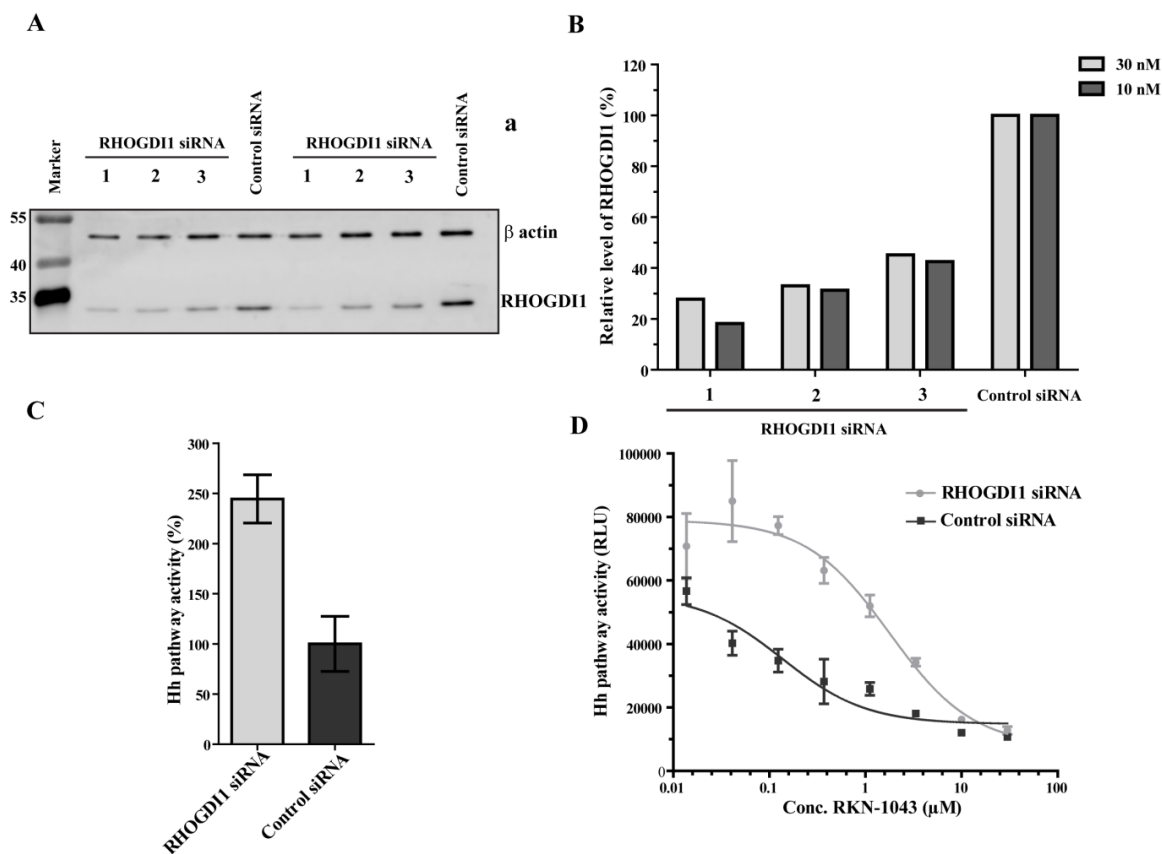


Figure 37. siRNA-mediated knockdown of RHOGDI1 and its influence on Hh signaling.

(A) C3H/10T1/2 cells were transfected with 10 and 30 nM RHOGDI1 siRNAs and control siRNA using 2% (v/v) DharmaFECT™ as a transfection reagent. Cells were lysed and RHOGDI1 knockdown was detected by immunoblotting using anti-RHOGDI1 antibody. (B) After densitometric analysis of the bands that were detected in A, the knockdown efficiency was calculated by first normalizing the band intensities of RHOGDI1 to the intensities for the bands for β-actin in respective samples. RHOGDI1 expression in the control siRNA samples were set to 100%. (C) C3H/10T1/2 cells were transfected with 10 nM RHOGDI1 siRNA-1 and control siRNA using 2% (v/v) DharmaFECT™ as a transfection reagent. 48 h later cells were treated with 1.5 μM purmorphamine and DMSO and osteoblast differentiation was monitored after 96 h. The Hh pathway activity in cells treated with control siRNA was set to 100%. (D) C3H/10T1/2 cells were transfected with 10 nM RHOGDI1 siRNA-1 and control siRNA using 2% (v/v) DharmaFECT™ as a transfection reagent. 48 h later cells were treated with 1.5 μM purmorphamine and different concentrations of RKN-1043 and osteoblast differentiation was monitored after 96 h. The curves represent the relative light units (RLU) as measure of Hh pathway activity. Data are mean values of three technical replicates and are representative of three biological replicates (N = 3, n = 3).

As summarized in section 5.3.6.1, RHO GTPases have been linked to Hh signaling as positive regulators. Thus, activation of RHO GTPases leads to activation of Hh signaling.¹¹² RHOGDI1 plays a critical role in the regulation of RHO GTPases as in the

absence of RHOGDI, cytosolic fractions constituting 90-95% of total RHO GTPases are unstable and are rapidly degraded by the proteasome (see 5.3.6). However, William Bozza *et al.*, have shown that knockdown of RHOGDI1 indeed led to slight decrease in the total RHO GTPase, while the levels of active RHO GTPases (GTP-bound) were significantly higher in RHOGDI-deficient cells compared to control cells.^{121,122} The depletion of RHOGDI in the cells leads to higher retention of inactive RHO GTPases (GDP-bound) at the membrane that are eventually activated by GEFs. As a result, more active RHO GTPases are detected at the membrane upon RHOGDI1 knockdown. Accordingly, depletion of RHOGDI1 was expected to mark activation of Hh signaling as a result of increased levels of active RHO GTPase (GTP-bound) that are positive regulators of Hh signaling. Agreeable results were obtained upon RHOGDI1 knockdown that led to activation of Hh signaling and therefore higher concentrations of RKN-1043 are needed to inhibit the Hh pathway (Figure 37).

The two-step binding process of RHOGDI to RHO GTPases leads to release of RHO GTPase from the membrane. The binding of regulatory arm at the N-terminal domain of RHOGDI to the switch I and II domains of RHO GTPase inhibits the interaction of GEFs with RHO GTPase.¹²³ This binding leads to slower isomerization of the RHOGDI and insertion of the GerGer moiety in the hydrophobic pocket of RHOGDI, resulting in RHO GTPase release from the membrane. The GerGer binding pocket of RHOGDI1 is crucial for maintaining the RHO GTPases in stable and soluble form in the cytosol. RKN-1043 is an inhibitor of Hh signaling that binds to the GerGer binding pocket of RHOGDI1. Therefore, it is tempting to speculate that RKN-1043 displaces the GerGer moiety from the binding pocket thus leading to release of the GerGer moiety in the cytosol. This release of GerGer moiety induces misfolding and proteasomal degradation of the RHO GTPases thus causing RHO GTPase and Hh pathway inhibition (Figure 38). The contradicting outcome of the RHOGDI1 knockdown indicates that perturbation by RKN-1043 and RNAi knockdown of RHOGDI1 have different impact on the RHO GTPase regulation cycle. In the case of RKN-1043 mediated RHOGDI1 perturbation, only the GerGer binding pocket at C terminus of RHOGDI1 is inhibited while the regulatory arm might remain bound to the switch I and II domains of RHO GTPase. The inactive RHO GTPase in complex with RHOGDI would be inaccessible to the GEFs that can facilitate the activation of RHO GTPase, thus causing RHO GTPase and Hh pathway inhibition. Whereas, upon RNAi knockdown, RHOGDI's binding at switch I and II domains and

GerGer moiety are reduced. Therefore, based on these observations, RHOGDI1 inhibition by RKN-1043 cannot be compared with RHOGDI1 knockdown by siRNA. Thus, the knockdown of RHOGDI1 does not lead to phenocopy of RKN-1043.

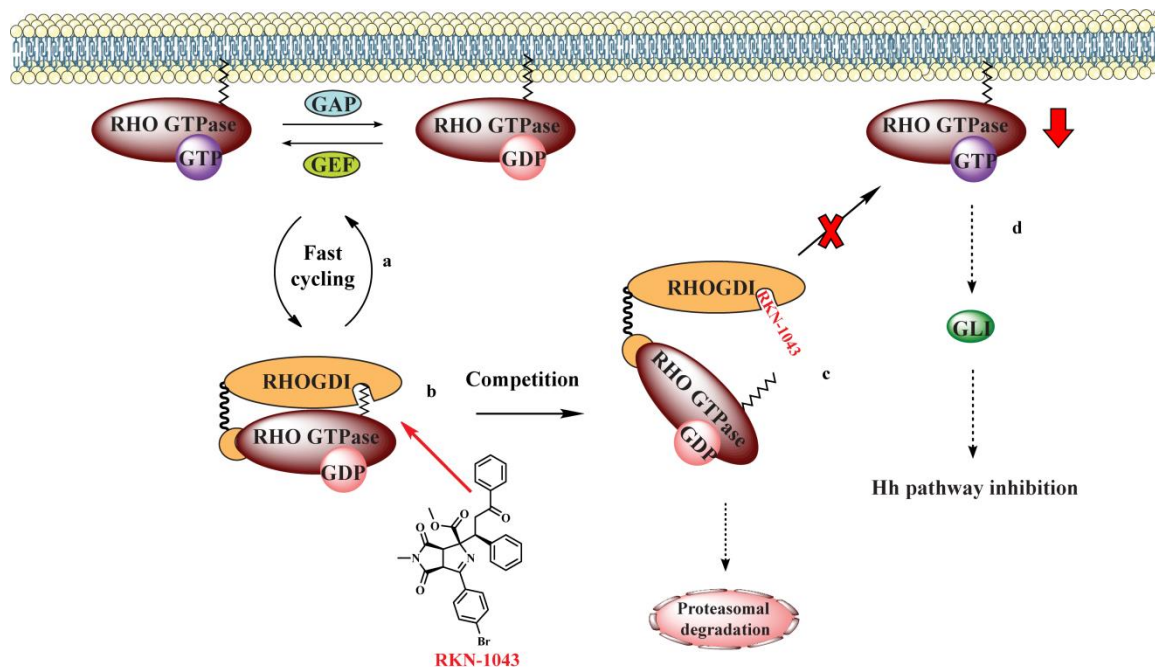


Figure 38. Schematic representation of proposed mode of action for Hh pathway inhibition by RKN.

(a) The prenylated RHO GTPase cycle at the membrane between an active GTP-bound and inactive GDP-bound state. GEFs promote activation of RHO GTPase, whereas, GAPs bind to activated RHO GTPase and stimulates their GTPase activity that leads to inactive RHO GTPases. (b) RKN-1043 binds to GerGer binding pocket of RHOGDI1 (c) Binding of RKN-1043 to GerGer binding pocket leads to release of the GerGer moiety in the cytosol. This release of GerGer moiety induces misfolding and proteasomal degradation of the RHO GTPases. (d) Inhibition of RHO GTPases leads to inhibition of Hh signaling pathway.

5.3.8.2 Effect of RHOGDI1 overexpression on Hh signaling

Similar to the siRNA-mediated knockdown of the RHOGDI1, the over-expression in the C3H/10T1/2 cells was optimized to achieve efficient transfection of RHOGDI1 expression plasmid. Over-expression increases the cellular protein levels, therefore allowing a complementary study to RHOGDI1 knockdown.

The transfections of the RHOGDI1 expression plasmid using the lipid-based transfection reagent Lipofectamine LTX & PlusTM were performed as described in the section 7.6.2. In the course of the optimization, different volumes of the transfection reagent as well as different plasmid DNA concentrations were tested. In order to evaluate the RHOGDI1 overexpression efficiency, C3H/10T1/2 cells were transfected with 400 and 800 ng/mL of N-FLAG-RHOGDI1 plasmid along with Lipofectamine LTX & PlusTM in the ratios of 1:4 and 1:8 (Plasmid [μ g] : Transfection reagents [μ L]). Figure 39 A and B show the successful overexpression of N-FLAG-RHOGDI1 in C3H/10T1/2 cells. All tested conditions led to overexpression of N-FLAG-RHOGDI1. As seen the Figure 39 B, 21-fold overexpression of RHOGDI1 was obtained when 800 ng/mL plasmid was used in the ratio of 1:8. On the basis of these results, 800 ng/mL of N-FLAG-RHOGDI1 plasmid with ratio of 1:8 to Lipofectamine LTX & PlusTM reagent were chosen for the following overexpression experiments.

In order to determine the effect of RHOGDI1 overexpression on Hh signaling pathway, an osteoblast differentiation assay was performed following RHOGDI1 overexpression. Two populations of C3H/10T1/2 cells were transfected with N-FLAG-RHOGDI1 plasmid and mock vector using the optimized conditions. The cells were reseeded in a 96-well plate and treated with 1.5 μ M purmorphamine and various concentrations of RKN-1043 or DMSO, as a control. The level of ALP was measured by using the CDP-*Star* reagent. The Hh pathway activation upon purmorphamine treatment in empty vector was normalized to 100% assuming that empty vector would not have any effect on the Hh signaling (Figure 39 C). In the case of N-FLAG-RHOGDI1 overexpression, nearly 40% reduced activation of Hh signaling was observed upon purmorphamine treatment. Thus, indicating that RHOGDI1 is a negative regulator of Hh signaling. Figure 39 D shows the luminescence values upon treatment of the N-FLAG-RHOGDI1 transfected cells with various concentrations of RKN-1043. Both curves show an RKN-1043 concentration-dependent reduction in the Hh pathway activity. However, no major difference in the

potency of RKN-1043 in N-FLAG-RHOVDI1 and mock vector transfected cells was observed. The increased concentration of N-FLAG-RHOVDI1 causing inhibition of Hh signaling confirms the RHOVDI1 involvement in Hh signaling as a negative regulator.

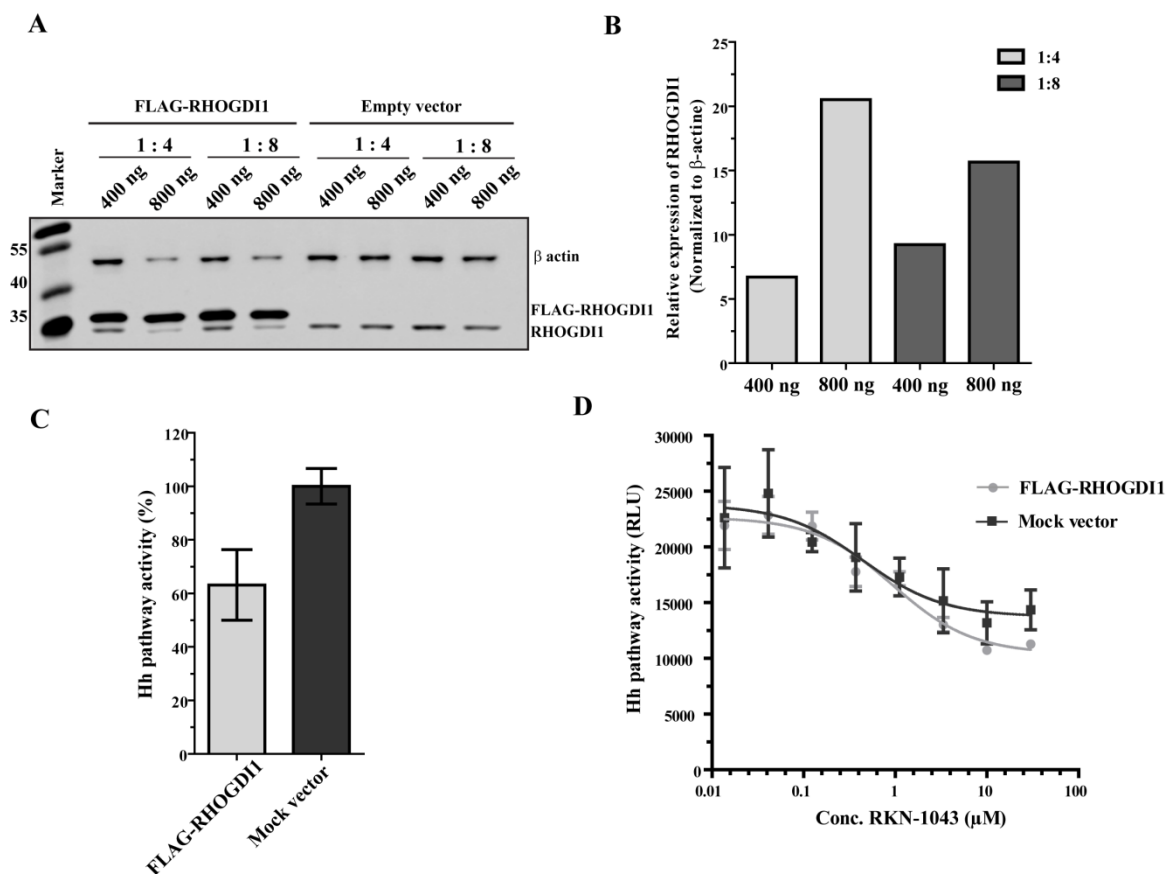


Figure 39. RHOVDI1 overexpression and its influence on Hh signaling.

(A) C3H/10T1/2 cells were transfected with 400 and 800 ng of N-FLAG-RHOVDI1 plasmid or mock vector using 1:4 or 1:8 ratios with respect to Lipofectamine LTX & Plus as a transfection reagent. Cells were lysed and RHOVDI1 overexpression was detected by means of immunoblotting using an anti-RHOVDI1 antibody. (B) After densitometric analysis, the overexpression efficiency was calculated by first normalizing band intensities for RHOVDI1 to the band intensities for β-actin in respective samples. RHOVDI1 expression levels for the mock vector sample were set to 1. (C) C3H/10T1/2 cells were transfected with 800 ng N-FLAG-RHOVDI1 plasmid or mock vector Lipofectamine LTX & PlusTM as transfection reagent (ratio 1:4). 24 h later cells were treated with 1.5 μM purmorphamine and DMSO and osteoblast differentiation was monitored after 72 h. The Hh pathway activity in cells that were transfected with the mock vector were set to 100%. (D) C3H/10T1/2 cells were transfected with 800 ng N-FLAG-RHOVDI1 plasmid or mock vector Lipofectamine LTX & PlusTM as transfection reagent (ratio 1:4). 24 h later cells were treated with 1.5 μM purmorphamine and different concentrations of RKN-1043 and osteoblast differentiation was monitored after 72 h. The curves represent the relative light units (RLU) as a measure of Hh pathway activity. Data are mean values of three technical replicates and are representative of three biological replicates (N = 3, n = 3).

These findings are complementary to the RHOVDI1 knockdown results, wherein knockdown led to stronger activation of Hh signaling. The increased stoichiometric ratios

of RHOGDI1 in the cells might have led to capture of RHO GTPases in GDP-bound inactive state in the cytosol. The inactive RHO GTPase in complex with RHOGDI would be inaccessible to the GEFs that can facilitate the activation of RHO GTPase, thus causing RHO GTPase and Hh pathway inhibition. As a result of 20-fold RHOGDI1 overexpression, the Hh pathway is inhibited to the maximum levels. Therefore further inhibition by RKN-1043 is not significant to exert additional Hh inhibitory effect. Therefore, there is no shift in the potency of RKN-1043 in N-FLAG-RHOGDI1 and mock vector transfected cells.

5.3.9 Effect of RKN-1043 on stress fibers

A non-canonical Hh signaling pathway has been reported in endothelial cells, which regulates actin stress fibers in response to Hh *via* GLI-independent mechanism. The non-canonical Hh signaling activates the small RHO GTPases RHOA and RAC1 *via* SMO-coupled $G\alpha_i$ proteins and regulates the actin cytoskeleton in fibroblasts and endothelial cells *via* RHO-associated protein kinase (ROCK).^{111,124,125} Therefore, the effect of RKN-1043-mediated RHOGDI1 inhibition on the actin cytoskeleton was determined by staining cells with phalloidin-rhodamine. NIH/3T3 cells were treated with 1.5 μ M purmorphamine and the ROCK inhibitor H1152, RKN-1043 or DMSO as a control (Figure 40). As expected, H1152 abolished stress fibers formation at all tested time points. In contrast, a dense network of parallel stress fibers was observed upon treatment with RKN-1043 and DMSO. Alteration in the total level of RHO GTPase as result of RKN-1043 treatment was expected to influence stress fibers. Although RKN-1043 inhibited Hh signaling and RHOGDI1 function, it did not have significant measurable effect on stress fibers. It is proposed that even in the absence of RHOGDIs, a fraction of RHO GTPases continue to be transported to the plasma membrane through vesicular trafficking which is sufficient to account for the observed phenotypes (e.g. stress fiber formation).¹⁰⁶ Therefore, inhibition of RHOGDI1 by RKN-1043 might have no influence on the stress fiber formation.

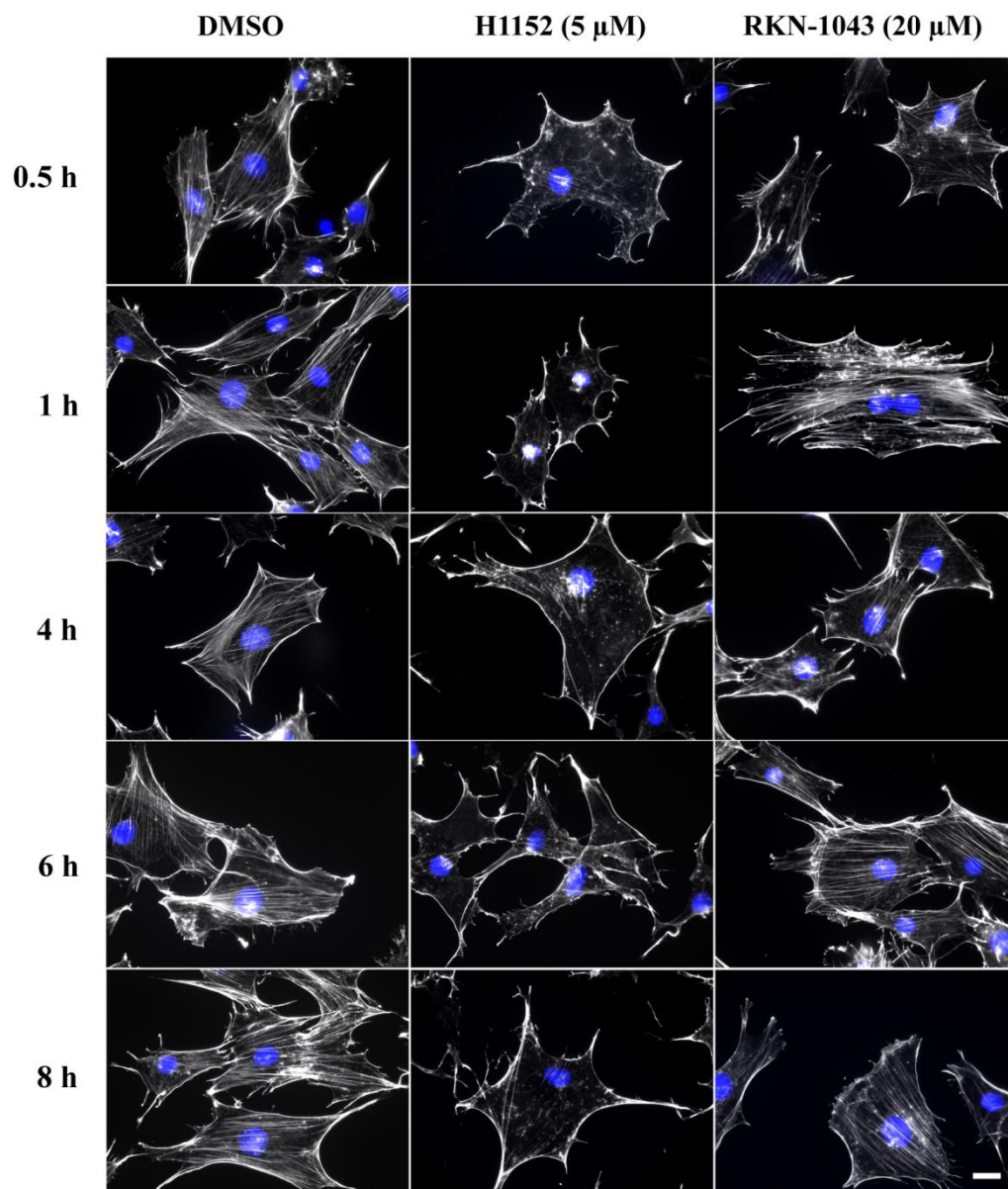


Figure 40. Effect of RKN-1043 on stress fibers.

NIH/3T3 cells were treated with H1152, RKN-1043 or DMSO as a control for various times. Cells were fixed and stained with DAPI to visualize the nuclei (blue), whereas actin filaments were stained with phalloidin-rhodamin (gray). The images shown are representative images of three biological replicates. Scale bar: 10 μm.

5.3.10 Summary and outlook for RKN-1043

RKN-1043 was identified as Hh signaling pathway inhibitor acting downstream of SMO. Target identification and validation efforts revealed RHOGDI1 as a potential target of RKN-1043. Competition with binding of a GerGer-RAB1 peptide to the GerGer binding pocket of RHOGDI1 makes RKN the first molecule to bind to the GerGer binding pocket of RHOGDI1, thus inhibiting its function. Investigation of the crystal structure of the RHOGDI1-RKN1043 complex would further help in understanding the binding mode of RKN-1043.

RHOGDI1 knockdown enhances Hh signaling, whereas RKN-1043-mediated inhibition of RHOGDI1 inhibits Hh signaling which highlights the complexity of RHOGDI1 involvement in Hh signaling. It was speculated that RKN-1043 displaces the GerGer moiety from the binding pocket thus leading to release of the GerGer moiety in the cytosol. Thus induces misfolding and proteasomal degradation of the RHO GTPases which causes RHO GTPase and Hh pathway inhibition

In-depth analysis of the effect of RKN-1043 on the activation state of RHO GTPases will further support the mechanism of action for RKN-1043-mediated Hh inhibition. Fluorescence lifetime imaging microscopy (FLIM)-based fluorescence resonance energy transfer (FRET) measurements¹²⁶ would address the speculation whether RKN-1043 indeed affects the interaction of RHOGDI1 with RHO GTPase in live cells. This can further be extended to assess the specificity towards RHOA, RAC1 and CDC42. FLIM-FRET would also shed light of spatial and temporal effects of RKN-1043 on RHO GTPase regulation by RHOGDI1. Alternatively, implementation of proximity ligation assay would facilitate the understanding of RKN-1043 on localization of the RHO GTPase-RHOGDI1 in complex and on RHO GTPase-RHOGDI1 complex formation.

Overall, RKN-1043 is a novel inhibitor of Hh signaling as well as for RHOGDI1 function. It can be used as a tool compound to study the effect of small molecule mediated RHOGDI1 modulation on various cellular processes.

5.4 Biological evaluation of bis-nitrophenyl-bipyridines

5.4.1 Confirmation of biological activity by secondary assays

In the working group of Prof. Adam Nelson (School of Chemistry, University of Leeds, Leeds, UK) a compound library with diverse scaffolds was prepared as a result of diversity-oriented synthesis by using metathesis cascades to prepare substrates for inter- and intramolecular Diels-Alders reactions.¹²⁷ The resulting compound library was screened by COMAS for modulation of several biological signaling pathways. Among the tested assays, Hh pathway activity in osteoblast differentiation assay was inhibited by LDS-000764 with an IC_{50} of 1.3 μ M. Since LDS-000764 was a racemic mixture, pure enantiomers MJD-1314 and MJD-1320 (see Figure 41) were synthesized by Dr. Mark Dow (School of Chemistry, University of Leeds, Leeds, UK) and analyzed for Hh pathway inhibition by employing the osteoblast differentiation assay. A significant difference in Hh pathway inhibition was observed for MJD-1314 and MJD-1320 with IC_{50} values of 0.60 ± 0.13 μ M and 11.2 ± 0.6 μ M, respectively (Figure 41.)

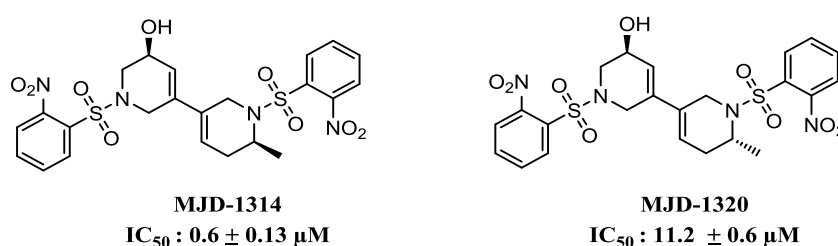


Figure 41. Chemical structures of MJD-1314 and MJD-1320 and biological activity.

IC_{50} s were determined upon treatment of C3H/10T1/2 cells with various concentrations of test compounds and DMSO as control. The Hh pathway was activated upon treatment with 1.5 μ M purmorphamine and ALP activity was measured after 96 h. All data are mean values of three independent experiments ($n = 3$) \pm s.d.

The Hh inhibitory activity of MJD-1314, being the most potent analogue, was confirmed in the orthogonal GLI-reporter gene assay with an IC_{50} value of 1.53 ± 0.4 μ M (Figure 42 A). Analysis of Hh target gene expression further confirmed the Hh specific transcriptional inhibition by MJD-1314, which dose dependently inhibited the expression of *Ptch1* and *Gli1* (Figure 42 B). The inhibition of Hh target gene expression along with the GLI-reporter gene assay confirm the GLI-transcription factor dependent inhibition of the Hh pathway by MJD-1314.

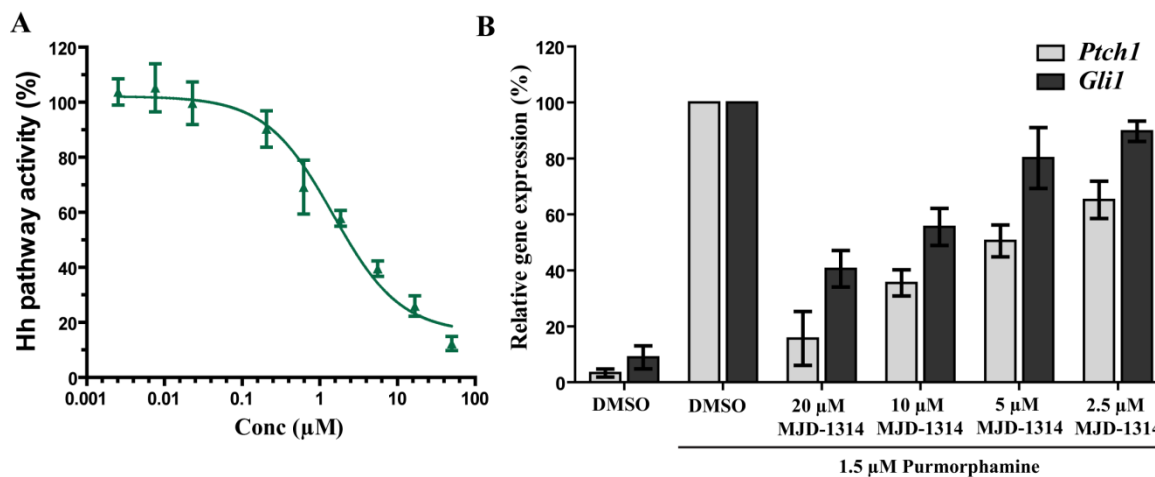


Figure 42. Influence of MJD-1314 on the GLI-mediated transcription.

(A) MJD-1314 inhibits GLI-dependent reporter gene expression in Shh-LIGHT2 cells. Cells were treated with 1.5 μ M purmorphamine and different concentrations of MJD-1314 for 48 h. Firefly and Renilla luciferase activities were determined and ratios of firefly luciferase/Renilla luciferase signals were calculated, which are a measure of Hh pathway activity. Nonlinear regression analysis was performed using a four parameter fit. All data are mean values of three independent experiments ($n = 3$) \pm s.d. (B) C3H/10T1/2 cells were treated with purmorphamine (1.5 μ M) and different concentrations of MJD-1314 or DMSO as a control for 48 h before isolation of total RNA. Following cDNA preparation, the relative expression levels of *Ptch1*, *Gli1* and *Gapdh* were determined by means of quantitative PCR employing specific oligonucleotides for *Ptch1* and *Gli1* or *Gapdh* as a reference gene. Expression levels of *Ptch1* and *Gli1* were normalized to the levels of *Gapdh* and are depicted as percentage of gene expression in cells activated with purmorphamine (100%). All data are mean values of three independent experiments ($n = 3$) \pm s.d.

Furthermore, MJD-1314 treatment failed to displace BODIPY-cyclopamine from the cells indicating that MJD-1314 most likely does not bind to the cyclopamine binding site of SMO (Figure 43 A). In order to quantify the displacement of BODIPY-cyclopamine, flow cytometry was used to count the cells displaying green fluorescence due to bound BODIPY-cyclopamine. Cells that were treated with BODIPY-cyclopamine and DMSO displayed the maximum BODIPY intensity (Figure 43 B). However, treatment with various concentrations of MJD-1314 failed to displace BODIPY-cyclopamine from the cells, therefore confirming the microscopy results.

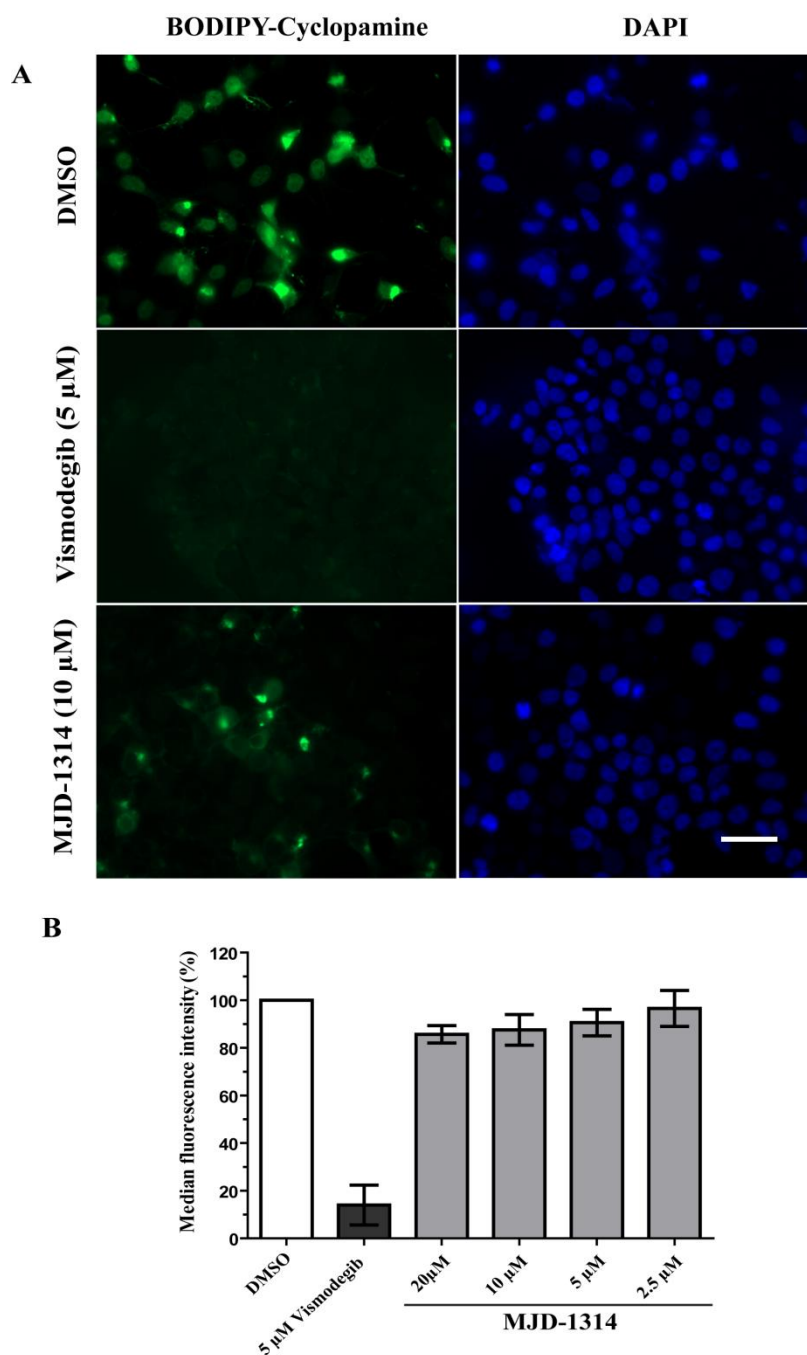


Figure 43. Effect of MJD-1314 on SMO-bound BODIPY-cyclopamine.

(A) HEK293T cells were transiently transfected with a SMO-expressing plasmid or empty vector. 48 h later cells were treated with BODIPY-cyclopamine (5 nM, green) followed by addition of 10 μM of MJD-1314 or 5 μM vismodegib and DMSO as controls and further incubation for 1 h. Cells were then fixed and stained with DAPI to visualize the nuclei (blue). Scale bar: 20 μm. (B) HEK293T cells ectopically expressing SMO were treated with different concentrations of MJD-1314, vismodegib or DMSO as a control in the presence of BODIPY-cyclopamine (5 nM) for 5 h. The graph shows the percentage of cell-bound BODIPY-cyclopamine as detected by fluorescence-activated cell sorting. Data are mean values of three independent experiments ($n=3$) \pm s.d.

To rule out the interference of MJD-1314 with SMO localization to cilia, cells were treated with MJD-1314 along with purmorphamine and co-localization of SMO with cilia

was analyzed by microscopy. However, MJD-1314 did not affect the localization of SMO in cilia indicating that MJD-1314 might be acting downstream of SMO for inhibition of Hh pathway.

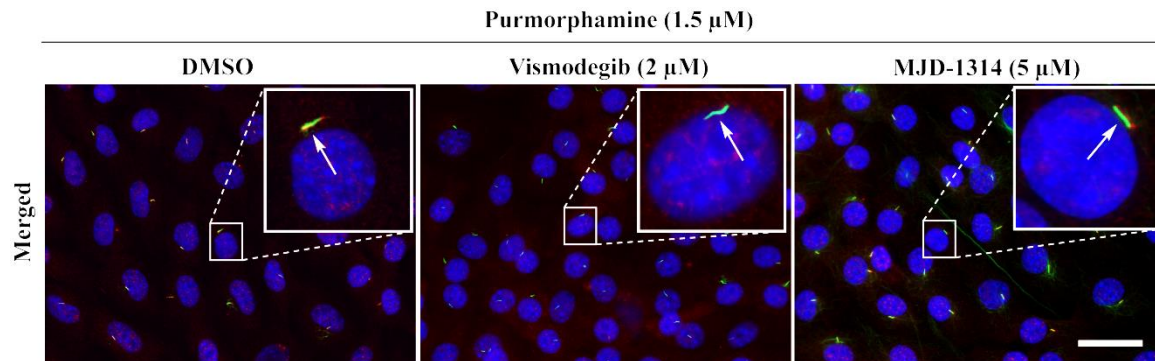


Figure 44. Effect of MJD-1314 on the ciliary localization of SMO.

NIH/3T3 cells were treated with 1.5 μ M purmorphamine for 2 h followed by addition of 2 μ M vismodegib or 5 μ M MJD-1314, and further incubation for 12 h. Cells were then fixed and stained to visualize the nuclei (blue), SMO (red) and cilia (acetylated tubulin; green). Inset: representative single cilia. Scale bar: 10 μ m.

5.4.2 Influence of MJD-1314 on kinases involved in Hh signaling

The effect of MJD-1314 on the kinases that are known to regulate Hh signaling was determined by Eurofins. The biochemical inhibition of the tested kinase by 10 μM MJD-1314 was determined by activity based assays (Table 11). However, MJD-1314 did not influence the tested kinases and therefore needs further efforts on identification of the novel regulators of Hh signaling pathway.

5.4.3 Target identification

In order to identify the molecular targets of MJD-1314, affinity-based chromatography was performed. For this technique, positive and negative affinity probes are required to enrich the molecular targets in *pull-down* experiments, which can be analyzed by mass spectrometry. In order to synthesize the positive and negative probes knowledge of the SAR is critical. Unfortunately, due to limited availability of derivatives, a complete understanding of the SAR for MJD-1314 was not possible. Nonetheless, Dr. Matthias Bischoff (COMAS) synthesized the *pull-down* probes by attaching the linker on the alcohol group of the bipyridine that was amenable to modification. It was assumed that coupling of a PEG-linker to 1-tosylpiperidin-3-ol would lead to a simplified negative probe MB-63 (Figure 45). MB-64 inhibited Hh signaling with an IC_{50} of $6.4 \pm 1.2 \mu\text{M}$ in the GLI-reporter gene assay, whereas the control probe MB-63 failed to inhibit the Hh signaling. Therefore, MB-64 was used as positive probe, whereas MB-63 was used as negative probe for the following chemical proteomics experiments.

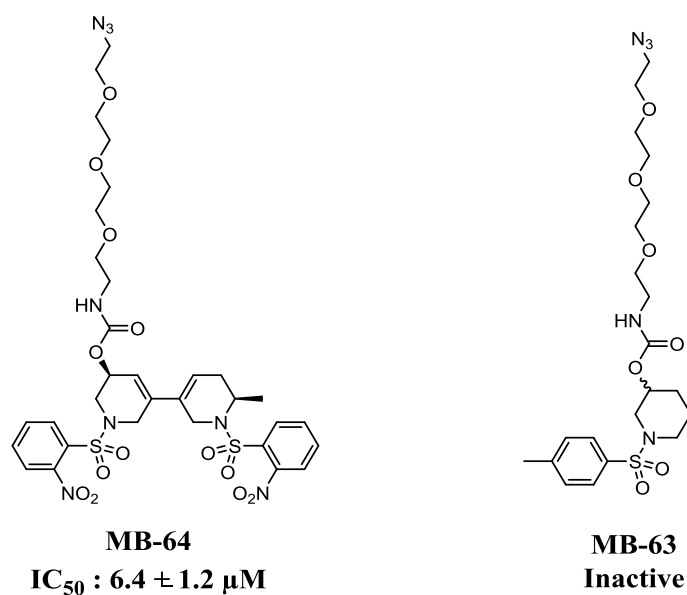


Figure 45. Chemical structures of the *pull-down* probes MB-64 and MB-63 and biological activity.

MB-64 and MB-63 were tested in GLI-dependent reporter gene assay in Shh-LIGHT2 cells. Cells were treated with 1.5 μM purmorphamine and different concentrations of MB-64 and MB-63 for 48 h. Firefly and Renilla luciferase activities were determined and ratios of firefly luciferase/Renilla luciferase signals were calculated, which are a measure of Hh pathway activity. Nonlinear regression analysis was performed using a four parameter fit. All data are mean values of three independent experiments ($n = 3$) \pm s.d.

For the *pull-down* experiments the free amine derivatives of MB-64 and MB-63 were immobilized on NHS ester magnetic beads. NIH/3T3 cell lysates were incubated with the immobilized probes to enable protein binding. Non-specifically bound proteins were removed by washing the immobilized probes with lysis buffer containing 25 mM magnesium chloride. For the enzymatic digestion of bound proteins, the magnetic beads were incubated with trypsin and LysC endopeptidases that cleave within polypeptides.

The resulting peptides were purified as mentioned in section 7.4.4 and analyzed by means of nano-HPLC / MS / MS. The mass spectrometry experiments were done at the HRMS facility at the MPI Dortmund and the subsequent data analysis was performed by Dr. Petra Janning (MPI Dortmund). Statistical analysis was performed to quantify the proteins that were selectively enriched by the active probe as opposed to the inactive probe. Table 4 represents the proteins that were identified using the label-free quantification. Based on the fold enrichment ratio, 10 statistically significant proteins were identified as potential targets. The protein enrichment using the positive probe indicates the success of *pull-down* probe synthesis immobilization strategy.

Table 4. List of proteins enriched by active probe MB-64 as identified by means of affinity chromatography.

The active probe MB-64 and the inactive probe MB-63 were immobilized on NHS ester magnetic beads. NIH/3T3 lysate was passed on to the probes and target proteins were identified upon enrichment using mass spectrometry and label-free quantification. The ratios indicate the fold excess for protein enriched using active probe MB-64 as compared to the inactive probe MB-63. The *pull-down* experiments were performed in two independent biological duplicates with three technical replicates.

Protein names	Gene names	Ratio (A/I)
Stomatin-like protein 2	Stoml2	29
Acid ceramidase subunit alpha	Asah1	12
60S acidic ribosomal protein P0	Rplp0	10
Sterol-4-alpha-carboxylate 3-dehydrogenase, decarboxylating	Nsdhl	10
Acyl-CoA-binding protein	Dbi	9
S-methyl-5-thioadenosine phosphorylase	Mtap	5
26S proteasome non-ATPase regulatory subunit 11	Psm11	5
60S ribosomal protein L14	Rpl14	5
Phosphatidylethanolamine-binding protein 1	Pebp1	4
Carboxypeptidase;Lysosomal protective protein	Ctsa	3

In order to achieve better quantification of the identified proteins, next SILAC lysates were used in the affinity chromatography experiments. Several proteins were identified as bound to the active and the inactive probe. SILAC-based quantification of proteins bound to the active probe MB-64 and inactive probes MB-63 was performed by Dr. Petra Janning (MPI, Dortmund) to identify proteins that were enriched in active probe as compared to inactive probe. Statistical analysis of the enriched proteins led to positive ratios for heavy isotope-labelled proteins bound to the active probe (AH) and light isotope labelled protein bound to inactive probe (IL) (AH/IL) and negative ratios for the heavy isotope labelled protein bound to inactive probe (IH) and light isotope labelled protein bound to active probe (AL) (IH/AL) indicating the enrichment of proteins using the positive as compared to the negative probe. Table 5 shows the proteins that were identified as significant hits and the ratios are indicative of fold enrichment by the positive probe MB-64 as compared to the negative probe MB-63. Among the identified proteins, noticeably, acid ceramidase (ASAHI), S-methyl-5-thioadenosine phosphorylase (MTAP) and Sterol-4-alpha-carboxylate 3-dehydrogenase (NSDHL) were identified with higher ratios using the label-free as well as SILAC-based quantifications after the *pull-downs*. Because of the reproducibility in identification of ASAHI, MTAP and NSDHL

across two label free quantifications and one SILAC *pull-down* experiment, these proteins were regarded as potential targets which needed further validation.

Table 5. List of protein identified by SILAC *pull-down* experiment.

The active probe MB-64 and the inactive probe MB-63 were immobilized on NHS ester magnetic beads. Heavy and light isotope labelled NIH/3T3 lysates were passed on to the probes and target proteins were identified upon enrichment using mass spectrometry and SILAC-quantification. The ratios indicate the fold excess for protein enriched using active probe MB-64 as compared to the inactive probe MB-63. The *pull-down* experiments were performed in once with three technical replicates.

Protein name	Gene name	SILAC ratio
Acid ceramidase subunit alpha	Asah1	6.72
S-methyl-5-thioadenosine phosphorylase	Mtap	6.02
Phosphatidylethanolamine-binding protein 1	Pebp1	3.85
A-kinase anchor protein 8	Akap8	3.53
Ras-related protein Rab-2A;Ras-related protein Rab-2B	Rab2a;Rab2b	2.91
Sterol-4-alpha-carboxylate 3-dehydrogenase, decarboxylating	Nsdhl	2.52
Signal transducer and activator of transcription 3	Stat3	2.37
Ras-related protein Rab-10	Rab10	1.93
Acyl-protein thioesterase 1	Lypla1	1.90
Retinol dehydrogenase 11	Rdh11	1.40
Clathrin heavy chain 1	Cltc	1.27

5.4.4 Target validation

5.4.4.1 Determination of target engagement of MJD-1314 by immunoblotting

In order to validate the results of the affinity chromatography experiments and prioritize a potential target, immunoblotting after the *pull-down* was performed. Initially ASAH1 and MTAP were prioritized because of their identification in SILAC experiments with high SILAC ratios of 6.72 and 6.02, respectively. MTAP and ASAH1-specific antibodies were used to detect the enrichment of the proteins after affinity *pull-down* experiments (Figure 46). Enrichment of the MTAP protein only using the active *pull-down* probe was detected by immunoblotting. (Figure 46 A), whereas ASAH1 was not enriched using the positive or negative probe (Figure 46 B). The failed detection of ASAH1 could be a result of weaker binding of ASAH1 to the linker. The weakly bound ASAH1 protein might have been washed away during the washing steps, therefore making it difficult to identify by immunoblotting. Although the washing steps remain the same in the proteomics based *pull-down*, the HRMS instrument sensitivity would have led to identification of ASAH1. Therefore, these results confirm the selective enrichment of only MTAP by active probe MB-64.

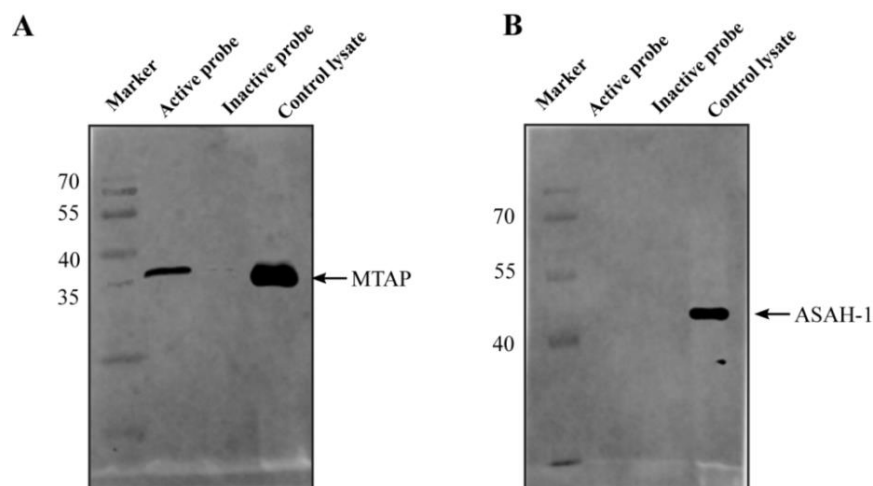


Figure 46. Validation of MTAP and ASAH-1 enrichment by active probe MB-64 by immunoblotting after the *pull-down*.

The active probe MB-64 and the inactive probe MB-63 were immobilized on NHS ester magnetic beads and exposed to NIH/3T3 lysates. Bound proteins were eluted and analyzed by immunoblotting using (A) MTAP-specific antibody and (B) ASAH-1-specific antibody and secondary antibody that was coupled to infra-red fluorescent dye *IR800*. Data is representative of three independent biological replicates. (n=3)

In order to further demonstrate target engagement of MTAP by the active *pull-down* probe, competition-based *pull-down* was performed. At this stage, the potential target NSDHL was also followed for validation because of its involvement in cholesterol biosynthesis regulation, which has been linked to Hh pathway regulation. For competition-based *pull-down*, the active probe MB-64 was immobilized on magnetic beads and exposed to NIH/3T3 lysates that were pre-incubated for 2 h with various concentrations of MJD-1314 and DMSO as a control. It was expected that MJD-1314 would compete with the active probe MB-64 for binding to the target protein, therefore leading to differential enrichment by the active probe as a function of MJD-1314 concentration in the lysates. As seen in Figure 47 A, NSDHL was enriched by the active probe, however, exposure of lysates to MJD-1314 did not lead to competitive binding indicating the nonspecific binding of NSDHL with the *pull-down* probes. In contrast, pre-incubation of the lysate with MJD-1314 led to competition with the active probe for binding to MTAP as indicated by diminished band intensities in the samples with high (i.e. 10, 30 and 50 μ M) concentration of MJD-1314.

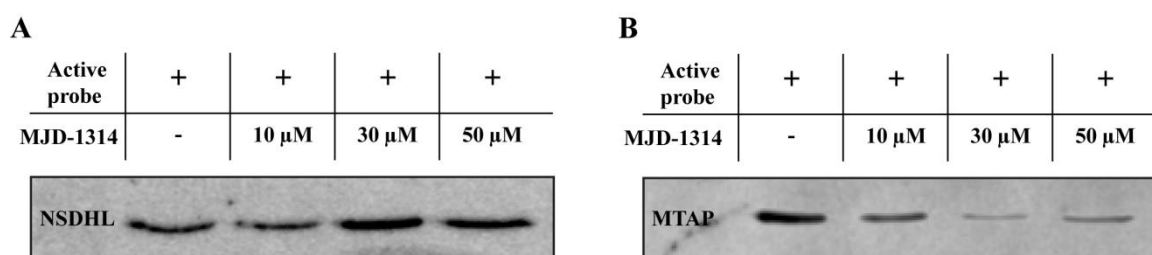


Figure 47. Validation of potential targets by immunoblotting after a competitive *pull-down*.

The active probe MB-64 and the inactive probe MB-63 were immobilized on NHS ester magnetic beads and exposed to NIH/3T3 lysates that were pre-incubated with increasing concentrations of MJD-1314 or DMSO as a control. Bound proteins were eluted and analyzed by immunoblotting using (A) NSDHL-specific antibody and (B) MTAP-specific antibody and secondary antibody that was coupled to infrared fluorescent dye *IR800*. Data is representative of three independent biological replicates.

These results confirm the target engagement of MTAP by MJD-1314. Therefore, further biophysical and genetic validation experiments were carried out to confirm MTAP as a target of MJD-1314.

5.4.4.2 MJD-1314 induces thermal stabilization of MTAP

In order to further investigate the binding of MJD-1314 to MTAP, the effect of MJD-1314 on MTAP thermal stability was investigated by means of the cellular thermal shift assay. Small-molecule binding to a target protein may cause changes in the thermodynamic properties of the protein leading to thermal stabilization or destabilization.¹²⁸ NIH/3T3 cell lysates were incubated with 30 μ M MJD-1314 or DMSO as a control. As seen in Figure 48, MTAP band intensities in DMSO treated lysates diminish with increasing temperatures indicating melting of MTAP at higher temperature. Upon treatment with MJD-1314 the MTAP band intensities remain relatively stable at higher temperatures (>60 $^{\circ}$ C) compared to the DMSO-treated lysates. These results confirm the target engagement and thermal stabilization of MTAP protein in lysate by MJD-1314.

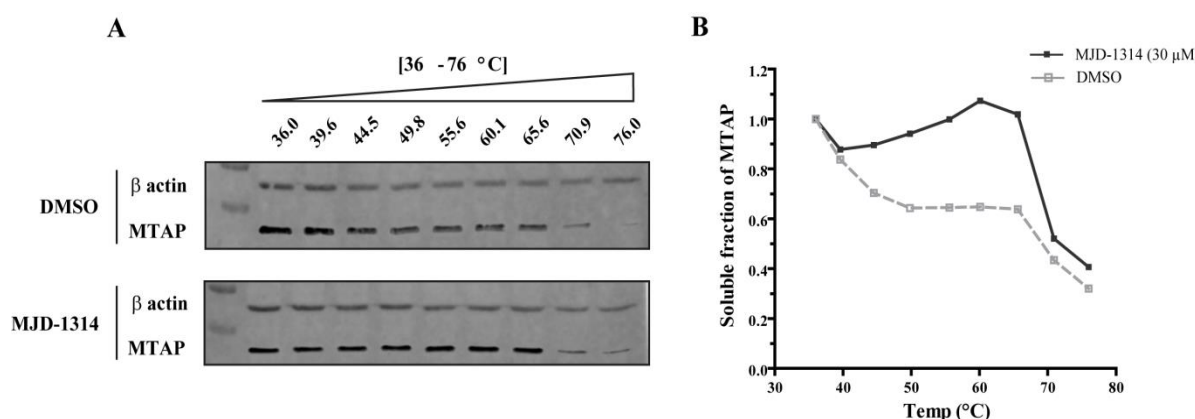


Figure 48. Cellular thermal shift assay for MTAP.

(A) NIH/3T3 cell lysates were incubated with 30 μ M of MJD-1314 followed by heating at increasing temperatures to denature the proteins. Upon ultracentrifugation, MTAP and β -actin (used as a reference) were detected in the soluble fractions by means of immunoblotting. (B) Quantification of MTAP abundance in the soluble fractions upon normalization to the band intensities for β -actin and MTAP at 36 $^{\circ}$ C (set to 1). Data is representative of three independent biological replicates.

In order to demonstrate thermal stabilization of purified human MTAP by MJD-1314, differential scanning fluorimetry experiments were performed. The assay principle is similar to CETSA with differences in the detection method and the use of purified protein. Purified MTAP protein along with SYPRO-orange dye was incubated with various concentrations of MJD-1314 and DMSO as a control and exposed to increasing temperatures. As a result of heating, hydrophobic sequences of the protein become exposed to solvent as the protein starts to unfold. The fluorescence of SYPRO-orange dye increases as a result of binding to the solvent-exposed hydrophobic regions of the protein.

Therefore, the change in the fluorescence intensity of SYPRO-orange dye was measured to determine protein stability.¹²⁹ As seen in Figure 49, thermal stabilization of MTAP was observed upon exposure to MJD-1314. The maximum melting temperature shift (ΔT_m) was observed at 80 and 100 μM MJD-1314. Moreover, saturation of ΔT_m with 80 μM and 100 μM of MJD-1314 indicates the highest degree of thermal stabilization of MTAP.

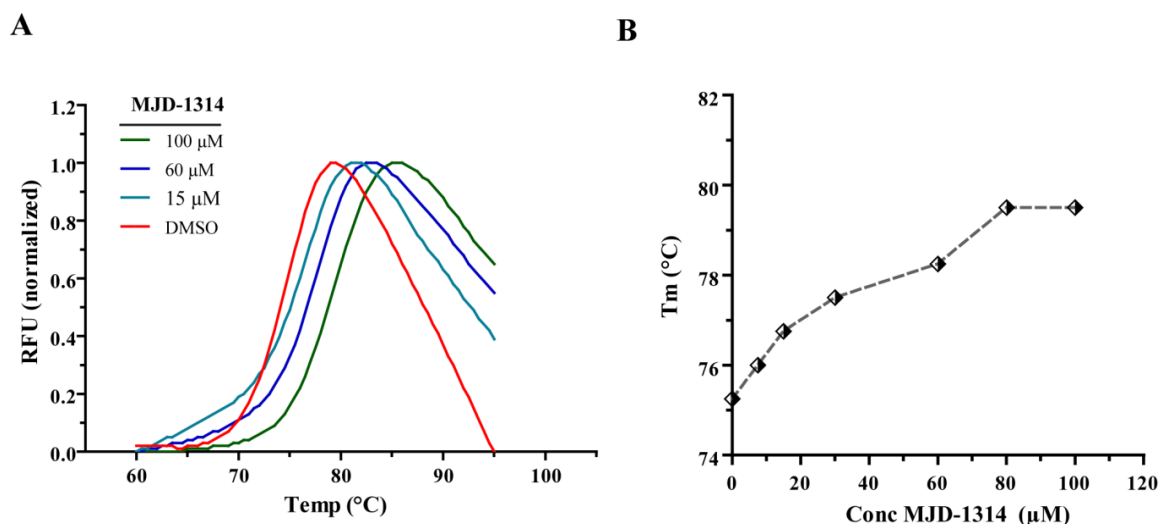


Figure 49. Thermal stability of MTAP as detected by differential scanning fluorimetry.

(A) Purified human MTAP protein was incubated with various concentrations of MJD-1314 or DMSO as a control. The change in the fluorescence intensity of SYPRO-orange was used as a measure of the melting behavior of MTAP. (B) Melting temperature (T_m) were determined by the maximum fluorescence intensity of SYPRO-orange in A and are plotted against the concentration of MJD-1314. Data is representative of three independent biological replicates

Table 6. Change in the melting temperature of MTAP in the presence of MJD-1314.

Melting temperature (T_m) and differences of T_m (ΔT_m) between MJD-1314 and DMSO-treated samples are given. T_m were determined by the maximum fluorescence intensity of SYPRO-orange measured using differential scanning fluorimetry. All data shown are mean values ($N = 3$, $n = 2-3$).

MJD-1314 (μM)	T_m ($^{\circ}\text{C}$)	ΔT_m ($^{\circ}\text{C}$)
100	79.5	4.25
80	79.5	4.25
60	78.25	3.0
30	77.5	2.25
15	76.75	1.5
7.5	76.0	0.75
DMSO	75.25	-

The results so far demonstrate the target engagement of MTAP with MJD-1314 that leads to thermal stabilization of MTAP.

5.4.5 Polyamine biosynthesis

MTAP is an enzyme ubiquitously expressed in normal tissues and plays a central role in the salvage of adenine and methionine. Biochemical evidence suggests that mammalian MTAP is a trimer made up of three identical subunits of 32 kDa (Figure 50)¹³⁰ although in at least one case the enzyme was reported as a dimer.¹³¹ MTAP catalyzes the phosphorylation of S-methyl-5'-thioadenosine (MTA), a product of both spermidine and spermine synthases in the polyamine biosynthesis pathway. As a result of phosphorylation, MTA is cleaved into adenine and 5-methylribose-D-ribose-1-phosphate (MTR-1-P).^{132,133} Subsequently, adenine is salvaged to generate adenosine monophosphate (AMP), and the MTR-1-P is converted to methionine (Figure 51). These products are further recycled to S-adenosyl-L-methionine (SAM) which, *via* decarboxylation, serves as a precursor for MTA synthesis. Moreover, spermine and spermidine are produced from putrescine by the subsequent addition of an aminopropyl group derived from SAM.¹³⁴ Thus, this metabolic pathway represents an alternative to *de novo* purine biosynthesis.

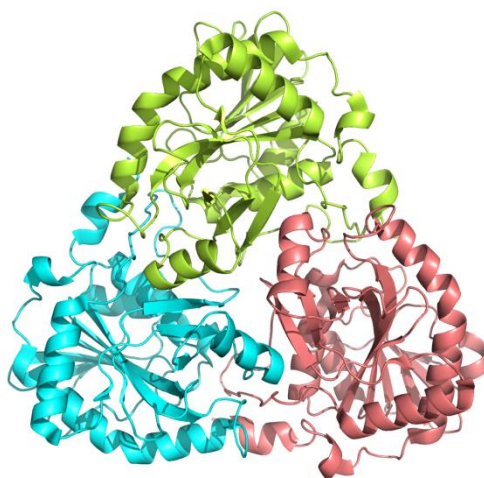


Figure 50. Crystal structure of MTAP trimer (1V4N).

MTAP is a trimer with three identical subunits. Each identical subunit is shown in a different color.¹³⁵

Inhibition of MTAP leads to increased intracellular MTA concentration that causes feedback inhibition of polyamine biosynthesis. MTA accumulation causes SAM-induced alterations in DNA methylation. Therefore, MTA accumulation is predicted to have different effects on cells by altering the DNA methylation.¹³⁶ Co-deletion of the MTAP gene together with the tumor suppressor cyclin-dependent kinase inhibitor 2A (*CDKN2A*) and other genes near the chromosomal locus 9p21 are frequent in non-Hodgkin

lymphoma and acute lymphoblastic leukemia and have also been observed in lung, bladder, pancreatic, endometrial, breast, ovarian cancer, mantle cell lymphoma, conventional chondrosarcomas, and biliary tract cancers.¹³⁷⁻¹⁴⁰ Recent studies have shown that deletion of *CDKN2A* is closely associated with tumor development than MTAP deletions. MTAP deletions in specific tumor cells *in vivo* have a metabolic effect different from whole organism inhibition of MTAP as MTA accumulation will not occur in MTAP-deficient tumor because of the MTA removal by MTAP produced by surrounding normal tissues.¹³⁶

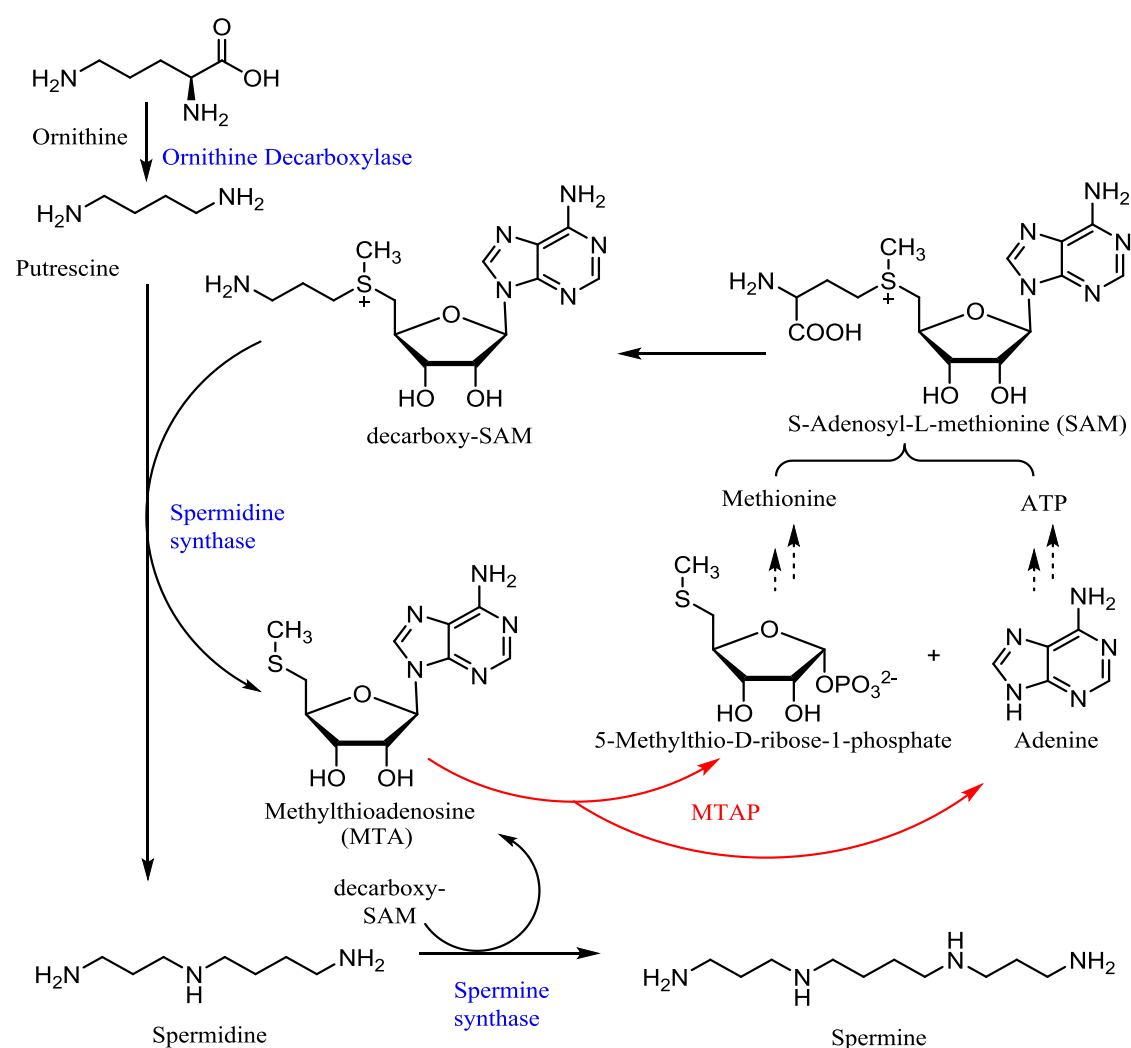


Figure 51. The polyamine biosynthesis pathway.

MTA is a common product of both spermidine and spermine synthetases and is proposed to act as a feedback product inhibitor for both enzymes. MTAP catalyzes the conversion of MTA to 5-methyl-D-ribose-1-phosphate and adenine that is recycled to S-adenosylmethionine. The enzymes involved in polyamine biosynthesis pathway are represented in color.

MT-DADMe-ImmA (MTDIA) is a transition state inhibitor of MTAP with $K_d = 1$ nM.¹⁴¹

MTDIA treatment led to accumulation of MTA and inhibition of A549 (human non-small

cell lung carcinoma) and H358 (human bronchioloalveolar non-smallcell lung carcinoma cells) xenograft tumor growth in immunodeficient mice which indicates that MTAP as a target for lung cancer therapy.¹⁴² Inhibition of MTAP by MTDIA in FaDu cells (hypopharynx squamous cell carcinoma cell line) and Cal27 cells (head and neck squamous cell carcinoma cell line) led to accumulation of MTA, decreased the levels of polyamines and induced apoptosis.¹³⁶ These results have shown that inhibition of MTAP enzymatic activity by MTDIA is an attractive strategy for targeting cancer.

Expression of MTAP in MTAP-deleted HT1080 cells decreased colony formation, migration and ability to form tumors in severe combined immunodeficiency mice, whereas treatment of MTAP-expressing cells with MTDIA did not result in MTAP deletion phenotype. Furthermore, expression of catalytically inactive MTAP in MTAP-deleted HT1080 cells resulted in reversal of the MTAP deletion phenotype, thus suggesting that in this particular case (inhibition of) MTAP enzymatic activity is not necessary for tumor suppressing function of MTAP.¹⁴³ These contradictory studies demonstrate a more complex role of MTAP in cancer progression that is not only limited to its enzymatic function.

5.4.5.1 Crosstalk between the polyamine biosynthesis pathway and Hh signaling

The effect of Hh pathway activation on polyamine metabolism was studied in cerebellar granule cell progenitors (GCPs), the cells of origin of Hh-dependent medulloblastoma.¹⁴⁴ Stimulation of GCPs with SHH increased proliferation and elevated the levels of putrescine, spermine and spermidine. An inhibitor of ornithine decarboxylase (ODC), Difluoromethylornithine (DFMO), inhibited SHH-induced GCP proliferation and decreased the levels of polyamines without affecting GLI-mediated transcription of Hh target genes. Furthermore, DFMO inhibited the proliferation of *Ptch1*^{-/-} mouse embryonic fibroblasts (MEFs) while it failed to inhibit the proliferation *Sufu*^{-/-} MEFs indicating a SUFU-mediated mode of action of DFMO. Immunoaffinity precipitation of proteins bound to SUFU revealed that SUFU binds and stabilizes cellular nucleic acid binding protein (CNBP) to regulate ODC translation. Later it was shown that the presence of an evolutionarily conserved AMPK-consensus site in CNBP is critical in Hh-dependent regulation of CNBP activity.^{145,146}

Although MTAP regulates ODC by production of downstream metabolites,¹⁴⁷ a direct involvement of MTAP in the Hh pathway has not been explored.

5.4.6 Influence of MJD-1314 on MTAP enzymatic activity

As discussed above, MTAP phosphorylates MTA and cleaves it into adenine and MTR-1-P. Therefore, for measuring the enzymatic activity of MTAP, MTA was used as a substrate and its conversion to adenine was monitored by conversion of adenine to 8-dihydroxyadenine by xanthine oxidase. The generation of 8-dihydroxyadenine was detected by monitoring the absorbance at 305 nm (Figure 52 A). Highest absorbance and linear rate of enzyme reaction was observed with 200 μ M MTA when used with 100 nM MTAP and 0.2 U of xanthine oxidase. Therefore these conditions were used for determining the effect of MJD-1314 on the enzymatic function of MTAP. MTDIA inhibited the conversion of MTA as indicated by a concentration-dependent inhibition of 8-dihydroxyadenine formation (Figure 52). However, MJD-1314 did not affect the MTAP enzyme activity as indicated by the complete conversion of MTA to adenine and then to 8-dihydroxyadenine thus implying that MJD-1314 had no effect on the enzymatic activity of xanthine oxidase as well.

The affinity *pull-down* and thermal stabilization assays clearly revealed the target engagement of MTAP with MJD-1314. However, MJD-1314 did not inhibit the enzymatic function of MTAP thus indicating an enzyme activity-independent mode of interaction of MJD-1314 and MTAP. To further understand the possible involvement of MTAP in Hh pathway regulation, the effect of MTDIA-mediated inhibition of MTAP on the Hh pathway was measured by GLI-reporter gene assay (Figure 53). However, MTDIA failed to inhibit purmorphamine-induced activation of the Hh pathway in Shh-LIGHT2 cells. These results show that inhibition of MTAP enzyme activity has no effect on the GLI-dependent Hh signaling pathway.

Failure of MJD-1314 to inhibit the enzymatic activity of MTAP and the inability of MTDIA to inhibit the GLI-dependent Hh signaling pathway led to the assumption that MTAP is involved in Hh signaling by a putative non-canonical function. Tang *et. al.*, have shown that expression of the catalytically inactive form of MTAP in MTAP-deleted HT1080 cells resulted in reversal of the MTAP deletion phenotype thus suggesting a non-canonical i.e. not related to enzymatic function of MTAP.¹⁴³

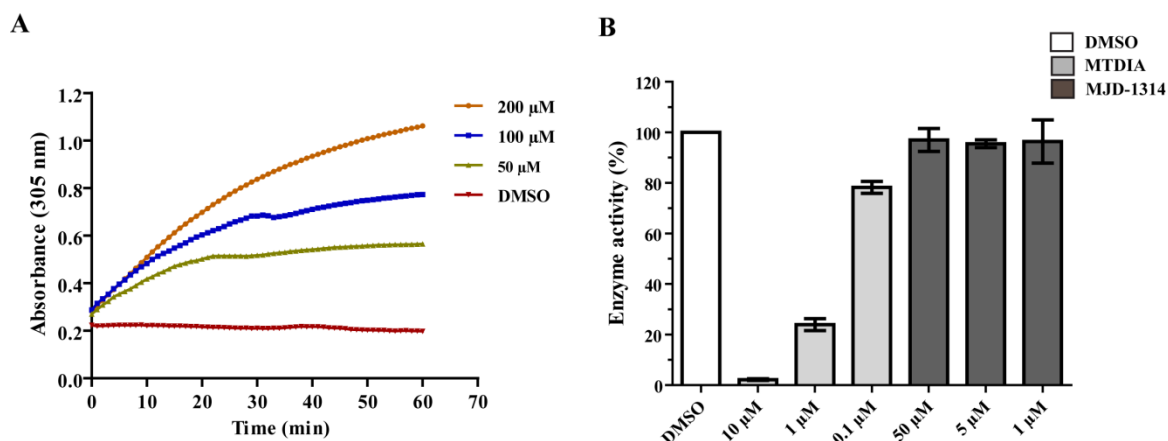


Figure 52. Effect of MJD-1314 on the enzymatic activity of MTAP.

(A) Liberation of adenine upon phosphorylation of methylthioadenosine (MTA) by MTAP was monitored by adenine conversion to 8-dihydroxyadenine by xanthine oxidase. Various concentrations of methylthioadenosine (MTA) were incubated with 100 nM MTAP and 0.2 U xanthine oxidase at 25 °C for 60 min. The resulting change in the absorbance at 305 nm was continuously monitored for 60 min. (B) Effect of MTDIA and MJD-1314 on the enzymatic activity of MTAP. 200 μ M methylthioadenosine (MTA), 0.2 U xanthine oxidase, and the test compounds were incubated at 25 °C. The enzymatic reaction was initiated by addition of 100 nM MTAP. The resulting change in the absorbance at 305 nm was continuously monitored for 60 min. All data are mean values of three independent experiments ($n = 3$) \pm s.d.

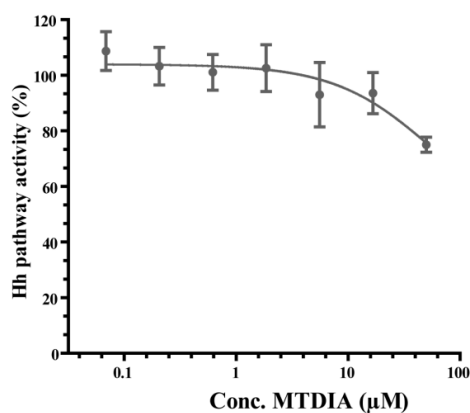


Figure 53. Effect of MTDIA on GLI mediated reporter gene assay.

Shh-LIGHT2 cells were treated with 1.5 μ M purmorphamine and different concentrations of MTDIA for 48 h. Firefly and Renilla luciferase activities were determined and ratios of firefly luciferase/Renilla luciferase signals were calculated, which are a measure of Hh pathway activity. Nonlinear regression analysis was performed using a four-parameter fit. All data are mean values of three independent experiments ($n = 3$) \pm s.d.

5.4.7 Genetic validations

In order to establish a putative non-canonical, role of MTAP in the regulation of Hh signaling pathway MTAP gene expression was altered by RNAi and plasmid-mediated overexpression.

The following genetic validation experiments were performed by Jana Flegel, a master student in the in the Department of Chemical Biology at the Max Planck Institute of Molecular Physiology, Dortmund, Germany.

5.4.7.1 Effect of MTAP knockdown on Hh signaling

In order to evaluate the influence of MTAP knockdown on Hh signaling pathway and osteoblast differentiation assay, siRNA-mediated MTAP knockdown efficiency was optimized with regard to the siRNA sequence and the concentration of the siRNA.

The effect of MTAP knockdown on the Hh signaling pathway was determined by osteoblast differentiation assay following MTAP knockdown. The Hh pathway activation upon purmorphamine treatment in samples with control siRNA was normalized to 100% assuming that the control siRNA would not have any effect on Hh signaling (Figure 54 A). In the case of 67% MTAP knockdown, 40% weaker activation of Hh signaling was observed upon purmorphamine treatment indicating the phenocopy of MJD-1314 treatment. Figure 54 B shows the absolute luminescence values upon treatment of the MTAP-siRNA-transfected cells with various concentrations of MJD-1314 upon Hh pathway activation. The Hh pathway inhibition by MJD-1314 is significantly enhanced in cells with depleted MTAP as compared to cells transfected with control siRNA. These results indicate the involvement of MTAP in Hh signaling as a positive regulator.

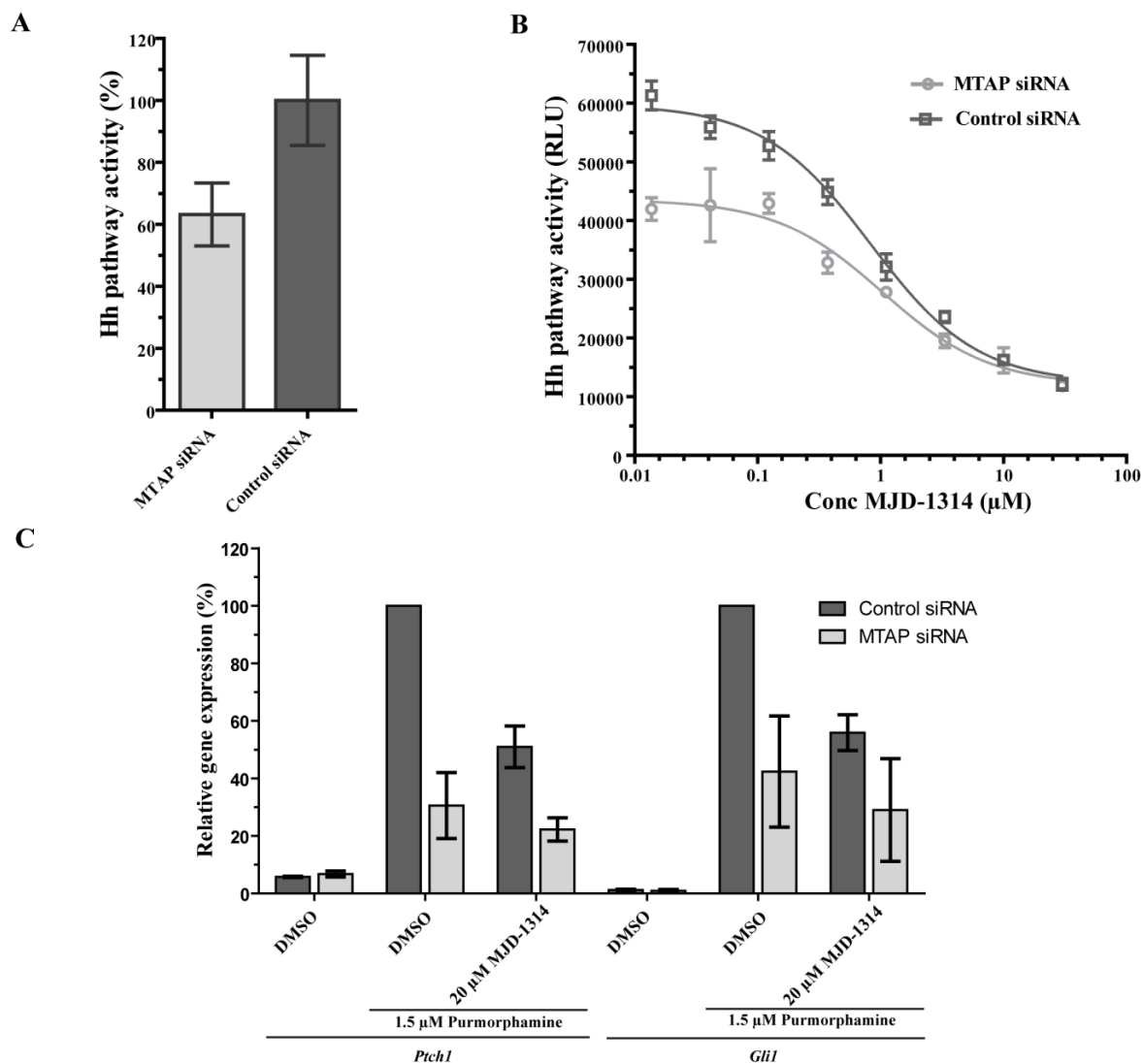


Figure 54. siRNA-mediated knockdown of MTAP and its influence on Hh signaling.

(A) C3H/10T1/2 cells were transfected with 10 nM MTAP siRNA-3 and control siRNA using 2% (v/v) DharmaFECTTM as a transfection reagent. 48 h after transfection cells were treated with 1.5 µM purmorphamine and DMSO and osteoblast differentiation was monitored after 96 h. The Hh pathway activity in cells that were treated with control siRNA was set to 100%. (B) C3H/10T1/2 cells were transfected as described above. 48 h after transfection cells were treated with 1.5 µM purmorphamine and different concentration of MJD-1314 and osteoblast differentiation was monitored after 96 h. The curves represent the relative light units (RLU) as a measure of Hh pathway activity. Data are mean values of three technical replicates and are representative of three biological replicates (N =3, n = 3) (C) C3H/10T1/2 cells were treated as described above and total RNA was isolated, cDNA was prepared and the relative expression levels of *Ptch1*, *Gli1* and *Gapdh* were determined by means of quantitative PCR employing specific oligonucleotides for *Ptch1*, *Gli1* or *Gapdh* as a reference gene. Expression levels of *Ptch1* and *Gli1* were normalized to the levels of *Gapdh* and are depicted as percentage of gene expression in cells activated with purmorphamine and transfected with control siRNA (100%). All data are mean values of three independent experiments (n = 3)±s.d.

To determine the effect of MTAP on GLI-mediated transcription, mRNA levels of Hh target genes *Ptch1* and *Gli1* were quantified following MTAP knockdown (Figure 54 C). *Ptch1* and *Gli1* expression upon purmorphamine treatment in control siRNA was

normalized to 100%. In the case of 63.8% MTAP knockdown, the expression of *Ptch1* and *Gli1* was reduced to 30-40% upon purmorphamine treatment indicating the phenocopy of the MJD-1314 treatment. The inhibition of *Ptch1* and *Gli1* expression under MTAP knockdown conditions was further reduced upon treatment with 20 μ M MJD-1314. The effect of MTAP knockdown on target gene expression as well suggests that MTAP could be involved in Hh signaling as a positive regulator. Since in the RT-qPCR experiments GLI-mediated transcription activity was measured after MTAP knockdown, it can be assumed that MTAP's involvement in Hh signaling is mediated by GLI transcription factors.

5.4.7.2 Effect of MTAP overexpression on Hh signaling

In order to determine the effect of MTAP overexpression on Hh signaling pathway, an osteoblast differentiation assay was performed following MTAP overexpression. The Hh pathway activation upon purmorphamine treatment in samples that were transfected with the mock vector was normalized to 100% (Figure 55.). Surprisingly, in the case of N-FLAG-MTAP 1.8 fold over expression, nearly 25% weaker activation of Hh signaling was observed upon purmorphamine treatment. This result indicates that MTAP can be involved in Hh signaling as a negative regulator.

Figure 55. B shows the absolute luminescence values upon treatment of N-FLAG-MTAP transfected cells with various concentrations of MJD-1314 upon Hh pathway activation. Increased potency of MJD-1314 was observed in MTAP overexpressing cells as compared to cells transfected with mock vector. The increased levels of N-FLAG-MTAP led to inhibition of Hh signaling suggesting that MTAP could be involved in Hh signaling as a negative regulator. However, the results obtained from overexpression studies do not correlate with the results obtained with MTAP knockdown. Although both approaches indicate the possible involvement of MTAP in Hh signaling, the contradictory observations in the knockdown and overexpression studies indicate a more complex involvement of MTAP in Hh signaling.

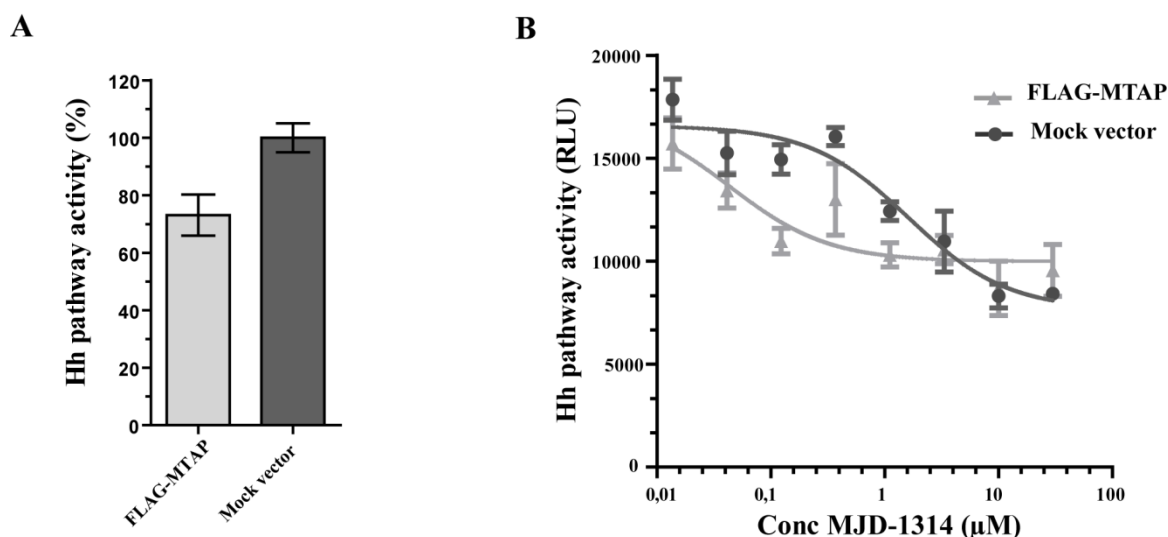


Figure 55. Plasmid-mediated MTAP overexpression and its influence on Hh signaling.

(A) C3H/10T1/2 cells were transfected with 800 ng/mL N-FLAG-MTAP plasmid or mock vector Lipofectamine LTX & PlusTM as transfection reagent in a ratio of 1:3. 24 h later cells were treated with 1.5 µM purmorphamine and DMSO and osteoblast differentiation was monitored after 72 h. The Hh pathway activity in cells that were transfected with the mock vector was set to 100%. (B) C3H/10T1/2 cells were transfected as described above. 24 h later cells were treated with 1.5 µM purmorphamine and different concentrations of MJD-1314 and osteoblast differentiation was monitored after 72 h. The curves represent the relative light units (RLU) as measure of Hh pathway activity. Data are mean values of three technical replicates and are representative of three biological replicates (N =3, n = 3).

A rationale that when more or fewer copies of the target are present, a higher or lower drug concentration is required to induce the phenotype do not appear to hold true for all compounds.¹⁴⁸ In studies carried out in bacterial systems it was shown, especially for enzymes, that target overexpression may confer resistance to the compounds if the target activity is inhibited by the compounds. However, enzyme overexpression might not confer resistance to a compound that acts by altering non-enzymatic functions.¹⁴⁹ Moreover, an overexpression or knockdown of a single component in the system disturbs the stoichiometric protein ratios that produce no effect or contradictory effects due to the disturbed stoichiometric ratios.¹⁵⁰

The genetic experiments reveal the involvement MTAP in Hh pathway regulation. However, further investigations are necessary to elucidate the function of MTAP in the regulation of Hh signaling. The GLI transcriptional activity is a direct measure of Hh pathway activity, therefore the outcome of the target gene expression is more reliable in order to determine the effect of MTAP alterations on Hh signaling. Hh target gene expression followed by MTAP knockdown indicated the involvement of MTAP in Hh signaling as a positive regulator, similarly, the effect of MTAP overexpression on target

gene expression needs to be analyzed to understand the effect of MTAP on GLI transcription activity.

5.4.8 Effect of MJD-1314 on the localization of MTAP

In order to check the possible change in the localization of MTAP upon MJD-1314 treatment, localization studies were undertaken by Jana Flegel, a Master student in the Department of Chemical Biology at the Max Planck Institute of Molecular Physiology, Dortmund, Germany. NIH/3T3 cells were transfected with N-mCherry-MTAP plasmid and the localization of the MTAP tagged with mCherry was studied by fluorescence microscopy. As seen in the representative images (Figure 56.), no effect of MJD-1314 or purmorphamine was seen on the localization of MTAP. Under physiological conditions MTAP is localized both in the cytosol and nucleus.¹⁵¹ However, treatment with purmorphamine and MJD-1314 did not affect the localization of MTAP within cellular compartments.

The binding of MJD-1314 to transiently expressed N-mCherry-MTAP is questionable as fusion of mCherry tag might lead to interference with binding. Also, the overexpression of N-mCherry-MTAP might have disturbed the stoichiometric protein ratios that produce no effect or contradictory effects. In order to overcome this issue, localization experiments can be performed with endogenous MTAP protein using antibodies against MTAP. Moreover, Fluorescence Resonance Energy Transfer (FRET) and Fluorescence Lifetime Imaging Microscopy (FLIM) can be performed to detect the binding of fluorophore-tagged MJD-1314 to MTAP and subcellular localization of MTAP.

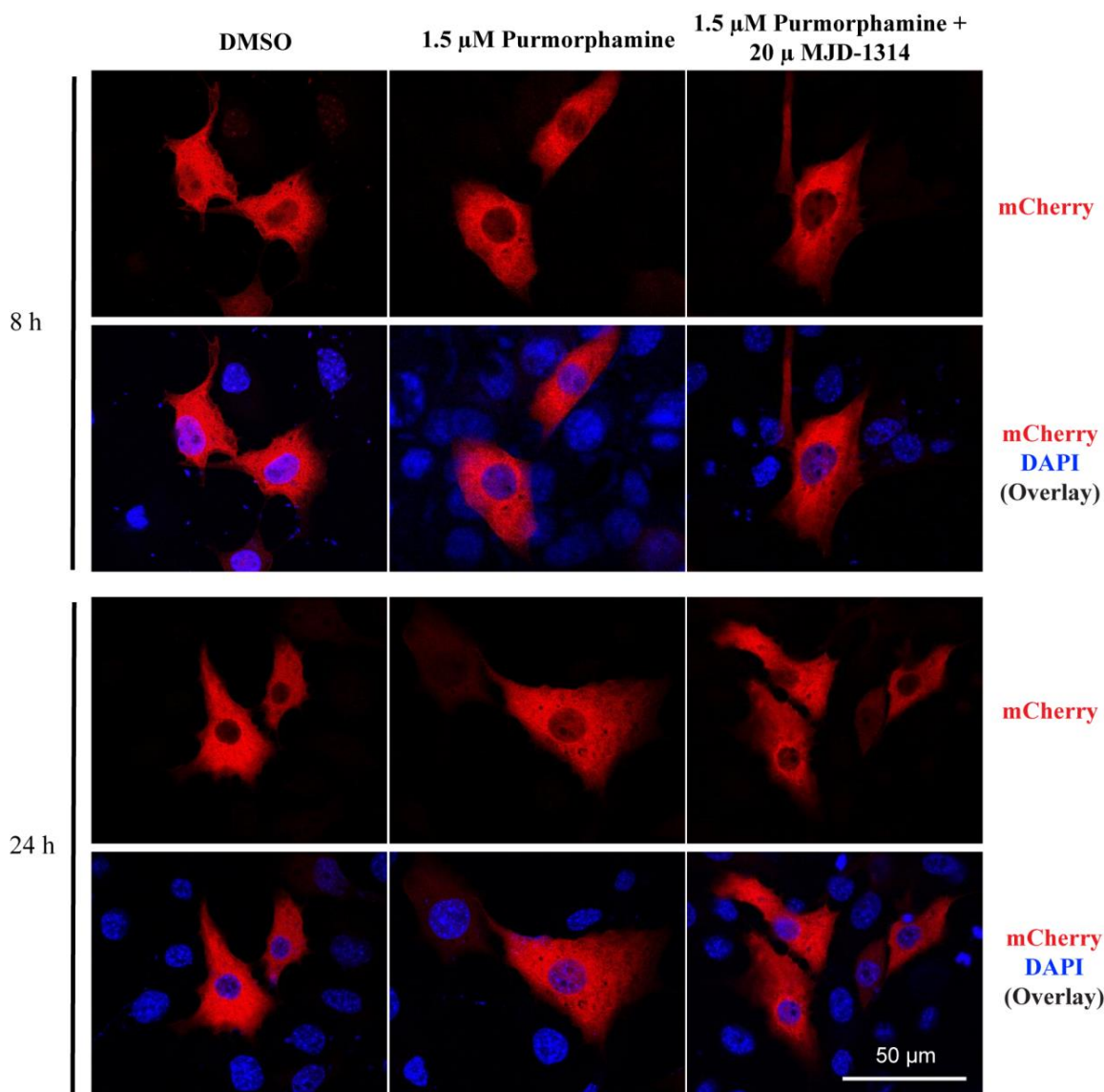


Figure 56. Effect of MJD-1314 on the subcellular localization of MTAP.

NIH/3T3 cells were transfected with N-mCherry MTAP plasmid (red). After 24 h cells were treated with 1.5 μM purmorphamine and 20 μM MJD-1314 or DMSO as a control. Cells were fixed and permeabilized after 8 h and 24 h. Cells were stained with DAPI (blue) to visualize nuclei and analyzed by using confocal microscopy. Representative images shown (n = 2).

5.4.9 Immunoprecipitation of interacting partners of MTAP

The outcome of MTAP enzymatic assay and localization studies did not shed light on the possible mode of involvement of MTAP in Hh signaling. Therefore, to decipher the non-canonical function of MTAP in Hh pathway regulation, protein-protein interaction of MTAP were analyzed by FLAG-immunoprecipitation. It was envisioned that MTAP might be a member of a protein complex that is being targeted by MJD-1314. In order to identify proteins that are interacting partners of MTAP, cell lysates of NIH/3T3 cells,

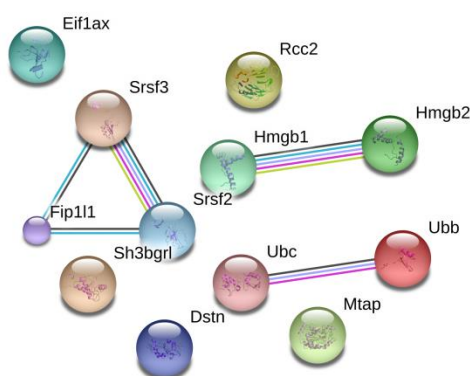
which were transfected with N-FLAG-MTAP or N-FLAG control vector, were exposed to anti-FLAG antibody-tagged magnetic beads. For the enzymatic digestion of bound proteins, magnetic beads were incubated with trypsin and LysC endopeptidases that cleave within the polypeptides. The resulting peptides were purified and analyzed by means of nano-HPLC / MS / MS. The mass spectrometry experiments were done at the HRMS facility at the MPI Dortmund and the resulting data analysis was performed by Dr. Petra Janning (MPI Dortmund). Statistical analysis was performed to quantify the proteins that were selectively enriched in the lysates of NIH/3T3 cells transfected with N-FLAG-MTAP as opposed to N-FLAG control vector transfected cells. It was expected that anti-FLAG tag would capture N-FLAG-MTAP protein along with the proteins that are bound to MTAP.

Table 7 summarizes the list of proteins that were enriched from lysates of N-FLAG-MTAP transfected cells. As expected, MTAP was identified with 927 fold enrichment ratio because of the transfection with N-FLAG-MTAP plasmid. Additional 10 proteins were identified to be selectively enriched from N-FLAG-MTAP lysates compared to the control samples. The known and predicted interactions of identified proteins were retrieved using version 10.0 of the STRING database (Figure 57).¹⁵² The interaction analysis indicates that none of the 10 identified proteins have known or predicted interactions with MTAP. Interaction analysis of each protein independently (data not shown) using the STRING database did not point out at direct interaction with Hh pathway regulation.

Table 7. List of proteins co-immunoprecipitated with N-FLAG-MTAP.

Two populations of NIH/3T3 cells were transfected with N-FLAG-MTAP plasmid or N-FLAG mock vector. The lysates from these transfected cells were exposed to anti-FLAG magnetic beads. The enriched proteins were eluted and analyzed by mass spectrometry. The ratios indicate the fold excess of protein enriched in beads exposed to lysates of N-FLAG-MTAP plasmid transfected beads compared to lysates of N-FLAG mock plasmid. The experiments were performed in technical triplicates. (N=3).

Protein name	Gene name	Ratio
S-methyl-5-thioadenosine phosphorylase	Mtap	927
SH3 domain-binding glutamic acid-rich-like protein	Sh3bgrl	10
High mobility group protein B2	Hmgb2	8
Serine/arginine-rich splicing factor 2	Srsf2	7
High mobility group protein B1	Hmgb1	5
Pre-mRNA 3-end-processing factor FIP1	Fip111	5
Serine/arginine-rich splicing factor 3	Srsf3	5
Destrin	Dstn	4
Protein RCC2	Rcc2	4
Ubiquitin-60S ribosomal protein L40	Ubc;Ubb	4
Eukaryotic translation initiation factor 1A	Eif1ax	2

**Figure 57. Known and predicted interaction analysis of proteins co-immunoprecipitated with N-FLAG-MTAP.**

The predominant identification of splicing factors such as Srsf2, Srsf3 and Fip111 indicates the modulation of splicing process by MTAP. Interestingly, alternative splicing

is an important regulatory mechanism for the modulation of repressor and activator properties of GLI2 protein.¹⁵³ Therefore, it is necessary to evaluate the effect of MJD-1314 on splicing process *via* modulation of MTAP.

5.4.10 Summary and outlook for the bis-nitrophenyl-bipyridine MJD-1314

A cell-based screen at COMAS identified MJD-1314 as a potent inhibitor of Hh signaling. Biological characterization of MJD-1314 revealed SMO independent and GLI-dependent inhibition of the Hh signaling pathway. Chemical proteomics efforts led to the identification of MTAP as a potential target of MJD-1314. Thermal stability experiments validated the target engagement for MJD-1314, which induced thermal stabilization of MTAP. Alterations in the expression levels of MTAP revealed complex involvement in the Hh signaling i.e. as a positive regulator or negative regulator.

The inability of MJD-1314 to inhibit MTAP enzyme function and the inability of MTDIA, an MTAP inhibitor, to inhibit Hh signaling indicates involvement of MTAP in Hh signaling independent of its enzymatic function. Efforts to decipher the non-canonical function of MTAP by analyzing the change in its localization upon compound treatment were unsuccessful. FLIM-FRET experiments¹²⁶ using fluorophore-tagged MJD-1314 and MTAP would illustrate the binding and subcellular localization of MTAP. The protein-protein interactions of MTAP with splicing factors and its possible effect on the Hh signaling needs to be further validated.

Although MJD-1314 did not inhibit the enzyme function of MTAP, it would be interesting to check the effect of MJD-1314 on the metabolic state of cells by metabolomics studies. Furthermore, gene expression profiling can shed light on non-canonical function of MTAP and mode of action of MJD-1314 in Hh pathway inhibition.

Overall, MJD-1314 is a novel inhibitor of Hh signaling acting downstream of SMO. The Hh pathway inhibition by MJD-1314 *via* MTAP needs to be addressed.

6 Materials

6.1 Chemicals

Chemicals	Provider
2-propanol	Fisher Scientific GmbH, Schwerte, GER
Acetonitrile	Fisher Scientific GmbH, GER
Acrylamide	AppliChem GmbH, Darmstadt, GER
Agar	Fisher Scientific GmbH, Schwerte, GER
Agarose	Life Technologies GmbH, Darmstadt, GER
Ammonium bicarbonate	Sigma-Aldrich Chemie GmbH, Munich, GER
Ammonium persulfate	SERVA Electrophoresis GmbH, Heidelberg, GER
Ammonium sulfate	AppliChem GmbH, Darmstadt, GER
Ampicillin	GERBU Biotechnik GmbH, Heidelberg, GER
Aqua/Polymount	Polysciences, Inc., PA, USA
BODIPY-Cycloamine	Carbosynth Limited, Compton, UK
Bovine Serum Albumin (BSA)	Invitrogen, Darmstadt, GER
Bromophenol blue	Sigma-Aldrich Chemie GmbH, Munich, GER
Cell dissociation buffer	PAN Biotech GmbH, Aidenbach, GER
Chloramphenicol	Carl Roth & Co. KG, Karlsruhe, GER
cOmplete protease Inhibitor, EDTA-free	Roche Diagnostics GmbH, Mannheim, GER
Coomassie Brilliant Blue G-250	SERVA Electrophoresis GmbH, Heidelberg, GER
Dimethylsulfoxide (DMSO)	SERVA Electrophoresis GmbH, Heidelberg, GER
Dithioerythritol (DTE)	GERBU Biotechnik GmbH, Heidelberg, GER
Dithiothreitol (DTT)	GERBU Biotechnik GmbH, Heidelberg, GER
Dulbecco's Modified Eagle Medium	PAN Biotech GmbH, Aidenbach, GER
Ethanol	Sigma-Aldrich Chemie GmbH, Munich, GER
Ethylenediaminetetraacetic acid (EDTA)	GERBU Biotechnik GmbH, Heidelberg, GER
Ethylenglycol tetraacetic acid (EGTA)	AppliChem GmbH, Darmstadt, GER
Formaldehyde	AppliChem GmbH, Darmstadt, GER
GelRed™ Nucleic Acid Gel Stain	Biotium, Inc., CA, USA
Geneticin (G418)	Sigma-Aldrich Chemie GmbH, Munich, GER
Glycerol	GERBU Biotechnik GmbH, Heidelberg, GER
Glycin	Carl Roth & Co. KG, Karlsruhe, GER
HEPES	GERBU Biotechnik GmbH, Heidelberg, GER
Hydrochloric acid (HCl)	AppliChem GmbH, Darmstadt, GER
Iodoacetamide	ACROS Organics, Geer, BEL
Kanamycine sulfate	GERBU Biotechnik GmbH, Heidelberg, GER
Magnesium chloride	AppliChem GmbH, Darmstadt, GER

Chemicals	Provider
Methanol	Sigma-Aldrich Chemie GmbH, Munich, GER
Non-essential amino acids (NEAA)	PAN Biotech GmbH, Aidenbach, GER
Nonfat dried milk powder	AppliChem GmbH, Darmstadt, GER
NP-40 Alternative	Calbiochem, Darmstadt, GER
Penicillin-Streptomycin (100x)	PAN Biotech GmbH, Aidenbach, GER
Phosphatase inhibitor	Roche Diagnostics GmbH, Mannheim, GER
Phosphate-buffered saline (PBS) Tablets	Jena Biosciences GmbH, Jena, GER
PhosStop, Phosphatase Inhibitor Cocktail	Roche, Mannheim, GER
PIPES	Sigma-Aldrich Chemie GmbH, Munich, GER
Ponceau S	SERVA Electrophoresis GmbH, Heidelberg, GER
Potassium chloride	AppliChem GmbH, Darmstadt, GER
Purmorphamine	Cayman Chemical, Ann Arbor, USA
RT PCR Water	Fisher Scientific GmbH, Schwerte, GER
SlimFast Schoko	SlimFast, Messel, GER
Sodium chloride	Sigma-Aldrich Chemie GmbH, Munich, GER
Sodium dodecyl sulfate	GERBU Biotechnik GmbH, Heidelberg, GER
Sodium hydrogencarbonate	Fisher Scientific GmbH, Schwerte, GER
Sodium pyruvate (100 mM)	PAN Biotech GmbH, Aidenbach, GER
Tetramethylethyldiamin (TEMED)	Carl Roth & Co. KG, Karlsruhe, GER
Trifluoroacetic acid	Sigma Aldrich, Steinheim, GER
Tris-HCl	Carl Roth & Co. KG, Karlsruhe, GER
Triton X-100	SERVA Electrophoresis GmbH, Heidelberg, GER
Trypan blue	Life Technologies GmbH, Darmstadt, GER
Trypsin	Roche Diagnostics GmbH, Mannheim, GER
Trypsin/EDTA	PAN Biotech GmbH, Aidenbach, GER
Tween 20	Santa Cruz Biotechnology, Inc., TX, USA
Vismodegib	Selleckchem, Munich, GER
Zeocin	InvivoGen, Toulpuse, France

6.2 Laboratory consumables

Consumable	Provider
Cell culture plates (6, 12, 24, 96 well plate)	Sarstedt AG & Co, Nümbrecht, GER
Cell culture flask (50, 250 750 mL)	Sarstedt AG & Co, Nümbrecht, GER
Cell culture 96-well plate, white	Greiner Bio-One GmbH, Frickenhausen, GER
Cell culture 384-well plate, white	Greiner Bio-One GmbH, Frickenhausen, GER
Countess® cell counter	Life Technologies GmbH, Darmstadt, GER
Coverslips	Carl Roth GmbH, Karlsruhe, GER
Gradient Protein Gel (4-20%)	Pierce, Thermo Fisher, GER

Consumable	Provider
Microscope slides	Diagonal, Münster, GER
iCycler iQ® PCR Plates, 96 well	Bio-Rad Laboratories Ltd., Hertfordshire, UK
PCR Sealers™, Microseal® 'B' Film	Bio-Rad Laboratories Ltd., Hertfordshire, UK
Cryovials	VWR International GmbH, Darmstadt, GER
Neubauer chamber	Sarstedt AG & Co, Nümbrecht, GER
Glass slides	Diagonal GmbH & Co. KG, Münster, GER
PVDF-Transfer membrane	Merck Chemicals Ltd, Beeston, GER
Serological pipettes	Sarstedt, Nümbrecht, GER
Whatman 3MM Paper	Whatman GmbH, Dassel, GER
Syringes (1, 5, 20, 50 mL)	Braun, Melsungen, GER
Test Tubes (0.5, 1.5, 2 mL)	Eppendorf, Hamburg, GER
Test Tubes (15, 50 mL)	Sarstedt, Nümbrecht, GER
Test Tubes (low protein bind, 1-5 mL)	Eppendorf, Hamburg, GER

6.3 Laboratory equipment

Equipment	Manufacturer
Agarose Gel Chamber	BioRad, München, GER
Cell Counter, Countess™	Life Technologies™, Darmstadt, GER
Centrifuge 5415R	Eppendorf Eppendorf, Hamburg, GER
Centrifuge, Minispin,	Eppendorf Eppendorf, Hamburg, GER
Gellogig 200 Imaging System	KODAK, Rochester, USA
iCycler Thermal Cycler (iQ5)	BioRad, München, GER
IncuCyt ZOOM	Essen BioScience, USA
Magnetic racks	Life Technologies™, Darmstadt, GER
Magnetic stirrer	IKA®Werke, Staufen, GER
NanoDrop 2000c UV-Vis Spectrophotometer	Thermo Scientific, Schwerte, GER
Odyssey® Fc imaging system	LI-COR Biosciences, Bad Homburg, GER
pH Meter	Mettler Toledo, Giessen, GER
Pierce™ G2 Fast Blotter	Thermo Scientific, Schwerte, GER
Plate Reader, Tecan Infinite M200	Tecan, Crailsheim, USA
Shaker/Thermomixer comfort	Eppendorf, Hamburg, GER
Sterile Bench	Nuaire NuAire, Fernwald, GER
Vortex Genie 2	Roth, Karlsruhe, GER
Waterbath	Hettich AG, Bäch, GER
Zeiss Observer Z.1, inverse fluorescence microscope	Zeiss, Jena, GER

6.4 Commercial Kits

Commercial kit	Manufacturer
Anti-Flag M2 Magnetic beads	Thermo Scientific, Schwerte, GER
CellTiter-Glo® Luminiscent Cell Viability Assay	Promega GmbH, Mannheim, GER
DC™ Protein Assay	Bio-Rad Laboratories GmbH, München, GER
Endofree Plasmid Maxi Kit	Qiagen GmbH, Hilden, GER
Lipofectamine® 2000 Transfection Reagent	Life Technologies GmbH, Darmstadt, GER
Phusion Flash High-Fidelity PCR Master Mix	Thermo Scientific, Schwerte, GER
QuantiTect Reverse Transcription Kit	Qiagen GmbH, Hilden, GER
Restore™ Western Blot Stripping Buffer	Thermo Scientific, Schwerte, GER
RNeasy mini Kit	Qiagen GmbH, Hilden, GER
SuperSignal® West Pico	Thermo Scientific, Schwerte, GER
SuperSignal® West Femto	Thermo Scientific, Schwerte, GER
FuGENE® 6 Transfection Reagent	Promega, Madison, USA
Qiagen® Plasmid Mini Purification Kit	Qiagen, Hilden, GER
Attractene Transfections Reagent	Qiagen, Hilden, GER
DharmaFECT™ 1	GE Healthcare Europe GmbH, Freiburg, GER
FuGene® 6	Promega GmbH, Mannheim, GER
Lipofectamine® 2000	Invitrogen GmbH, Darmstadt, GER
Lipofectamine® LTX & PLUS™	Invitrogen GmbH, Darmstadt, GER
CDP-Star® Chemiluminescence Substrate	Roche Diagnostics Deutschland GmbH, GER
Dual-Luciferase® Reporter Assay System	Promega GmbH, Mannheim, GER
QuantiFast SYBR Green PCR Kit	Bio-Rad Laboratories, Inc., California, USA

6.5 Buffers and solutions

Cell biology buffers	Composition
Fixation buffer	3.7% formaldehyd in PBS
Lysis buffer	50 mM PIPES 50 mM NaCl 5 mM MgCl ₂ 5 mM EGTA 0.1% (v/v) NP-40 0.1% (v/v) triton X-100 0.1% (v/v) tween 20 1 μM DTT protease Inhibitor PhosphoSTOP (pH 7.4)
PBS-T	0.1% tween20 in PBS
Permeabilization buffer	0.1% (v/v) triton X-100 in PBS
Protein biochemistry buffers	Composition
Colloidal coomassie staining solution	0.25% (w/v) coomassie brilliant blue G-250 45% (v/v) methanol 10% (v/v) acetic acid
Coomassie destaining solution	30% (v/v) methanol 10% (v/v) acetic acid
Immunoblotting blocking buffer	10 mM tris-HCl 150 mM NaCl 0.05% (v/v) tween-20 (pH 7.5) Blocking substances: 1-5% (w/v) skimmed milk or 2% (w/v) BSA or 2% (w/v) slim fast
Liposome assay buffer	20 mM HEPES, pH 7.4 150 mM NaCl 3 mM DTT
Liposome flotation assay buffer	20 mM HEPES, pH 7.4 150 mM NaCl 1 mM EDTA 1 mM DTT
Odyssey blocking buffer	LI-COR® GmbH, Bad Homburg, GER

Protein biochemistry buffers	Composition
RHOVDI1 FP buffer 1	30 mM Tris, pH 7.5 150 mM NaCl 3 mM DTE
RHOVDI1 FP buffer 2	30 mM TrisHCl, pH 7.5 10 mM KH ₂ PO ₄ /K ₂ HPO ₄ , 10 mM MgCl ₂
SDS running buffer (10x)	2.5 M glycine 250 mM Tris-HCl 35 mM SDS
SDS sample buffer (5x)	50% (v/v) glycerol 250 mM Tris-HCl (pH 6.8) 350 mM SDS 500 mM DTE 360 µM bromophenol blue
SDS separating gel (12%, 20 mL)	6.60 mL H ₂ O 8.00 mL acrylamide mix (30%) 5.00 mL Tris-HCl (1.5 M, pH 8.8) 0.20 mL SDS (10%) 0.20 mL ammonium persulfate (10%) 8 µL TEMED
SDS stacking gel (5%, 5 mL)	3.40 mL H ₂ O 0.83 mL acrylamide mix (30%) 0.63 mL tris-HCl (1.0 M, pH 6.8) 0.05 mL SDS (10% (w/v)) 0.05 mL ammonium persulfate (10%) 5 µl TEMED
Surface plasmon resonance buffer (SPR buffer)	20 mM HEPES, pH 7.4 50 mM NaCl 5 mM MgCl ₂ , 3 mM DTT
Transfer buffer	14.41 g/L glycine 3.03 g/L Tris-HCl 20% (v/v) methanol
Chemical proteomics buffers	Composition
Alkylation Buffer	50 mM chloroacetamide 8 M urea in 50 mM Tris-HCl, pH 7.9
Block A Solution	0.5 M ethanolamine 0.5 M NaCl, pH 8.3

Chemical proteomics buffers	Composition
Block B Solution	0.1 M sodium acetate 0.5 M NaCl, pH 4.0
In gel digestion alkylation Buffer	55 mM iodoacetamide in 25 mM NH ₄ HCO ₃
In-gel digestion reduction buffer	50 mM DTT in 25 mM NH ₄ HCO ₃
In-gel digestion solution	0.01 µg/mL trypsin (proteomic grade) in 25 mM NH ₄ HCO ₃
In-gel digestion wash solution I	25 mM NH ₄ HCO ₃ / acetonitrile (3:1)
In-gel digestion wash solution II	25 mM NH ₄ HCO ₃ / acetonitrile (1:1)
Reduction/ Denaturation Buffer	8 M urea in 50 mM Tris-HCl, pH 7.9
STAGE Elution Buffer	0.1% (v/v) formic acid 80% (v/v) acetonitrile in H ₂ O
STAGE Equilibration Buffer	0.1% (v/v) formic acid in H ₂ O
STAGE Reducing Buffer	0.05 M iodoacetamide, 8 M urea in 0.1 M Tris-HCl (pH 8.5) [always freshly prepared]
STAGE Urea Buffer	8 M urea in 0.1 M tris-HCl (pH 8.5) 5 µg/mL trypsin [always freshly prepared]
Molecular biology buffers	Composition
PBS	137 mM NaCl 2.7 mM KCl 10 mM Na ₂ HPO ₄ 2.0 mM KH ₂ PO ₄ (pH 7.4)
TAE	40 mM tris-HCl/ acetic acid (pH 7.5) 20 mM sodium acetate 1 mM EDTA
Enzyme assay buffers	Composition
PTP1b enzyme buffer	25 mM HEPES, 50 mM NaCl, 2.5 mM EDTA, 1 mM DTE, 0.025% NP-40 (pH 7.2)
MTAP enzyme buffer	200 mM NaH ₂ PO ₄ 200 mM Na ₂ HPO ₄ pH 7.0

6.6 Cell lines

Cell line	Description	Source
C3H/10T1/2	Mouse mesenchymal stem cells	ATCC (CCL-226)
HEK293T	Human embryonic kidney cells transformed with the SV-40 large T antigen	ATCC (CRL-3216)
HeLa	Human cervical cancer cells	ATCC (CCL-2)
NIH/3T3	Mouse embryonic fibroblast	DSMZ (ACC 59)
Shh-LIGHT2	NIH/3T3 cells stably transfected with a Gli-responsive firefly luciferase reporter plasmid and a pRL-TK constitutive renilla luciferase expression vector	(Sasaki et al., 1997) (Taipale et al., 2000)

6.7 Mammalian cell culture medium

Cell line	Medium
NIH/3T3	DMEM high Glucose (4.5 g/L) 10% FCS 1 mM Sodium pyruvate
Shh-LIGHT2	DMEM high Glucose (4.5 g/L) 10% FCS 1 mM Sodium pyruvate 400 µg/mL G418 150 µg/mL Zeocin
C3H/10T1/2	DMEM high Glucose (4.5 g/L) 10% FCS 6 mM L-Glutamine 1 mM Sodium pyruvate
HEK293T	DMEM high Glucose (4.5 g/L) 10% FBS 1% (v/v) Penicillin Streptomycin 1% (v/v) Sodium pyruvate 1% (v/v) Non-essential amino acids
HeLa	DMEM high Glucose (4.5 g/L) 10% FBS 1% (v/v) penicillin/streptomycin 1% (v/v) Sodium pyruvate 1% (v/v) MEM-NEAA

6.8 Bacterial strains

Bacterial Strains	Description	Medium
OmniMAX™ 2 T1	F' [proAB lacIq lacZΔM15 Tn10(TetR) Δ(ccdAB)] mcrA Δ(mrrhsdRMS-mcrBC) Φ80(lacZ)ΔM15Δ(lacZYA-argF)U169 endA1recA1 supE44 thi-1 gyrA96 relA1 tonA panD	LB Medium 0.5% (w/v) yeast extract 1% (w/v) tryptone 0.5% (w/v) NaCl LB agar plates 0.5% (w/v) yeast extract 1% (w/v) tryptone 0.5% (w/v) NaCl 1.5% (w/v) agar

6.9 PCR primers

Gene	Primer sequence	Amplicon size (bp)
<i>Gapdh</i>	Fwd: 5'-AGCCTCGTCCCG TAGACAAAAT-3' Rev: 5'-CCGTGAGTGGAGTCATACTGGA-3'	111
<i>Ptch1</i>	Fwd: 5'-CTCTGGAGCAGATTTCCAAGG-3' Rev: 5'-TGCCGCAGTTCTTTTGAATG-3'	116
<i>Gli1</i>	Fwd: 5'-GGAAGTCCTATTCACGCCTTGA-3' Rev: 5'-CAACCTTCTTGCTCACACATGTAAG-3'	90
<i>Arhgdia</i>	Fwd: 5'-GCAGCTTGTGTTGGGGTTTT-3' Rev: 5'-AGCAGACAACCTTGAGCCA-3'	94
<i>Mtap</i>	Fwd: 5'-GGTGGAACAGGCTTGGATGA-3' Rev: 5'-ATCGGATGGCTTGCCGAAT-3'	84

6.10 siRNAs

siRNA	Description and sequence	GE Healthcare Europe GmbH, catalog number
MTAP no-1	Mouse <i>Mtap</i> (66902) siRNA - GGUCAGAAACGCUCCGUAA	J-063657-09-0002
MTAP no-2	Mouse <i>Mtap</i> (66902) siRNA - CCACUACCCUACAGCGCUA	J-063657-10-0002
MTAP no-3	Mouse <i>Mtap</i> (66902) siRNA - CAGAUAGGGUCGAUGGAAU	J-063657-11-0002
RHOGDI no-1	Mouse <i>Arhgdia</i> (192662) siRNA - CGACUGACCUUGGUAUGCA	J-064240-05-0002

siRNA	Description and sequence	GE Healthcare Europe GmbH, catalog number
RHOGDI no-2	Mouse Arhgdia (192662) siRNA - UCAAGUCGCGCUUCACAGA	J-064240-06-0002
RHOGDI no-3	Mouse Arhgdia (192662) siRNA - GAGAUCGUGUCCGGCAUGA	J-064240-07-0002
Control siRNA	Non-targeting siRNA - UGGUUUACAUGUCGACUAA	D-001810-01-05

6.11 Plasmids

Plasmid	Description	Provider and catalogue number
pGEN-mSmo	Mammalian expression vector backbone: pEG with EGFP removed. The plasmid contains of neomycin resistance gene for selection.	Addgene, Cambridge, USA (37673)
pJ414-N-HIS-hMTAP	Bacterial expression vector backbone: pJ414 with synthetic human MTAP insert with N terminal HIS tag and ampicillin resistance gene.	Addgene, Cambridge, USA (64077)
pCMV3-N-FLAG-mMTAP	Mammalian expression pCMV3-N-FLAG vector with open reading frame of mMtap with N terminal FLAG tag. The size of the vector is 6098 base pairs with kanamycin resistance gene for selection.	Sino Biologicals, Beijing, China (MG5A1109-NF)
pCMV3-N-FLAG-mArhgdia	Mammalian expression pCMV3-N-FLAG vector with open reading frame of mArhgdia with N terminal FLAG tag. The size of the vector is 6098 base pairs with kanamycin resistance gene for selection.	Sino Biologicals, Beijing, China (MG52485-NF)
pCMV3-N-Flag-NCV	Mammalian expression pCMV3-N-FLAG vector as negative control for the pCMV3-N-FLAG clone multiple cloning sites are removed. The size of the plasmid is 6013 base pairs with kanamycin resistance gene for selection.	Sino Biologicals, Beijing, China (CV016)

6.12 Primary antibodies

Antibody	Catalogue number	Origin	Manufacturer
Anti-SMO	ab38686	Rabbit	Abcam, Cambridge, UK
anti-N-acetylated tubulin	T6793	Mouse	Sigma Alderich now Merck
Anti- β -Actin	ab8227	Rabbit	Abcam, Cambridge, UK
Anti-RHORHOGDIA-1	sc-373724	Mouse	Santa Cruz Biotechnology, Dallas, USA
Anti-MTAP	sc-100782	Mouse	Santa Cruz Biotechnology, Dallas, USA
Anti-NSDHL (D-11)	sc-390871	Mouse	Santa Cruz Biotechnology, Dallas, USA
Anti-ASEH1	sc-136275	Mouse	Santa Cruz Biotechnology, Dallas, USA

6.13 Secondary antibodies

Antibody	Catalogue number	Origin	Manufacturer
Anti-Rabbit-Alexa594	A11012	Goat	Invitrogen Life Technologies GmbH, Darmstadt, Germany
Anti-Mouse-Alexa488	A21202	Donkey	Invitrogen Life Technologies GmbH, Darmstadt, Germany
Anti-Mouse-IR800	926-32212	Donkey	LI-COR Biotechnology – GmbH, Bad Homburg, Germany
Anti-Mouse-HRP	31430	Goat	Thermo Fisher Scientific Inc., USA
Anti-Rabbit-IR680	926-68072	Donkey	LI-COR Biotechnology – GmbH, Bad Homburg, Germany

7 Methods

7.1 Cell culture

Cells were cultured in the corresponding cell culture medium in tissue culture flask T150 with growth area of 75 cm² at 37 °C and 5% CO₂. For sub-cultivation, the growth medium was removed at 80 – 85% confluency and cells were washed with 5 mL PBS. To detach cells from the bottom of the flask, 3 mL of trypsin / EDTA solution was added and cells were incubated for 5 min at 37 °C and 5% CO₂. Later, the cells were suspended in 7 mL of fresh growth medium. Whenever necessary for cell line maintenance, cells were transferred to new cell culture flask with corresponding medium.

7.1.1 Determination of cell number

The cell number was determined by mixing 10 µL cell suspension with 10 µL trypan blue and loading 10 µL of this mixture into the countess slide. This slide was then inserted into the automated counting device (CountessTM, InvitrogenTM) and cells were counted according to the manufacturer's instructions.

7.1.2 Osteoblast differentiation assay

For identification of the Hh signaling pathway modulators, an osteoblast differentiation assay was performed at the Compound Management and Screening Center (COMAS) in Dortmund, Germany. Briefly, 800 C3H/10T1/2C3H/10T1/2 cells were seeded per well in white 384-well plates. After incubation for 16 h, compounds were added to a final concentration of 10 µM using the acoustic nanoliter dispenser ECHO 520 (Labcyte). One hour later, osteogenesis was induced with addition of 1.5 µM purmorphamine. The plates were incubated for 96 h at 37 °C and 5% CO₂. In order to measure the activity of alkaline phosphatase, the medium from the 384 well plates was replaced with 35 µL osteogenesis-lysis buffer containing 1:100 chemiluminescent substrate CDP-Star®. The plates were incubated in the dark at 25 °C for one hour. The luminescence was monitored using the Paradigm plate reader (Molecular Devices, USA). Dose-response analysis was performed for all hit compounds using a three-fold dilution series starting from a concentration of 30 µM. Half-maximal inhibitory concentrations (IC₅₀) were calculated using the Quattro software suite (Quattro Research, Planegg, Germany).

Alternatively, osteogenesis assay was also performed in 96 well plates. 3000 C3H/10T1/2C3H/10T1/2 cells were seeded per well in white 96-well plates. After incubation for 16 h, compounds were added to a final concentration of 10 μM followed by addition of 1.5 μM purmorphamine after one hour. The plates were incubated for 96 h at 37 °C and 5% CO_2 . Subsequently the medium was replaced by 100 μL osteogenesis-lysis buffer containing 1:100 chemiluminescent substrate CDP-Star®. The plates were incubated in the dark at 25 °C for one hour and the luminescence was monitored using the Infinite® M200 plate reader (Tecan, Austria).

7.1.3 CellTiter-Glo® viability assay

The effect of test compounds on the viability of C3H/10T1/2C3H/10T1/2 cells was determined by the CellTiter-Glo® luminescence cell viability assay at COMAS, Dortmund, Germany. Cells were treated as described for the osteogenesis assay (see 7.1.2) prior to addition of the CellTiter-Glo® reagent according to manufacturer's protocol. Compounds causing at least a 50% reduction in the osteogenesis assay and retaining cell viability of at least 80% were considered as hits. Dose-response analysis was performed for all hit compounds using a three-fold dilution series starting from a concentration of 30 μM . Half-maximal inhibitory concentrations (IC_{50}) were calculated using the Quattro software suite (Quattro Research GmbH).

7.1.4 Gli-dependent reporter gene assay

2.5×10^4 Shh-LIGHT2 cells were seeded per well in 96-well plates. After incubation for 16 h, medium was replaced by low serum-containing medium (0.5% FCS) supplemented with 1.5 μM purmorphamine. One hour later various concentrations of the compounds or DMSO as a control were added and cells were further incubated for 48 h. Firefly and renilla luciferase activities were determined by means of the Dual-Luciferase® Reporter Assay System according to the manufacturer's protocol. Briefly, the medium was removed and cells were lysed by addition of 50 μL of 1X passive lysis buffer and continuous shaking at 25 °C for 20 min. 10 μL cell lysate was mixed with 10 μL firefly luciferase substrate in a white half-area 96 well plate and resulting firefly luminescence was measured. To this mixture 10 μL renilla luciferase substrate was added and the resulting renilla luciferase luminescence was measured using the Infinite® M200 plate reader (Tecan, Austria).

7.1.5 SMO binding assay using fluorescence microscopy

1.5×10^4 HEK293T cells were seeded on poly-D-lysine-coated coverslips placed in a 24-well plate. After overnight incubation, cells were transfected with the SMO expressing plasmid pGEN-mSmo (Addgene no. 37673) using Fugene HD (Promega) according to the manufacturer's protocol. After 48 h incubation at 37 °C cells were washed once with PBS and incubated further in fresh DMEM medium containing 0.5% FBS, 5 nM BODIPY-cyclopamine and various concentrations of the test compounds or DMSO as a control. One hour later cells were washed twice with PBS and fixed with 3% paraformaldehyde for 10 min at room temperature and subsequently permeabilized with 0.2% sodium azide in 1x PBS for 5 min at room temperature. Cells were then stained with 1 µg/ml DAPI for 10 min and were mounted on glass slides using Aqua Polymount (Polysciences Inc). Images were acquired on an Axiovert Observer Z1 microscope (Carl Zeiss, Germany) using a Plan-Apochromat 63x/1.40 Oil DIC M27 objective.

Alternatively, for washout experiments, the transfected cells were treated with 10 µM test compounds for 1 h. The medium was removed and cells were washed three times with fresh medium for 5 min followed by addition of medium supplemented with 5 nM BODIPY-cyclopamine for 1 h prior to fixation, staining and visualization as mentioned above.

7.1.6 SMO binding assay using flow cytometry

3×10^5 HEK293T cells per well were seeded in 6-well plate. After overnight incubation, cells were transfected with the SMO expressing plasmid pGEN-mSmo as described above. After 48 h of incubation the medium was replaced by DMEM containing 0.5% FBS, 5 nM BODIPY-cyclopamine and various concentrations of the test compounds or DMSO as a control. Following incubation for 5 h cells were washed once with PBS, detached using trypsin/EDTA (0.05/0.02% (v/v) in PBS), and collected by centrifugation at 250 x g for 5 min at room temperature. Cells were washed twice and then suspended in ice-cold PBS. Cell suspensions were subjected to flow cytometry analysis employing the BD LSR II Flow Cytometer (laser line: 488 nm, emission filter: 530/30) to detect the presence of BODIPY. Data analysis was performed using the FlowJo software, version 7.6.5 (Tree Star Inc., USA).

7.1.7 SAG1 competition assay

The competition assay was performed using the Gli-dependent reporter gene assay as described above (see 7.1.4) with exception of using 0.1 μM or 1 μM SMO agonist (SAG) to activate the pathway instead of purmorphamine.

7.1.8 Ciliary localization of SMO

3×10^4 NIH/3T3 cells per well were seeded in coverslip-containing 24-well plate and cultured overnight. Cells were further incubated for 12 h in DMEM containing 0.5% FCS to induce ciliation. Cells were then treated with 1.5 μM purmorphamine and various concentrations of the test compounds or DMSO as a control. 12 h later cells were washed with PBS followed by fixation in 4% ice-cold paraformaldehyde for 10 min at room temperature. Permeabilization and blocking was performed with a solution containing 0.1% Triton X-100 and 1% heat-inactivated horse serum in PBS for 30 min at room temperature. The samples were then incubated with mouse anti-N-acetylated tubulin antibody (dilution 1:5000) and rabbit anti-SMO antibody (dilution 1:200) overnight at 4 $^{\circ}\text{C}$ followed by washing and subsequent incubation with Alexa Fluor 594-conjugated goat anti-rabbit and Alexa Fluor 488-conjugated donkey anti-mouse antibodies (Invitrogen; 1:500 dilutions) and DAPI (0.1 $\mu\text{g}/\text{mL}$) for 45 min at room temperature. Coverslips were washed and mounted using Aqua Polymount (Polysciences Inc). Images were acquired with Axiovert Observer microscope Z1 (Carl Zeiss, Germany) using a Plan-Apochromat 63x/1.40 Oil DIC M27 objective.

7.2 Molecular biology methods

7.2.1 RNA isolation

2.0×10^4 C3H/10T1/2C3H/10T1/2 cells were seeded per well in 24-well plate and incubated overnight at 37 $^{\circ}\text{C}$. The medium was replaced by medium containing 1.5 μM purmorphamine and various concentrations of test compounds or DMSO and incubated for 48 h. Subsequently, the total RNA was isolated using the RNeasy mini kit (Qiagen) according to the manufacturer's protocol. Briefly, cells were lysed by adding 350 μL RLT buffer provided with the kit. The resulting cell lysates were added to the QIAshredder columns and centrifuged for 2 min at 8000 x g. The homogenized lysate was later mixed with equal volumes of 70% (v/v) ethanol. Total RNA was purified by transferring the

homogenized mixture into RNeasy columns and centrifugation for 15 s at 8000 x g. After centrifugation the flow-through was discarded and columns were washed with 700 μ L RW1 buffer for 15 s at 8000 x g. The columns were then washed twice with 500 μ L RPE buffer for 15 s and 2 min at 8000 x g. The columns were later placed in new 2 mL collection tubes and centrifuged at 8000 x g for 1 min. Finally, the RNA was eluted by adding 30 μ L RNase-free water to the column and centrifugation at 8000 x g for 1 min.

The concentration of purified RNA was measured by means of the Nanodrop 2000. The device was first calibrated with pure RNase-free water and the absorption of 1 μ L RNA was then measured at 260 nm. The RNA was shock-frozen for storage in liquid nitrogen and stored at -80 °C.

7.2.2 cDNA preparation

Total RNA (see 7.2.1) was used to prepare complementary DNA (cDNA) using QuantiTect Reverse Transcription Kit (Qiagen) according to the manufacturer's protocol. Briefly, 2 μ L gDNA Wipeout buffer was added to 12 μ L of total RNA diluted in RNase-free water to a final concentration of 500 ng per sample. The samples were incubated at 42 °C for 2 min in order to eliminate genomic DNA. 6 μ L of a mastermix containing 1 μ L Quantiscript Reverse Transcriptase, 4 μ L Quantiscript RT Buffer (5x) and 1 μ L RT primer mix were mixed with 14 μ L of RNA and incubated for 15 min at 42 °C. The reverse transcriptase was inactivated by incubating the reaction mixture at 96 °C for 3 min. The cDNA samples were stored at -20 °C.

7.2.3 Quantitative PCR

Quantitative PCR was performed using SsoAdvancedTM Universal SYBR[®] Green Supermix according the manufacturer's protocol. Briefly, 50 ng cDNA (from 7.2.2) was added to a master mix containing 1 μ M of the respective primer pairs (see 6.9), nuclease-free H₂O and 5 μ L SsoAdvancedTM Universal SYBR[®] Green Supermix. The final reaction volume was maintained at 10 μ L. The quantitative amplification was performed using iQTM5 Real-Time PCR Detection System (Biorad, Germany). In order to achieve polymerase activation and DNA denaturation, the reactions were incubated at 95 °C for 30 s. Subsequently, the fluorescence was recorded over 40 denaturation and annealing/extension cycles at 96 °C for 10 s followed by 30 s at 60 °C. The expression level of the genes was determined by using the $2^{-\Delta\Delta Ct}$ method.¹⁵⁴

7.2.4 Transformation of competent *E. coli* with plasmid DNA

For the transformation of plasmid DNA, chemically competent *E. coli* cells (One Shot® OmniMAX™ 2 T1) were used. To 100 µL of the *E. coli* cells 100 ng plasmid DNA were added and the cells were incubated for 30 min on ice. For heat shock transformation, cells were incubated for 1 min at 42 °C and subsequently incubated for 2 min on ice. 900 µL LB medium were added to the cells followed by incubation for 1 h at 37 °C in a shaker. Cells were centrifuged at 9300 x g for 5 min and the supernatant was discarded. The resulting pellet was suspended in 100 µL of LB medium. The resulting suspension was transferred onto LB agar plates containing the corresponding antibiotic and incubated overnight at 37 °C. A single colony was picked and inoculated into LB medium containing the appropriate antibiotic followed by preparation of glycerol stock.

7.2.5 Glycerol stock preparation

For the long-term preservation of the plasmids, 500 µL cell suspension of plasmid-transformed bacteria were mixed with 500 µL sterile glycerol and stored at -80 °C.

7.2.6 Plasmid DNA isolation

The plasmid DNA was isolated using QIAGEN Plasmid Maxi Kit (Qiagen, Germany) according to the manufacturer's protocol. Bacterial cells from glycerol stocks were inoculated into 300 mL of LB medium supplemented with an appropriate antibiotic and incubated overnight with continuous shaking at 37 °C. Cells were harvested by centrifugation at 6000 x g for 15 min at 4 °C. The supernatant was discarded and the cell pellet was suspended in 10 mL ice-cold P1 buffer supplemented with RNase. 10 mL buffer P2 were added to the suspension and incubated at room temperature for 5 min. Subsequently, 10 mL ice-cold buffer P3 was added and samples were incubated on ice for 20 min. The resulting cell suspension was centrifuged for 30 min at 20000 x g for 30 min at 4 °C. The supernatant was collected and passed over Qiagen-tip 500 column which was activated by passing 10 mL buffer QBT beforehand. The column was washed twice by with 30 mL of buffer QC. The plasmid DNA was eluted by adding two times 5 mL buffer QF to the column and the eluate was collected in fresh centrifuge tubes. The plasmid DNA was precipitated by adding 7 mL 2-propanol and centrifuged at 20000 x g for 30 min at 4 °C. The supernatant was discarded and the pellet was washed in 5 mL 70% (v/v) ethanol and centrifuged at 20000 x g for 5 min at 4 °C. The supernatant was discarded

and the pellet was air dried for 5 min and subsequently dissolved in 500 μ L TE buffer. The concentration of the plasmid DNA was determined by using the NanoDrop 2000 spectrophotometer as described in 7.2.1.

7.3 Biochemical methods

7.3.1 Purification of recombinant MTAP protein

The pJ414-N-HIS-hMTAP plasmid containing the human MTAP gene was transformed into BL21-CodonPlus(DE3)-RIL cells which were grown overnight at 37 °C in 25 mL of LB medium containing 100 μ g/mL ampicillin. This culture was transferred into 1 L of LB ampicillin-containing medium, and the cell growth was continued at 37 °C until the optical density (OD) at 600 nm (OD_{600}) reached 0.7. Protein expression was induced by adding IPTG to 1 mM final concentration. After 4 h of induction at 37 °C, the cells were harvested by centrifugation at 4500 x g for 30 min. The cell pellet was suspended in 20 mL of lysis buffer (15 mM imidazole, 300 mM NaCl, and 50 mM phosphate, 1 mM PMSF, 1 μ g/mL lysozyme pH 8.0), containing EDTA-free DNase inhibitor (2 tablets for 20 mL, Roche Diagnostics) added according to the supplier's recommendations.

Cells were disrupted twice with a fluidizer and centrifuged at 20000 x g for 30 min. The supernatant was loaded onto a 5 mL column of Ni-NTA Superflow resin pre-equilibrated with 15 mL of lysis buffer. The column was washed with 15 mL of wash buffer (80 mM imidazole, 300 mM NaCl, and 50 mM phosphate buffer, pH 8.0), and the enzyme was eluted with 12 mL of elution buffer (250 mM imidazole, 300 mM NaCl, and 50 mM phosphate, pH 8.0). The purified enzyme was dialyzed against 100 mM phosphate buffer, pH 7.4, with 2 mM DTT and concentrated to about 30.85 g/L. The enzyme was frozen at -80 °C for storage and had a purity of >95% determined by means of SDS-PAGE.

7.3.2 Protein concentration determination

The protein concentration of cell lysates was determined by employing the DC™ Protein Assay kit. Briefly, 5 μ L homogenized lysate were added per well to a clear bottom 96-well plate. 25 μ L per well working reagent A, that was prepared by mixing 20 μ L reagent S with 980 μ L reagent A, and added to the lysates. Subsequently, 200 μ L of reagent B was added per well and incubated in the dark for 20 min. The change in the absorbance was monitored at 750 nm using the Infinite® M200 plate reader (Tecan, Austria). To

calculate the protein concentration, a BSA concentration series of 4, 2, 1, 0.5, 0.25, 0.125, 0.062 and 0 mg/mL was measured as a standard. A linear regression equation was determined by plotting the BSA concentrations against the corresponding absorbance. The resulting linear equation was used to determine the protein concentration of the lysate.

7.3.3 SDS polyacrylamide gel electrophoresis (SDS-PAGE)

Cell lysates were mixed with 5x SDS sample buffer for 10 min at 95 °C. These lysates and 5 µL protein standard were applied to 12% or 15% polyacrylamide gels. The gels were immersed in 1x SDS running buffer and exposed to an electric field. For the first 10 min the proteins were separated under the 80 V and later with constant voltage of 120 V. After electrophoresis, gels were stained with a colloidal Coomassie solution or transferred on a PVDF membrane.

7.3.4 Immunoblotting

Immunoblotting describes the transfer the proteins from polyacrylamide gels to a PVDF membrane for subsequent detection of proteins using specific antibodies.

After the SDS-PAGE, the gel was transferred to a container and washed three times for 5 min with deionized H₂O. In parallel, the PVDF membrane was activated with methanol for 30 s and the Whatman filter paper was soaked for 10 min in Pierce™ 1-Step Transfer Buffer. The PVDF membrane was later equilibrated with Pierce™ 1-Step Transfer Buffer for 5 min prior to placing on to two layers of soaked filter paper. The polyacrylamide gel was placed on top of the membrane, followed by two layers of soaked filter paper. Air bubbles and excess buffer were removed from this assembly by carefully pressing this setup with a roller. The protein transfer was carried out at a constant voltage of 25 V for 7 min using the Pierce™ Fast Semi-Dry Blotter. The membrane was then washed twice with deionized water and swirled briefly in Ponceau S to stain the proteins. The stained membrane was washed with deionized water until the transferred proteins were visible on the membrane.

7.3.5 Colloidal coomassie staining of proteins

Proteins resolved using SDS-PAGE were stained with a colloidal Coomassie solution. After electrophoresis, the gel was transferred to a fresh container and rinsed with

deionized water. The gel was submerged in Coomassie-staining solution for 30 min. After the staining, excess of staining solution was removed by submerging the stained gel with destaining solution overnight.

7.3.6 PTP1B enzymatic assay

PTP1B-catalyzed hydrolysis of p-nitrophenyl phosphate (pNPP) to p-nitrophenol (pNP) was determined by measuring the absorbance at 405 nm. 15 nM of human full-length PTP1B was preincubated with various concentrations of the test compounds in PTP1B assay buffer for 30 min at 37 °C. The enzymatic reaction was initiated by the addition of 2 mM of pNPP. The reaction volume was maintained 200 µL and the reactions were carried out in 96-well clear bottom microtiter plates. The resulting change in the absorbance at 405 nm was continuously monitored for 60 min at 30 °C using Infinite® M200 plate reader (Tecan, Austria).

7.3.7 MTAP enzymatic assay

Liberation of adenine upon phosphorylation of methylthioadenosine (MTA) by MTAP was monitored by its conversion to 8-dihydroxyadenine by xanthine oxidase. 200 µM of MTA, 0.2 U xanthine oxidase, and test compounds were incubated at 25 °C for 5 min. The enzymatic reaction was initiated by the addition of 100 nM of MTAP. The reaction volume was maintained 200 µL and the reactions were carried out in 96 well flat µClear® bottom microtiter plates. The resulting change in the absorbance at 305 nm was continuously monitored for 60 min using Infinite® M200 plate reader (Tecan, Austria).

7.4 Chemical proteomics

7.4.1 Cell lysate preparation for affinity *pull-down* experiments

5×10^5 NIH/3T3 cells were grown in T150 cell culture flask up to 90-95% confluence with changing the medium intermittently. Cells were washed with 5 mL PBS and detached from the bottom of flask by adding 5 mL of cell dissociation solution for 5 min at 37 °C and 5% CO₂. Cells were suspended in cell culture medium and pelleted by centrifuged at 250 x g, 5 min at 4 °C. The cell pellets were then washed thrice with PBS by suspending the cells in ice-cold PBS followed by centrifugation. Finally, the cell pellets were either directly frozen in liquid nitrogen and stored at -80 °C or subsequently lysed in lysis buffer

(see 0) for 10 min on ice. To assure complete cell lysis, the suspension was passed through 0.9 μm and 0.45 μm cannula 10 times each and incubated on ice for 40 min with intermittent vortexing every five minutes until a homogeneous mixture was obtained. The resulting homogenate was centrifuged at 18000 x g for 30 min at 4 °C and the supernatant was carefully transferred into a new vial. The supernatant was subsequently snap frozen in liquid nitrogen and stored at -80 °C.

7.4.2 Cell lysate preparation for co-immunoprecipitation

The two populations of NIH3/T3 cells were transiently transfected with pCMV3-N-FLAG-mMTAP plasmid or pCMV3-N-FLAG-NCV plasmid using Lipofectamine® LTX & PLUS™ reagent according to manufacturer's protocol. Briefly, 2×10^6 NIH/3T3 cells were seeded in T175 flasks and incubated overnight at 37 °C and 5% CO₂. For the transfection, 500 ng/ μL plasmid DNA and PLUS reagent were diluted in Opti-MEM® medium and incubated for 5 min at room temperature. Lipofectamine® LTX reagent was directly added to this mixture and incubated for 30 min at room temperature. The Plasmid DNA to transfection reagent ratio of 1:4 was maintained during the transfections (Plasmid [μg]:Transfection reagent [μL]). The DNA-lipid complex was added dropwise to the T175 flask and cells were continued to grow for 24 h to achieve a confluency of up to 90-95%. The cells were washed with 5 mL PBS and detached from the bottom of flask by adding 5 mL of cell dissociation solution for 5 min at 37 °C and 5% CO₂. The cells were suspended in cell culture medium and pelleted by centrifugation at 250 x g, 5 min at 4 °C. The cell pellets were then washed thrice with PBS by suspending the cells in ice-cold PBS followed by centrifugation. Finally, the cell pellets were either directly frozen in liquid nitrogen and stored at -80 °C or subsequently lysed in lysis buffer for 10 min on ice. To assure complete cell lysis, the suspension was passed through 0.9 μm and 0.45 μm cannula 10 times each and incubated on ice for 40 min with intermittent vortexing every five minutes until a homogeneous mixture was obtained. The resulting homogenate was centrifuged at 18000 x g, 30 min at 4 °C and the supernatant was carefully transferred into a new vial. The supernatant was subsequently snap frozen in liquid nitrogen and stored at -80 °C.

7.4.3 Affinity chromatography enrichment of compound-bound proteins (Pull-down)

25 μL N-hydroxysuccinimide magnetic beads were activated by incubation with 500 μL 1 mM HCl for 1 min. HCl was replaced by 500 μL coupling buffer containing 10 μM of free amine affinity probes and incubated for 2 h at room temperature with overhead rotation. The residual active groups of the immobilized probes were quenched by alternating incubation with 500 μL block A buffer and block B buffer for 5 min three times each. For protein binding, the magnetic beads were equilibrated with 500 μL lysis buffer followed by incubation with 500 μL lysate (protein concentration: 2 mg/mL) 2 h at 4 $^{\circ}\text{C}$ with overhead rotation. In order to wash out non-specifically bound proteins, the beads were first washed with 500 μL lysis buffer containing 25 mM MgCl_2 followed by three times washing with 500 μL PBS. At this stage, the beads were either mixed with 5 x SDS sample buffer for 5 min at 95 $^{\circ}\text{C}$ or the beads were processed for on-bead tryptic digestion.

7.4.4 On bead tryptic digestion and STAGE (STop And Go Extraction) tips desalting

Tryptic digestion of bead-bound proteins was carried out in two stages. First, bound proteins were reduced by incubating the beads with 50 μL reducing buffer at 30 $^{\circ}\text{C}$ for 30 min with shaking. Later, the reduced proteins were alkylated by addition of 5.5 μL alkylating solution and further incubation in the dark at 30 $^{\circ}\text{C}$ for 30 min while shaking at 350 rpm. The reduced and alkylated proteins were digested by adding 1 μg LysC at 37 $^{\circ}\text{C}$ for 1 h while shaking at 350 rpm. The supernatant was transferred to a new tube and the beads were further incubated with 50 mM Tris-HCl (pH 7.5) containing 1 μg trypsin at 37 $^{\circ}\text{C}$ for 1 h while shaking at 350 rpm. Both the supernatants were combined together and further digested by adding 2 μg trypsin for 16 h at 37 $^{\circ}\text{C}$ with continuous shaking. The enzymatic digestion was stopped by addition of 2 μL proteomics grade TFA. In order to purify the resulting peptides, STAGE tips were prepared by loading the 200 μL microtips with 2 layers of C18 (octadecyl) disks. The tips with C18 disks were activated by addition of 100 μL methanol. Furthermore, the tips were calibrated by washing with 100 μL Buffer B and 100 μL Buffer A. The peptide purification was achieved by passing the digestion solution over the activated STAGE tips. Bound peptides were eluted twice

using 20 μ L Buffer B and the solvent was evaporated by means of rotary speed vacuum evaporator. The samples were stored at $-20\text{ }^{\circ}\text{C}$ until mass spectrometry analysis.

7.4.5 Cell lysate preparation for stable isotope labeling with amino acids in cell culture (SILAC)

In order to prepare 500 mL SILAC medium containing heavy isotope “heavy medium”, DMEM (Gibco, A14431-01) without L-arginine, L-lysine, L-glutamine and sodium pyruvate, the medium was supplemented with 50 mg $^{13}\text{C}_6,^{15}\text{N}_2$ L-lysine and 50 mg $^{13}\text{C}_6,^{15}\text{N}_4$ - L-arginine, 10% (v/v) dialyzed and heat-inactivated fetal bovine serum, 2 mM L-glutamine and 1 mM sodium pyruvate. Similarly, for preparing the SILAC medium with light isotope “light medium”, 50 mg $^{12}\text{C}_6,^{15}\text{N}_2$ L-lysine and 50 mg $^{12}\text{C}_6,^{14}\text{N}_4$ - L-arginine were used. Two populations of NIH/3T3 cells were either grown in “heavy” or “light” medium in T175 cell culture flask for seven day and up to 90-95% confluence with medium exchange after three days. The cells were washed with 5 mL PBS and detached from the bottom of flask by adding 5 mL of cell dissociation solution for 5 min at $37\text{ }^{\circ}\text{C}$ and 5% CO_2 . The cells were suspended in cell culture medium and pelleted by centrifugation at $250 \times g$ for 5 min at $4\text{ }^{\circ}\text{C}$. The cell pellets were then washed thrice by suspending the cells in ice-cold PBS followed by centrifugation. Finally, the cell pellets were either directly frozen in liquid nitrogen and stored at $-80\text{ }^{\circ}\text{C}$ or subsequently lysed in lysis buffer (see 0) for 10 min on ice. To assure complete cell lysis, the suspension was passed through $0.9\text{ }\mu\text{m}$ and $0.45\text{ }\mu\text{m}$ cannula 10 times each and incubated on ice for 40 min with intermittent vortexing every five minutes until a homogeneous mixture was obtained. The resulting homogenate was centrifuged at $18000 \times g$ for 30 min at $4\text{ }^{\circ}\text{C}$ and the supernatant was carefully transferred into a new vial. The supernatant was subsequently snap frozen in liquid nitrogen and stored at $-80\text{ }^{\circ}\text{C}$.

7.4.6 Determination of heavy amino acid incorporation efficiency

For checking the isotope-labelled amino acid incorporation efficiency, SILAC “heavy” and “light” lysates were mixed with 5 x SDS sample buffer and incubated for 10 min at $95\text{ }^{\circ}\text{C}$. These samples were separated using precast TGX 4-20% polyacrylamide gel by applying electric field for 15 min at 80 V. After the electrophoresis the gel was transferred to a glass petri dish and washed once with fixation solution. Protein bands indicated by bromophenol blue and empty gel were cut using scalpel and transferred to

fresh Eppendorf tube containing 500 μL fixation buffer and incubated overnight with shaking at 25 $^{\circ}\text{C}$. The fixation solution was replaced by 200 μL wash in-gel digestion wash solution I for 30 min at 37 $^{\circ}\text{C}$ followed by in-gel digestion wash solution II 2 and washed for another 45 min at 37 $^{\circ}\text{C}$. In order to reduce disulfide bridges, 200 μL reducing buffer was added to the gel pieces and incubated for 45 min at 37 $^{\circ}\text{C}$. Alkylation of the reduced proteins was carried out by addition of 200 μL of the alkylation solution for 1 h in the dark at 25 $^{\circ}\text{C}$. The gel pieces were washed twice with 200 μL in-gel digestion wash solution II for 15 min at 25 $^{\circ}\text{C}$. The gel pieces were dehydrated by incubating with 100 μL acetonitrile for 10 min at 25 $^{\circ}\text{C}$ and subsequent air drying for 15 min. Proteins inside the gel were digested by addition of 75 μL 25 mM NH_4HCO_3 containing 750 ng trypsin and incubated at 30 $^{\circ}\text{C}$ for 15 min. The digestion was continued by the addition of another 75 μL 25 mM NH_4HCO_3 at 30 $^{\circ}\text{C}$ for 16 h. The digestion was stopped by addition of 10 μL 10% (v/v) TFA and subsequent sonication for 30 min at 0 $^{\circ}\text{C}$. The supernatant was collected and transferred to fresh Eppendorf tube. 50 μL acetonitrile was added to the gel pieces and incubated for 15 min. The resultant supernatant was collected carefully. The combined supernatants were concentrated in a vacuum evaporator and the dried samples were stored at -80 $^{\circ}\text{C}$ until mass spectrometric analysis.

7.4.7 Co-immunoprecipitation

20 μL anti-Flag M2 Magnetic beads were added to 1.5 mL low-binding tubes. The storage solution was removed and the beads were washed with 500 μL TBS buffer followed by 500 μL lysis buffer (without protease inhibitor, PhosphoSTOP and DTT) for 5 min. For protein binding, 250 μL (3 mg/mL) lysate from 7.4.2 were added to the beads and incubated at 4 $^{\circ}\text{C}$ for 4 h with overhead rotation. The lysate was then removed and beads were washed with lysis buffer followed by washing thrice with 500 μL TBS for 5 min each. On bead tryptic digestion and STAGE tip desalting was performed according to 7.4.4 and the samples were analyzed by mass spectrometry.

7.4.8 Mass spectrometric and data evaluation

In order to identify the tryptic peptides, the samples were purified by UltiMateTM 3000 RSLCnano system (Dionex, Germany) and MS/MS analysis was carried out using Q ExactiveTM Plus Hybrid Quadrupole-Orbitrap Mass Spectrometer equipped with a nano-spray source (Nanospray Flex Ion Source, Thermo Scientific). Briefly, the tryptic

peptides were solubilized in 20 μL 0.1% (v/v) TFA in water and 3 μL were injected onto a pre-column cartridge (5 μm , 100 \AA , 300 μm ID * 5 mm, Dionex, Germany) using 0.1% (v/v) TFA in water as eluent with a flow rate of 30 $\mu\text{L}/\text{min}$. Desalting was performed for 5 min with eluent flow through followed by back-flushing of the sample during the whole analysis from the pre-column to the PepMap100 RSLC C18 nano-HPLC column (2 μm , 100 \AA , 75 μm ID \times 50 cm, nanoViper, Dionex, Germany) using a linear gradient starting with 95% water containing 0.1% (v/v) formic acid / 5% (v/v) acetonitrile containing 0.1% (v/v) formic acid and increasing to 70% water containing 0.1% (v/v) formic acid / 30% (v/v) acetonitrile containing 0.1% (v/v) formic acid after 95 min using a flow rate of 300 nL/min. The nano-HPLC was coupled to the Quadrupole-Orbitrap Mass Spectrometer using a standard coated SilicaTip (ID 20 μm , Tip-ID 10 μm , New Objective, Woburn, MA, USA), mass range of m/z 300 to 1650 was acquired with a resolution of 70000 for a full scan, followed by up to ten high energy collision dissociation (HCD) MS/MS scans of the most intense at least doubly charged ions with a resolution of 17500.

Data evaluation was performed using MaxQuant software¹⁵⁵ (v.1.5.3.30) including the Andromeda search algorithm and searching the mouse reference proteome of the uniprot database. Briefly, the search was performed for full enzymatic trypsin cleavages allowing two miscleavages. For protein modifications carbamidomethylation was chosen as fixed and oxidation of methionine and acetylation of the N-terminus as variable modifications. The mass accuracy for full mass spectra was set to 20 ppm for the first and 4.5 ppm for the second search. The mass accuracy for MS/MS spectra was set to 20 ppm. The false discovery rates for peptide and protein identification were set to 1%. Only proteins for which at least two peptides were quantified were chosen for further validation. For label-free experiments, label free quantification (LFQ) intensities were logarithmized (\log_2) and proteins which were not three times quantified in at least one of the groups were filtered. For SILAC experiments $^{13}\text{C}_6, ^{15}\text{N}_2$ L-lysine and $^{13}\text{C}_6, ^{15}\text{N}_4$ - L-arginine were chosen for the “heavy” labeled samples and the intensities were logarithmized (\log_2). Proteins which were quantified less than three times in at least one of the groups were filtered out. In both the cases missing values were imputed using small normal distributed values and a t-test was performed. Proteins which were statically significant outliers in at least one out of the three experiments were considered as hits.

7.4.9 Target engagement by affinity enrichment

To validate the target engagement of putative target proteins by the test compound, cell lysates were pre-incubated with various concentrations of the test compound or DMSO at 4 °C for 2 h followed by exposure to immobilized active probe. Briefly, 25 µL N-hydroxysuccinimide magnetic beads were activated by incubating with 500 µL of 1 mM HCl for 1 min. HCl was replaced by 500 µL of coupling buffer (0.15 M triethanolamine, 0.5 M NaCl pH 8.3) containing 10 µM of free amine affinity probes and incubated for 2 h at 25 °C with overhead rotation. The residual active groups on the immobilized probes were quenched by alternating incubation with 500 µL Block A buffer (0.5 M ethanolamine, 0.5 M NaCl, pH 8.3) and Block B buffer buffers for 5 min three times each. For protein binding, the immobilized probes were equilibrated with 500 µL of lysis buffer followed by incubation for 2 h at 4 °C with 500 µL of cell lysates that were pre-incubated with various concentration of the test compounds or DMSO. In order to wash out non-specifically bound proteins, the beads were first washed with 500 µL lysis buffer containing 25 mM MgCl₂ followed by three times washing with 500 µL PBS. The beads were mixed with 32 µL H₂O and 8 µL 5 x SDS sample buffer and incubated for 10 min at 95 °C. The enriched proteins of interest were detected by immunoblotting using protein specific antibody.

7.5 Biophysical methods

7.5.1 Cell lysate preparation for cellular thermal shift assay

5x10⁵ NIH/3T3 cells were grown in T175 cell culture flask up to 90-95% confluence. Cells were washed once with PBS and detached by adding 5 mL trypsin/EDTA followed by incubation for 5 min at 37 °C in the dark. The cells were suspended in cell culture medium and pelleted by centrifugation at 250 x g for 5 min at 4 °C. The cell pellet was washed thrice by suspending the cells in ice-cold PBS followed by centrifugation at 250 x g for 5 min at 4 °C. Cell pellets were snap frozen in liquid nitrogen and thawed in the water bath at 23 °C. The freeze-thaw cycle was repeated four times with intermittent vortexing. The resulting homogenate was centrifuged at 100000 x g for 20 min at 4 °C and the supernatant was carefully transferred into a new vial. The supernatant was subsequently snap frozen in liquid nitrogen and stored at -80 °C.

7.5.2 Cellular thermal shift assay

The test compound or DMSO were added to 600 μL NIH/3T3 lysate (protein concentration: 1 mg/mL) and incubated with continuous overhead rotation at 25 °C for 30 min. The lysates were splitted into nine aliquotes at 60 μL per tube (0.2 mL PCR tube) and incubated at different within a temperature gradient of 36 °C to 76 °C for 4 min in a gradient PCR cycler. These lysates were then transferred to 0.5 mL polycarbonate tubes and centrifuged at 100000 x g for 1 h at 4 °C to pellet the precipitated proteins. The supernatant was collected carefully and mixed with 5 x SDS sample buffer and incubated for 5 min at 95 °C. Later, the samples were loaded onto SDS-polyacrylamide gel and analyzed for the melting behavior of the protein under study by immunoblotting using specific antibodies for the protein of interest.

7.5.3 Differential scanning fluorimetry

To a PCR plate, 3.5 μL of distilled water, 5 μL of corresponding protein buffer, 4 μL of the protein of interest (0.1-1 mg/mL), various concentrations of the test compound or DMSO and 2.5 μL of SYPRO[®] Orange (40 x) were added in the mentioned sequence and the reaction volume was maintained to 20 μL . The PCR plate was sealed with optically clear film and centrifuged for 1 min at 200 x g to remove air bubbles. The plate was further placed iQTM5 Real-Time PCR Detection System (Biorad, Germany) and exposed to a gradient of temperature from 25 °C up to 95 °C with a step size of 0.5 °C every 30 s. The change in the fluorescence of SYPRO[®] Orange at 590 nm was recorded.

7.5.4 Fluorescence polarization

To investigate the binding of compound under investigation to the lipid binding pocket of human full length RHOGDI-1, fluorescence polarization of fluorescein-tagged RAB1 peptide (Fluorescein-SGGGSC(GerGer)-OMe)¹¹⁵ in the presence of RHOGDI-1 was monitored. The Fluorescein-GerGer-Rab1 peptide was prepared by that was prepared by Dr. Tom Mejuch, a post-doctoral researcher at the Max Planck Institute of Molecular Physiology, Dortmund, Germany. The 5 μM of fluorescently labeled RAB1 peptide was added to a cuvette containing the RHOGDI1 FP buffer 1. 50 μM of human full length RHOGDI-1 was added to the cuvette followed by addition of increasing concentrations of the compound RKN-1043 to the protein-peptide complex. The change in the fluorescence

polarization was monitored at an excitation and emission wavelengths of 495 nm and 520 nm, respectively, corresponding to the fluorescein label.

To determine the effect of RKN-1043 on the binding of RHOGDI1 and non-prenylated RAC1-GDP, fluorescence polarization experiments with TAMRA-GDP RAC1 and RHOGDI1 were performed in the research group of Prof. Reza Ahamadian by Mohammad Akbarzadeh at the Heinrich Heine University Düsseldorf, Germany.

Fluorescent polarization measurements were performed by titrating 1 μ M TAMRA-GDP-bound Rac1 with increasing concentrations of RHOGDI1 in the presence and absence of 50 μ M RKN-1043 in a RHOGDI1 FP buffer 2. The change in the fluorescence polarization was monitored at an excitation and emission wavelengths of 557 nm and 583 nm, respectively, corresponding to the TAMRA label.

7.5.5 Liposome sedimentation assay

The following experiments were performed in the research group of Prof. Reza Ahamadian by Mohammad Akbarzadeh at the Heinrich Heine University Düsseldorf, Germany.

Displacement of GerGer-RAC-1-GDP from synthetic liposomes by GST-RHOGDI-1 in the presence and absence of compound was studied using liposome sedimentation assay. Liposomes were prepared in 1 mL of liposome assay buffer by self-assembling of the lipids (194 μ g), containing 39% (w/w) phosphatidylethanolamine, 16% (w/w) phosphatidylcholine, 36% (w/w) phosphatidylserine, 4% (w/w) sphingomyelin, and 5% (w/w) phosphatidylinositol 4,5-bisphosphate. 10 μ M GerGer-RAC-1-GDP was added to the liposomes incubated for 20 min on ice. 15 μ M GST-RHOGDI-1 and the compound or DMSO was added to the liposome-GerGer-RAC-1-GDP complex prior to incubation on ice for 30 min. The samples were centrifuged at 20000 x g for 30 min at 4 °C. The resulting pellet and supernatant fractions were collected and analyzed by Western blotting.

7.5.6 Liposome flotation assay

The following experiments were performed in the research group of Prof. Reza Ahamadian by Mohammad Akbarzadeh at the Heinrich Heine University Düsseldorf, Germany.

10 μM of GerGer-RAC-1-GDP was added to liposomes suspended in liposome flotation assay buffer and incubated for 20 min on ice. The liposomes were prepared by using self-assembling the lipids (194 μg), containing 39% (w/w) phosphatidylethanolamine, 0.2% (w/w) NBD-PE (N-(7-nitrobenz-2-oxa-1,3-diazol-4-yl)-1,2-dihexadecanoyl-sn-glycero-3-phosphoethanolamine, triethylammonium salt), 16% (w/w) phosphatidylcholine, 36% (w/w) phosphatidylserine, 4% (w/w) sphingomyelin, and 5% (w/w) phosphatidylinositol 4,5-bisphosphate. 15 μM of GST-RHOGDI-1 and compound or DMSO was added to liposome-GerGer-RAC-1-GDP complex and samples were further incubated on ice for 30 min. The samples were added to 30% (w/v) sucrose solution. The resulting suspension was overlaid with protein buffer containing 25% (w/v) sucrose and finally with protein buffer without sucrose. The resulting samples were centrifuged at 140000 \times g for 1 h at 4 $^{\circ}\text{C}$. The upper liposome-containing phase (detected by fluorescent NDB-PE) was collected and analyzed by western blotting.

7.5.7 Surface plasmon resonance (SPR)

The following biophysical experiments were performed in the research group of Prof. Reza Ahamadian by Mohammad Akbarzadeh at the Heinrich Heine University Düsseldorf, Germany.

Biacore® 3000 instrument (Biacore, now GE Healthcare) was used to analyze the effect of a compound on GerGer-RAC-1-GDP and RHOGDI-1 interaction. Liposomes suspended in SPR buffer were immobilized by injecting 0.5 mM liposomes with flowrate of 5 $\mu\text{L}/\text{min}$ on the surface of a Pioneer® L1 sensor chip (GE Healthcare) for the period of 900 s, as indicated by a constant signal. Unbound liposomes were removed by passing the buffer and 10 mM NaOH with flowrate of 5 $\mu\text{L}/\text{min}$ for 30 s over the sensor chip. Buffer containing 15 μM GerGer-RAC-1-GDP was passed with flowrate of 5 $\mu\text{L}/\text{min}$ over the immobilized liposomes to facilitate the loading of GerGer-RAC-1-GDP on to the liposomes. The effect of compounds on the association of GerGer-RAC-1-GDP with liposomes and the resulting dissociation of GerGer-RAC1 upon passing 25 μM of RHOGDI-1 was monitored by the change in the signal.

7.6 Genetic validation

7.6.1 siRNA-mediated knockdown

2×10^4 C3H/10T1/2 cells were seeded per well in a 24-well plate and incubated overnight at 37 °C and 5% CO₂. In order to achieve highest knockdown efficiency, three different sequences of siRNA were used at different concentrations. For the transfection, siRNAs were diluted in the ratio of 1:20 in Opti-MEM® serum-free medium. Similarly, the DharmaFECT™ transfection reagent was separately mixed in the ratio of 1:50 and 1:25 with Opti-MEM® serum-free medium in a low-binding tube and incubated for 5 min at room temperature. Subsequently, the lipid solution was added to the siRNA solution in the ratio 1:1 and incubated for 20 min at room temperature. The corresponding lipid:siRNA solution was diluted 1:5 with the respective cell culture medium and was added to the overnight incubated cells by replacing the old medium and further incubated for 48-96 h at 37 °C. Alternatively, the transfections were carried out in T25 cell culture flask. 4×10^5 C3H/10T1/2 cells were seeded in a T25 cell culture flask and incubated overnight at 37 °C and 5% CO₂. The siRNA transfection was carried out in similar way as mentioned above with using the optimized transfection conditions.

7.6.2 Overexpression

The C3H/10T1/2 cells were transiently transfected with plasmid DNA containing gene expressing the protein of interest or a mock vector using Lipofectamine® LTX & PLUS™ reagent according to the manufacturer's protocol. For optimization of the transfection, various concentrations of plasmid DNA and DNA:lipid ratios were used. Briefly, 2×10^4 C3H/10T1/2 cells per well were seeded in a 24-well plate and incubated overnight at 37 °C and 5% CO₂. For the transfections, plasmid DNA and PLUS reagent were diluted 1:1 in Opti-MEM® medium and incubated for 5 min at room temperature. Lipofectamine® LTX reagent was directly added to this mixture and incubated for 30 min at room temperature. 100 µL of DNA:lipid complexes were added dropwise per well to the 24-well plate containing 400 µL cell culture medium. Alternatively, the transfections were carried out in T25 cell culture flask. 5×10^5 cells were seeded in the T25 cell culture flask and incubated overnight at 37 °C and 5% CO₂. The plasmid DNA transfections were carried out in similar way as mentioned above using optimized transfection conditions.

7.7 Kinase profiling at Eurofins

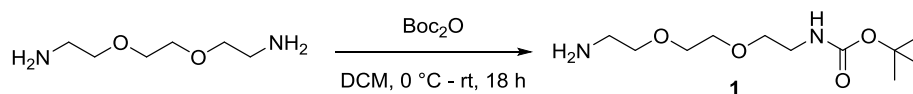
The kinase profiling assays were outsourced to Eurofins. Test compounds were assayed at single point concentration (10 μ M) for the effect on kinases involved in Hh signaling. The assay conditions can be taken from the Eurofins website: <http://www.eurofins.com/pharma-services/pharma-discovery-services/services/in-vitro-pharmacology/kinases/biochemical.aspx>.

7.8 GPCR screening at Eurofins

The GPCR binding assays were outsourced to Eurofins. Test compounds were assayed at single point concentration (10 μ M) for binding to the respective GPCR. The assay conditions can be taken from Eurofins website: <http://www.eurofins.com/biopharma-services/discovery/services/in-vitro-pharmacology/gpcrs/binding/>.

7.8.1 Synthesis of the *pull-down* probes

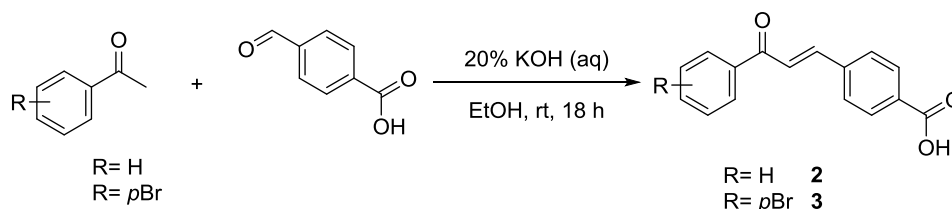
Preparation of *tert*-butyl (2-(2-(2-aminoethoxy)ethoxy)ethyl)carbamate (**1**)



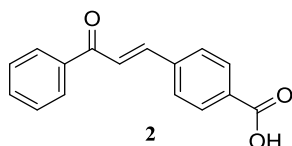
To the stirred solution of 2,2'-(ethylenedioxy)-bis(ethylamine) (3.395 g, 24.2 mM, 5 equiv.) in dichloromethane (10 mL) di-*tert*-butyl dicarbonate (1 g, 4.6 mM, 1 equiv.) solvated in dichloromethane (20 mL) was added over 8 h at 0°C. The reaction mixture was further stirred overnight at ambient temperature. The mixture was washed 2x with water, 1x with brine and dried over NaSO₄. The solvent was removed under vacuum to give the product **1**, which was used without further purification.

87% yield; colorless oil; ¹H NMR (600 MHz, CDCl₃): δ = 5.16 (br s, 1H), 3.62 (s, 4H), 3.57 – 3.51 (m, 4H), 3.35 – 3.28 (m, 2H), 2.90 (m, 2H), 1.44 ppm (s, 9H); ¹³C NMR (151 MHz, CDCl₃): δ = 156.18, 79.33, 73.26, 70.35, 70.33, 41.75, 40.46, 28.55 ppm; HRMS: calcd. for [M+H]⁺ C₁₁H₂₅O₄N₂ = 249.18088, found: 249.18125.

General procedure: Preparation of chalcones (**2** and **3**)

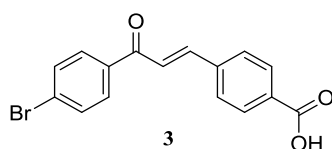


4-Carboxybenzaldehyde (1 mM, 1 equiv.) and acetophenone (1 mM, 1 equiv.) were dissolved in 5 mL ethanol. 600 μL of KOH (20% w/v aqueous solution) was added to the solution and the mixture was stirred overnight at ambient temperature. The mixture was cooled to 0°C and acidified with 10% aqueous HCl solution. The formed precipitate was filtered and dissolved in ethyl acetate. The organic phase was washed with a saturated NaCl solution and dried over MgSO₄. The solvent was removed under vacuum to give the chalcone as an amorphous solid, which was used without further purification.



4-Carboxy chalcone (2)

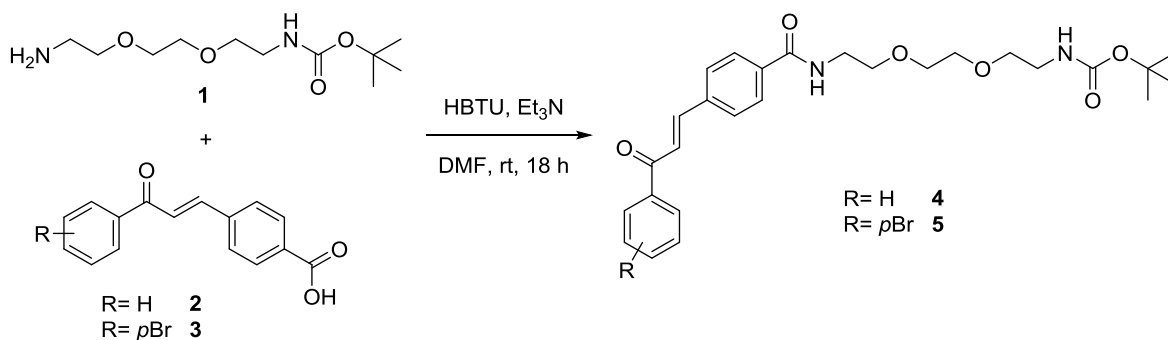
80% yield; slightly yellow amorphous solid; ^1H NMR (500 MHz, Acetone- d_6): δ = 11.45 (s, 2H), 8.21 – 8.16 (m, 6H), 8.11 (d, J = 8.3 Hz, 6H), 8.03 – 7.97 (m, 8H), 7.84 (d, J = 15.7 Hz, 3H), 7.68 (ddd, J = 8.5, 2.4, 1.2 Hz, 3H), 7.58 ppm (t, J = 7.6 Hz, 6H); ^{13}C NMR (126 MHz, Acetone- d_6): δ = 189.78, 167.04, 143.32, 140.27, 138.81, 133.92, 132.66, 130.96, 129.61, 129.51, 129.40, 125.04 ppm; HRMS: calcd. for $[\text{M}+\text{H}]^+$ $\text{C}_{16}\text{H}_{13}\text{O}_3$ = 253.08592, found: 253.08594.



4-Bromo-4-carboxy chalcone (3)

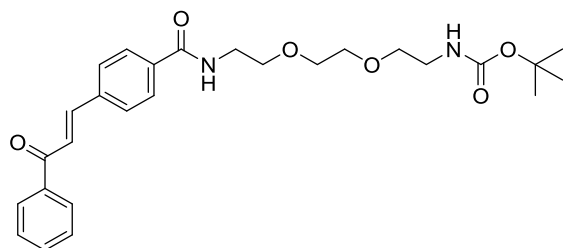
77% yield; colorless amorphous solid; ^1H NMR (500 MHz, THF- d_8): δ = 11.56 (s, 1H), 8.08 – 8.03 (m, 4H), 7.88 – 7.84 (m, 4H), 7.74 – 7.69 ppm (m, 2H); ^{13}C NMR (126 MHz, THF- d_8): δ = 188.42, 167.21, 144.06, 140.25, 138.11, 133.42, 132.90, 131.31, 131.13, 129.43, 128.65, 124.34 ppm; HRMS: calcd. for $[\text{M}+\text{H}]^+$ $\text{C}_{16}\text{H}_{11}\text{BrO}_3$ = 331.98711, found: 331.98725.

General procedure: Preparation of chalcone linker fragment (4 and 5)



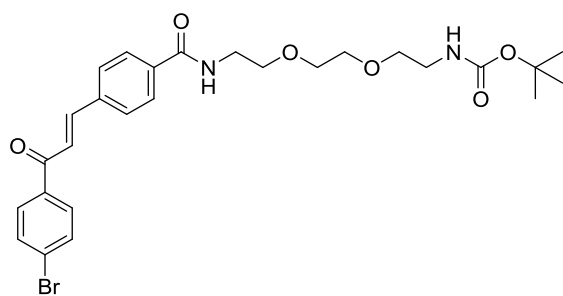
To the stirred solution of chalcone **2/3** (0.20 mM, 1 equiv.), linker **1** (0.30 mM, 1.5 equiv.) and triethylamine (0.70 mM, 3.5 equiv.) in 2.5 mL DMF was added HBTU (0.70

mM, 3.5 equiv.). The mixture was stirred at ambient temperature for 18 h. The solvent was removed under reduced pressure. The residue was solved in dichloromethane and washed with a saturated NaHCO₃ solution. The aqueous phase was extracted with dichloromethane and the combined organic phases were washed with brine and dried over MgSO₄. After removing the solvent under reduced pressure the purification was done by silica column chromatography and the product was obtained using ethylacetate/methanol as eluent (from 0% to 2%).



***tert*-butyl (*E*)-(2-(2-(2-(4-(3-oxo-3-phenylprop-1-en-1-yl) benzamido) ethoxy) ethoxy) ethyl)carbamate (4)**

86% yield; yellow oil; ¹H NMR (400 MHz, Acetone-d₆): δ = 8.18 – 8.14 (m, 2H), 8.01 – 7.91 (m, 5H), 7.81 (d, *J* = 15.7 Hz, 1H), 7.69 – 7.64 (m, 1H), 7.60 – 7.54 (m, 2H), 3.68 – 3.56 (m, 8H), 3.51 (t, *J* = 5.8 Hz, 2H), 3.22 (q, *J* = 5.8 Hz, 1H), 1.39 ppm (s, 9H); ¹³C NMR (101 MHz, Acetone-d₆): δ = 189.88, 166.78, 143.66, 138.97, 138.57, 137.29, 133.83, 129.60, 129.42, 129.38, 128.64, 124.34, 70.95, 70.72, 70.33, 41.07, 40.53, 28.63 ppm; HRMS: calcd. for [M+H]⁺ C₂₇H₃₅O₆N₂ = 483.24896, found: 483.24947.

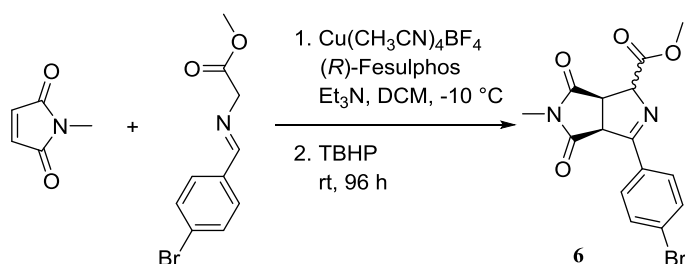


***tert*-butyl (*E*)-(1-(4-(3-(4-bromophenyl)-3-oxoprop-1-en-1-yl)phenyl)-1-oxo-5,8,11-trioxa-2-azatridecan-13-yl)carbamate (5)**

56% yield; yellow oil; ¹H NMR (600 MHz, CDCl₃): δ = 7.94 – 7.85 (m, 4H), 7.81 (d, *J* = 15.7 Hz, 1H), 7.69 (d, *J* = 8.1 Hz, 2H), 7.66 (d, *J* = 8.4 Hz, 2H), 7.54 (d, *J* = 15.7 Hz, 1H), 3.69 (s, 4H), 3.65 (s, 4H), 3.57 (t, *J* = 5.2 Hz, 2H), 3.31 (t, *J* = 5.0 Hz, 2H), 1.44 ppm

(s, 9H); ^{13}C NMR (151 MHz, CDCl_3): $\delta = 189.23, 166.82, 144.09, 137.63, 136.78, 136.27, 132.16, 130.22, 128.65, 128.33, 127.95, 123.06, 70.53, 70.35, 40.09, 28.54$ ppm; HRMS: calcd. for $[\text{M}+\text{H}]^+ \text{C}_{27}\text{H}_{34}^{79}\text{BrO}_6\text{N}_2 = 561.15948$, found: 561.16062; calcd. for $[\text{M}+\text{H}]^+ \text{C}_{27}\text{H}_{34}^{81}\text{BrO}_6\text{N}_2 = 563.15743$, found: 563.15847.

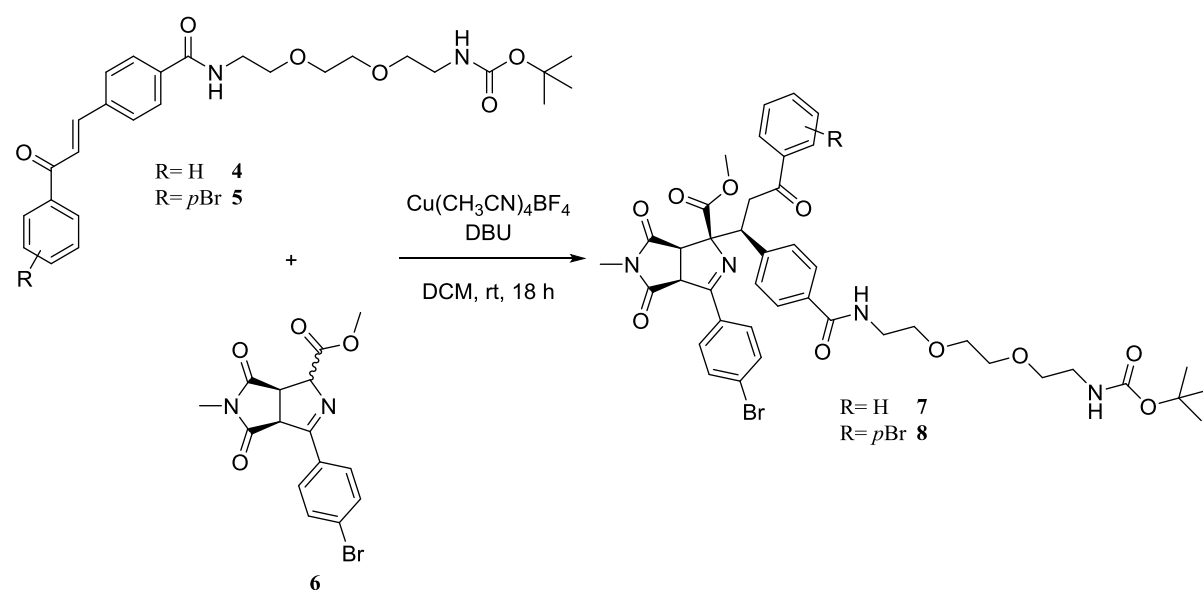
Preparation of methyl (3*a*S,6*a*R)-3-(4-bromophenyl)-5-methyl-4,6-dioxo-1,3*a*,4,5,6,6*a*-hexahydro-pyrrolo[3,4-*c*]pyrrole-1-carboxylate (6)



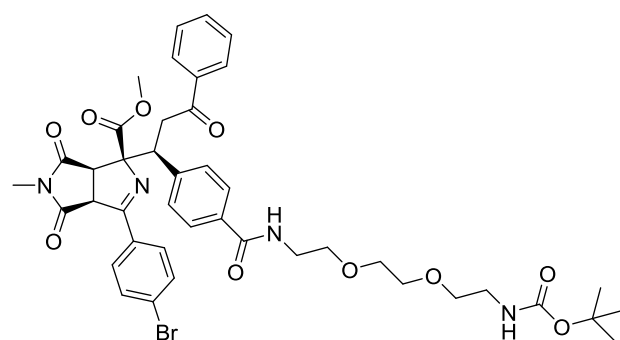
(*R_p*)-2-(*tert*-Butylthio)-1-(diphenylphosphino)ferrocene (1 mol%, 40 μM) and tetrakis-(acetonitrile)copper(I) tetrafluoroborate (1 mol%, 40 μM) were dissolved in dry dichloromethane and stirred at ambient temperature for 15 min. The resulting solution was cooled to 0°C and *N*-methylmaleimide (1.0 eq., 4.05 mM), α -iminoester (1.02 equiv., 3.9813 mM) and Et_3N (20 mol%, 0.81 mM) were added. The solution was allowed to stir at 0°C for 3 h. After the *N*-methylmaleimide was completely used up tetrakis-(acetonitrile)copper(I) tetrafluoroborate (4 mol%, 160 μM) and *tert*-butyl hydroperoxide (1.2 equiv., 4.69 mM) was added. The deep blue solution was allowed to stir at ambient temperature for 96 h. The crude mixture was directly loaded onto silica gel and the product was purified using petroleum ether / ethyl acetate as eluent.

74% yield; amorphous pale yellow solid; Inseparable mixture of isomers (55:45 ratio); For major isomer, ^1H NMR (600 MHz, CDCl_3): $\delta = 8.11 - 7.95$ (m, 2H), 7.66 – 7.53 (m, 2H), 5.25 – 5.22 (m, 1H), 4.71 (dd, $J = 8.4, 2.5$ Hz, 1H), 4.09 (dd, $J = 8.4, 3.0$ Hz, 1H), 3.84 (s, 3H), 2.96 ppm (s, 3H); For minor isomer, ^1H NMR (600 MHz, CDCl_3): $\delta = 8.11 - 7.95$ (m, 2H), 7.66 – 7.53 (m, 2H), 5.29 (dd, $J = 10.0, 1.3$ Hz, 1H), 4.63 (dd, $J = 8.9, 1.3$ Hz, 1H), 3.95 (t, $J = 9.4$ Hz, 1H), 3.79 (s, 2H), 2.96 ppm (s, 3H); For mixture of isomers: ^{13}C NMR (151 MHz, CDCl_3): $\delta = 176.14, 174.94, 172.44, 172.11, 170.24, 169.49, 168.72, 168.42, 131.80, 131.79, 131.31, 131.24, 130.17, 130.03, 127.14, 127.07, 76.65, 75.42, 60.42, 56.92, 56.45, 53.33, 52.84, 47.44, 46.83$ ppm, HRMS: calcd. for $[\text{M}+\text{H}]^+ \text{C}_{15}\text{H}_{14}^{79}\text{BrO}_4\text{N}_2 = 365.01315$, found: 365.01412; calcd. for $[\text{M}+\text{H}]^+ \text{C}_{15}\text{H}_{14}^{81}\text{BrO}_4\text{N}_2 = 367.01110$, found: 367.01170.

General procedure for Michael Addition (7 and 8)



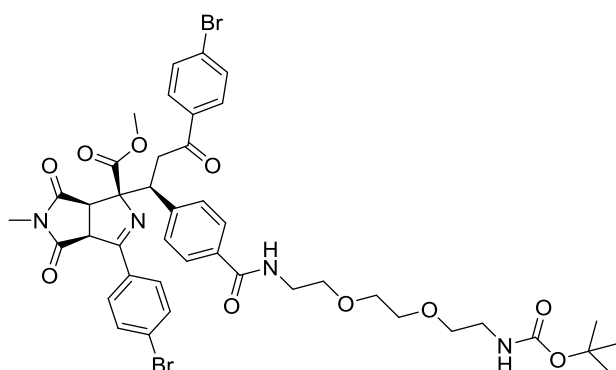
To the stirred solution of methyl (3a*S*,6a*R*)-3-(4-bromophenyl)-5-methyl-4,6-dioxo-1,3a,4,5,6,6a-hexahydro-pyrrolo[3,4-*c*]pyrrole-1-carboxylate (**6**) (0.18 mM, 2 equiv) in 1 mL of dry CH_2Cl_2 was added chalcone linker fragment (**4/5**) (0.09 mM, 1 equiv) solved in 1 mL of dry CH_2Cl_2 and stirred for 10 min at rt. Subsequently, tetrakis-(acetonitrile)copper(I) tetrafluoroborate (0.01 mM, 0.1 equiv) and 1,8-diazabicyclo (0.04 mM, 0.5 equiv) were added and the reaction was stirred at rt for 16 h. The crude reaction mixture was directly loaded on the silica column and separated using ethylacetate/petroleum ether (30-60%) mixture followed by follow by preparative HPLC. The products **7/8** are UV active and can be visualized under standard UV lamp.



Methyl (1*S*,3a*S*,6a*R*)-3-(4-bromophenyl)-1-((*R*)-1-(4-((2,2-dimethyl-4-oxo-3,8,11-trioxa-5-azatridecane-13-yl)carbamoyl)phenyl)-3-oxo-3-phenylpropyl)-5-methyl-4,6-dioxo-1,3a,4,5,6,6a-hexahydro-pyrrolo[3,4-*c*]pyrrole-1-carboxylate (7**)**

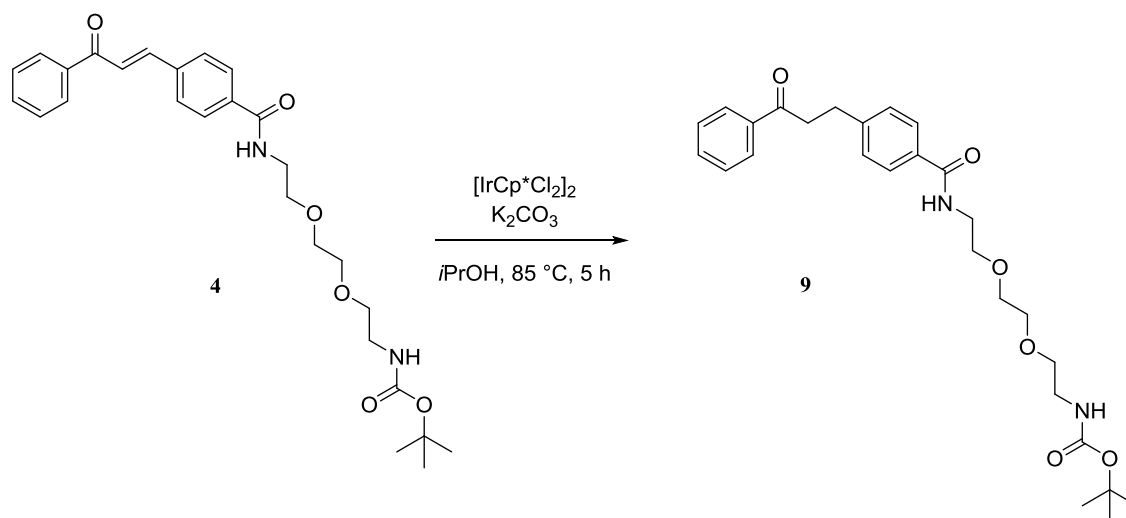
18% yield; amorphous white solid; ^1H NMR (600 MHz, CD_3CN): δ = 8.05 (d, J = 8.5 Hz, 2H), 7.91 (d, J = 7.8 Hz, 2H), 7.69 (d, J = 8.5 Hz, 2H), 7.58 (t, J = 7.4 Hz, 1H), 7.54 –

7.49 (m, 2H), 7.46 (t, $J = 7.7$ Hz, 2H), 7.21 (d, $J = 8.1$ Hz, 2H), 7.01 (s, 1H), 5.35 (s, 1H), 4.41 (dd, $J = 11.0, 2.3$ Hz, 1H), 3.90 (dd, $J = 17.6, 11.0$ Hz, 1H), 3.66 (s, 3H), 3.65 – 3.61 (m, 1H), 3.57 – 3.50 (m, 8H), 3.47 – 3.42 (m, 2H), 3.40 (t, $J = 5.3$ Hz, 2H), 3.10 (q, $J = 5.7$ Hz, 2H), 2.75 (s, 3H), 1.36 ppm (s, 9H); ^{13}C NMR (151 MHz, CD_3CN): $\delta = 198.84, 176.27, 173.19, 171.09, 170.51, 167.37, 156.89, 142.79, 137.77, 134.62, 134.18, 132.62, 132.43, 131.79, 131.45, 129.61, 128.97, 127.63, 127.07, 88.22, 79.25, 70.89, 70.86, 70.58, 70.16, 57.90, 53.54, 53.12, 49.60, 41.90, 40.99, 40.35, 28.60, 25.51$ ppm; HRMS: calcd. for $[\text{M}+\text{H}]^+ \text{C}_{42}\text{H}_{48}^{79}\text{BrO}_{10}\text{N}_4 = 847.25483$, found: 847.25687; calcd. for $[\text{M}+\text{H}]^+ \text{C}_{42}\text{H}_{48}^{81}\text{BrO}_{10}\text{N}_4 = 849.25279$, found: 849.25538.



Methyl (1*S*,3*aS*,6*aR*)-3-(4-bromophenyl)-1-((*R*)-3-(4-bromophenyl)-1-(4-((2,2-dimethyl-4-oxo-3,8,11-trioxo-5-azatridecan-13-yl)carbamoyl)phenyl)-3-oxopropyl)-5-methyl-4,6-dioxo-1,3*a*,4,5,6,6*a*-hexahydropyrrolo[3,4-*c*]pyrrole-1-carboxylate (8)

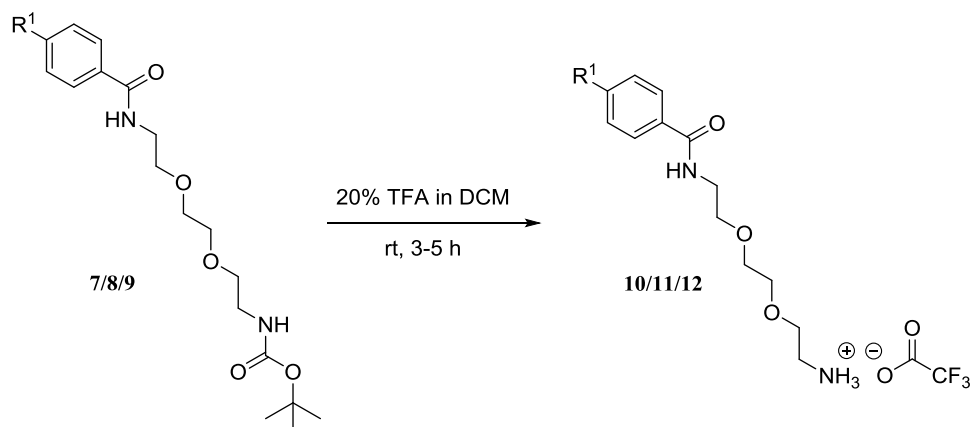
21% yield; amorphous white solid; ^1H NMR (600 MHz, CD_3CN): $\delta = 8.04$ (d, $J = 8.5$ Hz, 2H), 7.81 (d, $J = 8.5$ Hz, 2H), 7.69 (d, $J = 8.5$ Hz, 2H), 7.63 (d, $J = 8.5$ Hz, 2H), 7.51 (d, $J = 7.9$ Hz, 2H), 7.21 (d, $J = 7.90$ Hz, 2H), 7.01 (s, 1H), 5.34 (s, 1H), 4.39 (dd, $J = 10.8, 2.5$ Hz, 1H), 3.85 (dd, $J = 17.6, 10.8$ Hz, 1H), 3.65 (s, 3H), 3.63 (dd, $J = 17.6, 2.5$ Hz, 1H), 3.57 – 3.49 (m, 8H), 3.48 – 3.42 (m, 2H), 3.40 (t, $J = 5.2$ Hz, 2H), 3.10 (q, $J = 5.7$ Hz, 2H), 2.75 (s, 3H), 1.36 ppm (s, 9H); ^{13}C NMR (151 MHz, CD_3CN): $\delta = 198.05, 176.26, 173.18, 171.07, 170.57, 167.36, 156.91, 142.64, 136.67, 134.66, 132.77, 132.62, 132.44, 131.76, 131.44, 130.85, 128.60, 127.66, 127.10, 88.17, 79.26, 70.89, 70.86, 70.60, 70.17, 57.91, 53.56, 53.08, 49.51, 41.93, 40.99, 40.35, 28.60, 25.51$ ppm; HRMS: calcd. for $[\text{M}+\text{H}]^+ \text{C}_{42}\text{H}_{47}^{79}\text{Br}_2\text{O}_{10}\text{N}_4 = 925.16535$, found: 925.16781; calcd. for $[\text{M}+\text{H}]^+ \text{C}_{42}\text{H}_{47}^{79}\text{Br}^{81}\text{BrO}_{10}\text{N}_4 = 927.16330$, found: 927.16592; calcd. for $[\text{M}+\text{H}]^+ \text{C}_{42}\text{H}_{47}^{81}\text{Br}_2\text{O}_{10}\text{N}_4 = 929.16125$, found: 929.16440.

Preparation of *tert*-Butyl (2-(2-(2-(4-(3-oxo-3-phenylpropyl) benzamido) ethoxy)ethoxy) ethyl)carbamate (9)

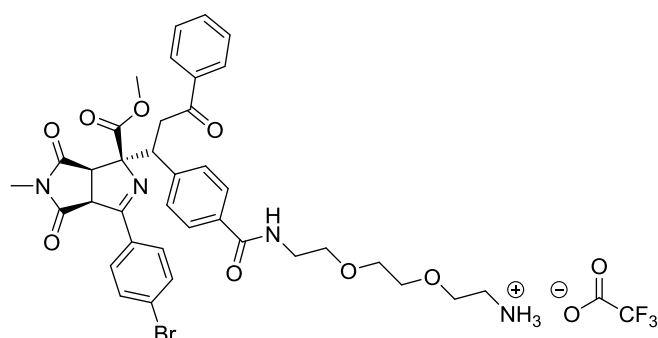
Chalcone **4** (1 equiv., 0.17 mM), $[\text{IrCp}^*\text{Cl}_2]_2$ (5 mol%, 8.3 μM) and K_2CO_3 (25 mol%, 41.4 μM) were solved in 4 mL *iso*-propanol. The reaction mixture was stirred under argon atmosphere for 5 h at 85 °C. The solvent was removed under reduced pressure and the product was purified by column chromatography using ethyl acetate / petroleum ether as eluent follow by preparative HPLC. A reversed Phase C18 column (Nucleodur C18, diameter 10 mm, Macherey & Nagel) was used. Method: flow rate 6.0 mL/min, (A = acetonitrile + 0.1% trifluoroacetic acid (TFA), B = water + 0.1% TFA). Gradient: 1-28 min: 30% A, 80% B.

15% yield; amorphous white solid; ^1H NMR (500 MHz, CD_3CN): δ = 7.97 (d, J = 7.4 Hz, 2H), 7.71 (d, J = 8.1 Hz, 2H), 7.60 (t, J = 7.4 Hz, 1H), 7.49 (t, J = 7.4 Hz, 2H), 7.35 (d, J = 8.1 Hz, 2H), 7.09 (s, 1H), 5.38 (s, 1H), 3.61 – 3.53 (m, 6H), 3.50 (q, J = 5.6 Hz, 2H), 3.44 (t, J = 5.6 Hz, 2H), 3.37 (t, J = 7.5 Hz, 2H), 3.15 (q, J = 5.6 Hz, 2H), 3.05 (t, J = 7.5 Hz, 2H), 1.38 ppm (s, 9H); ^{13}C NMR (126 MHz, CD_3CN): δ = 199.99, 167.74, 146.28, 137.86, 134.03, 133.47, 129.61, 129.48, 128.87, 128.05, 79.18, 70.87, 70.82, 70.55, 70.18, 40.94, 40.43, 40.27, 30.38, 28.53 ppm; HRMS: calcd. for $[\text{M}+\text{H}]^+$ $\text{C}_{27}\text{H}_{37}\text{O}_6\text{N}_2$ = 485.26461, found: 485.26530.

General procedure: Cleavage of the Boc-protecting group (10,11 and 12)



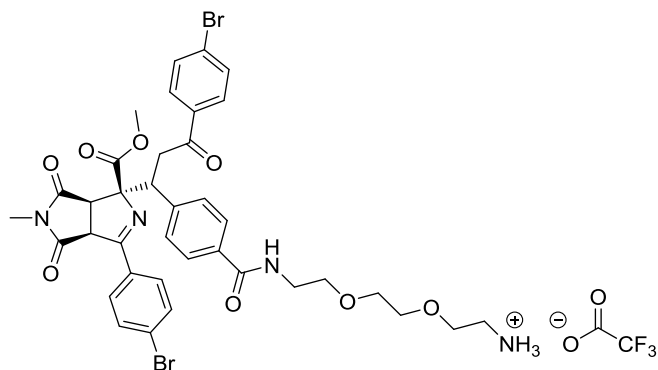
The Boc-protected amine (1 equiv., 3.5 μ M) was solved in 20% TFA in DCM. The solution was stirred for 3-5 h at ambient temperature. The solvent was removed under reduced pressure and the product was dried under high vacuum.



2-(2-(2-(4-((S)-1-((1S,3aS,6aR)-3-(4-bromophenyl)-1-(methoxycarbonyl)-5-methyl-4,6-dioxo-1,3a,4,5,6,6a-hexahydropyrrolo[3,4-c]pyrrol-1-yl)-3-oxo-3-phenylpropyl)benz-amido)ethoxy)ethoxy)ethan-1-aminium 2,2,2-trifluoroacetate (10)

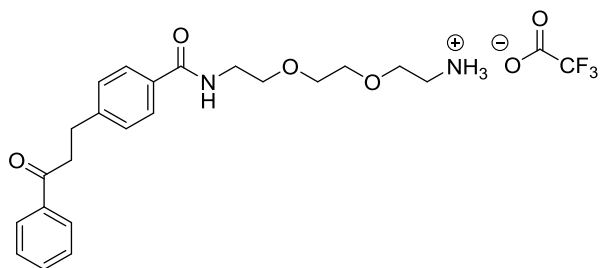
Quantitative yield; amorphous white solid; ¹H NMR (400 MHz, CD₃CN): δ = 8.04 (d, J = 8.6 Hz, 2H), 7.96 – 7.90 (m, 2H), 7.70 (d, J = 8.6 Hz, 2H), 7.59 (t, J = 7.4 Hz, 1H), 7.53 (d, J = 8.3 Hz, 2H), 7.47 (t, J = 7.7 Hz, 2H), 7.25 (d, J = 8.2 Hz, 3H), 6.79 (s, 3H), 4.42 (dd, J = 11.0, 2.5 Hz, 1H), 3.92 (dd, J = 17.6, 11.0 Hz, 1H), 3.71 – 3.63 (m, 4H), 3.63 – 3.46 (m, 12H), 3.06 – 2.97 (m, 2H), 2.76 (s, 3H); ¹³C NMR (101 MHz, CD₃CN): δ = 198.93, 176.25, 173.20, 171.05, 170.50, 143.28, 137.74, 134.26, 132.63, 132.43, 131.82, 131.59, 129.65, 128.99, 127.68, 127.10, 88.22, 71.11, 70.74, 67.01, 57.91, 53.57, 53.13, 49.62, 41.83, 40.67, 40.34, 25.54 ppm; HRMS: calcd. for [M+H]⁺ C₃₇H₄₀⁷⁹BrO₈N₄ =

747.20240, found: 747.20523; calcd. for $[M+H]^+$ $C_{37}H_{40}^{81}BrO_8N_4 = 749.20036$, found: 749.20256.



2-(2-(2-(4-((S)-3-(4-bromophenyl)-1-((1S,3aS,6aR)-3-(4-bromophenyl)-1-(methoxycarbonyl)-5-methyl-4,6-dioxo-1,3a,4,5,6,6a-hexahydropyrrolo[3,4-c]pyrrol-1-yl)-3-oxopyrrol)benz-amido)ethoxy)ethoxy)ethan-1-aminium 2,2,2-trifluoroacetate (11)

Quantitative yield; amorphous white solid; 1H NMR (400 MHz, CD_3CN): $\delta = 8.04$ (d, $J = 8.6$ Hz, 2H), 7.82 (d, $J = 8.6$ Hz, 2H), 7.70 (d, $J = 8.6$ Hz, 2H), 7.64 (d, $J = 8.6$ Hz, 2H), 7.53 (d, $J = 8.2$ Hz, 2H), 7.24 (d, $J = 8.2$ Hz, 3H), 6.90 (s, 3H), 4.40 (dd, $J = 10.8, 2.6$ Hz, 1H), 3.86 (dd, $J = 17.6, 10.8$ Hz, 1H), 3.66 (d, $J = 5.8$ Hz, 3H), 3.63 – 3.46 (m, 12H), 3.02 (d, $J = 3.1$ Hz, 2H), 2.76 ppm (s, 3H); ^{13}C NMR (101 MHz, CD_3CN): $\delta = 198.12, 176.24, 173.18, 171.04, 170.56, 143.08, 136.65, 134.23, 132.80, 132.63, 132.43, 131.79, 131.56, 130.87, 128.67, 127.71, 127.12, 88.18, 71.08, 70.75, 67.04, 57.92, 53.59, 53.07, 49.52, 41.86, 40.62, 40.35, 25.53$ ppm; HRMS: calcd. for $[M+H]^+$ $C_{37}H_{39}^{79}Br_2O_8N_4 = 825.11292$, found: 825.11557; calcd. for $[M+H]^+$ $C_{37}H_{39}^{79}Br^{81}BrO_8N_4 = 827.11087$, found: 827.11329; calcd. for $[M+H]^+$ $C_{37}H_{39}^{81}Br_2O_8N_4 = 829.10882$, found: 829.11166.



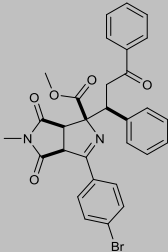
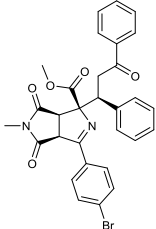
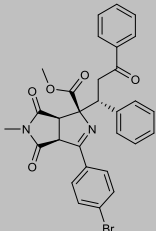
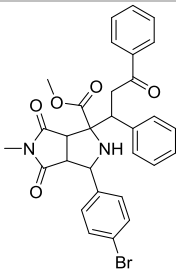
2-(2-(2-(4-(3-oxo-3-phenylpropyl)benzamido)ethoxy)ethoxy)ethan-1-aminium 2,2,2-trifluoroacetate (12)

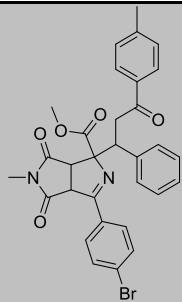
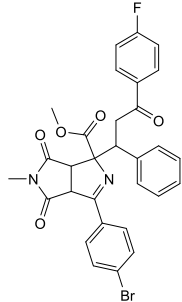
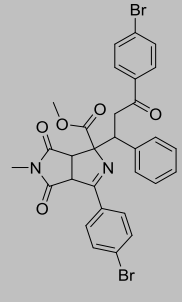
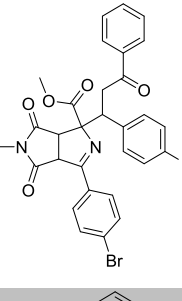
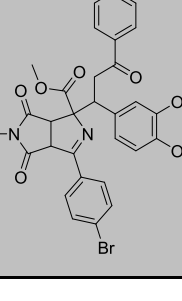
Quantitative yield; amorphous white solid; ^1H NMR (500 MHz, CD_3CN): $\delta = 7.97$ (d, $J = 8.2$ Hz, 2H), 7.74 (d, $J = 8.2$ Hz, 2H), 7.63 – 7.58 (m, 1H), 7.57 – 7.43 (m, 5H), 7.35 (d, $J = 8.0$ Hz, 2H), 3.68 – 3.63 (m, 2H), 3.63 – 3.49 (m, 8H), 3.36 (t, $J = 7.5$ Hz, 2H), 3.05 ppm (t, $J = 7.4$ Hz, 4H); ^{13}C NMR (126 MHz, CD_3CN): $\delta = 200.01, 168.45, 146.55, 137.84, 134.06, 133.10, 129.62, 129.53, 128.87, 128.16, 118.34, 70.96, 70.71, 70.61, 67.20, 40.36, 40.32, 40.31, 30.37, 1.82, 1.65, 1.48, 1.32, 1.15, 0.99, 0.82$ ppm; HRMS: calcd. for $[\text{M}+\text{H}]^+ \text{C}_{22}\text{H}_{29}\text{O}_4\text{N}_2 = 385.21218$, found: 385.21311.

8 Appendix

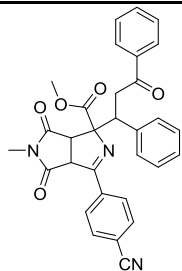
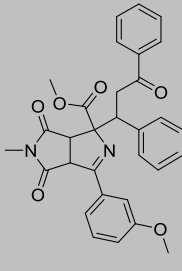
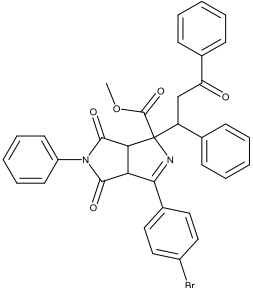
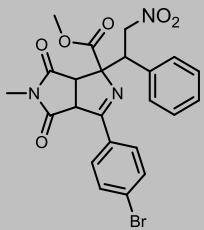
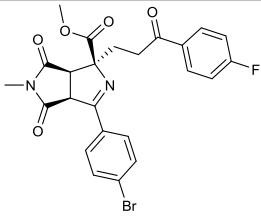
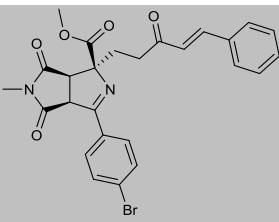
Table 8. Biological activities of bispyrrolidines

Inhibition potencies of Hh pathway are shown. Inhibition was measured in the osteogenesis assay. *IC₅₀ measured in GLI-reporter gene assay. Data shown are mean values ± SD (N ≥ 3).

Entry	Structure	Provider ID	IC ₅₀ ± SD (μM)
1	 <p>Racemic</p>	MPI_RNARAYAN_924 MPI_SHANG_207	2.94 (1.44)
2	 <p>Epimer 1</p>	MPI_RNARAYAN_1043 MPI_SHANG_208	1.5 (0.2)
3	 <p>Epimer 2</p>	MPI_SHANG_244	1.8 (0.0)
4		MPI_RNARAYAN_1117	>10 μM

Entry	Structure	Provider ID	IC ₅₀ ± SD (μM)
5		MPI_RNARAYAN_1084	inactive
6		MPI_RNARAYAN_1083	16.8 (1.3)*
8		MPI_RNARAYAN_1082	>10*
9		MPI_RNARAYAN_1072	13.6 (1.03)*
10		MPI_RNARAYAN_1087	2.9*

Entry	Structure	Provider ID	IC ₅₀ ± SD (μM)
11		MPI_RNARAYAN_1075	5.3 (0.6)*
12		MPI_RNARAYAN_1076	5.12 (0.8)*
13		MPI_RNARAYAN_1094	3.03 (0.4)
14		MPI_RNARAYAN_1095	inactive
15		MPI_RNARAYAN_1096	inactive
16		MPI_RNARAYAN_1097	inactive

Entry	Structure	Provider ID	IC ₅₀ ± SD (μM)
17		MPI_RNARAYAN_1098	inactive
18		MPI_RNARAYAN_1099	inactive
19		MPI_RNARAYAN_1110	inactive
20		MPI_RNARAYAN_903	inactive
21		MPI_RNARAYAN_1025	inactive
22		MPI_RNARAYAN_1024 MPI_SHANG_233	2.3 (0.8)

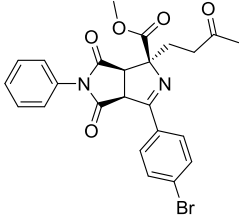
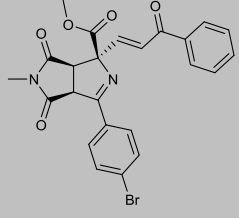
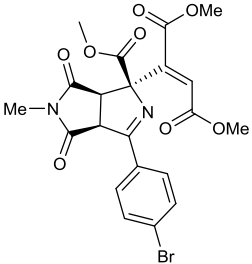
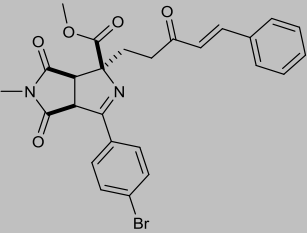
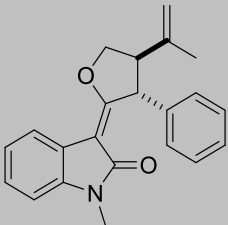
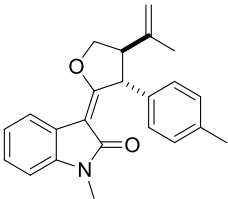
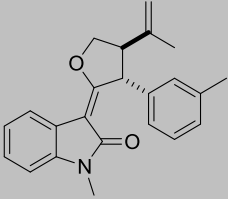
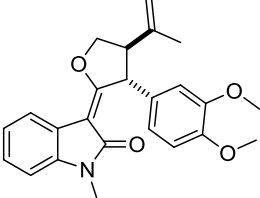
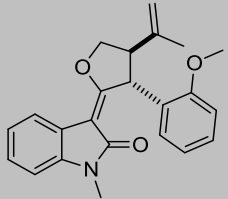
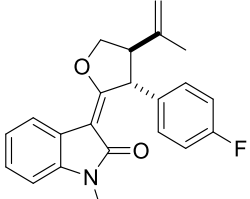
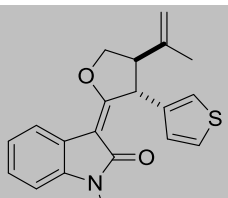
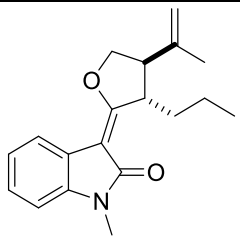
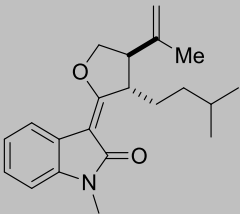
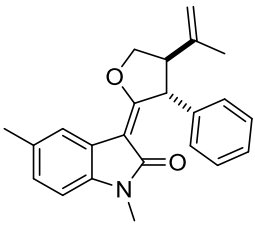
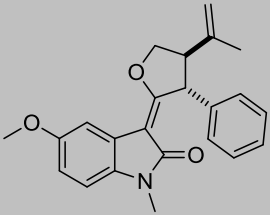
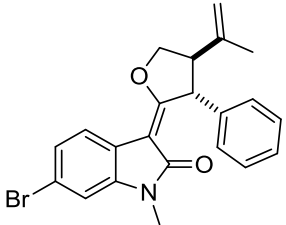
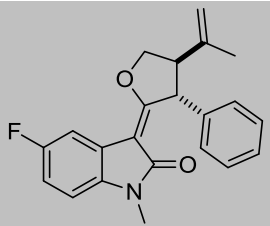
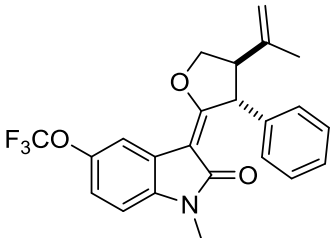
Entry	Structure	Provider ID	IC ₅₀ ± SD (μM)
23		MPI_RNARAYAN_1050	inactive
24		MPI_RNARAYAN_970	3.13 (0.2)
25		MPI_RNARAYAN_1023	inactive
26		MPI_RNARAYAN_957 MPI_SHANG_222	3.15 (1.65)

Table 9. Biological activities of *df*-oxindoles

Inhibition potencies of Hh pathway are shown. Inhibition was measured in the osteogenesis assay. Data shown are mean values \pm SD ($N \geq 3$).

Entry	Structure	Provider's ID	IC ₅₀ \pm SD (μ M)
1		MPI_YENLEE_YCL_168	5.26 (1.25)
2		MPI_YENLEE_YCL_318	inactive
3		MPI_YENLEE_YCL_658	inactive
4		MPI_YENLEE_YCL_254	inactive
5		MPI_YENLEE_YCL_320	6.96 (2.66)
6		MPI_YENLEE_YCL_319	inactive
7		MPI_YENLEE_YCL_488	inactive

Entry	Structure	Provider's ID	IC ₅₀ ± SD (μM)
8		MPI_YENLEE_YCL_248	inactive
9		MPI_YENLEE_YCL_247	inactive
10		MPI_YENLEE_YCL_216	inactive
11		MPI_YENLEE_YCL_224	inactive
12		MPI_YENLEE_YCL_222	inactive
13		MPI_YENLEE_YCL_217	6.53 (0.56)
14		MPI_YENLEE_YCL_223	inactive

Entry	Structure	Provider's ID	IC ₅₀ ± SD (μM)
15		MPI_YENLEE_YCL_218	inactive
16		MPI_YENLEE_YCL_219	inactive
17		MPI_YENLEE_YCL_225	2.75 (0.62)
18		MPI_YENLEE_YCL_220	3.13 (1.02)
19		MPI_YENLEE_YCL_347	9.56 (3.32)
20		MPI_YENLEE_YCL_348	6.33 (0.65)

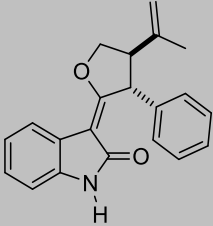
Entry	Structure	Provider's ID	IC ₅₀ ± SD (μM)
21		MPI_YENLEE_YCL_683	inactive

Table 10. Effect of RKN-1043 on the kinases involved in Hh signaling.

Influence of 10 μ M RKN-1043 on the activity of selected kinases. Kinase activities were determined at Eurofins by means of a radiometric-based assay using K_m -ATP for each enzyme. Data are mean values of two independent measurements.

Method	ATP (tested) / μ M	Kinase tested	% inhibition		
			n1	n2	mean
ZLYTE	Km app	ADRBK1 (GRK2)	7	15	11
ZLYTE	Km app	ADRBK2 (GRK3)	-1	-1	-1
ZLYTE	Km app	AKT1 (PKB alpha)	8	9	8
ZLYTE	Km app	AKT3 (PKB gamma)	-6	1	-2
ZLYTE	Km app	CSNK1A1 (CK1 alpha 1)	5	2	3
ZLYTE	Km app	CSNK1D (CK1 delta)	3	3	3
ZLYTE	Km app	CSNK1E (CK1 epsilon)	-2	5	2
ZLYTE	Km app	CSNK1G1 (CK1 gamma 1)	8	7	7
ZLYTE	Km app	CSNK1G2 (CK1 gamma 2)	13	10	11
ZLYTE	Km app	CSNK1G3 (CK1 gamma 3)	3	9	6
ZLYTE	Km app	CSNK2A1 (CK2 alpha 1)	4	6	5
ZLYTE	Km app	CSNK2A2 (CK2 alpha 2)	10	8	9
ZLYTE	Km app	DYRK1A	-2	1	0
ZLYTE	Km app	DYRK1B	-1	4	2
ZLYTE	Km app	GRK4	3	0	1
ZLYTE	Km app	GRK5	4	7	5
ZLYTE	Km app	GRK6	6	2	4
ZLYTE	Km app	GRK7	8	2	5
ZLYTE	Km app	GSK3A (GSK3 alpha)	2	3	3
ZLYTE	Km app	GSK3B (GSK3 beta)	6	7	7
ZLYTE	100	MAP2K1 (MEK1)	6	9	8
ZLYTE	Km app	MAPK3 (ERK1)	7	4	6
Adapta	10	PI4KA (PI4K alpha)	-3	2	-1
Adapta	Km app	PI4KB (PI4K beta)	-3	14	6
Adapta	Km app	PIK3C2A (PI3K-C2 alpha)	2	4	3
Adapta	10	PIK3C2B (PI3K-C2 beta)	-6	9	2
Adapta	Km app	PIK3CA/PIK3R1 (p110 alpha/p85 alpha)	13	-1	6
Adapta	Km app	PIK3CD/PIK3R1 (p110 delta/p85 alpha)	-24	-15	-19
Adapta	Km app	PIK3CG (p110 gamma)	-6	1	-3
ZLYTE	Km app	PIM1	4	7	5
ZLYTE	Km app	PRKACA (PKA)	-8	2	-3
ZLYTE	Km app	PRKCD (PKC delta)	-8	0	-4
ZLYTE	Km app	STK23 (MSSK1)	4	9	6
ZLYTE	Km app	SYK	17	8	13

Table 11. Effect of MJD-1314 on the kinases involved in Hh signaling.

Influence of 10 μM MJD-1314 on the activity of selected kinases. Kinase activities were determined at Eurofins by means of a radiometric-based assay using K_m -ATP for each enzyme. Data are mean values of two independent measurements.

Method	ATP (tested) / μM	Kinase tested	% inhibition		
			n1	n2	mean
ZLYTE	Km app	ADRBK1 (GRK2)	2	2	2
ZLYTE	Km app	ADRBK2 (GRK3)	2	0	1
ZLYTE	Km app	AKT1 (PKB alpha)	7	7	7
ZLYTE	Km app	AKT2 (PKB beta)	11	9	10
ZLYTE	Km app	AKT3 (PKB gamma)	5	-6	0
ZLYTE	Km app	CSNK1A1 (CK1 alpha 1)	7	5	6
ZLYTE	Km app	CSNK1D (CK1 delta)	2	3	3
ZLYTE	Km app	CSNK1E (CK1 epsilon)	-2	1	0
ZLYTE	Km app	CSNK1G1 (CK1 gamma 1)	4	6	5
ZLYTE	Km app	CSNK1G2 (CK1 gamma 2)	5	2	3
ZLYTE	Km app	CSNK2A1 (CK2 alpha 1)	5	5	5
ZLYTE	Km app	CSNK2A2 (CK2 alpha 2)	3	2	2
ZLYTE	Km app	DYRK1A	-1	-1	-1
ZLYTE	Km app	GRK4	-10	-7	-9
ZLYTE	Km app	GRK5	0	-6	-3
ZLYTE	Km app	GRK6	-5	2	-1
ZLYTE	Km app	GRK7	1	5	3
ZLYTE	Km app	GSK3A (GSK3 alpha)	3	4	4
ZLYTE	Km app	GSK3B (GSK3 beta)	-1	10	4
Adapta	10	PI4KA (PI4K alpha)	3	9	6
Adapta	Km app	PI4KB (PI4K beta)	28	26	27
Adapta	Km app	PIK3C2A (PI3K-C2 alpha)	5	7	6
Adapta	10	PIK3C2B (PI3K-C2 beta)	8	-4	2
Adapta	Km app	PIK3CA/PIK3R1 (p110 alpha/p85 alpha)	27	13	20
Adapta	Km app	PIK3CD/PIK3R1 (p110 delta/p85 alpha)	28	47	37
Adapta	Km app	PIK3CG (p110 gamma)	0	4	2
ZLYTE	Km app	PIM1	-12	-15	-14
ZLYTE	Km app	PRKACA (PKA)	-3	2	-1
ZLYTE	Km app	PRKCD (PKC delta)	-15	-13	-14
ZLYTE	Km app	STK23 (MSSK1)	2	2	2
ZLYTE	Km app	SYK	4	8	6

10 List of abbreviations

°C	Degrees Celsius
ALP	Alkaline phosphatase
aq.	Aqueous
Ar	Aryl
calcd.	Calculated
CETSA	Cellular thermal shift assay
COMAS	Compound Management and Screening Center
Conc	Concentration
DARTS	Drug affinity responsive target stability
DFMO	Difluoromethylornitine
DHH	Desert hedgehog
DIPEA	N,N-diisopropylethylamine
DMAP	4-dimethylamino pyridine
DMF	Dimethyl formamide
DMSO	Dimethyl sulfoxide
DSF	Differential scanning fluorimetry
equiv.	Equivalents
FDA	Food and drug administration
FLIM	Fluorescence Lifetime Imaging Microscopy
FP	Fluorescence polarization
FRET	Fluorescence Resonance Energy Transfer
GAP	Gtpase activating proteins
GEF	Guanine nucleotide exchange factor
GerGer	Geranylgeranyl
GFP	Green fluorescent protein
GLI	Glioma-associated oncogene homolog
GRK2	G protein-coupled receptor kinase
Hh	Hedgehog
Hhat	Hedgehog acyl transferase
HPLC	High performance liquid chromatography
HR	High resolution
HTS	high throughput screening
Hz	Hertz
IC ₅₀	Half-maximal inhibitory concentration
IHH	Indian hedgehog
J	Coupling constant

K _d	Dissociation constant
LC-MS	Liquid chromatography mass spectrometry
LFQ	Label free quantification
MEF	Mouse embryonic fibroblast
MS	Mass spectrometry
MTA	Methylthioadenosine
MTAP	Methylthioadenosine phosphorylase
NHS	N-hydroxysuccinimide
NMR	Nuclear magnetic resonance
PAGE	Polyacrylamide gel electrophoresis
PE	Phosphatidylethanolamine
PEG	Polyethylene glycol
PTC1	Patched 1
qPCR	Quantitative polymerase chain reaction
R.L.U.	Relative light units
RAS	Rat sarcoma
RHO	RAS homologous
RISC	RNA-induced silencing complex
RNAi	RNA interference
rt	Room temperature
s.d	Standard deviation
SAG	SMO Agonist
SAR	Structure-activity relationship
SDS	Sodium dodecyl sulfate
SDS-PAGE	Sodium dodecyl sulfate polyacrylamide gel electrophoresis
SEA	Similarity ensemble approach
SHH	Sonic hedgehog
shRNA	Small hairpin RNA
SILAC	Stable isotope labeling with amino acids in cell culture
SPiDER	Self-organizing map-based prediction of drug equivalence relationship
SPROX	stability of proteins from rates of oxidation
T _m	Melting temperature
TMT	Tandem mass tag

11 References

- 1 Hartwell, L. H. Twenty-five years of cell cycle genetics. *Genetics* **129**, 975-980 (1991).
- 2 Hartwell, L. H. *Saccharomyces cerevisiae* cell cycle. *Bacteriological Reviews* **38**, 164-198 (1974).
- 3 Driscoll, M. Molecular genetics of cell death in the nematode *Caenorhabditis elegans*. *Journal of Neurobiology* **23**, 1327-1351, doi:10.1002/neu.480230919 (1992).
- 4 Nusslein-Volhard, C. & Wieschaus, E. Mutations affecting segment number and polarity in *Drosophila*. *Nature* **287**, 795-801 (1980).
- 5 Schreiber, S. L. Chemical genetics resulting from a passion for synthetic organic chemistry. *Bioorganic & medicinal chemistry* **6**, 1127-1152 (1998).
- 6 Schenone, M., Dancik, V., Wagner, B. K. & Clemons, P. A. Target identification and mechanism of action in chemical biology and drug discovery. *Nat Chem Biol* **9**, 232-240 (2013).
- 7 MacBeath, G. Chemical genomics: what will it take and who gets to play? *Genome Biology* **2**, comment2005.2001-comment2005.2006 (2001).
- 8 An, W. F. & Tolliday, N. Cell-Based Assays for High-Throughput Screening. *Molecular Biotechnology* **45**, 180-186, doi:10.1007/s12033-010-9251-z (2010).
- 9 Koo, J. *et al.* A GUS/Luciferase Fusion Reporter for Plant Gene Trapping and for Assay of Promoter Activity with Luciferin-Dependent Control of the Reporter Protein Stability. *Plant and Cell Physiology* **48**, 1121-1131, doi:10.1093/pcp/pcm081 (2007).
- 10 Chen, J. K., Taipale, J., Young, K. E., Maiti, T. & Beachy, P. A. Small molecule modulation of Smoothed activity. *Proc. Natl. Acad. Sci. U. S. A.* **99**, 14071-14076, doi:10.1073/pnas.182542899 (2002).
- 11 Stoddart, M. J. Cell viability assays: introduction. *Methods in molecular biology (Clifton, N.J.)* **740**, 1-6, doi:10.1007/978-1-61779-108-6_1 (2011).
- 12 Ziegler, S., Pries, V., Hedberg, C. & Waldmann, H. Target identification for small bioactive molecules: finding the needle in the haystack. *Angewandte Chemie (International ed. in English)* **52**, 2744-2792, doi:10.1002/anie.201208749 (2013).
- 13 Ong, S. E. *et al.* Stable isotope labeling by amino acids in cell culture, SILAC, as a simple and accurate approach to expression proteomics. *Molecular & cellular proteomics : MCP* **1**, 376-386 (2002).
- 14 Rix, U. & Superti-Furga, G. Target profiling of small molecules by chemical proteomics. *Nat Chem Biol* **5**, 616-624, doi:10.1038/nchembio.216 (2009).
- 15 Voigt, T. *et al.* A natural product inspired tetrahydropyran collection yields mitosis modulators that synergistically target CSE1L and tubulin. *Angewandte Chemie (International ed. in English)* **52**, 410-414, doi:10.1002/anie.201205728 (2013).
- 16 Bretkopf, S. B., Oppermann, F. S., Kéri, G., Grammel, M. & Daub, H. Proteomics Analysis of Cellular Imatinib Targets and their Candidate Downstream Effectors. *Journal of Proteome Research* **9**, 6033-6043, doi:10.1021/pr1008527 (2010).
- 17 Kruger, M. *et al.* SILAC mouse for quantitative proteomics uncovers kindlin-3 as an essential factor for red blood cell function. *Cell* **134**, 353-364, doi:10.1016/j.cell.2008.05.033 (2008).
- 18 Krijgsveld, J. *et al.* Metabolic labeling of *C. elegans* and *D. melanogaster* for quantitative proteomics. *Nat Biotech* **21**, 927-931 (2003).
- 19 Titov, D. V. & Liu, J. O. Identification and validation of protein targets of bioactive small molecules. *Bioorganic & medicinal chemistry* **20**, 1902-1909, doi:<http://dx.doi.org/10.1016/j.bmc.2011.11.070> (2012).
- 20 Lee, J. & Bogyo, M. Target deconvolution techniques in modern phenotypic profiling. *Current opinion in chemical biology* **17**, 118-126, doi:10.1016/j.cbpa.2012.12.022 (2013).
- 21 Mamidyala, S. K. & Finn, M. G. In situ click chemistry: probing the binding landscapes of biological molecules. *Chemical Society Reviews* **39**, 1252-1261, doi:10.1039/B901969N (2010).

- 22 He, G. *et al.* Gamma-secretase activating protein is a therapeutic target for Alzheimer's disease. *Nature* **467**, 95-98, doi:10.1038/nature09325 (2010).
- 23 Hernandez-Boluda, J. C. & Cervantes, F. Imatinib mesylate (Gleevec, Glivec): a new therapy for chronic myeloid leukemia and other malignancies. *Drugs of today (Barcelona, Spain : 1998)* **38**, 601-613 (2002).
- 24 Martinez Molina, D. *et al.* Monitoring drug target engagement in cells and tissues using the cellular thermal shift assay. *Science* **341**, 84-87, doi:10.1126/science.1233606 (2013).
- 25 Fry, D. W. *et al.* Specific inhibition of cyclin-dependent kinase 4/6 by PD 0332991 and associated antitumor activity in human tumor xenografts. *Molecular cancer therapeutics* **3**, 1427-1438 (2004).
- 26 Pai, M. Y. *et al.* in *Chemical Biology: Methods and Protocols* (eds Jonathan E. Hempel, Charles H. Williams, & Charles C. Hong) 287-298 (Springer New York, 2015).
- 27 Lomenick, B. *et al.* Target identification using drug affinity responsive target stability (DARTS). *Proceedings of the National Academy of Sciences* **106**, 21984-21989, doi:10.1073/pnas.0910040106 (2009).
- 28 West, G. M., Tang, L. & Fitzgerald, M. C. Thermodynamic analysis of protein stability and ligand binding using a chemical modification- and mass spectrometry-based strategy. *Analytical chemistry* **80**, 4175-4185, doi:10.1021/ac702610a (2008).
- 29 West, G. M. *et al.* Quantitative proteomics approach for identifying protein-drug interactions in complex mixtures using protein stability measurements. *Proceedings of the National Academy of Sciences* **107**, 9078-9082, doi:10.1073/pnas.1000148107 (2010).
- 30 Kapoor, S., Waldmann, H. & Ziegler, S. Novel approaches to map small molecule-target interactions. *Bioorganic & medicinal chemistry* **24**, 3232-3245, doi:<http://dx.doi.org/10.1016/j.bmc.2016.05.020> (2016).
- 31 de Waal, L. *et al.* Identification of cancer-cytotoxic modulators of PDE3A by predictive chemogenomics. *Nat Chem Biol* **12**, 102-108, doi:10.1038/nchembio.1984 (2016).
- 32 Moffat, J. *et al.* A lentiviral RNAi library for human and mouse genes applied to an arrayed viral high-content screen. *Cell* **124**, 1283-1298, doi:10.1016/j.cell.2006.01.040 (2006).
- 33 Wang, J. *et al.* Cellular phenotype recognition for high-content RNA interference genome-wide screening. *Journal of biomolecular screening* **13**, 29-39, doi:10.1177/1087057107311223 (2008).
- 34 Ito, M., Kawano, K., Miyagishi, M. & Taira, K. Genome-wide application of RNAi to the discovery of potential drug targets. *FEBS Letters* **579**, 5988-5995, doi:<http://dx.doi.org/10.1016/j.febslet.2005.08.015> (2005).
- 35 Castoreno, A. B. *et al.* Small molecules discovered in a pathway screen target the Rho pathway in cytokinesis. *Nat Chem Biol* **6**, 457-463, doi:http://www.nature.com/nchembio/journal/v6/n6/supinfo/nchembio.363_S1.html (2010).
- 36 Lenart, P. *et al.* The small-molecule inhibitor BI 2536 reveals novel insights into mitotic roles of polo-like kinase 1. *Curr. Biol.* **17**, 304-315, doi:10.1016/j.cub.2006.12.046 (2007).
- 37 Burkard, M. E., Santamaria, A. & Jallepalli, P. V. Enabling and disabling Polo-like kinase 1 inhibition through chemical genetics. *ACS Chemical Biology* **7**, 978-981, doi:10.1021/cb200551p (2012).
- 38 Keiser, M. J. *et al.* Relating protein pharmacology by ligand chemistry. *Nat Biotech* **25**, 197-206, doi:http://www.nature.com/nbt/journal/v25/n2/supinfo/nbt1284_S1.html (2007).
- 39 Self-organizing molecular fingerprints: a ligand-based view on drug-like chemical space and off-target prediction. *Future Medicinal Chemistry* **1**, 213-218, doi:10.4155/fmc.09.11 (2009).
- 40 Riddle, R. D., Johnson, R. L., Laufer, E. & Tabin, C. Sonic hedgehog mediates the polarizing activity of the ZPA. *Cell* **75**, 1401-1416, doi:[http://dx.doi.org/10.1016/0092-8674\(93\)90626-2](http://dx.doi.org/10.1016/0092-8674(93)90626-2) (1993).

- 41 Echelard, Y. *et al.* Sonic hedgehog, a member of a family of putative signaling molecules, is implicated in the regulation of CNS polarity. *Cell* **75**, 1417-1430 (1993).
- 42 Krauss, S., Concordet, J. P. & Ingham, P. W. A functionally conserved homolog of the *Drosophila* segment polarity gene *hh* is expressed in tissues with polarizing activity in zebrafish embryos. *Cell* **75**, 1431-1444 (1993).
- 43 Chang, D. T. *et al.* Products, genetic linkage and limb patterning activity of a murine hedgehog gene. *Development* **120**, 3339 (1994).
- 44 Varjosalo, M. & Taipale, J. Hedgehog: functions and mechanisms. *Genes & development* **22**, 2454-2472, doi:10.1101/gad.1693608 (2008).
- 45 Heretsch, P., Tzagkaroulaki, L. & Giannis, A. Modulators of the hedgehog signaling pathway. *Bioorganic & medicinal chemistry* **18**, 6613-6624, doi:<http://dx.doi.org/10.1016/j.bmc.2010.07.038> (2010).
- 46 Briscoe, J. & Therond, P. P. The mechanisms of Hedgehog signalling and its roles in development and disease. *Nat Rev Mol Cell Biol* **14**, 416-429, doi:10.1038/nrm3598 (2013).
- 47 Mann, R. K. & Beachy, P. A. Novel lipid modifications of secreted protein signals. *Annual review of biochemistry* **73**, 891-923, doi:10.1146/annurev.biochem.73.011303.073933 (2004).
- 48 Heretsch, P., Tzagkaroulaki, L. & Giannis, A. Modulators of the hedgehog signaling pathway. *Bioorganic & medicinal chemistry* **18**, 6613-6624, doi:10.1016/j.bmc.2010.07.038 (2010).
- 49 Ding, Q. *et al.* Diminished Sonic hedgehog signaling and lack of floor plate differentiation in *Gli2* mutant mice. *Development* **125**, 2533-2543 (1998).
- 50 Corbit, K. C. *et al.* Vertebrate Smoothed functions at the primary cilium. *Nature* **437**, 1018-1021, doi:10.1038/nature04117 (2005).
- 51 Goetz, S. C. & Anderson, K. V. The primary cilium: a signalling centre during vertebrate development. *Nature reviews. Genetics* **11**, 331-344, doi:10.1038/nrg2774 (2010).
- 52 Gorojankina, T. Hedgehog signaling pathway: a novel model and molecular mechanisms of signal transduction. *Cellular and molecular life sciences : CMLS* **73**, 1317-1332, doi:10.1007/s00018-015-2127-4 (2016).
- 53 Mukhopadhyay, S. *et al.* The ciliary G-protein-coupled receptor *Gpr161* negatively regulates the Sonic hedgehog pathway via cAMP signaling. *Cell* **152**, 210-223, doi:10.1016/j.cell.2012.12.026 (2013).
- 54 Pan, Y., Bai, C. B., Joyner, A. L. & Wang, B. Sonic hedgehog signaling regulates *Gli2* transcriptional activity by suppressing its processing and degradation. *Molecular and cellular biology* **26**, 3365-3377, doi:10.1128/mcb.26.9.3365-3377.2006 (2006).
- 55 Wang, B. & Li, Y. Evidence for the direct involvement of β TrCP in *Gli3* protein processing. *Proc. Natl. Acad. Sci. U. S. A.* **103**, 33-38, doi:10.1073/pnas.0509927103 (2006).
- 56 Kovacs, J. J. *et al.* Beta-arrestin-mediated localization of smoothed to the primary cilium. *Science* **320**, 1777-1781, doi:10.1126/science.1157983 (2008).
- 57 Yang, C., Chen, W., Chen, Y. & Jiang, J. Smoothed transduces Hedgehog signal by forming a complex with *Evc/Evc2*. *Cell research* **22**, 1593-1604, doi:10.1038/cr.2012.134 (2012).
- 58 Tukachinsky, H., Lopez, L. V. & Salic, A. A mechanism for vertebrate Hedgehog signaling: recruitment to cilia and dissociation of *SuFu-Gli* protein complexes. *The Journal of cell biology* **191**, 415-428, doi:10.1083/jcb.201004108 (2010).
- 59 Mukhopadhyay, S. & Rohatgi, R. G-protein-coupled receptors, Hedgehog signaling and primary cilia. *Seminars in cell & developmental biology* **33**, 63-72, doi:10.1016/j.semcdb.2014.05.002 (2014).
- 60 Beachy, P. A., Hymowitz, S. G., Lazarus, R. A., Leahy, D. J. & Siebold, C. Interactions between Hedgehog proteins and their binding partners come into view. *Genes & development* **24**, 2001-2012, doi:10.1101/gad.1951710 (2010).

- 61 Ruiz i Altaba, A., Mas, C. & Stecca, B. The Gli code: an information nexus regulating cell fate, stemness and cancer. *Trends in cell biology* **17**, 438-447, doi:10.1016/j.tcb.2007.06.007 (2007).
- 62 Brennan, D., Chen, X., Cheng, L., Mahoney, M. & Riobo, N. A. Noncanonical Hedgehog signaling. *Vitamins and hormones* **88**, 55-72, doi:10.1016/b978-0-12-394622-5.00003-1 (2012).
- 63 Taipale, J., Cooper, M. K., Maiti, T. & Beachy, P. A. Patched acts catalytically to suppress the activity of Smoothed. *Nature* **418**, 892-897, doi:10.1038/nature00989 (2002).
- 64 Huang, P. *et al.* Cellular Cholesterol Directly Activates Smoothed in Hedgehog Signaling. *Cell* **166**, 1176-1187.e1114, doi:10.1016/j.cell.2016.08.003 (2016).
- 65 Vuolo, L., Herrera, A., Torroba, B., Menendez, A. & Pons, S. Ciliary adenylyl cyclases control the Hedgehog pathway. *Journal of cell science* **128**, 2928-2937, doi:10.1242/jcs.172635 (2015).
- 66 Sharpe, H. J., Wang, W., Hannoush, R. N. & de Sauvage, F. J. Regulation of the oncoprotein Smoothed by small molecules. *Nat Chem Biol* **11**, 246-255, doi:10.1038/nchembio.1776 (2015).
- 67 Wu, F., Zhang, Y., Sun, B., McMahon, A. P. & Wang, Y. Hedgehog Signaling: From Basic Biology to Cancer Therapy. *Cell chemical biology* **24**, 252-280, doi:10.1016/j.chembiol.2017.02.010 (2017).
- 68 Pressey, J. G., Anderson, J. R., Crossman, D. K., Lynch, J. C. & Barr, F. G. Hedgehog Pathway Activity in Pediatric Embryonal Rhabdomyosarcoma and Undifferentiated Sarcoma: A Report from the Children's Oncology Group. *Pediatric blood & cancer* **57**, 930-938, doi:10.1002/pbc.23174 (2011).
- 69 Ng, J. M. & Curran, T. The Hedgehog's tale: developing strategies for targeting cancer. *Nat Rev Cancer* **11**, 493-501, doi:10.1038/nrc3079 (2011).
- 70 Pan, S. *et al.* Discovery of NVP-LDE225, a Potent and Selective Smoothed Antagonist. *ACS medicinal chemistry letters* **1**, 130-134, doi:10.1021/ml1000307 (2010).
- 71 Munchhof, M. J. *et al.* Discovery of PF-04449913, a Potent and Orally Bioavailable Inhibitor of Smoothed. *ACS medicinal chemistry letters* **3**, 106-111, doi:10.1021/ml2002423 (2012).
- 72 Gendreau, S. B. *et al.* Abstract B192: Preclinical characterization of BMS-833923 (XL139), a hedgehog (HH) pathway inhibitor in early clinical development. *Molecular cancer therapeutics* **8**, B192-B192, doi:10.1158/1535-7163.targ-09-b192 (2009).
- 73 Bender, M. H. *et al.* Abstract 2819: Identification and characterization of a novel smoothed antagonist for the treatment of cancer with deregulated hedgehog signaling. *Cancer Research* **71**, 2819 (2014).
- 74 Maun, H. R. *et al.* Hedgehog pathway antagonist 5E1 binds hedgehog at the pseudo-active site. *The Journal of biological chemistry* **285**, 26570-26580, doi:10.1074/jbc.M110.112284 (2010).
- 75 Petrova, E., Rios-Esteves, J., Ouerfelli, O., Glickman, J. F. & Resh, M. D. Inhibitors of Hedgehog acyltransferase block Sonic Hedgehog signaling. *Nat Chem Biol* **9**, 247-249, doi:<http://www.nature.com/nchembio/journal/v9/n4/abs/nchembio.1184.html#supplementary-information> (2013).
- 76 Stanton, B. Z. *et al.* A small molecule that binds Hedgehog and blocks its signaling in human cells. *Nat Chem Biol* **5**, 154-156, doi:10.1038/nchembio.142 (2009).
- 77 Edison, R. J. & Muenke, M. Central Nervous System and Limb Anomalies in Case Reports of First-Trimester Statin Exposure. *New England Journal of Medicine* **350**, 1579-1582, doi:10.1056/nejm200404083501524 (2004).
- 78 Cooper, M. K. *et al.* A defective response to Hedgehog signaling in disorders of cholesterol biosynthesis. *Nature genetics* **33**, 508-513, doi:10.1038/ng1134 (2003).
- 79 Lauth, M., Bergström, Å., Shimokawa, T. & Toftgård, R. Inhibition of GLI-mediated transcription and tumor cell growth by small-molecule antagonists. *Proc. Natl. Acad. Sci. U. S. A.* **104**, 8455-8460, doi:10.1073/pnas.0609699104 (2007).

- 80 Kim, J. *et al.* Itraconazole and arsenic trioxide inhibit Hedgehog pathway activation and tumor growth associated with acquired resistance to smoothened antagonists. *Cancer cell* **23**, 23-34, doi:10.1016/j.ccr.2012.11.017 (2013).
- 81 Hosoya, T., Arai, M. A., Koyano, T., Kowithayakorn, T. & Ishibashi, M. Naturally occurring small-molecule inhibitors of hedgehog/GLI-mediated transcription. *Chembiochem : a European journal of chemical biology* **9**, 1082-1092, doi:10.1002/cbic.200700511 (2008).
- 82 Wu, X., Ding, S., Ding, Q., Gray, N. S. & Schultz, P. G. A Small Molecule with Osteogenesis-Inducing Activity in Multipotent Mesenchymal Progenitor Cells. *Journal of the American Chemical Society* **124**, 14520-14521, doi:10.1021/ja0283908 (2002).
- 83 Sinha, S. & Chen, J. K. Purmorphamine activates the Hedgehog pathway by targeting Smoothened. *Nat Chem Biol* **2**, 29-30, doi:10.1038/nchembio753 (2006).
- 84 Wang, X.-D. *et al.* Mutations in the Hedgehog Pathway Genes SMO and PTCH1 in Human Gastric Tumors. *PLOS ONE* **8**, e54415, doi:10.1371/journal.pone.0054415 (2013).
- 85 Wu, X., Walker, J., Zhang, J., Ding, S. & Schultz, P. G. Purmorphamine Induces Osteogenesis by Activation of the Hedgehog Signaling Pathway. *Chemistry & Biology* **11**, 1229-1238, doi:<http://dx.doi.org/10.1016/j.chembiol.2004.06.010> (2004).
- 86 GmbH, R. D. <http://netdocs.roche.com/DDM/Effective/pdf_0900b2fc80b66db4.pdf> (
- 87 Taipale, J. *et al.* Effects of oncogenic mutations in Smoothened and Patched can be reversed by cyclopamine. *Nature* **406**, 1005-1009, doi:http://www.nature.com/nature/journal/v406/n6799/supinfo/4061005a0_S1.html (2000).
- 88 di Magliano, M. P. & Hebrok, M. Hedgehog signalling in cancer formation and maintenance. *Nat Rev Cancer* **3**, 903-911 (2003).
- 89 Sharpe, H. J., Wang, W., Hannoush, R. N. & de Sauvage, F. J. Regulation of the oncoprotein Smoothened by small molecules. *Nat Chem Biol* **11**, 246-255, doi:10.1038/nchembio.1776 (2015).
- 90 Cho, H. Protein tyrosine phosphatase 1B (PTP1B) and obesity. *Vitamins and hormones* **91**, 405-424, doi:10.1016/b978-0-12-407766-9.00017-1 (2013).
- 91 Trist, D. G. & Corsi, M. Cholecystokinin (CCK) assays. *Current protocols in pharmacology* **Chapter 4**, Unit 4.13, doi:10.1002/0471141755.ph0413s04 (2001).
- 92 Lok, S. *et al.* The human glucagon receptor encoding gene: structure, cDNA sequence and chromosomal localization. *Gene* **140**, 203-209 (1994).
- 93 Authier, F. & Desbuquois, B. Glucagon receptors. *Cellular and Molecular Life Sciences* **65**, 1880-1899, doi:10.1007/s00018-008-7479-6 (2008).
- 94 Wondrusch, D., Böhme, A., Thaens, D., Ost, N. & Schüürmann, G. Local Electrophilicity Predicts the Toxicity-Relevant Reactivity of Michael Acceptors. *The Journal of Physical Chemistry Letters* **1**, 1605-1610, doi:10.1021/jz100247x (2010).
- 95 Etienne-Manneville, S. & Hall, A. Rho GTPases in cell biology. *Nature* **420**, 629-635 (2002).
- 96 Ridley, A. J. & Hall, A. The small GTP-binding protein rho regulates the assembly of focal adhesions and actin stress fibers in response to growth factors. *Cell* **70**, 389-399 (1992).
- 97 Ridley, A. J., Paterson, H. F., Johnston, C. L., Diekmann, D. & Hall, A. The small GTP-binding protein rac regulates growth factor-induced membrane ruffling. *Cell* **70**, 401-410 (1992).
- 98 Nobes, C. D. & Hall, A. Rho, rac, and cdc42 GTPases regulate the assembly of multimolecular focal complexes associated with actin stress fibers, lamellipodia, and filopodia. *Cell* **81**, 53-62 (1995).
- 99 Tapon, N. & Hall, A. Rho, Rac and Cdc42 GTPases regulate the organization of the actin cytoskeleton. *Current opinion in cell biology* **9**, 86-92 (1997).
- 100 Cook, D. R., Rossman, K. L. & Der, C. J. Rho guanine nucleotide exchange factors: regulators of Rho GTPase activity in development and disease. *Oncogene* **33**, 4021-4035, doi:10.1038/onc.2013.362 (2014).

- 101 van Buul, J. D., Geerts, D. & Huveneers, S. Rho GAPs and GEFs: controlling switches in endothelial cell adhesion. *Cell adhesion & migration* **8**, 108-124 (2014).
- 102 Ota, T., Maeda, M., Okamoto, M. & Tatsuka, M. Positive regulation of Rho GTPase activity by RhoGDIs as a result of their direct interaction with GAPs. *BMC systems biology* **9**, 3, doi:10.1186/s12918-015-0143-5 (2015).
- 103 Dovas, A. & Couchman, John R. RhoGDI: multiple functions in the regulation of Rho family GTPase activities. *Biochemical Journal* **390**, 1-9, doi:10.1042/BJ20050104 (2005).
- 104 Ueda, T., Kikuchi, A., Ohga, N., Yamamoto, J. & Takai, Y. Purification and characterization from bovine brain cytosol of a novel regulatory protein inhibiting the dissociation of GDP from and the subsequent binding of GTP to rhoB p20, a ras p21-like GTP-binding protein. *The Journal of biological chemistry* **265**, 9373-9380 (1990).
- 105 Boulter, E. *et al.* Regulation of Rho GTPase crosstalk, degradation and activity by RhoGDI1. *Nature cell biology* **12**, 477-483, doi:10.1038/ncb2049 (2010).
- 106 Garcia-Mata, R., Boulter, E. & Burrige, K. The 'invisible hand': regulation of RHO GTPases by RHOGDIs. *Nat Rev Mol Cell Biol* **12**, 493-504 (2011).
- 107 Gandhi, P. N. *et al.* An activating mutant of Rac1 that fails to interact with Rho GDP-dissociation inhibitor stimulates membrane ruffling in mammalian cells. *Biochemical Journal* **378**, 409-419, doi:10.1042/BJ20030979 (2004).
- 108 Gibson, R. M. *et al.* An activating mutant of Cdc42 that fails to interact with Rho GDP-dissociation inhibitor localizes to the plasma membrane and mediates actin reorganization. *Experimental cell research* **301**, 211-222, doi:10.1016/j.yexcr.2004.07.033 (2004).
- 109 Tiedje, C., Sakwa, I., Just, U. & Höfken, T. The Rho GDI Rdi1 Regulates Rho GTPases by Distinct Mechanisms. *Molecular Biology of the Cell* **19**, 2885-2896, doi:10.1091/mbc.E07-11-1152 (2008).
- 110 Tnimov, Z. *et al.* Quantitative analysis of prenylated RhoA interaction with its chaperone, RhoGDI. *The Journal of biological chemistry* **287**, 26549-26562, doi:10.1074/jbc.M112.371294 (2012).
- 111 Chinchilla, P., Xiao, L., Kazanietz, M. G. & Riobo, N. A. Hedgehog proteins activate pro-angiogenic responses in endothelial cells through non-canonical signaling pathways. *Cell cycle (Georgetown, Tex.)* **9**, 570-579, doi:10.4161/cc.9.3.10591 (2010).
- 112 Kasai, K. *et al.* The G12 family of heterotrimeric G proteins and Rho GTPase mediate Sonic hedgehog signalling. *Genes to cells : devoted to molecular & cellular mechanisms* **9**, 49-58 (2004).
- 113 Choi, S. S. *et al.* Activation of Rac1 promotes Hedgehog-mediated acquisition of the myofibroblastic phenotype in rat and human hepatic stellate cells. *Hepatology (Baltimore, Md.)* **52**, 278-290, doi:10.1002/hep.23649 (2010).
- 114 Newcombe, A. R., Stockley, R. W., Hunter, J. L. & Webb, M. R. The Interaction between Rac1 and Its Guanine Nucleotide Dissociation Inhibitor (GDI), Monitored by a Single Fluorescent Coumarin Attached to GDI. *Biochemistry* **38**, 6879-6886, doi:10.1021/bi9829837 (1999).
- 115 Mejuch, T. *et al.* Small-Molecule Inhibition of the UNC119–Cargo Interaction. *Angewandte Chemie International Edition* **56**, 6181-6186, doi:10.1002/anie.201701905 (2017).
- 116 Pelish, H. E. *et al.* Secramine inhibits Cdc42-dependent functions in cells and Cdc42 activation in vitro. *Nat Chem Biol* **2**, 39-46, doi:10.1038/nchembio751 (2006).
- 117 Sioud, M. Therapeutic siRNAs. *Trends in pharmacological sciences* **25**, 22-28, doi:10.1016/j.tips.2003.11.006 (2004).
- 118 DerMardirossian, C. & Bokoch, G. M. GDIs: central regulatory molecules in Rho GTPase activation. *Trends in cell biology* **15**, 356-363, doi:10.1016/j.tcb.2005.05.001 (2005).
- 119 Carthew, R. W. & Sontheimer, E. J. Origins and Mechanisms of miRNAs and siRNAs. *Cell* **136**, 642-655, doi:10.1016/j.cell.2009.01.035 (2009).

- 120 Wittrup, A. & Lieberman, J. Knocking down disease: a progress report on siRNA therapeutics. *Nature reviews. Genetics* **16**, 543-552, doi:10.1038/nrg3978 (2015).
- 121 Bozza, W. P., Zhang, Y., Hallett, K., Rosado, L. A. R. & Zhang, B. RhoGDI deficiency induces constitutive activation of Rho GTPases and COX-2 pathways in association with breast cancer progression. *Oncotarget* **6**, 32723-32736 (2015).
- 122 Boulter, E. *et al.* Regulation of Rho GTPase crosstalk, degradation and activity by RhoGDI1. *Nature cell biology* **12**, 477-483, doi:http://www.nature.com/ncb/journal/v12/n5/supinfo/ncb2049_S1.html (2010).
- 123 Ota, T., Maeda, M., Okamoto, M. & Tatsuka, M. Positive regulation of Rho GTPase activity by RhoGDIs as a result of their direct interaction with GAPs. *BMC Systems Biology* **9**, 3, doi:10.1186/s12918-015-0143-5 (2015).
- 124 Riobo, N. A., Saucy, B., DiLizio, C. & Manning, D. R. Activation of heterotrimeric G proteins by Smoothed. *Proceedings of the National Academy of Sciences of the United States of America* **103**, 12607-12612, doi:10.1073/pnas.0600880103 (2006).
- 125 Polizio, A. H. *et al.* Heterotrimeric Gi proteins link Hedgehog signaling to activation of Rho small GTPases to promote fibroblast migration. *The Journal of biological chemistry* **286**, 19589-19596, doi:10.1074/jbc.M110.197111 (2011).
- 126 Wouters, F. S., Verveer, P. J. & Bastiaens, P. I. H. Imaging biochemistry inside cells. *Trends in Cell Biology* **11**, 203-211, doi:[http://dx.doi.org/10.1016/S0962-8924\(01\)01982-1](http://dx.doi.org/10.1016/S0962-8924(01)01982-1) (2001).
- 127 O'Leary-Steele, C. *et al.* Synthesis of Small Molecules with High Scaffold Diversity: Exploitation of Metathesis Cascades in Combination with Inter- and Intramolecular Diels–Alder Reactions. *Chemistry – A European Journal* **16**, 9563-9571, doi:10.1002/chem.201000707 (2010).
- 128 Cimmperman, P. *et al.* A Quantitative Model of Thermal Stabilization and Destabilization of Proteins by Ligands. *Biophysical Journal* **95**, 3222-3231, doi:10.1529/biophysj.108.134973 (2008).
- 129 Niesen, F. H., Berglund, H. & Vedadi, M. The use of differential scanning fluorimetry to detect ligand interactions that promote protein stability. *Nature protocols* **2**, 2212-2221, doi:10.1038/nprot.2007.321 (2007).
- 130 Appleby, T. C., Erion, M. D. & Ealick, S. E. The structure of human 5'-deoxy-5'-methylthioadenosine phosphorylase at 1.7 Å resolution provides insights into substrate binding and catalysis. *Structure* **7**, 629-641, doi:[http://dx.doi.org/10.1016/S0969-2126\(99\)80084-7](http://dx.doi.org/10.1016/S0969-2126(99)80084-7) (1999).
- 131 Toorchen, D. & Miller, R. L. Purification and characterization of 5'-deoxy-5'-methylthioadenosine (MTA) phosphorylase from human liver. *Biochemical Pharmacology* **41**, 2023-2030, doi:[http://dx.doi.org/10.1016/0006-2952\(91\)90145-U](http://dx.doi.org/10.1016/0006-2952(91)90145-U) (1991).
- 132 Pegg, A. E. & Williams-Ashman, H. G. Phosphate-stimulated breakdown of 5'-methylthioadenosine by rat ventral prostate. *The Biochemical journal* **115**, 241-247 (1969).
- 133 Berger, B. J., Dai, W.-W. & Wilson, J. Methionine formation from α -ketomethiobutyrate in the trypanosomatid *Crithidia fasciculata*. *FEMS Microbiology Letters* **165**, 305-312, doi:10.1111/j.1574-6968.1998.tb13162.x (1998).
- 134 Hanfrey, C., Sommer, S., Mayer, M. J., Burtin, D. & Michael, A. J. Arabidopsis polyamine biosynthesis: absence of ornithine decarboxylase and the mechanism of arginine decarboxylase activity. *The Plant Journal* **27**, 551-560, doi:10.1046/j.1365-313X.2001.01100.x (2001).
- 135 *Crystal structure of Sulfolobus tokodaii MTAP.* (<http://www.rcsb.org/pdb/explore/explore.do?structureId=1V4N>).
- 136 Basu, I. *et al.* A transition state analogue of 5'-methylthioadenosine phosphorylase induces apoptosis in head and neck cancers. *The Journal of biological chemistry* **282**, 21477-21486, doi:10.1074/jbc.M702287200 (2007).
- 137 Chow, W. A. *et al.* Methylthioadenosine phosphorylase gene deletions are frequently detected by fluorescence in situ hybridization in conventional chondrosarcomas. *Cancer*

- Genetics and Cytogenetics* **166**, 95-100, doi:<http://dx.doi.org/10.1016/j.cancergencyto.2005.10.009> (2006).
- 138 Christopher, S. A., Diegelman, P., Porter, C. W. & Kruger, W. D. Methylthioadenosine Phosphorylase, a Gene Frequently Codeleted with p16^{INK4A}/ARF, Acts as a Tumor Suppressor in a Breast Cancer Cell Line. *Cancer Research* **62**, 6639 (2002).
- 139 Gerner, E. W. & Meyskens, F. L. Polyamines and cancer: old molecules, new understanding. *Nat Rev Cancer* **4**, 781-792 (2004).
- 140 Schmid, M. *et al.* Homozygous deletions of methylthioadenosine phosphorylase (MTAP) are more frequent than p16 INK4A (CDKN2) homozygous deletions in primary non-small cell lung cancers (NSCLC). *Oncogene* **17** (1998).
- 141 Guan, R., Tyler, P. C., Evans, G. B. & Schramm, V. L. Thermodynamic Analysis of Transition-State Features in Picomolar Inhibitors of Human 5'-Methylthioadenosine Phosphorylase. *Biochemistry* **52**, 8313-8322, doi:10.1021/bi401188w (2013).
- 142 Basu, I. *et al.* Growth and metastases of human lung cancer are inhibited in mouse xenografts by a transition state analogue of 5'-methylthioadenosine phosphorylase. *The Journal of biological chemistry* **286**, 4902-4911, doi:10.1074/jbc.M110.198374 (2011).
- 143 Tang, B., Kadariya, Y., Chen, Y., Slifker, M. & Kruger, W. D. Expression of MTAP Inhibits Tumor-Related Phenotypes in HT1080 Cells via a Mechanism Unrelated to Its Enzymatic Function. *G3: Genes/Genomes/Genetics* **5**, 35-44, doi:10.1534/g3.114.014555 (2015).
- 144 Schüller, U. *et al.* Acquisition of Granule Neuron Precursor Identity Is a Critical Determinant of Progenitor Cell Competence to Form Shh-Induced Medulloblastoma. *Cancer cell* **14**, 123-134, doi:<https://doi.org/10.1016/j.ccr.2008.07.005> (2008).
- 145 D'Amico, D. *et al.* Non-canonical Hedgehog/AMPK-Mediated Control of Polyamine Metabolism Supports Neuronal and Medulloblastoma Cell Growth. *Developmental cell* **35**, 21-35, doi:10.1016/j.devcel.2015.09.008 (2015).
- 146 Zhao, X. & Segal, R. A. A Polyamine Twist on Hedgehog Signaling. *Developmental cell* **35**, 1-2, doi:10.1016/j.devcel.2015.09.024 (2015).
- 147 Subhi, A. L. *et al.* Methylthioadenosine phosphorylase regulates ornithine decarboxylase by production of downstream metabolites. *The Journal of biological chemistry* **278**, 49868-49873, doi:10.1074/jbc.M308451200 (2003).
- 148 Chan, J. N. Y., Nislow, C. & Emili, A. Recent advances and method development for drug target identification. *Trends in pharmacological sciences* **31**, 82-88, doi:<http://dx.doi.org/10.1016/j.tips.2009.11.002> (2010).
- 149 Palmer, A. C. & Kishony, R. Opposing effects of target overexpression reveal drug mechanisms. *Nature communications* **5**, 4296, doi:10.1038/ncomms5296 (2014).
- 150 Gibson, T. J., Seiler, M. & Veitia, R. A. The transience of transient overexpression. *Nat Meth* **10**, 715-721, doi:10.1038/nmeth.2534 (2013).
- 151 MTAP_HUMAN. <<http://www.uniprot.org/uniprot/Q13126>> (
- 152 Szklarczyk, D. *et al.* STRING v10: protein–protein interaction networks, integrated over the tree of life. *Nucleic acids research* **43**, D447-D452, doi:10.1093/nar/gku1003 (2015).
- 153 Speek, M., Njunkova, O., Pata, I., Valdre, E. & Kogerman, P. A potential role of alternative splicing in the regulation of the transcriptional activity of human GLI2 in gonadal tissues. *BMC Molecular Biology* **7**, 13-13, doi:10.1186/1471-2199-7-13 (2006).
- 154 Pfaffl, M. W. A new mathematical model for relative quantification in real-time RT-PCR. *Nucleic acids research* **29**, e45 (2001).
- 155 Cox, J. & Mann, M. MaxQuant enables high peptide identification rates, individualized p.p.b.-range mass accuracies and proteome-wide protein quantification. *Nature biotechnology* **26**, 1367-1372, doi:10.1038/nbt.1511 (2008).

12 Acknowledgements

I would like to take this opportunity to thank many people who have supported me during my doctoral research in Germany.

I would like to thank Prof. Dr. Herbert Waldmann for accepting me in his group and for allowing me to work on very interesting and challenging projects. I am grateful for his continuous support, supervision and helpful suggestions throughout the doctoral study. I would also thank Dr. Slava Ziegler for her supervision and also for proof reading my PhD thesis. Additionally, my thanks go to Dr. Luca Laraia and Prof. Dr. Shobhna Kapoor for intellectual discussions and for proof reading my thesis. I would like to thank Dr. Leif Dehmelt for agreeing to be my second examiner of my PhD thesis.

Special thanks go to my collaborators, Prof. Adam Nelson and Prof. Reza Ahmadian for their support for the ongoing fruitful collaboration. I would like to explicitly mention Dr. Mark Dow and Mohammad Akbarzadeh for their contribution in the collaborative projects. Jana Flegel deserves a special mention for her contributing to my PhD research work.

Big thanks to my master thesis supervisor Dr. Sudipta Basu for encouraging me to broaden by research interest and recommending me to this wonderful work group.

I would like to give my sincere thanks to Yen-Chun Lee, Dr. Rishikesh Narayan, Dr. Erchang Shang, Dr. Marco Potowski, Dr. Michael Sheremet, Dr. Matthias Bischoff and Walter Hofer for their collaboration in order to accomplish the research projects. Besides, I thank all the lab mates and friends in the MPI, including Dr. Tim Förster, Dr. Lucas Robke, Elena Reckzeh, Dr. Andrei Ursu, Dr. Zhi-Jun Jia, Dr. Yasemin Akbulut, Lea Kremer, Stefan Zimmerman, Michael Winzker, Ranganath Gopalakrishnan, Juhi Sardana, Adithi Danda. I also acknowledge all other members of our department, especially those working in the bio group for creating a lively working environment. Special thanks go to Dr. Sonja Sievers, Dr. Claude Ostermann and all the other members of COMAS for contributing to this work with biological screenings.

I would also like to thank Amit Mahamne, Aditya Desai, Vivek Raina, Divya Singh and Dr. Shweta Bendre for making my stay in Germany comforting.

Further I would like to acknowledge the financial support by IMPRS-CMB (the International Max-Planck-Research School in Chemical and Molecular Biology).

Finally, I want to thank my family and my wife Kalyani for sharing my pain and happiness during the PhD.

13 Eidesstattliche Versicherung (Affidavit)

Patil, Sumersing

Name, Vorname
(Surname, first name)

172364

Matrikel-Nr.
(Enrollment number)

Belehrung:

Wer vorsätzlich gegen eine die Täuschung über Prüfungsleistungen betreffende Regelung einer Hochschulprüfungsordnung verstößt, handelt ordnungswidrig. Die Ordnungswidrigkeit kann mit einer Geldbuße von bis zu 50.000,00 € geahndet werden. Zuständige Verwaltungsbehörde für die Verfolgung und Ahndung von Ordnungswidrigkeiten ist der Kanzler/die Kanzlerin der Technischen Universität Dortmund. Im Falle eines mehrfachen oder sonstigen schwerwiegenden Täuschungsversuches kann der Prüfling zudem exmatrikuliert werden, §63 Abs. 5 Hochschulgesetz NRW.

Die Abgabe einer falschen Versicherung an Eides statt ist strafbar.

Wer vorsätzlich eine falsche Versicherung an Eides statt abgibt, kann mit einer Freiheitsstrafe bis zu drei Jahren oder mit Geldstrafe bestraft werden, § 156 StGB. Die fahrlässige Abgabe einer falschen Versicherung an Eides statt kann mit einer Freiheitsstrafe bis zu einem Jahr oder Geldstrafe bestraft werden, § 161 StGB.

Official notification:

Any person who intentionally breaches any regulation of university examination regulations relating to deception in examination performance is acting improperly. This offence can be punished with a fine of up to EUR 50,000.00. The competent administrative authority for the pursuit and prosecution of offences of this type is the chancellor of the TU Dortmund University. In the case of multiple or other serious attempts at deception, the candidate can also be unenrolled, Section 63, paragraph 5 of the Universities Act of North Rhine-Westphalia.

The submission of a false affidavit is punishable.

Any person who intentionally submits a false affidavit can be punished with a prison sentence of up to three years or a fine, Section 156 of the Criminal Code. The negligent submission of a false affidavit can be punished with a prison sentence of up to one year or a fine, Section 161 of the Criminal Code.

I have taken note of the above official notification.

Ort, Datum

(Place, date)

Unterschrift

(Signature)

Titel der Dissertation:

(Title of the thesis):

Discovery of Novel Targets in the Hedgehog Signaling Pathway

Ich versichere hiermit an Eides statt, dass ich die vorliegende Dissertation mit dem Titel selbstständig und ohne unzulässige fremde Hilfe angefertigt habe. Ich habe keine anderen als die angegebenen Quellen und Hilfsmittel benutzt sowie wörtliche und sinngemäße Zitate kenntlich gemacht. Die Arbeit hat in gegenwärtiger oder in einer anderen Fassung weder der TU Dortmund noch einer anderen Hochschule im Zusammenhang mit einer staatlichen oder akademischen Prüfung vorgelegen.

I hereby swear that I have completed the present dissertation independently and without inadmissible external support. I have not used any sources or tools other than those indicated and have identified literal and analogous quotations. The thesis in its current version or another version has not been presented to the TU Dortmund University or another university in connection with a state or academic examination.

14 Curriculum vitae

Name Sumersing Patil
Date of birth 15th June 1990
Place of birth Bodwad, Tal: Bodwad, India.

Education

2013-Present **Ph.D. in Chemical Biology**
Max Planck Institute of Molecular Physiology, Department of
Chemical Biology. Dortmund, Germany.

2008-2013 **Integrated B.Sc.-M.Sc. in Bioinformatics and Biotechnology**
Institute of Bioinformatics and Biotechnology, University of Pune.
Pune, India

Publications

1. Lee Y-C., **Patil S.**, et. al., (2017) A ligand-directed divergent catalytic approach to establish structural and functional scaffold diversity. *Nature Communications*. 8:14043, 1-12.
2. Kötzner L., Leutzsch M., Sievers S., **Patil S.**, et. al., (2016) The Organocatalytic Approach to Enantiopure 2H- and 3H-Pyrroles: Inhibitors of the Hedgehog Signaling Pathway. *Angewandte Chemistry International Edition*. 55:27, 7693-7697.
3. Ghosh S., **Patil S.**, et. al., (2016). Gnidia glauca Leaf and Stem Extract Mediated Synthesis of Gold Nanocatalysts with Free Radical Scavenging Potential. *Journal of Nanomedicine & Nanotechnology*. 7:2, 1-10.
4. **Patil, S.**, Gawali, et. al., (2013). Synthesis, characterization and in vitro evaluation of novel vitamin D3 nanoparticles as versatile platform for drug delivery in cancer. *Journal of Material Chemistry B*. 1:42, 5742-5750.
5. **Patil, S.**, Patil, S., et. al., (2013). Novel self-assembled lithocholic acid nanoparticles for drug delivery in cancer. *RSC Advances*. 3:43, 19760-19764.
6. Ghosh, S., **Patil S.**, et. al., (2012). Gnidia glauca flower extract mediated synthesis of gold nanoparticles and evaluation of its chemocatalytic potential. *Journal of Nanobiotechnology*, 10: 17, 1-9.
7. Ghosh, S., **Patil S.**, et. al., (2012). Synthesis of silver nanoparticles using Dioscorea bulbifera tuber extract and evaluation of its synergistic potential in combination with antimicrobial agents. *International Journal of Nanomedicine*, 7: 483-496.
8. Ghosh, S., **Patil, S.**, et. al., (2011). Synthesis of Gold Nanoanisotrops Using Dioscorea bulbifera Tuber Extract. *Journal of Nanomaterials*, 2011:1, 1-9.
9. Ghosh, S., Ahire, M., **Patil, S.**, et. al., (2011). Antidiabetic Activity of Gnidia glauca and Dioscorea bulbifera: Potent Amylase and Glucosidase Inhibitors. *Evidenced Based Complementary and Alternative Medicine*, 2012:1, 1-9.

